TOJSAT
The Online Journal of Science and Technology

ISSN 2146-7390

The Online Journal of Science and Technology

Volume 7 Issue 2

April 2017

www.tojsat.net
April 2017

Published in TURKEY

Contact Address:

Prof. Dr. Mustafa Şahin Dündar - TOJSAT, Editor Sakarya-Turkey

Message from the Editor-in-Chief

TOJSAT welcomes you.

I am happy to inform you that The Online Journal of Science and Technology (TOJSAT) has been published volume 7 issue 2 in 2017. This issue has research papers from all around the world.

The Online Journal of Science and Technology (TOJSAT) is an international journal in the field of science and technology. TOJSAT is an online and peer-reviewed journal that accepts papers on all aspects of science and technology. The aim of TOJSAT is to diffuse new developments in science and technology. The mission of TOJSAT is to provide educators, teachers, administrators, parents and faculties with knowledge about the very best research in science and technology. TOJSAT's acceptance rate is almost 30%. TOJSAT is now a major resource for knowledge about science and technology.

TOJSAT publishes research and scholarly papers in the fields of science and technology. All papers are reviewed at least by two international members of the Editorial Board with expertise in the areas(s) represented by a paper, and/or invited reviewers with special competence in the area(s) covered. The Editors reserve the right to make minor alterations to all papers that are accepted for publication.

TOJSAT is interested in various researches in science and technology. Therefore, we are pleased to publish this issue which different papers from various fields are shared with professionals. TOJSAT thanks and appreciate the editorial board members who have acted as reviewers for one or more submissions of this issue for their valuable contributions.

TOJSAT is confident that readers will learn and get different aspects on science and technology. Any views expressed in this publication are the views of the authors and are not the views of the Editor and TOJSAT.

TOJSAT will organize ISTECEurope - 2017 at Freie University in Berlin, Germany and ISTECAmerica - 2017, in Harvard University, Boston, USA. ISTEC series is an international educational activity for academics, teachers and educators. This conference is now a well-known science and technology event. It promotes the development and dissemination of theoretical knowledge, conceptual research, and professional knowledge through conference activities. Its focus is to create and disseminate knowledge about science and technology.

Call for Papers
TOJSAT invites our authors to submit a research paper. Submitted articles should be about all aspects of science and technology. The articles should be original, unpublished, and not in consideration for publication elsewhere at the time of submission to TOJSAT. Manuscripts must be submitted in English.

TOJSAT is guided by its' editors, guest editors and advisory boards. If you are interested in contributing to TOJSAT as an author, guest editor or reviewer, please send your CV to tojsateditor@gmail.com.

April 01, 2017
Editor-in-Chief
Prof. Dr. Aytekin İŞMAN
Sakarya University, Turkey

Message from the Editor

Dear Tojsat Readers,

Now, we are reading 2nd issue of 7th volume of The Online Journal of Science and Technology. We finished the istec 2016 conference hold in Vienna, Austria. The papers submitted from Saudi Arabia to Turkey receives interests from all over the areas of science and technology. The selected, peer-reviewed papers were accepted for publication apart from contributions from all over the World.

Prof.Dr. Mustafa S. Dundar

Editor

Table of Contents

ANALYSES OF ABA RESPONSES GENES IN *ARABIDOPSIS THALIANA sos5* MUTANT UNDER NaCI STRESS

Tuba ACET

Gümüşhane University, Engineering and Applied Sciences Faculty, Department of Genetic and Bioengineering, Gümüşhane- TURKEY

tubaacet@hotmail.com

Abstract: Abscisic acid (ABA) is an important phytohormone that regulates a lot of physiological, biochemical and molecular processes during plants life and response stress conditions. In this paper, *Arabidopsis thaliana salt overly sensitive* (*sos5*) mutant which known hyper sensitive to NaCI stress was used to investigate ABA regulation. Because of this, ABA depended genes determined by q-RT PCR method under 2h. 100 mM NaCI stress. Findings indicated that RD29A, RD 29B and RD22 which ABA dependent gene expressions were highly lower than *Col-gl* (wild type); however ERD1 which ABA in depended gene expression was higher than WT. Based on these results, we suggest that defect of ABA responses gene regulation might be responsible for hypersensitivity to Arabidopsis *sos5* mutant under salt stress.

Keywords: ABA, *Arabidopsis thaliana*, *sos5* mutant, salt stress

Introduction

Salinity is one of the most serious problems limiting the productivity of agricultural crops, with adverse effects on germination, plant defense system and crop yield (Munns & Tester, 2008). More than 45 million hectares of irrigated land have been damaged by salt, and 1.5 million hectares are taken out of production each year as a result of high salinity levels in the soil around the world (Munns & Tester, 2008). High salinity affects plants in several ways: water stress, ion toxicity, nutritional disorders, oxidative stress, alteration of metabolic processes, membrane disorganization, reduction of cell division and expansion, genotoxicity (Hasegawa, Bressan, Zhu, & Bohnert, 2000; Munns, 2002; Zhu, 2007). According to them, plant growth, development and survival highly reduced. Plants effected from salt stress in some different aspects such as osmotic, ionic and toxic. Meanwhile, plants have evolved several mechanisms to cope with salt stress. One of the most related defense mechanism is that produce ABA and express ABA related genes under salinity. For example, some researches showed that ABA-deficient mutants perform poorly under salinity stress (Xiong, Gong, Rock, Subramanian, Guo, Xu, et al., 2001). On the other hand, it has been shown that ABA-dependent and -independent transcription factors may also cross talk to each other in a synergistic way to amplify the response and improve stress tolerance (Shinozaki & Yamaguchi-Shinozaki, 2000).

There are some mutants characterized related to ABA and these are giving clues about ABA's role under stresses. But, we have very few ideas about Arabidopsis *sos5* mutant related to ABA. Shi et. al., (2003) has been shown firstly the *sos5* mutant of *A. thaliana* by root growth under salt stress. The root of *sos5* shows a drastic reduction of elongation growth combined with radial swelling of the elongation zone. Cell walls appear abnormally thin in *sos5*, apparently lacking the middle lamella (Shi et al., 2003).

To better understand the ABA related genetic pathway linking *sos5* mutant with salt tolerance and root growth, we exposed 2 hour 100 mM NaCI both WT and mutant. Then, we compared some ABA dependent and independent gene expression levels. We found that abscisic acid (ABA) dependent genes lower on *sos5* mutant compared to WT. We propose that Arabidopsis *sos5* mutant is hypersensitive to salt stress because of does not able to expressed ABA dependent genes enough and seem very sensitive.

Materials and Methods

Growth conditions

Arabidopsis thaliana ecotype *Col gl* wild type and the mutant (*sos5-1*) were kindly provided by Jian-Kang Zhu (University of California, Riverside, CA, USA). Growth conditions were as previously described (Blaukopf et al.,

2011). For phenotypic observation, ten seedlings were manually transferred to test media containing standard medium alone or also including the NaCI, and were examined using a dissecting microscope (Leica EZ4 HD). Stock ABA solution was prepared that was dissolved in 0.01 M NaOH.

Quantitative real-time PCR (qRT-PCR)

Samples were treated in biological triplicates. For each biological replicate, 150 seedlings were grown on a nylon mesh (20 mmmesh size; Prosep, Belgium) for 4 d and were transferred to standard medium with or without 100 mM NaCl and incubated for 120 min. Roots were removed from the seedlings, frozen in liquid nitrogen, ground in a ball mill (Retsch, Germany) for 2 min and RNA was extracted using peqGOLD Trifast (Peqlab, Germany) according to the manufacturer's instructions. The RNA concentration was measured using a Nano Drop 2000c Spectrophotometer (Thermo Scientific, USA). For each sample, 1 mg of total RNA was reverse-transcribed with oligo(dT) primers using a first-strand cDNA synthesis kit (Thermo Scientific, USA) according to the manufacturer's instructions.
Real-time PCR was performed using Solis BioDyne 5 × HOT FIREPol EvaGreen qPCR Mix Plus (no ROX) (Medibena, Austria), and a CFX96 TM Real-Time PCR Detection System (Bio-Rad, USA) was used for detection. Information on the oligonucleotides used can be found in Data Table 1. For real-time PCR, the following program was used: 95.0 8C for 15 min, 40 cycles of 95.0 8C for 10 s, 55.0 8C for 30 s, 72.0 8C for 30 s. Each biological replicatewas analysed in technical duplicates. The average technical error was 0.5 (+1) Ct values. Technical outliers were identified when the DCt between technical replicates was 2.5, and the higher Ct value was removed. The remaining technical replicates were averaged and the DCt (Ct test – CtUBQ5) was calculated.The effect of genotypes and treatments was tested by subjecting the DCt values of three biological replicates to a two-sided t-test.
For this study, the relative mRNA levels of three ABA dependent genes and one independent gene were analysed.

Results and Discussion

The mechanisms of genetic control of salt tolerance in plants have not yet fully understood. Because, salt stress sensed by different sensors. For instance, when plants exposed to salt stress, cell wall, cell surface and vacuole affected immediately and then triggered genes that over come to this case. One of the significant sensors that cell surface proteoglycans have been implicated in many aspects of plant growth and development, but genetic evidence supporting their function has been lacking. Shi et. al., (2003), reported in their paper that the Salt Overly Sensitive5 (SOS5) gene encodes a putative cell surface adhesion protein and is required for normal cell expansion. They isolated *sos5* mutant in a screen for Arabidopsis salt-hypersensitive mutants. According to them, under salt stress, the root tips of *sos5*mutant plants swell and root growth is arrested. The root-swelling phenotype is caused by abnormal expansion of epidermal, cortical, and endodermal cells. So, it means SOS5 gene is responsible for plant growth and development. Even under salt stress, the roots of the wild-type plants exhibit highly organized and defined cell shapes. Cell wall architecture, cytoskeleton, wall–membrane interactions and interaction between neighboring cells play a vital role in the control of cell expansion (Darley et. al., 2001). When this gene function knock out, in response to salt stress, the root tips of *sos5* plants swell and the root growth and elongation was arrested. We hypothesized that the certain phenotypic abnormalities of *sos5* related to ABA regulation.
According to our qRT-PCR results (**Figure 1.**), *At*-RD29A, *At*-RD29B and *At*-RD22 which are ABA dependent genes were highly expressed in WT plants, compare to *sos5* mutants. On the other hand, when we checked *At*-ERD1 which is ABA independent gene was higher in *sos5* mutants than WT under 100 mM NaCI. These results suggested that SOS5 gene have a synergistic function with ABA gene regulation. If there is no SOS5, in other word *sos5* mutant plants, there is a problem with ABA regulation and plants do not able to handle with salt stress affects. Based on this, Seifert et., al., (2014) pointed out that application of ABA suppresses the non-redundant role of *At*-SOS5 in the salt response and Salt oversensitivity in *At-sos5* is suppressed by the exogenous ABA applications. All tested ABA-dependent genes displayed a significant repression in *At-sos5*, suggesting that the effect of *At*-SOS5 on stress signaling might be specific for ABA.

Table 1: Oligonucleotides used for qRT-PCR.

1-) RD29A: At5g52310.1	RD29A-F: AAGTTACTGATCCCACCAAAGAAGAAAC
	RD29A-R: TTTCCTCCCAACGGAGCTCCTAAAC
2-) RD29B: At5g52300.1	RD29B-F: TCCGGTTTACGAAAAAGTCAAAGAAAC
	RD29B-R: AATCCGAAAACCCCATAGTCCCAAC
3-) RD22: At5g25610	RD22-F: ACGTCAGGGCTGTTTCCACTGAGGTG
	RD22-R: TAGTAGCTGAACCACACAACATGAG
4-) ERD1: At5g51070	ERD1-F: ACTTGGAAGGGGTGAACTTCAGTG
	ERD1-R: AGGTCCCACCAGTATAGGCTCATCG

Figure 1. Expression level of ABA related genes during under 100 mM NaCI. Error bars on each point indicate ±SE from three independent replicates.

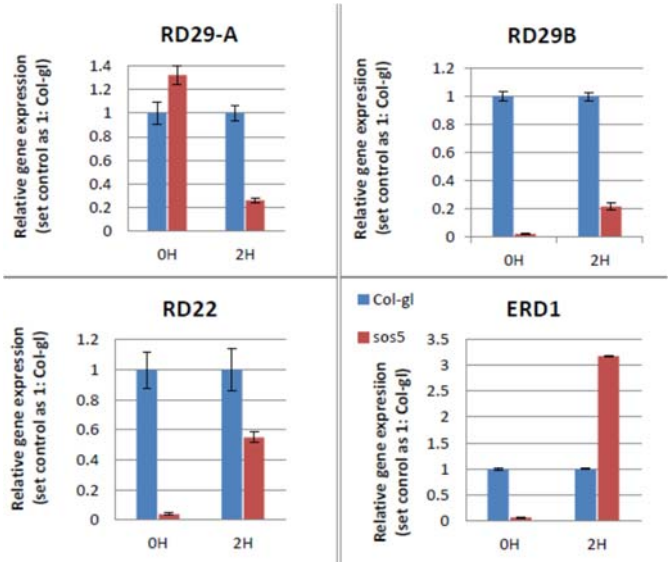

Conclusion

The predicted lipid-anchored glycoprotein *At*-SOS5 positively regulates cell wall biosynthesis and root growth by modulating ABA signalling. Taken together, we suggest that *At*-SOS5 and ABA signalling act in genetic synergy, leading to suppression of At-sos5 by ABA. Overall, we conclude that *At*-SOS5 regulates normal root growth via an ABA-depedent signalling pathway that might be upstream of cell wall biosynthesis.

Acknowledgements

We thank Dr. Georg Seifert (University of Natural Resources and Life Science, Vienna, Austria; Department of Applied Genetics and Cell Biology, Muthgasse 18, A-1990 Vienna, Austria) for hosted me in his laboratory and supervised my all works.
This work was supported by the Austrian Science Fund (P21782-B12, I1182-B22) and supported by The Council of Higher Education (PhD Research Scholarship), Turkey.

References

Blaukopf C., Krol M.Z., Seifert G.J. (2011). New insights into the control of cell growth. *Methods in Molecular Biology*. 715: 221–244.

Darley, C.P., Forrester, A.M., McQueen-Mason, S.J., (2001). *Plant Mol. Biol.* 47 179–195.

Hasegawa, P. M., Bressan, R. A., Zhu, J. K., & Bohnert, H. J. (2000). Plant cellular and molecular responses to high salinity. *Annual Review of Plant Physiology and Plant Molecular Biology*, 51, 463-499.

Munns, R. (2002). Comparative physiology of salt and water stress. *Plant, Cell & Environment*, 25(2), 239-250.

Munns & Tester, Munns, R., & Tester, M. (2008). Mechanisms of salinity tolerance. *Annual Review of Plant Biology*, 59, 651-681.

Shinozaki, K., & Yamaguchi-Shinozaki, K. (2000). Molecular responses to dehydration and low temperature: differences and cross-talk between two stress signaling pathways.*Current Opinion in Plant Biology*, 3(3), 217-223.

Shi H, KimY, GuoY, Stevenson B, Zhu J.K. (2003). The arabidopsis SOS5 locus encodes a putative cell surface adhesion protein and is required for normal cell expansion. *The Plant Cell*, 15: 19–32.

Seifert, G. J., Xue, H.,1 and Acet, T., (2014). The Arabidopsis thaliana *FASCICLIN LIKE ARABINOGALACTAN PROTEIN 4* gene acts synergistically with abscisic acid signalling to control root growth. *Annals of Botany*. Page 1 of 9, doi:10.1093/aob/mcu010.

Zhu, J.-K. (2007). Plant Salt Stress: *John Wiley & Sons*, Ltd.

CALCULUS WRITING PROMPTS

Jason D. Johnson
Zayed University, Department of Mathematics and Statistics, P.O. Box 19282, Dubai – UAE
Email: jason.johnson@zu.ac.ae

Carla A. Rudder
Rabdan Academy, Department of Mathematics, Al Dhafeer Street, Abu Dhabi – UAE
Email: cruder@ra.ac.ae

Abstract: In this paper, a study was designed to explore mathematics majors engaged in Calculus writing prompts. The paper also provides mathematics instructors benefits for instruction and students for the importance of writing to make sense of mathematics. An analysis for both the derivative and integral writing prompts was completed. The results indicate that mathematics majors were able to solve derivative and integral problems, however, some were unable to articulate their mathematical thinking and the thinking of others.

Key Words: Calculus, writing prompts, higher education, mathematics

"You know what I mean….I just can't explain it!"

Introduction

The above response was expressed by a mathematics major who participated in the study. University instructors have experienced leaners who are unable to articulate their mathematical understanding verbally and/or in written form. Why are some learners unable to convey their mathematical thinking in writing? Many learners view writing as a skill that should be practiced in History or English courses, rather than mathematics. The purpose of this paper is to record the results from a research study designed to examine the influence of calculus writing prompts and provide implications for instructors.

Ideas About Writing to Learn Mathematics

In a course designed for mathematics majors, learners explore some mathematics topics using writing prompts. For this study, writing prompts are defined as a situation where a learner explains a mathematical topic so that another learner would understand without simply restating a formula. Many participants in this study expressed disappoint for the idea of using calculus writing prompts to explain their mathematical thinking. This could be due to the lack of experience with writing to explain one's mathematical understanding. Morgan (1998) noted learners in mathematics might complete practice exercises without writing a single sentence to explain their solutions. Learners were asked to explain their mathematical thinking and the thinking of others for various topics in mathematics. Instructors may not perceive any relationship between writing and learning mathematics (Davision and Pearce, 1988; Ntenza, 2006). Learners must be given an opportunity to write about their mathematical thoughts. This can only be accomplished if the instructor is aware of the benefits for having learners articulate their thoughts in writing. Davision and Pearce (1980), further explain when instructor's use structured writing activities regularly the performance of learners improves drastically.

The Purpose of the Study

A study analyzed the mathematical thinking of twenty-three students' responses to various open writing prompts in order to decipher the students' mathematical understanding (Aspinwall and Aspinwall, 2003). The mathematical thinking of the students was classified into four categories: 1) algorithms and computation, 2) limited understanding, 3) utilitarian value, and 4) conceptual understanding. Do learners view mathematics as a procedural process rather than a conceptual process? Or do the views illustrate a limited understanding and/or a utilitarian value? The purpose of the current study was to determine the mathematics majors (n=9) written explanations for the derivative and integral calculus concepts based on the four categories, see table 1.

Table 1 Calculus writing prompts

Prompt 1 (derivative)	A learner in class is confused with the idea of *the derivative*. How would you explain this concept so that the learner gains a greater understanding without simply restating the formula?
Prompt 2 (integral)	A learner claims that the *integral* is used to find the area under the curve by using rectangles but is experiencing difficulty when finding the integrals for her homework assignment. She then says "I don't understand; I know what I'm supposed to find, I just can't find it." Is this learner correct about the concept? How would you help this learner achieve understanding of the concept? Explain.

Discussion

The calculus writing prompts were presented in a courses designed for mathematics majors in the beginning of a spring semester. Various calculus writing prompts were required; however, the derivative and integral writing prompts were of importance for this study. The derivative and integral calculus writing prompt is the first assignment where my learners are asked to think about writing to explain their understanding. The calculus writing prompts for the derivative and integral were given as a homework assignment, where each learner was able to use resources in order to create a well written response in their explanation for the derivative and integral. I have identified responses from three learners who are identified as: Mary, Billy, and Heather (pseudonyms). These learners were selected since their responses represent diverse mathematical understanding. The following sections describe four categorizes of mathematical understanding and the mathematics majors' responses are organized accordingly.

Algorithms and Computation

Algorithms and computation is when a learners' response is illustrated by evidence of a procedure in nature in order to explain the learners' mathematical understanding. For instance, Mary wrote, "say we're given the $f(x) = x^4 - 3x^3$ the derivative of this function is $f(x) = 4x^3 - 9x^2$." She then proceeds to illustrate a procedure in order to find the derivative. Below is Billy's example who describes given the learner another problem to solve, while he watches to determine if the learner has errors in their work.

> First, I would have the learner state the definition of the limit for me $\lim_{h\to 0} \frac{f(x+h)-f(x)}{h}$. Once that is stated, I would have the learner walk through a problem with me watching, to see if I can see what they aren't understanding. If there is a problem somewhere I would correct it.

Utilitarian Value

Utilitarian value is a response that reflects the usefulness of mathematics, either now or in the future; however, lack a valid response that would lead to a greater mathematical understanding. Evidence of this is demonstrated in Billy's response:

> This learner does have a limited understanding of the integral function, because there are many uses for the integral function not just to find the area under a curve. It is also used to find the volume of a solid rotated about a given point, as well as for optimizing different kinds of formulas. In the real world, there is a science called physics that uses the integral function to determine how much work it takes to do something. Also, farmer brown uses the integral function to maximize the amount of area he can enclose with a certain amount of fencing.

Billy has clearly identified several instances where the integral is useful. He has yet to offer a well written interpretation so that a learner would have a greater understanding for the integral.

Limited Understanding

Limited understanding is a response that lacks conceptual understanding, while identifying more than one procedure. Heather demonstrated a lack of understanding in her response. For instance, Heather's response was "I would explain to the learner that a derivative of *f(x)* is the same as the instantaneous rate of change, or slope, of a function at any

value x." Heather's response for the derivative indicates she understands the concept, however, lack to interpret a well written explanation to help another learner make sense of the derivative. Another example, was Heather's response to the integral writing prompt was:

> This learner is on the right track, but she does not realize that there is more than one way to find the integral of a problem. Using rectangles to find the area under a curve is a good way to work the problem. First, the learner should set a subinterval for the rectangles with in the given interval of the integral. The learner should know how to find the area of a rectangle. Using this, the learner can add the area of the subintervals that he or she created and multiply the sum of the subintervals to the difference of the main interval divided by the number of subintervals. These are all things the learner should know by the time they reach calculus. The learner just needed something that he or she already knows to relate what they are learning.

Heather's response, indicates a limited understanding since using rectangles will not yield the most accurate area under a curve.

Conceptual Understanding

Conceptual understanding is when a learner is able to articulate a well written mathematical explanation. Mary's response indicates conceptual understanding of an integral:

> This learner has the right concept; the integral is the area under the curve of a function. However, her understanding is limited. I would explain to this learner that even though an integral IS the area under the curve, you cannot just draw rectangles and add up the areas because the number of rectangles you draw will affect the answer. Depending on the shape of the curve, you may end up with too much area or too little. But we want to be precise. So in order to find the exact area under that curve we need an infinite number of rectangles.

In Mary's response, she explains to the learner the idea for using rectangles will yield a solution, however, the solution will not be precise. She concludes by helping the learner to understand that an infinite number of rectangles must be used to arrive to an accurate solution.

Responses Evaluated

All learners were able to calculate derivatives and integrals, as demonstrated on various assessments, however, this research project analyzed the learners' ability to provide well written explanations for the derivative and integral calculus concepts. The learners were all able to provide valid elucidations for the derivative and integral concepts, however, not all explanations lead to conceptual understanding. For instance, Heather's response for the derivative and integral showed that she was able to provide a definition for both, however, lacked a concise explanation to help a learner without restating a procedure. Billy and Mary's response for the derivative writing prompt was categorized as procedural understanding, while Mary's response for the integral writing prompt was conceptual understanding and Billy's was utilitarian value, see table 2.

Table 2. Writing prompt (1 & 2) responses for Mary, Billy, and Heather

CALCULUS WRITING PROMPTS	Mary	Billy	Heather
Prompt 1 (derivative)	AC	AC	LU
Prompt 2 (integral)	CU	UV	LU
Key: CU: Conceptual Understanding LU: Limited Understanding UV: Utilitarian Value AC: Algorithms and Computation			

As for all nine learners, their responses varied for both the derivative and integral writing prompts, see table 3. For both the derivative and integral writing prompts, approximately 55.5% of the learner written responses were conceptual understanding & algorithms and computation, while approximately 66.6% were utilitarian value. From the data, it is apparent that the learners view the derivative and integral as procedural mathematics and they are able to articulate the usefulness.

Table 3. Approximate percentages for all nine learner's responses

CALCULUS WRITING PROMPTS	Conceptual Understanding	Utilitarian Value	Limited Understanding	Algorithms and Computation
Prompt 1 (derivative)	3 (33.3%)	2 (22.2%)	1 (11.1%)	3 (33.3%)
Prompt 2 (integral)	2 (22.2%)	4 (44.4%)	1 (11.1%)	2 (22.2%)

Benefits for Learner

Some learners in the study were unable to articulate a well written explanation for the derivative and integral calculus concepts. With further opportunities to express their mathematical thoughts, learners will be able to formulate well written ideas. There are many benefits for allowing learners opportunities to write about their mathematical thinking:

- allow learners to dialog with teacher (Miller, 1992)
- learners express and reflect their attitudes, knowledge, processes, and belief about mathematics (Miller, 1991)
- improve learning (Miller, 1991)
- improve problem solving (Johnson, 1983)
- learners do considerable thinking and organizing of their thoughts (Johnson, 1983; McCarthy, 2008)
- experience expressing mathematical thoughts (Johnson, 1983)
- stimulate thinking about mathematics (Johnson, 1983)
- improve learner writing (Sjoberg, Slavit, Coon, 2004)
- improve ability to make connections to real-life applications with confidence (Sjoberg, Slavit, Coon, 2004)
- allow learners' opportunities to think about mathematical ideas (Porter and Masingila, 2000)
- increased learners' ability to understand higher levels of mathematics (Sjoberg, Slavit, Coon, 2004)

Learners need opportunities to reflect and gather their thoughts about new mathematics learned; and possibly make connections to mathematics already learned.

Benefits for Instructor

Allowing learner's, the opportunity to write their mathematical thinking provides the instructor with valuable information. A list of benefits for the instructor are:

- improve instruction (Miller, 1992)
- allow learners to dialog with instructor (Miller, 1992)
- informal assessment (Miller, 1991)
- writing is for all levels of mathematics (i.e., abstract algebra, and analysis) (Johnson, 1983)

Instructors also acquire information about learner's progress and/or development through allowing learners opportunities to write in mathematics. Furthermore, the instructor can determine struggling learners and/or those who have misconceptions. Some instructors even use writing in mathematics to detect learner's beliefs, attitudes, and/or ability to question the world using mathematics.

Conclusion

In this study, writing prompts were implemented with undergraduate mathematics majors, however, the results of the study yield a greater perspective for higher education instructors. Mathematics majors also need opportunities to explain their mathematical understanding, regardless of mathematics or statistics course. Writing prompts allow learners' the opportunity to write about their mathematical thinking, which will inform the instructor of their learners' mathematical development.

References

Aspinwall, L. and Aspinwall, J. S. (2003). Investigating mathematical thinking using open writing prompts. Mathematics Teaching in the Middle School. 8, 7, 350 – 353.

Davison, D.M. and Pearce, D. L. (1990). Perspectives on writing activities in the mathematics classroom. Mathematics Education Research Journal. 2, 1, 15 – 22.

Davison, D. M. and Pearce, D. L. (1998). Teacher use of writing in junior high Mathematics classrooms. School Science and Mathematics,88, 6 – 15.

Johnson, M. L. (1983). Writing in mathematics classes: A valuable tool for learning. Mathematics Teacher, 117– 119.

McCarthy, D. S. (2008). Communication in mathematics: Preparing preservice teachers to include writing in mathematics teaching and learning. School Science and Mathematics. 108, 7, 334 – 340.

Miller, L. D. (1991). Writing to learn mathematics. Mathematics Teacher, 516 – 521.

Miller, L. D. (1992). Teacher benefits from using impromptu writing prompts in algebra classes. Journal for Research in Mathematics Education. 23, 4, 329 – 340.

Morgan, C. (1998). Writing Mathematically: the discourse of investigation, Studies in mathematics education, Falmer Press London.

Ntenza, S. P. (2006). Investigating forms of children's writing in grade 7 mathematics classroom. Educational Studies in Mathematics. 61, 321 – 345.

Porter, M. and Masingila, J.O. (2000). Examining the effects of writing on conceptual and procedural knowledge in calculus. Educational Studies in Mathematics. 42, 165 – 177.

Sjoberg, C. A., Slavit, D., and Coon, T. (2004). Improving writing prompts to improve student reflection. Mathematics Teaching in the Middle School. 9, 9, 490 – 493.

CMAS BASED CERAMICS PRODUCTION USING DOLOMITE, KAOLIN AND ZIRCONIA

Nil Toplan and H. Özkan Toplan

Sakarya University, Engineering Faculty, Metallurgy and Materials Engineering Department, Esentepe Campus, 54187, Sakarya, Turkey

Email:toplano@sakarya.edu.tr

Abstract: CMAS (CaO-MgO-Al_2O_3-SiO_2) based ceramics were fabricated by using dolomite, kaoline and zirconia as raw materials. Natural calcia and magnesia containing material (dolomite) and silica and alümina containing kaolin were used to develop a new ceramic of CMAS system. The calculated amounts of oxides for the indicated compositions were ball milled for 3 h using distilled water as the milling media. After drying, the powders pressed in cylindrical mould under the pressure of 300 MPa. The samples were fired in an electric furnace with a heating rate of 10ºC.minute^{-1} at 900ºC to 1200ºC for periods of 1, 3, and 5 hours. Then, the fired samples were cooled to room temperature in the furnace. Microstructure of produced CMAS ceramics were investigated and their phases analysis was determined. The effects of ZrO_2 oxide on microstructure and phase structure of CMAS ceramics were also investigated.

Keywords: CMAS ceramics, anorthite, diopside, dolomite, kaoline

Introduction

Glass-ceramic materials, prepared by the controlled crystallization of glasses, have a variety of established uses that depend on their uniform reproducible fine-grained microstructures, absence of porosity and other wide-range of properties, which can be tailored by an adjustment of composition and the heat treatment procedure applied. Recently, glass-ceramics based on chain silicate structures have been developed (Khater, 2010). The glass-ceramics based on CMAS quaternary system, which are mainly produced from inexpensive natural or synthetic materials, such as fly ash, blast furnace slag, basalt, oil shale, granite and tuff, lithium porcelain clay tailings have received increasing attention during the past few decades. Blast furnace (BF) slag is one of the most abundant solid by-products in steel plants. Currently most of BF slag in China has been used for cement manufacturing and civil engineering, and the remaining amount is deposited in landfill. BF slag, which is mainly composed of CaO, SiO_2, Al_2O_3 and MgO, is the excellent raw material for the production of glass-ceramics. Recycling these slags is necessarily beneficial not only for economy, but also for environmental friendly steel plants (Yang et al, 2015). CMAS ceramic is one of the most promising glass–ceramic systems, and has excellent mechanical properties, high abrasive resistance and good chemical resistance due to the precipitation of crystals like diopside [$CaMgSi_2O_6$], anorthite [$CaAl_2Si_2O_8$] and cordierite [$Mg_2Al_4Si_5O_{18}$]. CMAS ceramics have become good candidates for functional applications such as sealant for solid oxide fuel cells, architectural applications such as building materials for interior and exterior walls, and heavy industrial applications such as protective materials for bunker, funnel and chute. As well known, the crystallization of CMAS glass–ceramics is very difficult, and also hard to control, which largely restricts the preparation and application of CMAS glass–ceramics. Sintering process and body crystallization process are two main preparation methods of CMAS glass–ceramics. Sintering process is derived from the sintering of fine ceramics, consisting of glass melting, water quenching, particle molding and high-temperature sintering, while body crystallization process is similar to the production procedures of plate glass, including glass melting, molding, annealing, nucleation and crystallization. In comparison with body crystallization process, it is relatively easy to control the crystallization of CMAS glass, but it is too difficult to obtain the fully dense glass–ceramics, for sintering process. Recently improving the crystallization of CMAS glass by adding nucleation agent has received considerable attentions. However, the present researches mainly focus on the crystallization of CMAS glass–ceramics prepared by sintering process (Yang et al,2014)

Controlled bulk crystallization is the method most frequently used for producing glass-ceramics through controlled crystallization. The study of the CMAS system was also important for understanding the reactions taking place in rocks, blast furnace slags and MgO refractories. In most cases, published phase diagrams are related to equilibrium conditions that are not usually encountered in glass-ceramic preparations. Therefore, it is necessary to determine

the relationship between the compositions of glass-ceramics and the crystal phases developed under conditions in which such polycrystalline materials were actually produced. In a previous paper Khater (2006) managed to obtain a glass-ceramic material based on by-pass silica sand and magnesite. From cement kiln dust which made up about 57 wt.% of the batch constituents depending on the composition. Cement kiln dust is generated in the cement kiln and associated equipment. Dust from the raw mix and the surroundings of the plant is normally suppressed with closed systems and through water sprays. During the burning process, the gas flows entrain a substantial quantity of dust that forms part of the kiln exit gasses. The production of cement kiln dust strongly depends upon the chemistry of raw materials, type of process and the design of gas velocities in the kiln. Other factors such as kiln performance and dust collection systems also play vital roles in kiln dust generation. The production of alkaline-earth aluminosilicate glasses in the system CMAS has been broadly investigated in the past decade. Crystalline phases such as cordierite, diopside, wollastonite, mullite, etc., have been precipitated from glasses under controlled conditions resulting in glass-ceramics with attractive dielectric properties and high mechanical and chemical resistance (Khater, 2010).

The CMAS ceramic system has attracted much attention due to its low densification temperature, low thermal expansion coefficient (TCE < 5.10^6 /1C), low dielectric constant ($\varepsilon r<10$) and better chemical durability. To facilitate CMAS glass crystallization different nucleating agents, such as TiO_2, CaF_2, and ZrO_2 have been used. It is well known that the flexural strength and fracture toughness can be improved by precipitating nano-size tetragonal ZrO_2 particles into the bulk glass. However, the pure glass easily bloats or softens during firing, leading to distortion of the components and requires the addition of ceramic fillers (such as alumina, cordierite, and rutile etc.) to eliminate softening at 800–900°C (Wang et al, 2014). Hanning et al (2006) explained that the glass compositions, the kind and content of nucleating agent and the schedule of heat-treatment, all greatly affect the microstructure and properties of glass–ceramics. In this work, sintering behaviors and microstructural properties of CMAS ceramics in the presence of the ZrO_2 nucleation agent was investigated.

Experimental procedures

Kaolin, dolomite, and zirconia were used as starting materials for preparations of CMAS based ceramics. ZrO_2 was added as a nucleation agent after the heat treatment schedule was determined, in attempt to promote the crystallization and improve performance of ceramics. The method of preparation of CMAS ceramics in present study is illustrated in Fig. 1. As shown in Figure the calculated amounts of the starting oxides for the indicated compositions were ball milled for 3 h using distilled water as the milling media and dried than sintering different temperature and times. Table 1 presents the chemical analyses of the raw materials, and Table 2 presents the chemical composition of the two CMAS ceramics. ZrO_2 was added into the CMAS-D ceramics compositon for preparations of CMAS-DZ coded ceramics.

Scanning electron microscopy (SEM, Jeol 6060LV) and energy-dispersive X-ray spectroscopy (EDS) were used to characterization of produced CMAS ceramics microstructure. X-ray diffraction (XRD) analysis was performed with RIGAKU D/Max/2200/PC to determine the crystalline phases occured in the produced CMAS ceramics. The volume density was measured by Archimedes method. The Vickers hardness (H_V) of the samples were measured using a microhardness tester (LEICA VMHT MOT) with a 100 g load, its load time was 15 s along the whole cross-section. Chemical durability of CMAS ceramic specimens was analyzed by measuring weight loss after chemical attacked at 2h later in 10% NaOH solutions at 100ºC.

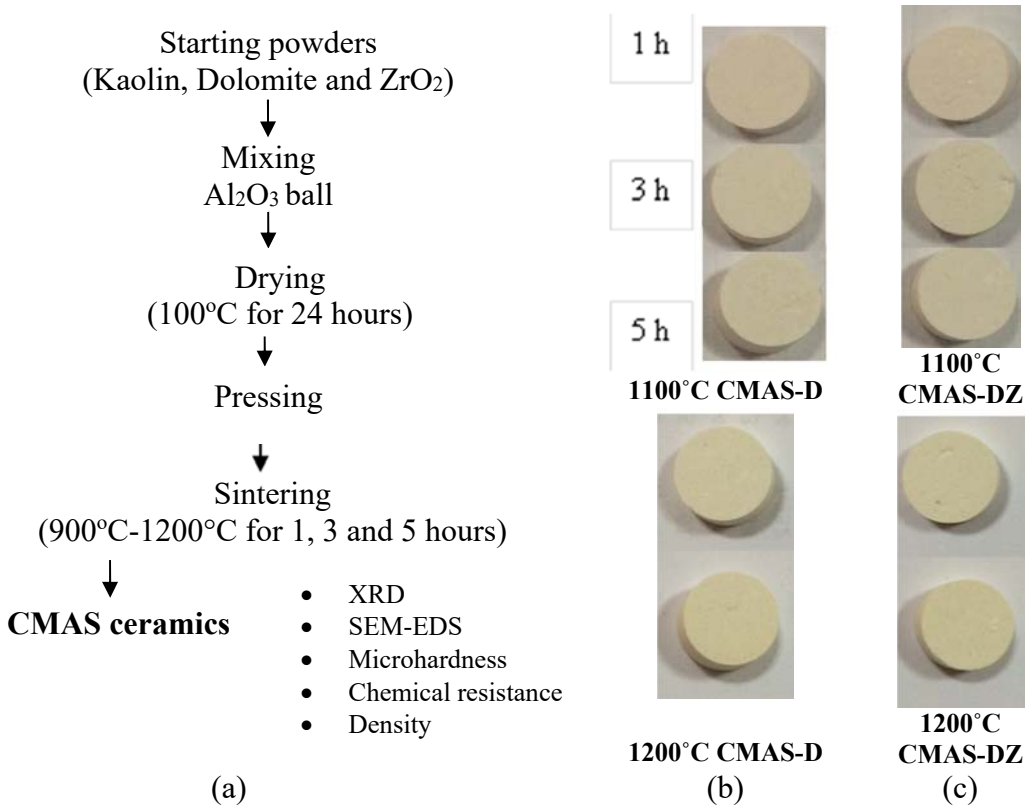

Figure 1. (a) Flow chart for the CMAS ceramics production, (b) and (c) macro structure of CMAS-D and CMAS-DZ coded ceramics

Table 1. Chemical analysis of the used raw materials (wt.%)

Raw Materials	CaO	MgO	Al_2O_3	SiO_2	H_2O	ZrO_2
Dolomite	50	50	-	-	-	-
Kaolin	-	-	39.5	46.54	13.96	-
Zirconia	-	-	-	-	-	100

Table 2. Chemical composition of the investigated CMAS ceramics (wt.%)

Composition (wt. %)	SiO_2	Al_2O_3	CaO and MgO	ZrO_2
	Kaolin		Dolomite	
CMAS-D	64		36	-
CMAS-DZ	64		36	5

Results and discussion

Fig. 2 shows the SEM micrographs of two coded ceramic samples crystallized at 1100 °C to 1200° C for 1 and 3 hours. It can be seen that the complex nucleation agents have an important role on the shape of crystals. With the addition of ZrO_2 (CMAS-DZ sample), the crystals irregularly arrange with sheet shape and low crystallinity (Khater, 2010). According to the SEM image of CMAS, a large number of granular crystals and a small quantity of lamellar shape crystal were distributed in the glass matrix after treated at 1100°C. S. Banijamali et al. (2009) explained that sintered CMAS ceramics reveals a coarser microstructure in which the needle-like crystals have been extended from the surface toward the center of glass particles. This behavior has led to the crack-like defects in the middle of particles.

In Fig. 3, the columnar and small granular crystalline phases were distributed in CMAS specimen after crystallization at 1100 °C. It is well known diopside is a columnar crystal in ceramics. Furthermore, the EDS microanalyses were carried out on different areas of CMAS specimens. The magnesium content of 1 coded area is higher than other areas. The aluminium and oxygen content of 4 and 5 areas is apparently higher than 1, 2 and 3 coded areas, which showed that the columnar crystalline phases were diopside. The addition of zirconia which can enhance the heterogeneous nucleation of phases, and limit the growth of long anisotropic anorthite grains which will result in new voids where equiaxed grains are originally located.

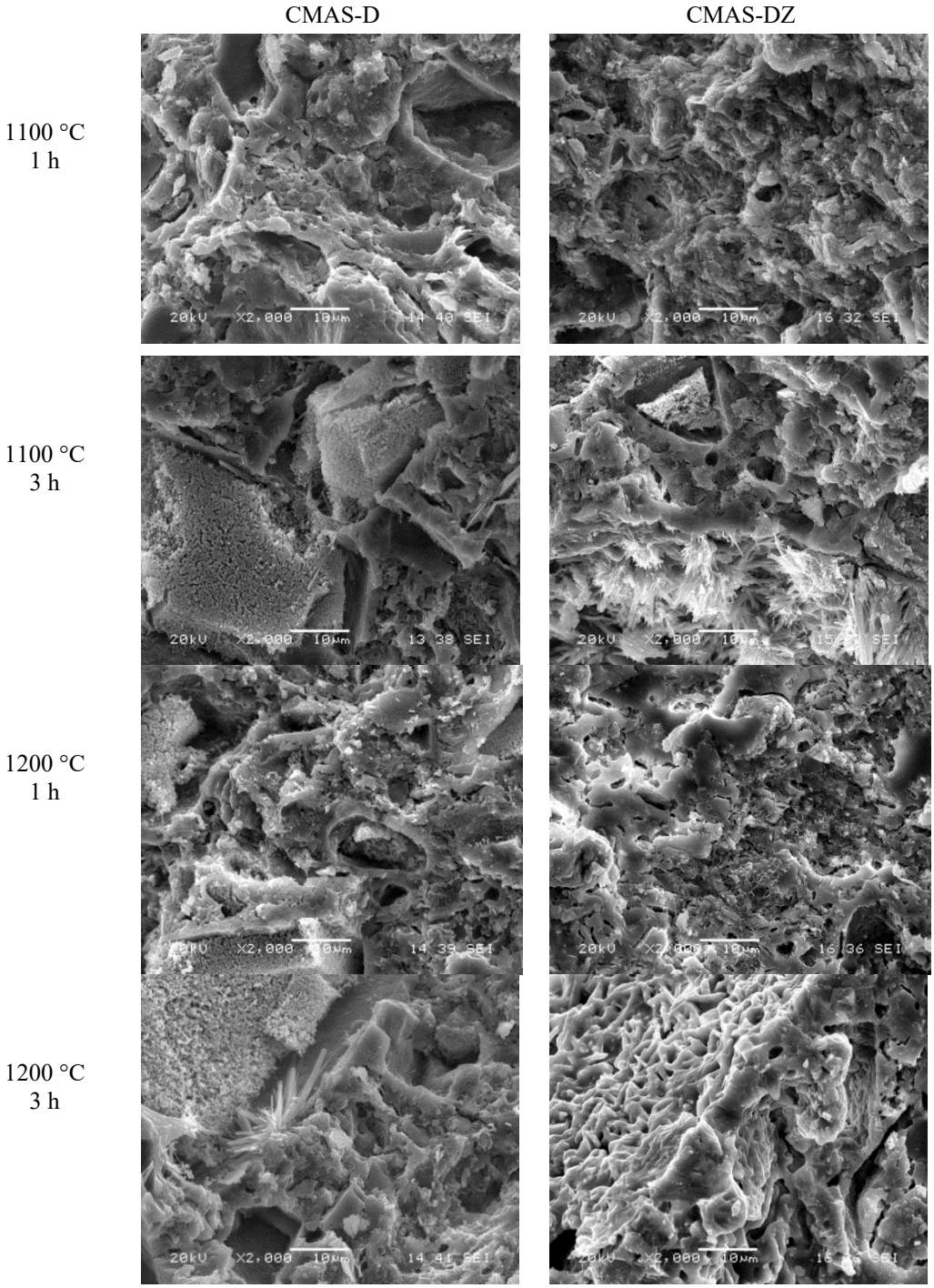

Figure 2. SEM images of the CMAS-D and DZ coded samples in the sintering of 1100 °C to 1200 °C for 1 and 3 hours

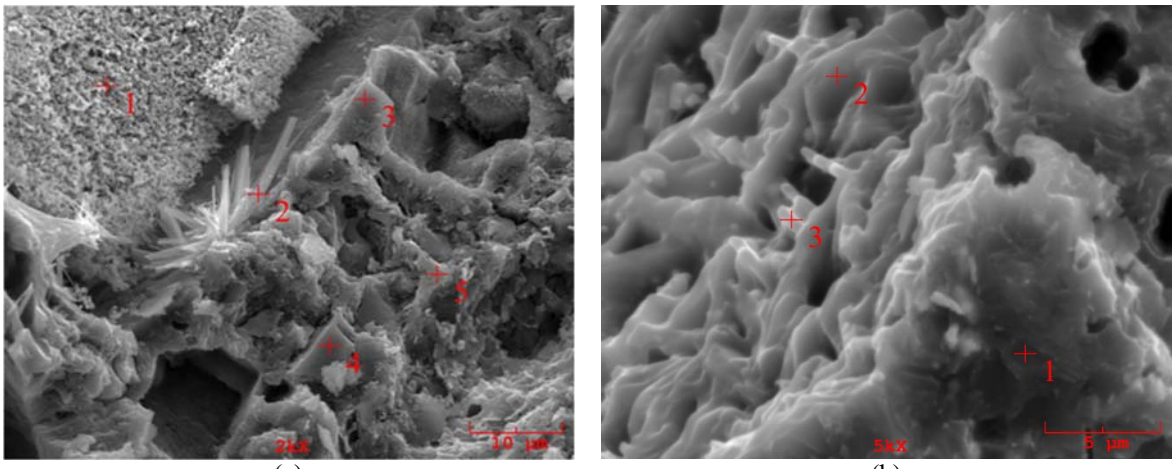

(a) (b)

Elementler	Miktar (%)				
	1	2	3	4	5
O	36.893	48.117	40.688	42.623	44.007
Mg	60.474	6.927	4.660	1.041	1.194
Al	0.704	12.893	14.711	25.653	21.825
Si	1.493	10.829	17.436	29.334	32.024
Ca	0.436	21.234	22.505	1.349	0.950

(c)

Elementler	Miktar(%)		
	1	2	3
O	28.393	30.556	43.716
Mg	0.728	1.729	3.251
Al	23.232	12.992	15.095
Si	27.582	20.047	19.157
Ca	17.194	32.147	14.937
Zr	2.871	2.530	3.844

(d)

Figure 3. SEM-EDS analysis of (a), (c) CMAS-D and (b), (d) CMAS-DZ samples sintered at 1200°C for 3h

Fig. 4 shows XRD patterns of the CMAS-D and CMAS-DZ coded samples crystallized at 900°C, 1000°C, 1100°C and 1200°C for 3 h. It can be seen that the CMAS-D, and CMAS-DZ samples have the same main crystalline phases, such as diopside and anorthite, their frequency depending largely on the base composition and crystallization parameters. It can be noticed that, with increasing the ZrO_2 content, the intensity of diopside becomes stronger gradually. In the Khater's (2014) X-ray diffraction showed that monoclinic or triclinic wollastonite ($CaSiO_3$), diopside ($CaMgSi_2O_6$) and anorthite ($CaAl_2Si_2O_8$) were the main crystalline phases developed in the CMAS ceramics.

CMAS-DZ ceramics exhibited slightly higher relative density and less porosity than CMAS-D ceramics, which is consistent with the results of Table 3. The corrosion resistance of CMAS ceramics is evaluated from the weight losses after leaching in alkali solution. The results are given in Table 3. Samples weight loss values for CMAS-D ceramics change between the ranges of 2.12 % to 3.73 % and for CMAS-DZ ceramics change between the ranges of 2.02% to 2.98%. It can be seen that, in general, the durability of CMAS ceramic is increased depend on crystallization temperature and adding ZrO_2 nucleating agent.

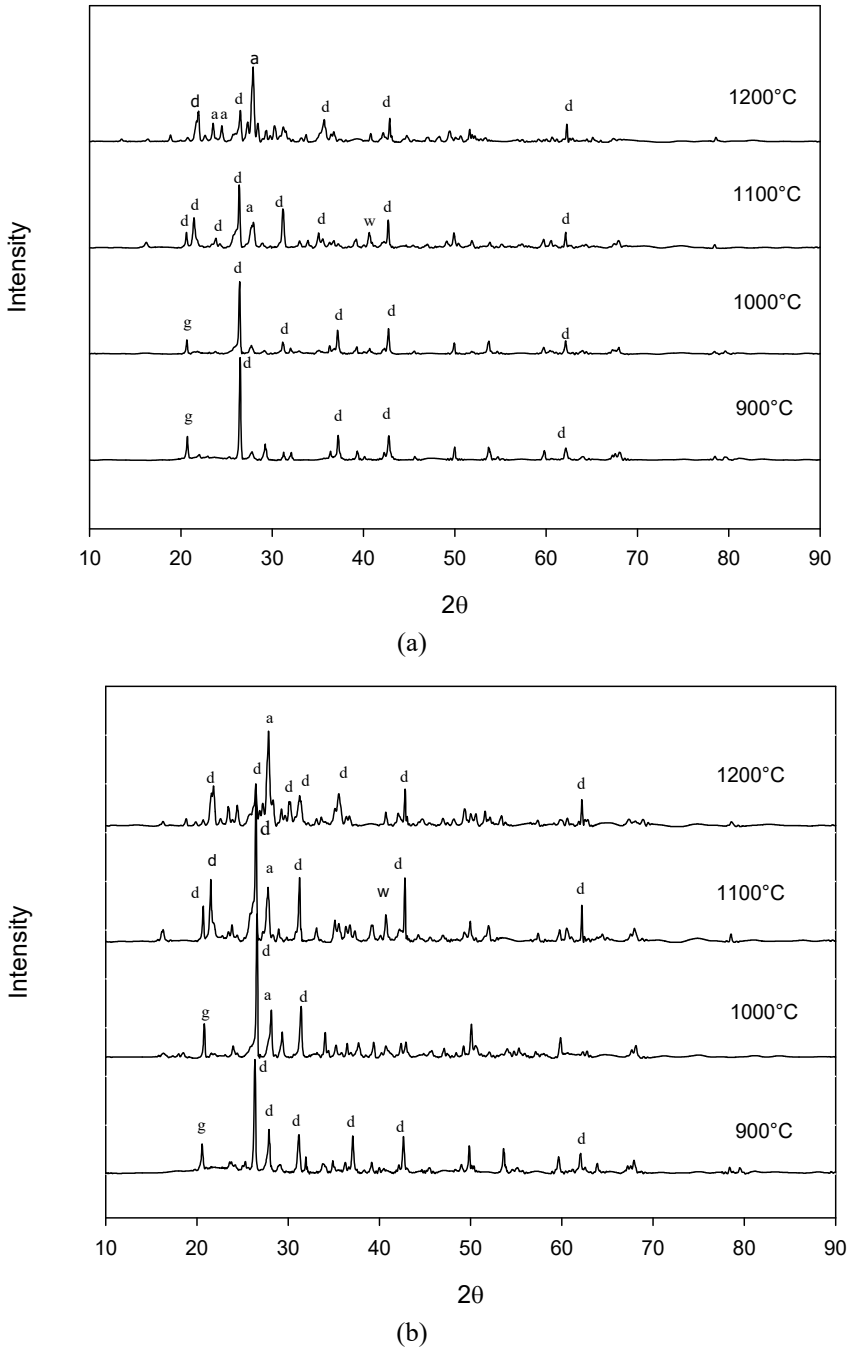

Figure 4. (a) XRD patterns of the CMAS-D and (b) CMAS-DZ samples crystallized at 900°C, 1000°C, 1100°C and 1200°C for 3 h (a:anorthite, d: diopsite, w: wollastonite, g:gehlenite)

Indentation microhardness measured for the obtained CMAS ceramic materials (Table 3) was found to lie in the range 522–844 HV, indicating high abrasion resistance of these materials and making them suitable for many applications under aggressive mechanical conditions. Samples hardness values for CMAS-D ceramics change between 522 HV to 787 HV and for CMAS-DZ ceramics change between 612 HV to 844 HV. The hardness of the samples drops from a value of about HV=844 for CMAS-DZ to about HV=522 for CMAS-D. Vickers hardness of CMAS ceramics were observed to increase with addition of ZrO_2. Average value of HV for the desert sand glass was found to be 6.37 GPa. This value of Vickers microhardness for desert sand glass falls is smaller than in this study results (Choi et al., 2015).

S. Banijamali et al. (2009) chose raw materials from commercial grade calcium carbonate, corundum, silicon oxide, titanium oxide, zirconium oxide and calcium fluoride. The homogenized mixture of raw materials was transferred to a zircon crucible and melted at 1450 °C for 1 h in an electric furnace. The melts were water quenched and the obtained frits were dried and milled to the required particle sizes (<75μm). According to the obtained results, in spite of less crystallization in SZ6 (ZrO_2 containing specimens), this sample shows the highest Vickers hardness and improved chemical resistance rather than fluorine containing specimens.

Tablo 3. Various properties of the CMAS-D and CMAS-DZ ceramics

Sample name	Sintering temperature (°C)	Time (h)	Density (g/cm^3)	Hardness (HV)	Mass loss in NaOH (wt.%)
CMAS-D	1000	1	1.70	522	3.73
		3	-	532	-
		5	1.72	568	-
	1100	1	1.72	570	2.65
		3	1.73	582	-
		5	1.77	612	2.35
	1200	1	1.84	747	2.31
		3	1.92	787	2.12
CMAS-DZ	1000	1	-	612	2.98
		3	1.805	634	-
		5	1.825	673	-
	1100	1	1.845	705	2.5
		3	1.88	736	-
		5	1.95	765	2.33
	1200	1	1.97	827	2.27
		3	1.99	844	2.02

Marques et al. (2010) reported that, the glass-ceramics based on diopside, with excellent mechanical properties, high abrasive resistance and good chemical resistance, were good candidates for decorative materials in construction field.

Conclusions

In the present work, the reported results show that dolomite, kaoline and zirconia can be used to develop a new ceramic of CMAS system. For sintering temperature lower than 1100°C, the CMAS specimen were digested. Diopside and anorthite were found as major crystalline phases. With the raise of sintering temperature, the crystal shape changed from spherical to needle and the crystal size became much larger. Vickers hardness of CMAS ceramics were observed to increase with the addition of ZrO_2.

References

Khater, G.A. (2010) Journal of Non-Crystalline Solids 356 (2010) 3066–3070.

Qing-chun YU, Chun-pei YAN, Yong DENG, Yue-bin FENG, Da-chun LIU, Bin YANG, (2015) Trans. Nonferrous Met. Soc. China 25, 2279-2284

Xingzhong Guo, Xiaobo Cai, Jie Song, Guangyue Yang, Hui Yang, (2014) Journal of Non-Crystalline Solids, 405 63–67

Khater, G.A. (2006) Advances in Applied Ceramics, 105-107.

Hsing-I Hsianga, Shi-Wen Yung, Chung-Ching Wang, (2014Ceramics International 40, 15807–15813.

Hanning Xiao, Yin Cheng, Liping Yu, Huabin Liu, (2006), Materials Science and Engineering, A 431, 191–195.

Narottam P. Bansal, Sung R. Choi, (2015) Ceramics International,41, 3901–3909.

S. Banijamali, B. Eftekhari Yekta, H. R. Rezaie, V. K. Marghussian, (2009) Thermochimica Acta, 488, 60–65.

Marques V M F, Tulyaganov D U, Agathopoulos S, Ferrira J M F., (2008). Ceramics International, 27: 661-668,

COMPARISON OF DIFFERENT TEMPORAL DATA WAREHOUSES APPROACHES

Georgia GARANI
Technological Educational Institute of Larisa, Department of Computer Science and Engineering, Greece
garani@teilar.gr

Canan Eren ATAY
Dokuz Eylul University, Department of Computer Engineering, Izmir, Turkey
canan@cs.deu.edu.tr

Abstract: Data warehouses are mainly used for business data analysis by querying and reporting huge collections of data. For the management of historical data, temporal data warehouses have been developed. Two current approaches for dealing with temporal data in data warehouses are compared in this paper, Object-Relational Temporal Data Warehouse (O-RTDW) model and Starnest Temporal Data Warehouse (S-TDW) model. The O-RTDW model enables data values to be associated with facts, and specifies when facts are valid, thereby providing a complete history of the data values and their changes. To accurately and completely store all data changes, the valid time should be kept at the attribute level. On the other hand, the S-TDW model uses the starnest schema for the modeling of time-varying data in dimensions. The temporal starnest schema expresses naturally hierarchy levels by the clustering of data in nested tables, with result the description of aggregation levels for a dimension in a natural way. By comparing these two temporal data warehouses models, object-oriented and nesting approaches are also compared and evaluated.

Keywords: Data Warehouse, Temporal Data Warehouse, Object-Relational Model, Starnest Schema

Introduction

Data warehouses play a critical part in the success of businesses. Decision support systems, data mining, business analysis, forecasting and product line analysis are all good examples of where data warehouses can be used.

Two IBM researchers, Barry Devlin and Paul Murphy, introduced the term 'Business Data Warehouse' in 1988 (Devlin and Murphy, 1988). It was described as a 'single logical storehouse of all the information used to report on the business'. In 1990, Ralph Kimball introduced Red Brick Warehouse, a database management system specifically for data warehousing. In the following year, 1991, a software for developing a data warehouse was built by Bill Inmon, the Prism Warehouse Manager.

Since then, a data warehouse (DW) is considered to be the main component of every business intelligence environment. It is mainly used for business data analysis by querying and reporting huge collections of data. Data in a DW must be stored in a way that is secure, reliable, easy to retrieve and to manage.

According to Bill Inmon (Inmon, 2002) a DW is "a collection of subject-oriented, integrated, non-volatile and time-variant data to support management's decisions". The non-volatile and time-variant data features of data warehousing suggest that it should allow changes to the data values without overwriting the existing values.

The main characteristics of a DW are given briefly below: A DW stores current and historical data. Stored data cannot change. Insertions, deletions and updates do not take place in a DW. Data is used only for querying and consequently, it is essential that querying performance is as high as possible.

For the management of historical data, temporal DWs have been developed. Temporal DWs use the knowledge obtained from temporal databases for the treatment of time domain. Temporal databases have built-in support for representing and managing information varying over time. They are divided in three categories, valid time databases, transaction time databases and bitemporal databases according to the type of time they support, valid time, transaction time or both respectively. Valid-time expresses the time when a fact is true in the real world and transaction-time represents the time when a fact is current in the database.

Time can be added at the tuple level in a relation and this relation is called tuple timestamping relation or at the attribute level, called attribute timestamping relation, when individual time varying attributes are timestamped. SQL has also been extended to support features introduced in temporal databases.

In this paper, two temporal DWs models are evaluated and compared, the Object-Relational Temporal Data Warehouse (O-RTDW) model and the Starnest Temporal Data Warehouse (S-TDW) model.

The O-RTDW model uses the object-relational approach for the representation of time-varying data. This model inherently groups related facts into a single row, hence allowing changes to the data value and timestamps to be kept together. Dimensions may have levels. Multivalued attributes of data type T_ATOM are used for temporal

support of a level attribute. The levels and dimensions can have many time-varying attributes stored as nested tables.
The S-TDW model uses the starnest schema for storing dimension's hierarchy. The starnest schema proposed in Garani and Helmer (2012) is based on the nested approach, where hierarchies are represented as nested tables. The starnest schema is extended in Garani, Adam and Ventzas (2016) to support time. In the temporal starnest schema every temporal dimension, i.e., dimension table dependent on time, contains time attributes for the support of time. Several queries expressed in SQL are implemented and executed using Oracle 11g in both approaches. Same data and queries are used. Execution time and result data are compared and useful results are obtained.
The remainder of the paper is structured as follows. Firstly, related research work is discussed. Afterwards, the two temporal DW models, O-RTDW model and S-TDW model are presented. The hospital's admission temporal DW case study is described in both models. Implementation issues are discussed and finally, last section concludes the paper.

Related Work

Temporal DWs have been the subject of research in recent years. In what follows, a brief description of research studies on this field is presented.
The term 'slowly changing dimensions' was introduced by Kimball (Kimball, 1996). It was used for storing slowly changing historical data. Three different techniques for dealing with attributes changing over time were proposed, either by overwriting the value, adding a dimension row, or adding a dimension column as well as a number of hybrid methods. In this research work, schema evolution and dimension updates have not been generally considered.
In Bliujute et. al. (1998) the temporal star schema proposed does not include a time dimension. Instead, every row appeared either in fact or dimension tables is timestamped which causes the increase of redundancy.
A bitemporal DW model proposed in Koncilia (2003) is an extended version of the COMET metamodel (Eder, Koncilia & Morzy, 2002). It supports valid time and transaction time both at instance and schema levels. The model allows all possible changes of schema and structure of a DW with the introduction of suitable transformation functions.
Malinowski and Zimanyi (2006) extended the conceptual multidimensional MultiDimER model for supporting valid time and transaction time. The model is suitable for representing time-varying levels, attributes and hierarchies. It distinguishes time variant elements from time invariant elements and treats them separately. The proposed model also supports DW loading time.
The bitemporal versioning of multidimensional schemas is used for defined the conceptual evolution DW model in Rechy-Ramírez and Edgard (2006). The model supports many versions with the same valid time and different transaction times. Sixteen schema evolution operators are defined for dimensions and cubes and a SQL-like language for the proposed model is also presented.
A review of issues associated to temporal data warehousing is presented in Golfarelli and Rizzi (2009). Three different topics are distinguished, handling changes in the DW, handling data changes in the data mart and handling schema changes in the data mart.
A graph based temporal semi-structured DW is presented in Combi, Oliboni & Pozzi (2009) and an appropriate query language for the modeling and querying of temporal data.
A multiversion DW management system called SysVersDW is defined in Turki, Jedidi & Bouaziz (2010). Versioning of schema and instance components is supported in the model. A number of integrity constraints are also included for data and structure consistency. The constraints presented are classified in three classes, structural constraints, temporal constraints and versioning constraints.
A new schema proposed in Garani and Helmer (2012), the starnest schema, is based on the nested approach. It is extended in (Garani, Adam, and Ventzas, 2014) for supporting time. The key component of the temporal starnest schema is the inclusion of time attributes in every dimension table depended on time.
A bitemporal DW model where both valid time and transaction time are attached to attributes is introduced by Atay and Alp in (Atay and Alp, 2016). DW objects and cubes are created with multidimensional bitemporal relational database.

Temporal Data Warehouse Models

For the management of historical data, temporal DWs have been developed for describing information changing over time. Two of the most recent proposed approaches are discussed and compared in this research work, O-RTDW and S-TDW models.

Object-Relational Temporal Data Warehouse (O-RTDW) model

The O-RTDW model uses the specifications provided by the Object-Relational model. It consists of a fact table and several dimension tables connected to it. A dimension is composed of one or more levels, whereas each level belongs to only one dimension. O-RTDW enables data values to be associated with facts and specifies when facts

were valid, thereby providing a complete history of data values and their changes. To accurately and completely store all data changes, the valid time should be kept at the attribute level. Attributes can be temporal or non-temporal. Temporal attributes consist of temporal atoms (T-ATOM). A temporal atom is defined as <valid time, value> where valid time component can be applied as a time point, a time interval, or a temporal element. Therefore, a temporal atom in the form of <[VT_{lb}, VT_{ub}), V> represents valid time lower bound as VT_{lb}, valid time upper bound as VT_{ub} and data value as V, respectively. In Figure 1 the conceptual model for the O-RTDW model is shown.

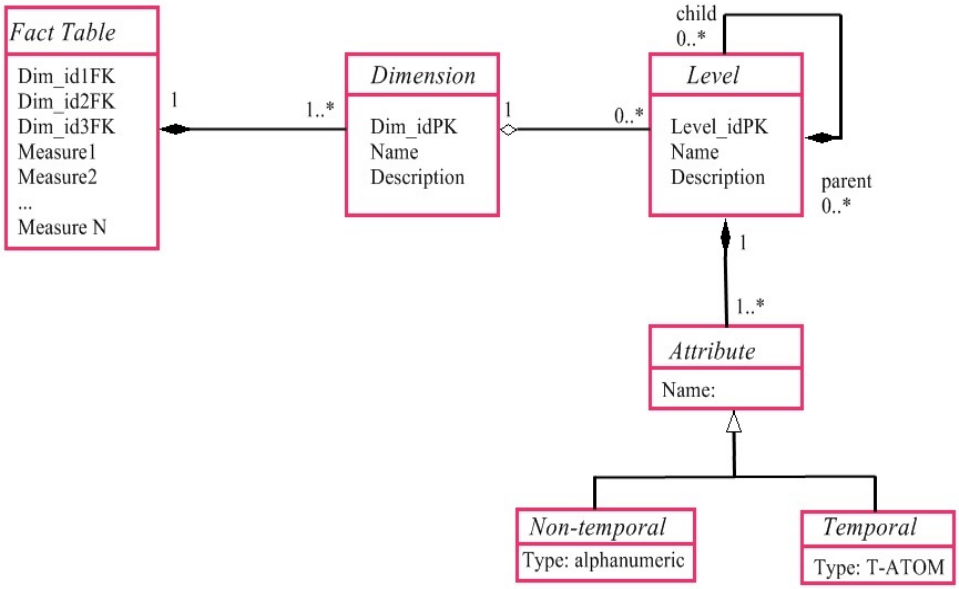

Figure 1. The conceptual model for the O-RTDW

Starnest Temporal Data Warehouse (S-TDW) model

S-TDW model uses the temporal starnest schema (Garani, Adam and Ventzas, 2014) for the modeling of time-varying data in dimensions. The starnest schema forms the integration of the star and snowflake schemas (Garani and Helmer, 2012). It expresses naturally hierarchy levels by the clustering of data in nested tables, with result the description of aggregation levels for a dimension in a natural way. It consists of a temporal fact table and a number of dimension tables. A temporal fact table can be timestamped by adding one or two time attributes representing a time point or a time interval respectively.

Dimension tables can also be timestamped similarly. Timestamped dimension tables are called temporal dimension tables. Temporal dimension tables are nested, since time attributes are inserted in a dimension in a nested way, where more detailed attributes are nested inside less detailed attributes. Therefore, dimension tables are not normalized. In each temporal dimension two valid time attributes are included, the start and stop time points of the corresponding time interval.

The fact table is linked to dimension tables with one to many relationships by foreign key attributes with a reference to the most detailed hierarchical attribute of each dimension. The conceptual model for the S-TDW model is shown in Figure 2.

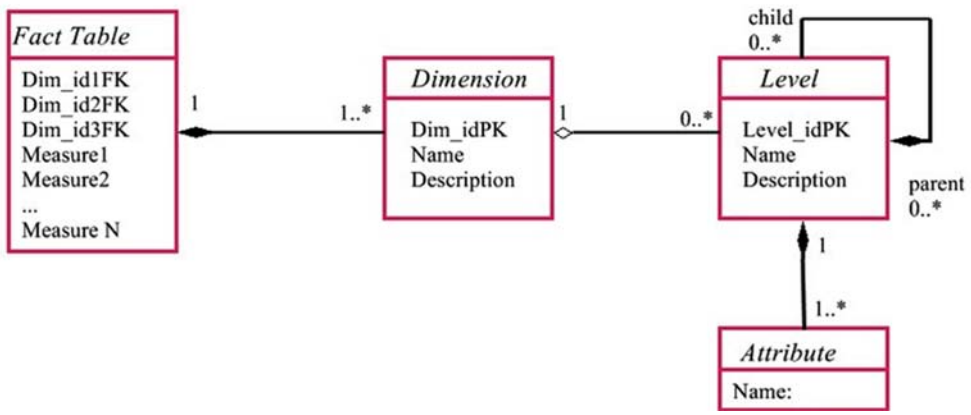

Figure 2. The conceptual model for the S-TDW

The main differences between O-RTDW and S-TDW models are presented in Table 1.

Table 1: The main differences between O-RTDW and S-TDW models

O-RTDW model	S-TDW model
Snowflake schema	Starnest schema
Object-Oriented approach	Nested approach
Temporal atom	Time attribute
Time interval	Time point (Start/Stop)

The Hospital's Admission Temporal Data Warehouse Case Study

A hospital's admission temporal DW has been used for the comparison of O-RTDW and S-TDW models. The hospital's admission temporal DW concerns the admission in the hospital of patients who suffer from different diseases and therefore, have different diagnoses and treatments.

In Figure 3 the schema of the O-RTDW model is shown. The schema is represented in snowflake format where dimension tables are split up into smaller normalized tables that express each dimension's hierarchy. Transitive functional dependencies do not exist.

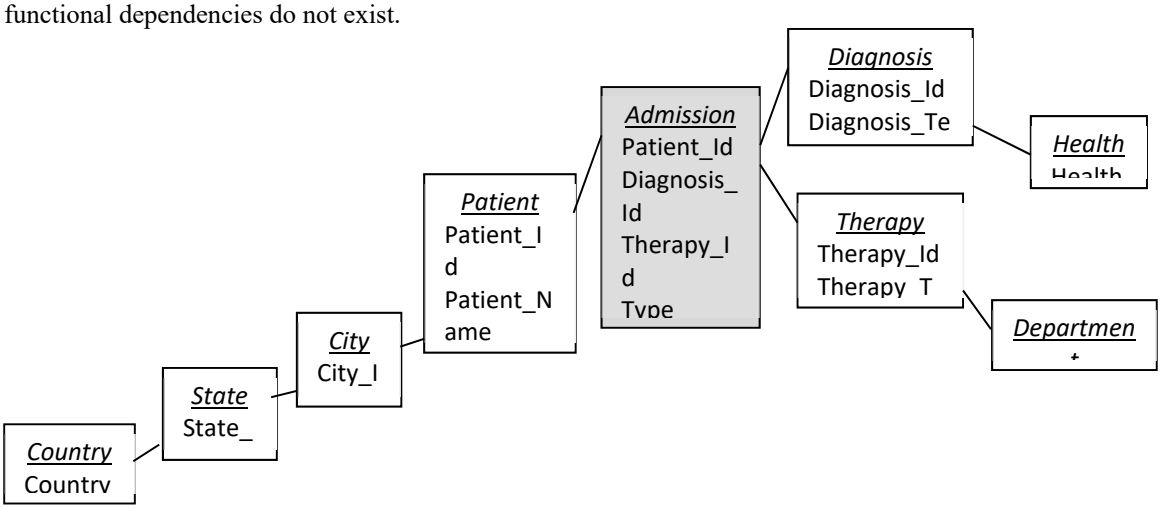

Figure 3. The schema for the O-RTDW model

Figure 4 presents the schema for the S-TDW model of the hospital's admission temporal DW. S-TDW model uses the starnest schema at the logical design. In the starnest schema a dimension's hierarchy is expressed as a nested table where hierarchy levels are expressed naturally and attributes can easily be associated within their corresponding levels. Each dimension table has a hierarchical attribute which is referred to a foreign key attribute of the fact table. The above mentioned hierarchical attribute is located in the most nested level of the dimension table.

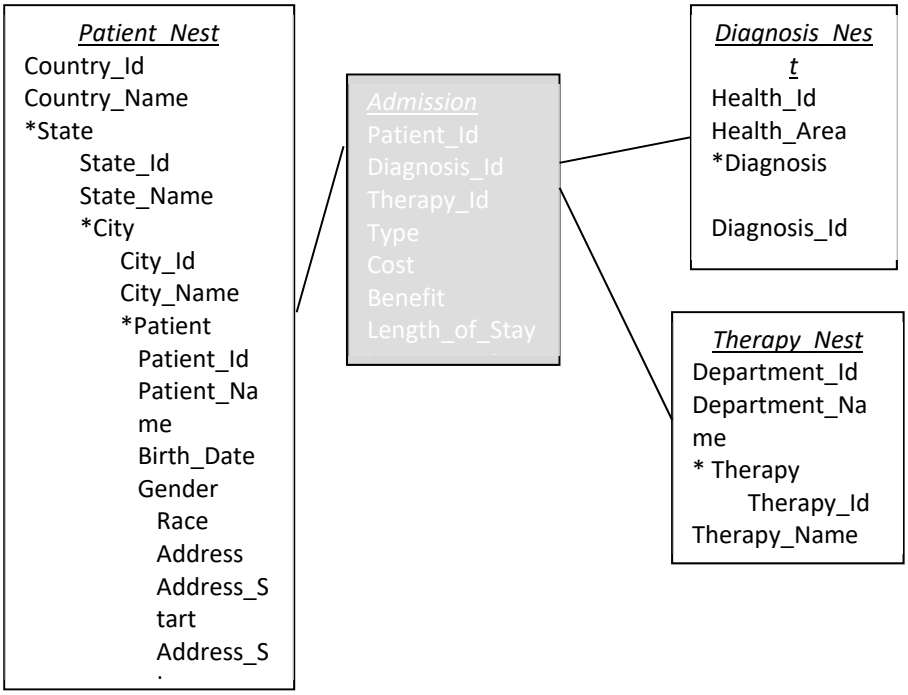

Figure 4. The schema for the S-TDW model

Figure 5 shows an instance of Patient dimension in the O-RTDW model. Address_Temporal attribute, as its name denotes, is temporal. It contains temporal atoms of the form <[VT_{lb}, VT_{ub}), V> where VT_{ub} can be either a time point representing the valid time upper bound of the corresponding time interval or 'now' denoting present time instant which increases as time advances.

PatientID	FirstName	LastName	BirthDate	Gender	Race	
101	JACKY	WANDA	03.03.1980	F	White	
102	TOM	BROWN	01.30.1989	M	White	
103	BILL	LAWRENCE	04.25.1977	F	Asian	
104	AMY	ANGEL	10.05.1985	F	Black	

Race	Address_Temporal	CityID
	< [01.30.1955, now], "625 13th Avenue">	45
	{< [03.03.1980, 06.06.2005), "55 Hamilton Avenue">, < [06.06.2005, 01.01.2008), "7 Leona Street">, < [01.01.2008, now], "96 Market Street">}	11
	< [01.30.1955, now], "111 Madison Avenue" >	18
	{<[04.25.1977, 11.12.2000), "5 Valley Road">, < [11.12.2000, now], "6255 Broadway">}	01

Figure 5. An instance of Patient dimension in the O-RTDW model

An instance of Patient dimension in the S-TDW model is presented in Figure 6. Patient dimension is a temporal dimension table since it is dependent on time. It is also nested since hierarchies in dimensions are presented as nested tables. Therefore, a temporal nested dimension table consists of hierarchical attributes, dimensional attributes and time attributes which can also be nested inside less detailed attributes. In Patient dimension *AddressDetails is a temporal nested attribute consisting of three attributes, one atomic, Address and two time attributes, AddressStart and AddressStop indicating the start and stop points of the time interval during which the corresponding address is valid.

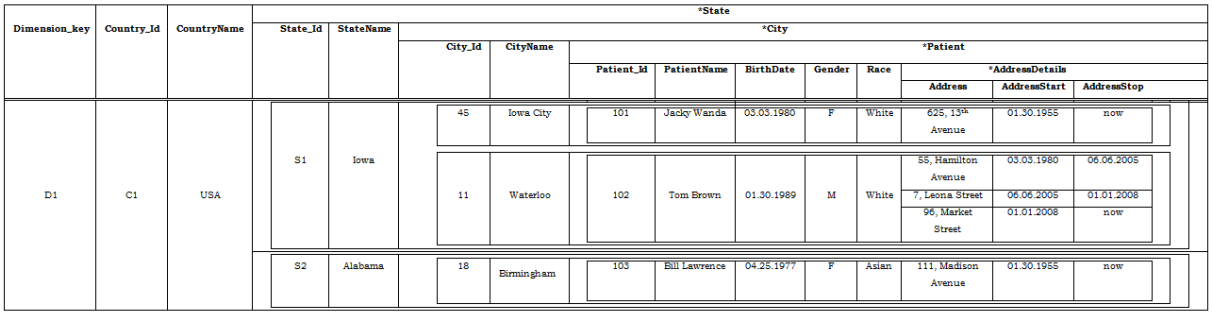

Dimension_key	Country_Id	CountryName	*State										
			State_Id	StateName	*City								
					City_Id	CityName	*Patient						
							Patient_Id	PatientName	BirthDate	Gender	Race	*AddressDetails	
												Address	AddressStart	AddressStop
D1	C1	USA	S1	Iowa	45	Iowa City	101	Jacky Wanda	03.03.1980	F	White	625, 13th Avenue	01.30.1955	now
					11	Waterloo	102	Tom Brown	01.30.1989	M	White	55, Hamilton Avenue	03.03.1980	06.06.2005
												7, Leona Street	06.06.2005	01.01.2008
												96, Market Street	01.01.2008	now
			S2	Alabama	18	Birmingham	103	Bill Lawrence	04.25.1977	F	Asian	111, Madison Avenue	01.30.1955	now

Figure 6. An instance of Patient dimension in the S-TDW model

Implementation

All queries have been executed on an Intel(R) Core(TM) i5 processor, running at 2.3 GHz, with 2.5 GB ram memory, under Windows 7 (32bit). The DW was built in Oracle Data Warehouse builder 11.2.0.1 and Oracle SQL Developer 4.0.3 was used.

The hospital's admission temporal DW consists of 9 tables in the O-RTDW model and 4 tables in the S-TDW model. Consequently, the number of joins in the O-RTDW model is much higher than in the S-TDW model. Relationship between a dimension and the number of tables it contains is one-to-one in the S-TDW model compared to one-to-many in the O-RTDW model. Tables in both models do not contain any data redundancy. Implementation of O-RTDW approach is platform independent in comparison to S-TDW approach which is platform dependent. The disk space required is more than three times higher in the O-RTDW approach than the S-TDW approach as it is shown in Table 2. In particular, the total space for the O-RTDW model is 14.3125 Mb in comparison to the S-TDW model where it is 4.1875 Mb.

Similarly, the number of rows is much higher in the O-RTDW approach than in the S-TDW model. Specifically, O-RTDW contains about 200,000 rows while S-TDW contains about 50,000 rows.

Table 2: O-RTDW model

Table name	Schema name	Size (Mb)	Number of rows
ADMISSION_O_CUBE_TAB	Admission	4.0	48,000
ADM_DEPARTMENTS	Department	0.0625	502
THERAPY_DIMENSION_O_TABLE	Therapy	3.0	50,200
ADM_HEALTH	Health	0.0625	501
DIAGNOSIS_DIMENSION_O_TABLE	Diagnosis	3.0	50,100
ADM_COUNTRIES	Country	0.0625	10
ADM_STATES	State	0.0625	100
ADM_CITIES	City	0.0625	1,000
PATIENT_DIMENSION_O_TABLE	Patient	4.0	50,000

Table 3: S-TDW model

Table name	Schema name	Size (Mb)	Number of rows
ADMISSION_N_CUBE_TAB	Admission_Nest	4.0	48,000
THERAPY_DIMENSION_TABLE	Therapy _Nest	0.0625	502
DIAGNOSIS_DIMENSION_TABLE	Diagnosis_Nest	0.0625	501
P_PATIENT_DIMENSION_TABLE	Patient_Nest	0.0625	10

Five different temporal and non-temporal queries are presented below in SQL. The same queries are expressed in both approaches and compared.

Query 1:
Which diagnoses have the same treatment? (non temporal)

O-RTDW model

```
SELECT Diagnosis1.Value AS Diagnosis1, Diagnosis2.Value AS Diagnosis2
FROM ADMISSION_O_CUBE_TAB A1, ADMISSION_O_CUBE_TAB A2,
DIAGNOSIS_DIMENSION_O_TABLE D1, DIAGNOSIS_DIMENSION_O_TABLE D2,
Table(D1.Diagnosis_Temporal) Diagnosis1,
Table(D2.Diagnosis_Temporal) Diagnosis2
WHERE D1.Diagnosis_Id < D2.Diagnosis_Id
```



```
AND A1.Therapy_Id = A2.Therapy_Id
AND D1.Diagnosis_Id = A1.Diagnosis_Id
AND D2.Diagnosis_Id = A2.Diagnosis_Id
```

S-TDW model

```
SELECT V1.DIAGNOSIS_NAME, V2.DIAGNOSIS_NAME
FROM ADMISSION_N_CUBE_TAB A1, ADMISSION_N_CUBE_TAB A2,
DIAGNOSIS_DIMENSION_TABLE D1, DIAGNOSIS_DIMENSION_TABLE D2,
Table(D1.Diagnosis) V1, Table(D2.Diagnosis) V2
WHERE V1.Diagnosis_Id < V2.Diagnosis_Id
AND A1.Therapy_Id = A2.Therapy_Id
AND V1.Diagnosis_Id = A1.Diagnosis_Id
AND V2.Diagnosis_Id = A2.Diagnosis_Id
```

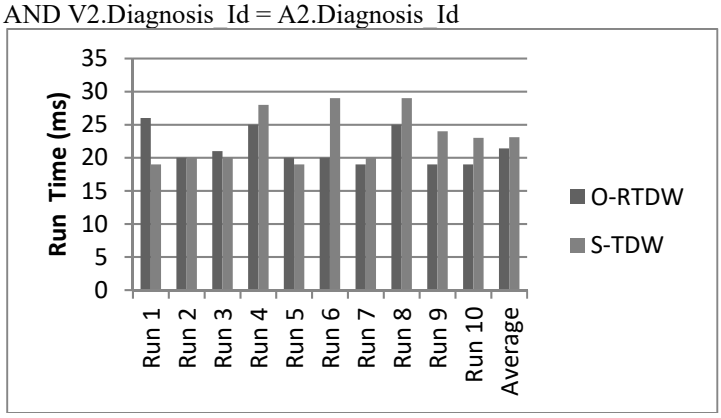

Figure 7. Query 1 run comparison chart

Query 2:
What is the average number of days for therapy in each department? (temporal)

O-RTDW model

```
SELECT Department_Id, AVG(Therapy.VALID_TIME_UB- Therapy.VALID_TIME_LB )
FROM THERAPY_DIMENSION_O_TABLE T, Table(T.Therapy_Temporal) THERAPY
GROUP BY Department_Id
```

S-TDW model

```
SELECT Department_Id, AVG( H.Therapy_Stop - H.Therapy_Start )
FROM Therapy_Dimension_Table T, Table(Therapy) H
GROUP BY Department_Id
```

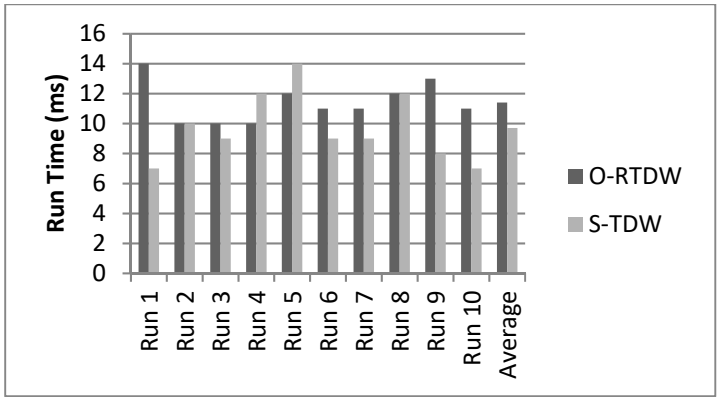

Figure 8. Query 2 run comparison chart

Query 3:
For each patient find the amount he/she paid for each admission and where he/she lived at that time. (temporal)

O-RTDW model

```
SELECT A.Patient_Id, A.Cost, ADDRESS1.Value
FROM ADMISSION_O_CUBE_TAB A, PATIENT_DIMENSION_O_TABLE P,
TABLE(P.Address_Temporal) ADDRESS1
WHERE ADDRESS1.VALID_TIME_LB <= A.Admission_Time
AND ADDRESS1.VALID_TIME_UB >= A.Admission_Time
AND A.Patient_Id = P.Patient_Id
ORDER BY A.Patient_Id
```

S-TDW model

```
SELECT A.Patient_Id, A.Cost, F.Address
FROM P_PATIENT_DIMENSION_TABLE P, ADMISSION_N_CUBE_TAB A,
Table(P.State) S, Table(S.City) C, Table(C.Patient) F
WHERE F.Address_Start <= A.Admission_Time
AND F.Address_Stop >= A.Admission_Time
AND F.Patient_Id = A.Patient_Id
ORDER BY A.Patient_Id
```

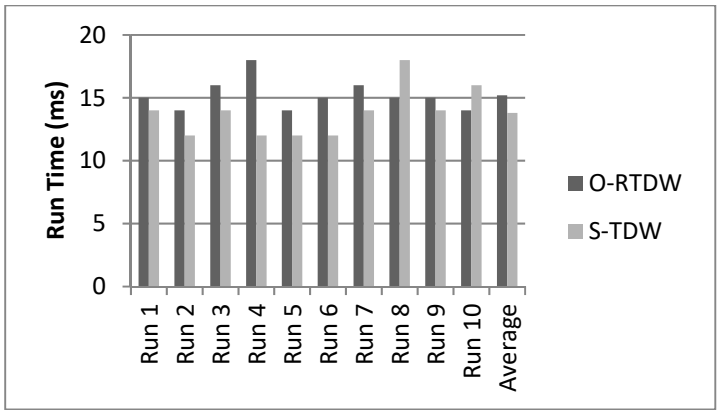

Figure 9. Query 3 run comparison chart

Query 4:
Which patients had cancer at New York in 2013? (temporal)

O-RTDW model

```
SELECT P.Patient_Name
FROM DIAGNOSIS_DIMENSION_O_TABLE D, ADMISSION_O_CUBE_TAB A,
Patient_Dimension_o_table P, ADM_CITIES C, TABLE(D.Diagnosis_Temporal) DIAGNOSIS1
WHERE D.description_d LIKE '%Cancer%'
AND A.Diagnosis_Id= D.Diagnosis_Id
AND A.Patient_Id=P.Patient_Id
AND C.City_Id=P.City_Id
AND   C.City_Name='New York'
AND ( EXTRACT(YEAR FROM DIAGNOSIS1.VALID_TIME_UB) = 2013
      OR EXTRACT(YEAR FROM DIAGNOSIS1.VALID_TIME_LB) = 2013 )
```

S-TDW model

```
SELECT F.Patient_Name
FROM   DIAGNOSIS_DIMENSION_TABLE D, ADMISSION_N_CUBE_TAB A,
P_PATIENT_DIMENSION_TABLE P, table(Diagnosis)   V, table(State) S, table(S.City) C,   table(C.Patient) F
WHERE V.description_d LIKE '%Cancer%'
AND V.Diagnosis_Id= A.Diagnosis_Id
AND A.Patient_Id=F.Patient_Id
AND C.City_Name='New York'
AND ( EXTRACT(YEAR FROM V.Diagnosis_Start) = 2013
```


OR EXTRACT(YEAR FROM V.Diagnosis_Stop) = 2013)

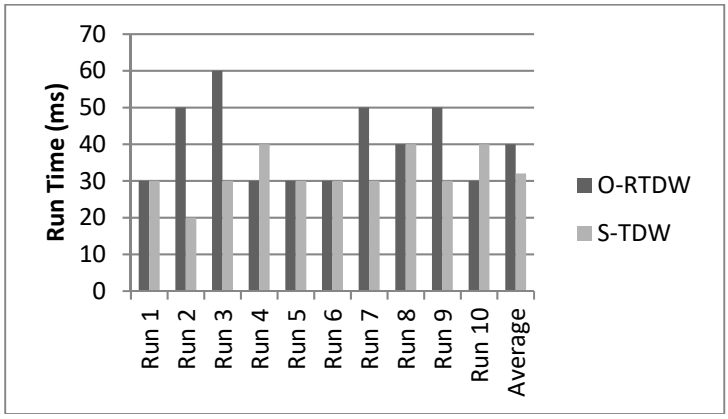

Figure 10. Query 4 run comparison chart

Query 5:
Which patients lived at the same city at the same time and had the same diagnosis? (temporal)

O-RTDW model

```
SELECT P1.Patient_Name, P2.Patient_Name, P1.City_Id, A1.Diagnosis_Id
FROM ADMISSION_O_CUBE_TAB A1, ADMISSION_O_CUBE_TAB A2, Patient_Dimension_o_table P1,
TABLE(P1.Address_Temporal) ADDRESS1, Patient_Dimension_o_table P2, TABLE(P2.Address_Temporal)
ADDRESS2
WHERE P1.Patient_ID < P2.Patient_ID
AND P1.City_Id = P2.City_Id
AND ((ADDRESS1.VALID_TIME_LB <= ADDRESS2.VALID_TIME_LB
        AND ADDRESS2.VALID_TIME_LB <= ADDRESS1.VALID_TIME_UB)
    OR (ADDRESS2.VALID_TIME_LB <= ADDRESS1.VALID_TIME_LB
        AND ADDRESS1.VALID_TIME_LB <= ADDRESS2.VALID_TIME_UB))
AND A1.Patient_Id = P1.Patient_Id
AND A2.Patient_Id = P2.Patient_Id
AND A1.Diagnosis_Id = A2.Diagnosis_Id
```

S-TDW model

```
SELECT F1.Patient_Name, F2.Patient_Name, C1.City_Id, A1.Diagnosis_Id
FROM P_PATIENT_DIMENSION_TABLE P1, Table(P1.State) S1, Table(S1.City) C1, Table(C1.Patient) F1,
P_PATIENT_DIMENSION_TABLE P2, Table(P2.State) S2, Table(S2.City) C2, Table(C2.Patient) F2,
ADMISSION_N_CUBE_TAB A1, ADMISSION_N_CUBE_TAB A2
WHERE   F1.Patient_Id < F2.Patient_Id
AND C1.City_Id = C2.City_Id
AND ((F1.Address_Start <= F2.Address_Start AND F2.Address_Start <= F1.Address_Stop)
    OR (F2.Address_Start <= F1.Address_Start AND F1.Address_Start <= F2.Address_Stop))
AND A1.Patient_Id=F1.Patient_Id
AND A2.Patient_Id = F2.Patient_Id
AND A1.Diagnosis_Id = A2.Diagnosis_Id
```

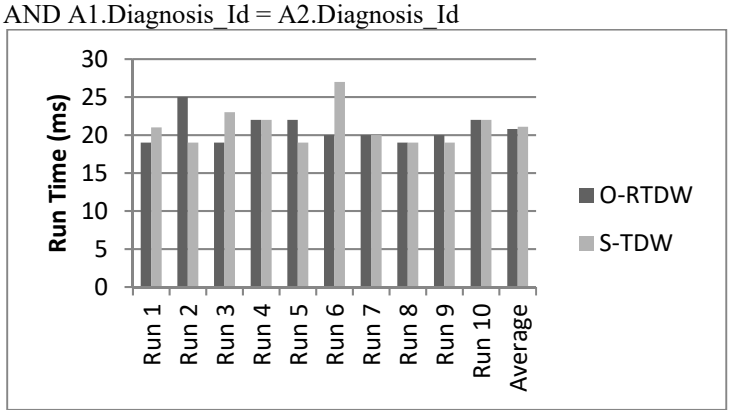

Figure 11. Query 5 run comparison chart

Overall, run times of the two approaches are similar, though S-TDW model is a little bit faster than O-RTDW as shown in Figure 12.

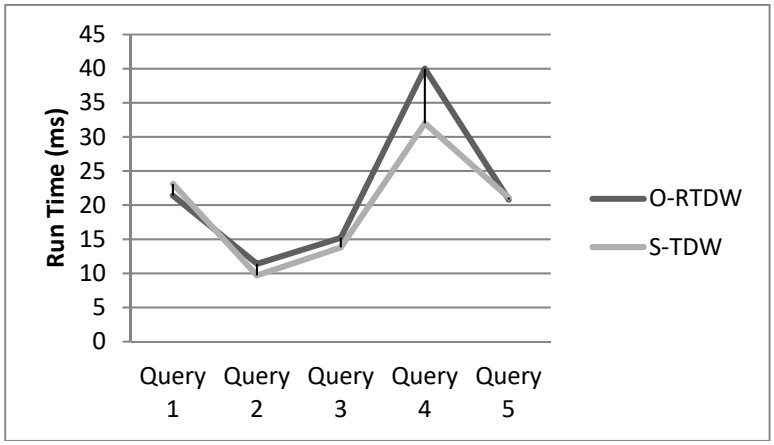

Figure 12. Queries' average run time comparison chart

Conclusion

Two current approaches for dealing with temporal data in DWs have been evaluated and compared in this research work, Object-Relational Temporal Data Warehouse (O-RTDW) model and Starnest Temporal Data Warehouse (S-TDW) model. Results showed that the S-TDW model requires significantly less space and it is a little faster on average than the O-RTDW model.

Future work includes implementation of optimization techniques for efficient evaluation of complex temporal nested queries, and the addition of transaction time to the implemented model.

Acknowledgements

The authors would like to thank George Tsaprazlis, undergraduate student from the Department of Computer Science and Engineering of the Technological Educational Institute of Thessaly, who helped with the implementation of this research work during his diploma thesis.

References

Atay, C. E. & Alp, G. (2016). Modeling and Querying Multidimensional Bitemporal Data Warehouses. *International Journal of Computer and Communication Engineering*, 5(2) (pp.110-119). San Bernardino, California : International Academy Publishing.

Bliujute, R., Saltenis, S., Slivinskas, G. & Jensen, C.S. (1998). Systematic Change Management in Dimensional Data Warehousing. In *Proceedings of the 3rd International Baltic Workshop on Databases and Information Systems*, Riga, Latvia (pp.27–41). Riga, Latvia: Latvian Academic Library.

Combi, C., Oliboni, B. & Pozzi, G. (2009). Modeling and Querying Temporal Semistructured Data Warehouses. In Kozielski, S. and Wrembel, R. (Eds.), *New Trends in Data Warehousing and Data Analysis, Annals of Information Systems*, 3 (pp.299–324). New York, USA: Springer.

Devlin, B. & Murphy, P.T. (1988). An Architecture for a Business and Information System. *IBM Systems Journal* 27(1) (pp.60-80). Yorktown Heights, New York, USA: IBM.

Eder, J., Koncilia, C. & Morzy, T. (2002). The COMET Metamodel for Temporal Data Warehouses. In *Proceedings of the 14th International Conference on Advanced Information Systems Engineering (CAiSE)*, Toronto, Canada (pp.83-99). Lecture Notes in Computer Science, Berlin-Heidelberg, Germany: Springer-Verlag.

Garani, G., Adam, G.K. & Ventzas, D. (2016). Temporal Data Warehouse Logical Modeling, *International Journal of Data Mining, Modelling and Management*, 8(2) (pp.144-159). Olney, Bucks, UK: Inderscience Publishers.

Garani, G. & Helmer, S. (2012). Integrating Star and Snowflake Schemas in Data Warehouses. *International Journal of Data Warehousing and Mining* 8(4) (pp.22-40). Hershey, Pennsylvania, USA : IGI Global.

Golfarelli, M. & Rizzi, S. (2009). A Survey on Temporal Data Warehousing. *International Journal of Data Warehousing & Mining* 5(1) (pp.1-17). Hershey, Pennsylvania, USA : IGI Global.

Inmon, W. (2002). *Building the Data Warehouse*. Indianapolis, Indiana, USA: John Wiley & Sons Publishers.

Kimball, R. (1996). *The Data Warehouse ToolKit*. Indianapolis, Indiana, USA: John Wiley & Sons Publishers.

Koncilia, C. (2003). A Bi-Temporal Data Warehouse Model. In *Proceedings of the 15th International Conference*

on Advanced Information Systems Engineering (CAiSE), Klagenfurt, Austria (pp.77-80). Lecture Notes in Computer Science, Berlin-Heidelberg, Germany: Springer-Verlag.

Malinowski, E. & Zimányi, E. (2006). A Conceptual Solution for Representing Time in Data Warehouse Dimensions. *In Proceedings of the 3rd Asia-Pacific Conference on Conceptual Modeling (APCCM)*, Hobbart, Australia (pp.45-54). Darlinghurst, Australia: Australian Computer Society.

Rechy-Ramírez, E.-J. & Edgard, B.-G. (2006). A Model and Language for Bitemporal Schema Versioning in Data Warehouses. In *Proceedings of the 15th International Conference on Computing (CIC)*, Mexico City, Mexico (pp.309-314). Los Alamitos, California, USA:IEEE Computer Society.

Turki, I.Z., Jedidi, F.G. & Bouaziz, R. (2010). Multiversion Data Warehouse Constraints. In *Proceedings of the 13th ACM International Workshop on Data Warehousing and OLAP (DOLAP)* (pp.11-18). New York, USA: ACM.

COMPARISONS OF POLYPROPYLENE COMPOSITES: THE EFFECT OF COUPLING AGENT ON MECHANICAL PROPERTIES

Umit HUNER[1*]

Trakya University, Faculty of Engineering, Department of Mechanical Engineering, Edirne 22030, Turkey

umithuner@trakya.edu.tr

Abstract: The aim of this work is to compare the glass fiber (GF)/polypropylene (PP) and black rice husk (BRH)/black rice husk ash (BRHA)/polypropylene (PP) composites on mechanical properties. Tensile, flexural and falling weight impact test was conducted to investigate the effect of filler content and coupling agent (MAPP) on the mechanical properties of the BRH/BRHA/PP composites. Using a coupling agent, the mechanical properties of glass fiber reinforced material is intended to reach. By incorporating up to 10% (by weight) fillers, the tensile strength of GF/PP increased by 21%, BRH/PP and BRHA/PP were decreased by 20% and 10%, respectively, compare to neat polypropylene. Using MAPP provided to enhance the tensile strength of BRH/PP and BRHA/PP composites. And also the effect of water absorption on GF/BRH/BRHA was investigated. Results showed that increasing BRH and BRHA concentration and increasing water contact time greatly increase water absorption.

Keyword: composites, mechanical properties, FTIR, rice husk, polypropylene

Introduction

In recent years, natural filler have a potential usage for composite production. Cellulosic fibers, like wheat straw, rice husk, flax, wood in their nature, as well as, several waste cellulosic products such as husk, shell flour and wood fiber have been used as reinforcement of different plastic resins. Cellulosic material reinforced plastics, are low cost, light-weighted, have enhanced mechanical properties, and are nonhazardous (Turmanova et al., 2008; Razavi-Nouri et al., 2006; Gupta et al., 2006). Despite the advantages of natural fiber reinforced plastic composites, they have lower impact resistance, lower strength and relatively poor moisture resistance compare to synthetic fiber reinforced composites such as glass fiber reinforced plastics (GFRP) (Lee & Jang, 1999; Rozman et al., 2010). Natural fillers have hydrophilic character in their nature and this cause incompatibility between filler and matrix. Water absorption can cause degeneration of dimensional stability and micro crack can be occurred in structure. This leads to decrease of strength of composite (Arbelaiz et al., 2005; Ershad-Langroudi et al., 2008; Premalal et al., 2002; de Carvalho et al., 2012). Therefore, interface of composite should be improved by chemically or coupling agent. Coupling agent provides to enhance the bonding between filler and matrix. This causes increase of strength and reducing of water absorption value.

Recently publications give information about using of natural fillers as reinforcements in composite applications. Turmanova et al. (2008) studied water absorption and mechanical properties of polypropylene filled raw rice husk and rice husk ash. The mechanical properties like tensile strength and Young's modulus that depend on filler content were determined. They investigated the water absorption and treatment of fillers how changes the mechanical properties. Razavi-Nouri et al. (2006) studied the reinforcing effect of chopped rice husk into polypropylene. And also the effect of coupling agent MAPP was investigated. Arbelaiz et al. (2005) have reported the effects of using different coupling agent for determining the coupling effectiveness for composites. Also they compared the influence of both fiber surface and matrix modification on mechanical properties. Ershad-Langroudi et al. (2008) studied modifying the chopped rice husk reinforced PP by recycled PET. They have investigated the potential usage of rPET on composite production and how can change the mechanical/thermal properties. Two kind of form of natural filler was chosen in this study because of its special properties. Black rice husk and black rice husk ash (obtained burned rice husk). Low cost, low density, high modulus etc. are some of properties that bring about to choose these fillers. In Turkey BRH production is not much but have potential. After harvesting rice husk has no special usage as filler or something like that. Black rice husk is the outer covering of paddy and accounts for 20% of its weight (Ershad-Langroudi et al., 2008). BRHA is form of BRH that is obtained by burning the BRH. It contains higher rate of silica which is usually used as filler. Also using BRHA as reinforcement in certain polymers gives composites with better dimensional stability, toughness, as well as processing properties, and cheap process cost. This characteristic structure may not be used as waste so it should be estimated valuable technical filler.

This study aims to determine physical, mechanical and spectroscopic properties of BRH and BRHA reinforced PP composites. Therefore, tensile, bending tests, water absorption and FT-IR were carried out. The mechanical properties of the composite material obtained with natural fibers compared with neat polypropylene and glass fiber reinforced composite which is quite widely used in composite production. MAPP is used as a coupling agent on natural fiber reinforced PP to enhance the fiber-matrix interface bonding. This study was conducted to determine whether to use natural fibers instead of synthetic fibers. And also which form of rice husk more can be more effective for production compared to glass fiber reinforced composite.

Materials and method

Materials

In this study, the base resin used was S.R.L., a polypropylene homopolymer by ROM Petrol Petrochemicals with density of 0.90 g/cm³ and melt flow index of 9.36 g per 10 min (200 ^{0}C per 2.16 kg load cell). Poly-propylene-grafted maleic anhydride (PP-*g*-MA (Sigma Aldrich), MA content= 1% wt). Chopped glass fiber (E-glass) (PA2-4.5) was supplied by Cam Elyaf A.Ş. It has 10.5 µm diameter and 4.5 mm length (the nominal value from manufacturer's data sheet). And also it was treated by coupling agent silane 0.6%. The lignocellulosic material used as the reinforced filler in the composite was black rice husk (BRH) has been collected from Thrace region in Turkey at 2011 harvest time with moisture content (unseasoned) of 5.88 % according to AACC Method No: 44-15A. Rice husk was burnt in Protherm PLF 120/7 model ashing furnace at 600˚C for 6 hours according to AACC Method No: 08-01. Ash content of 77.64% and average particle size of 500 µm were obtained (Anonymous, 2000). As it has been shown table 1, BRHs contain cellulose, hemicelluloses, lignin, waxes, and water-soluble substances (Turmanova et al., 2008).

Composites preparation

Rice husks were dried in a vacuum oven Ecocell 55 at 103 ±2 ^{0}C for 24 h to adjust the moisture content to 1–3% and then stored over desiccant before compounding. For this study moisture content decreased from 5.88% to 1.58%. Figure 1 shows drying and burning process.

Figure1. a) Drying process b) burning process

TABLE 1: Typical composition of some of natural fillers (Turmanova et al., 2008; Arbelaiz et al., 2005; Julson et al., 2009).

Natural fibers	Density (g/cm^3)	Cellulose %	Hemicelluloses %	Lignin %	Mineral Ash %	Water Soluble M. %
Flax	1,51	65-85	18-20	1-4	5	1,5
Hemp	1,47	77,5	10	3,7-13	0,8	1,8
Kenaf	1,52	45-57	21,5-23	15-19	2-5	1,9
Sisal	1,45	50-64	10-24	7-11	0,6-1	1,7
Black Rice Husk	0,09-0,15	31-34	22-26	22-23	11-14	7-9
Chemical analysis of Black Rice Husk Ash						
Composition	SiO_2	K_2O	MgO	Al_2O_3	CaO	Fe_2O_3
%	93,19	3,84	0,87	0,78	0,74	0,58

Water causes lower adhesion between filler and matrix. Therefore, it should be removed from composite structure by drying process. Reinforced plastics granules were produced by single screw extruder (L/D= 28). The extruder has four zones with controlled temperature. The setting for these zones was: Z1 = 160^0C, Z2 = 175^0C, Z3 = 185^0C and Z4 = 185°C. The screw velocity used was 55 rpm. Sheets of dimensions 180x180x4 mm^3 were prepared using a hydraulic press under a pressure of 150 kg cm^2. Tensile strength, elongation at break were recorded and calculated by automatically. And elastic modulus was calculated from tensile test data by manually.

Mechanical properties

Tensile, flexural and impact are used for determining mechanical properties of reinforced plastics. In this study, both, tensile and flexural tests were performed using an Instron Universal Testing Machine Model 8501, equipped with a 500 kg load cell, strain-gauge extensometer (Instron, model 2620) after conditioning at 23 ±2 ^{0}C according to ISO 527 standard and ASTM D790, respectively. The cross-head speed used for the type IA tensile specimens was 5 mm/min. For the Flexural test (three point bending) a specimen with nominal dimensions of 80x10x4 mm^3, a span of 32 mm and a cross-head of 1 mm/min were used (Franco-Herrera & Gonzalez, 2005). Gardner impact test was carried out using a Devostrans Drop Impact Test Machine according to ASTM standard D5420. For the test a specimen with nominal dimensions of 60x60x3.2 mm^3, striker diameter 12.70±0.10 mm and support plate inside diameter 16.26 ±0.025 mm. Three specimens of each sample were tested for tensile and flexural tests, and the average results were reported. Gardner impact test was carried out according to Bruceton Staircase Method by 20 samples for each calculated value.

TABLE 2: Formulations of the Composites in Weight Percent

Sample ID	Ingredients (%)			
	PP	GF	BRH/MAPP	BRHA/MAPP
PP	100	0	0/0	0
PPGF10	90	10	0/0	0
PPGF20	80	20	0/0	0
PPGF30	70	30	0/0	0
PPBRH10	85	0	10/5	0
PPBRH20	75	0	20/5	0
PPBRH30	65	0	30/5	0
PPBRHA10	85	0	0	10/5
PPBRHA20	75	0	0	20/5
PPBRHA30	65	0	0	30/5

Water absorption properties

Water absorption tests were carried out according to the ASTM D 570-98 method. Composite samples were immersed in distilled water in Memmert WBN 22 model water bath at 90 ° C. After that samples were dried an

oven for 24 h at 103±2°C. The dried specimens were weighed with a precision of 0.0001 g by Sartorius ED224S precision balance. The samples were removed from the distilled water, dried with blotting paper, and weight values were determined. Water absorption percent was calculated using the following formula,

$$M\ (\%) = M_t - M_o / M_o \times 100$$

Where, M_o and M_t denote the oven-dry weight and weight after time t, respectively.

Spectroscopic characterization

Fourier transform infrared (FT-IR) spectroscopy was used to detect the presence of the functional group that exists in rice husk/rice husk ash/glass fibers. The IR spectrometer (Perkin-Elmer spectrum BX, Perkin-Elmer Canada) was used for detecting of spectra of samples. FT-IR spectra of the samples were collected in the range of 4000-400 cm^{-1} with a resolution of 4 cm^{-1}.

Morphological study

SEM was used for detecting morphology of interface of composite materials. SEM micrographs of the surfaces of impact fractured specimens were taken using a ZEISS Evo® LS 10 scanning electron microscope and FEI F50 SEM. The samples were first sputter-coated with a fine layer of gold under vacuum for 60 sec.

Results and discussion

Tensile properties

Tensile strength and modulus of PPGF composites increased by about 70% and 188%, respectively, according to neat PP at 30% filler content. Gupta et al. (2006) has reported that increase of tensile strength and modulus values reached 50% according to neat PP at same filler content. The increase of tensile strength, as a result of glass fiber incorporation, can be attributed to the good stress transfer to the glass fiber by the glass fiber-matrix interface. This good stress transfer from the polymer matrix to glass fibers leads to increase in tensile strength due to the strength of glass fiber. Figure 2 shows tensile strength and modulus of composites that depends on filler contents. Figure 3 depicts one set of BRH/BRHA reinforced composites' stress-strain graphs which have been obtained from test machine software.

The tensile strength of composites that containing PPBRH decrease by increasing filler content. At 20 % filler content, value of tensile strength reached 42% decrease according to neat PP (Tensile strength, 28 MPa). Tensile modulus of PPBRH composite had a small tendency to increase, at 20% filler content obtained value of 7% increase. Turmanova et al. (2008) has reported 14% tensile strength decrease and 5% tensile modulus increase at 20% raw rice husk content. After using MAPP, tensile strength of the PPBRH increased, and the value was obtained to be lower by 20% compared to the neat PP. The tensile modulus of PPBRH changed the upward and increased by 47% compared to reinforced PP. Tensile strength of PPBRHA decreased 21% and modulus increased 20% according to neat PP, at 20% filler content. Similar results have been reported by Turmanova et al. (2008). After incorporating MAPP, the tensile strength of PPBRHA reached similar value with neat PP. The modulus of PPBRHA decreased by 38% compared to PPBRHA without MAPP.

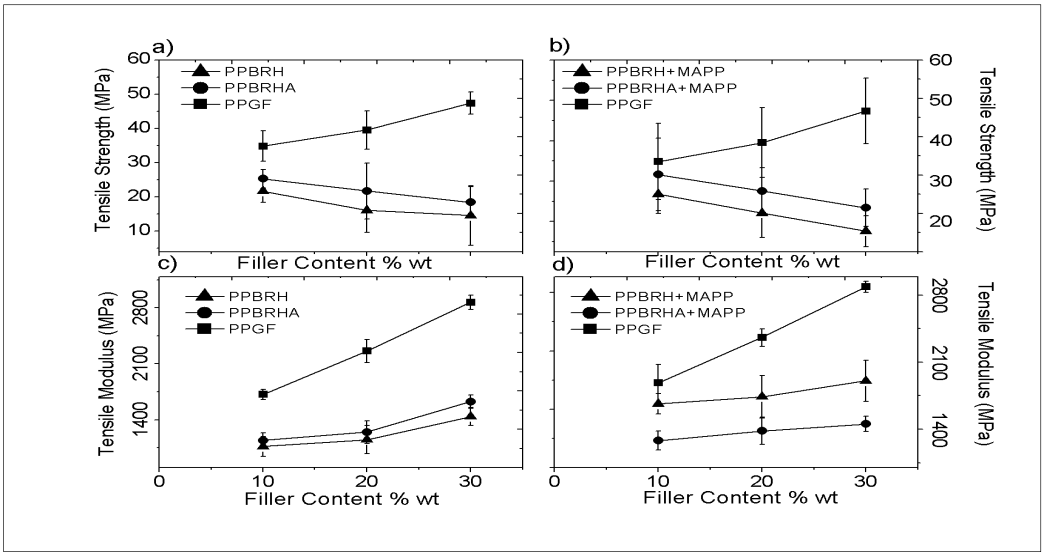

Figure 2. Tensile modulus and strength of composites a) tensile strength of composites depend on filler content, b) tensile strength of composites with %5 MAPP c) tensile modulus of composites depends on filler content d) tensile modulus of composites with %5 MAPP

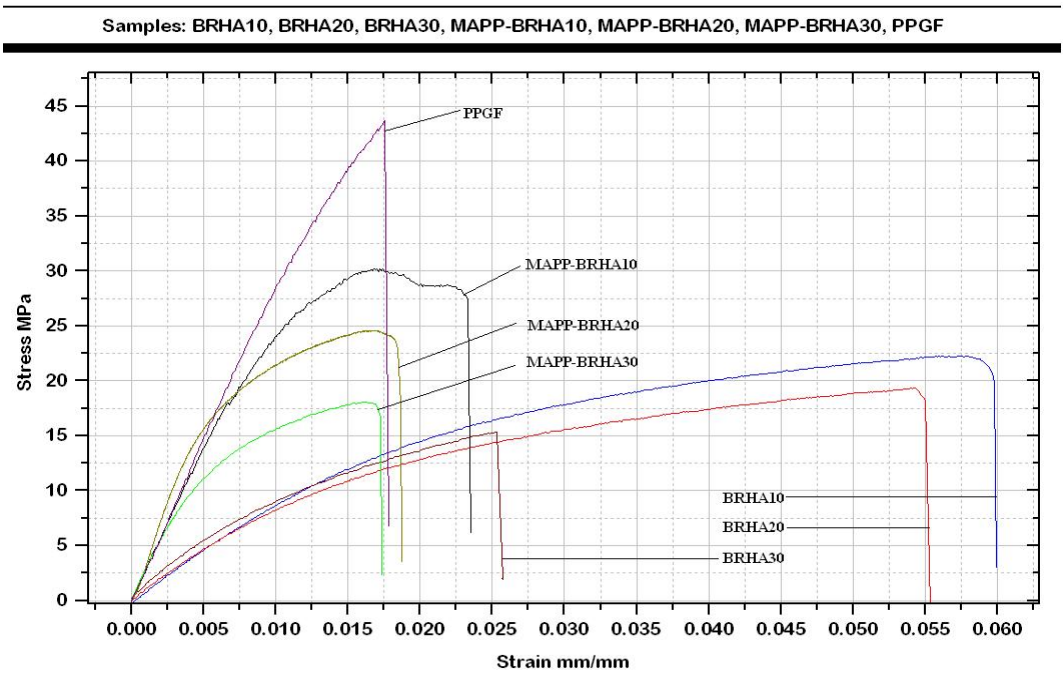

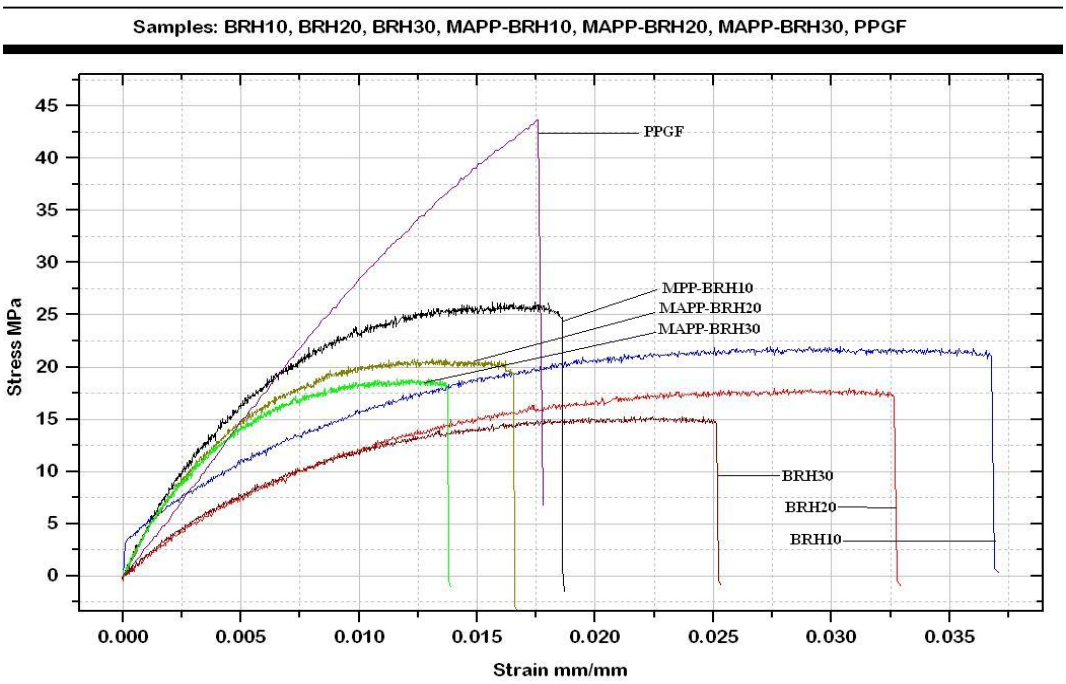

Figure 3. Stress-strain graph of BRH/BRHA composites

PPBRH and PPBRHA composites have lower tensile strength according to neat PP and PPGF composite. This mainly attributed to restricting of stress transfer by interface of composite. Weak adhesion force between filler and matrix cause not good interface bonding. It should be noted that BRHA composites have good dispersion because of its smaller size. And this provides higher strength due to better interaction between filler and matrix compared to BRH composites.

Composites had tensile moduli which tend to increase in all composition. This mainly attributed to presence of rigid filler in their structure. Fillers restrict the free motion of matrix and deformation has been avoided. This caused increase of elastic modulus with increase filler content (Crespo et al., 2008; George et al., 2001). It is more likely the rice husk/ash acts as stress concentrators in the PP matrix. Therefore, dispersion of fillers can provide reinforcing affect due to having higher modulus than PP matrix.

Flexural Properties

It was found that although the flexural strength of BRH reinforced PP relatively remained constant, in addition to this PPBRHA increased weakly. The flexural modulus of PPBRH and PPBRHA increased by about 44% and 71%, respectively, comparing to the neat PP. Razavi-Nouri et al. (2006) has reported for BRH composites 10% and 45% increase on flexural strength and flexural modulus, respectively. And also Fuad et al. (1995) reached 40% flexural strength value at BRHA composite.

Figure 4 shows comparison of flexural strength and modulus depend on filler content of composites. PPGF composite showed the highest flexural strength and modulus by about 90% and 153%, respectively, comparison to the others. Gupta et al. (2006) has reported 63% and 258% increase for the 30% filler content. Incorporating glass fibers to polymer matrix increases the stiffness of composite. This is mainly attributed to having higher stiffness according to polymer matrix.

The MAPP is a good coupling agent that is physically stronger and has thermally stable bonds, attributed to hydrogen bonding with BRH/BRHA and chain entanglements and co-crystallization with PP (Khalil, 2008). Using MAPP enhanced the compatibility of fiber-matrix and provided to increase flexural strength and modulus. Flexural strength of BRHPP and BRHAPP increased by 10% and 29% compared to neat PP. The flexural modulus of PPBRH and PPBRHA increased by about 94% and 97%, respectively, comparing to the neat PP.

Tension, compression and shear stress occurs during the flexural loading. Failure is mainly attributed to occurring bending and shearing in bending test. Incorporating of glass fiber provides to resist the shearing of composite and this cause an increase of flexural strength (Gupta et al., 2006; Lee & Jang, 1999).

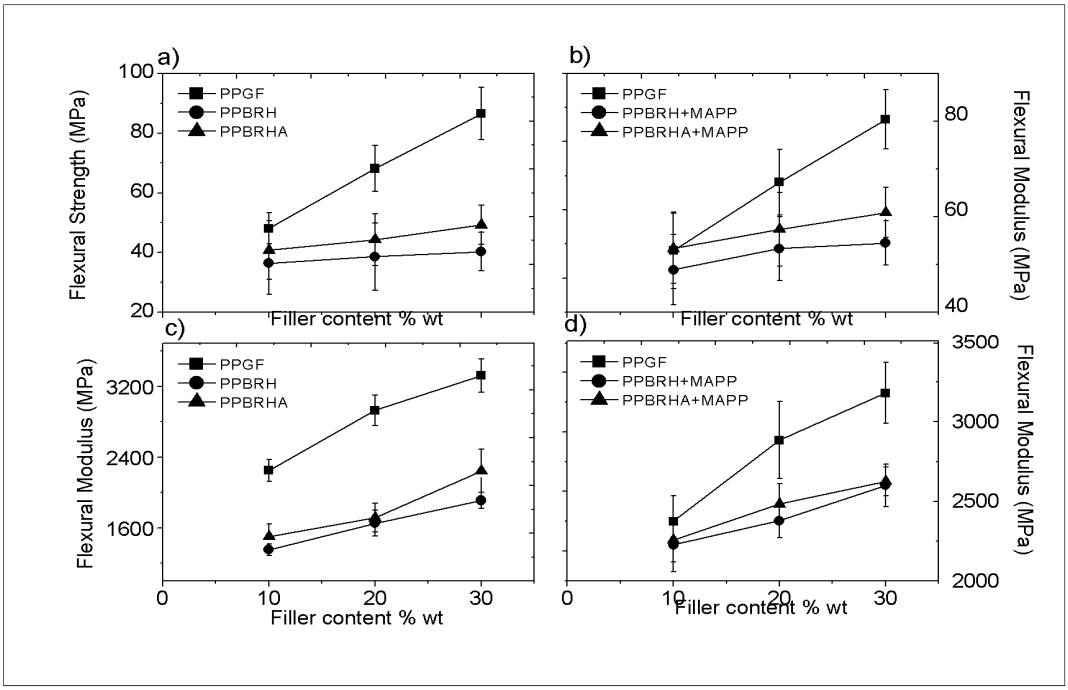

Figure 4. a) Flexural strength depends on filler content b) after using coupling agent, flexural strength-filler content c) flexural modulus without coupling agent d) flexural modulus of composites with coupling agent

Water absorption test results

PP is a non-polar polymer which has less tends to bound with water. In normal conditions, while the PP may contain 0.1% of water; at 90 degrees the water absorption value can reach 0.25 percent. The natural fillers are hydrophilic which restrict of their usage in production. The hydrophilic character of reinforcement in composites causes reduction of mechanical properties. Therefore polymers are required to undergo some operations before the additive into the matrix. Due to the high hydrophilic character of the components of natural fillers water absorption is a severe handicap for some applications of natural fiber polymer composites. Generally speaking, polypropylene hardly absorbs water due to its hydrophobic structure; however, rice husk can absorb water because of its hydrophilic character (Rozman et al., 2010; Nourbakhsh, et al., 2011; Yang, et al., 2006; Starks & Rowland, 2003; Julson et al., 2009; Jacoby et al., 2001; Thwe & Liao, 2002).

The study reports the effect of filler type and content on water absorption value of composite. Figures 5a reveals that the water absorption increases with increase of natural filler content. And also results showed that increasing BRH and BRHA concentration and increasing water contact time greatly increased water absorption, as it can be seen in Figure 5c. Figures 5b and 5d depicts that the water uptake and BRH filler content. Because of the free OH groups contained in cellulose, PP matrix composite acts as hydrophilic structure. Therefore, the water absorption increases with increasing rate of reinforcements. Similar curves were obtained by Turmanova et al. (2008). MAPP use, while ensuring the improvement of the interface between the reinforcement and the matrix, this improvement causes a lowering of water absorption. Reason behind this is considered to be a change in the diffusion mechanism of natural reinforcements. Water molecules are transferred to micro-gaps in the polymer by diffusion mechanism. In the fiber matrix interface, the water molecules are transferred by capillary action due to the lack of wetting. And also micro cracks can be occurred during production process, this cause water transportation to the gaps. Incorporating MAPP decreases the micro gaps due to enhance the bonding mechanism between filler and matrix. So water absorption value reduces by adding coupling agent.

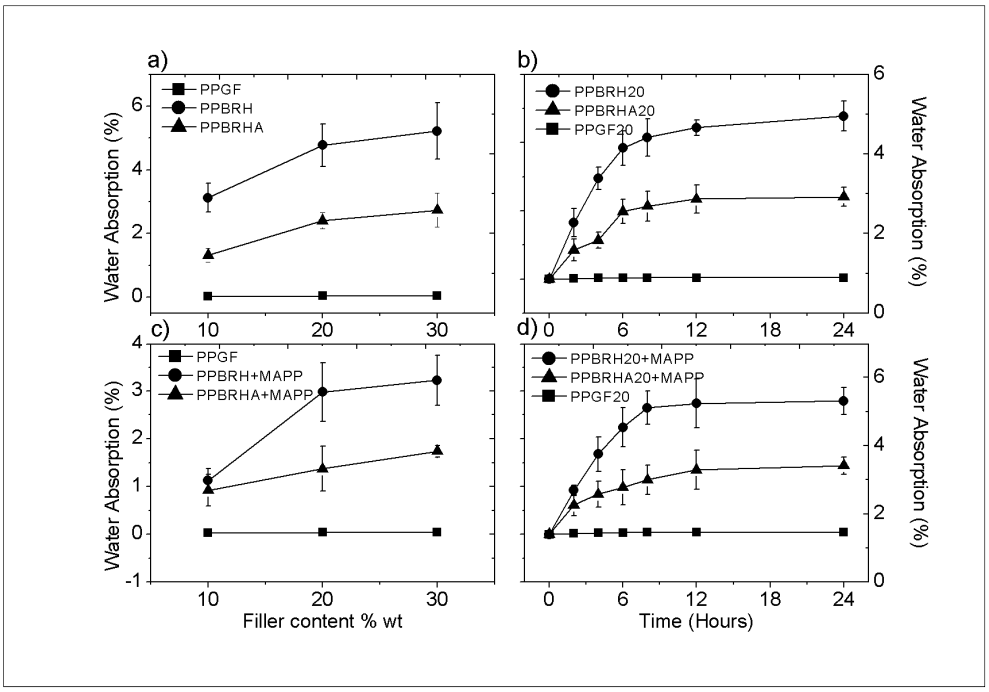

Figure 5. a) Water absorption according to filler content, b) Effect of coupling agent on water absorption, c) water absorption value at 90 ^{0}C, d) Dependences of water absorption after using coupling agent MAPP

It can be seen from Fig. 4c-d BRH20 had the highest water absorption value, PPGF20 had the lowest value. It means that the, PPGF is basically a hydrophobic polymer composite.

Gardner impact properties

Impact failures are the result of rapid crack propagation through the material. The crack's growth rate is inversely proportional to the impact resistance of the material. For a polymer to be considered as having good impact resistance, it should be able to absorb most of the impact energy and slows the rate of crack propagation (Bigg, 1987).

Gardner test is used for determining impact energy required for crack or failure on flat surface. A striker is used for impact by drop weight. Figure 6 shows the impact tester and one of the deformed 20% PPGF sample. The procedure determines the energy (mass x gravity x height) that will cause 50% of the specimens tested to fail. Incorporation of glass fibers provide to increase of impact strength. This is mainly attributed to having higher energy absorb capacity of fibers and it cause less fiber breakage and a higher residual strength to the composite (Gupta et al., 2006). PPGF composite reached maximum impact energy value at 10% filler content according to others. Lee et al. (1999) has reported the maximum impact energy at 20% glass fiber reinforced composite. Increasing glass fiber makes the composite structure more brittle and free motion of matrix chains is restricted by fibers. During the loading, matrix cannot damp the force due to less matrix transport are between fibers. This causes decrease of impact strength of composite. Some others explained that is mainly attributed to increase in the crystallinity orientation factor of PP by GF.

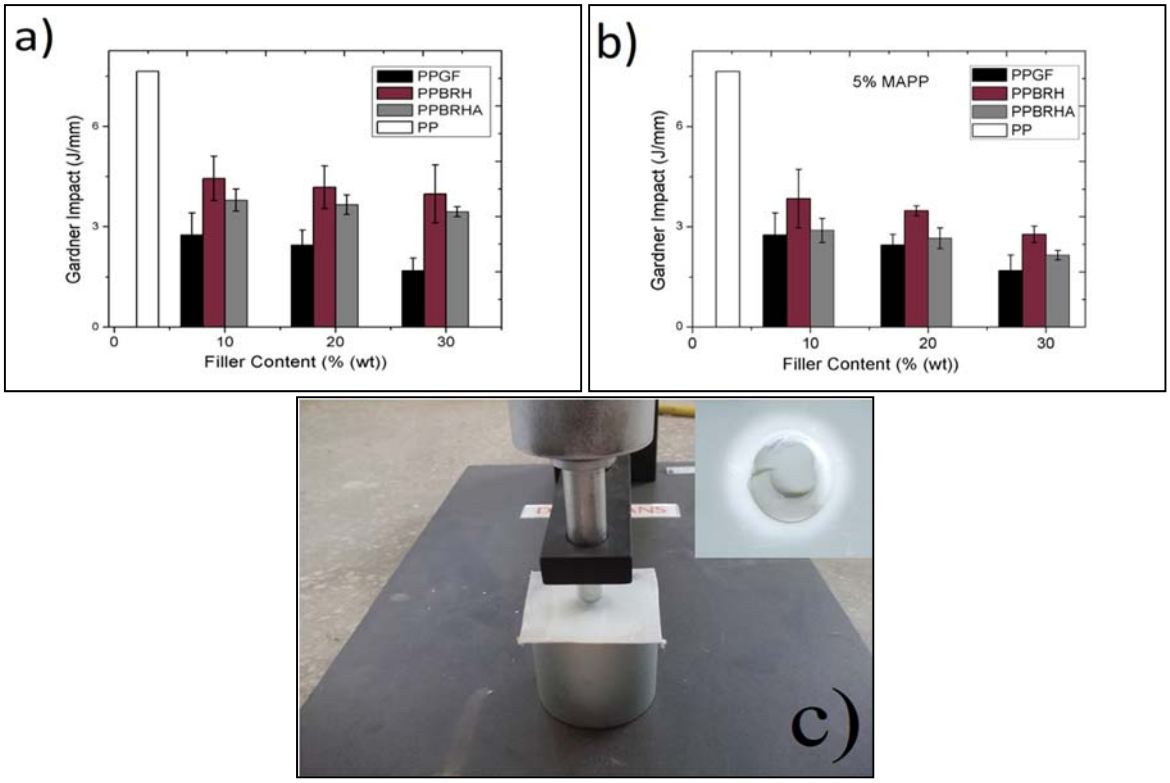

Figure 6. a) Gardner impact energy depend on filler content, b) Gardner impact energy of composites with MAPP c) test set-up

Adding BRH/BRHA filler into the polypropylene causes decrease of the impact strength. Interfacial adhesion effect the impact strength of composite. The weak bonding between filler and matrix cannot handle the energy of impact (Fuad et al., 1995). Crack moves along the weak interface. Polymer matrix cannot block the crack propagation and this cause lower impact strength. Increasing the rate of filler, increases the regions where the weak bonds and cannot prevent crack propagation.

Figure 6a) reveals that the BRH composite have higher impact strength than the BRHA composite. This may be explained higher agglomeration of BRHA that cause restriction of stress transfer to matrix. Agglomeration of the reinforcing particles has been suggested in previous studies by the effect of the adhesion forces within the composite structure (Fuad et al., 1995). BRHA particles make structure more brittle and tend to crack failure. Figure 6b) shows composites including MAPP. Adding MAPP to the structure of composite material makes the structure more brittle. Although, having stronger bond between fillers and matrix, the agglomeration of fillers is not inhibited in the composite structure. During the impact test, external mechanical energy is transferred to brittle structure of matrix and this cause a sudden damage.

Spectroscopic Results

FT-IR gives information about internal structure of composite. These curves present both PP and filler characteristic chemical bands. Figure 7 depicts that the IR spectra of filled PP. 2985-2640 cm^{-1} band give information about symmetric and asymmetric vibration of ethylene, methylene and CH groups (Turmanova et al., 2008). 1436-452 cm^{-1} have number of absorption bands (Hummel & Scholl 1968). The BRH are characterized by band between 3500 and 2700 cm^{-1}. Absorbed water and OH groups can be placed to this band. This band's position gives proof about presence of strong hydrogen bonds. 1600 cm^{-1} and 1500 cm^{-1} band give information about H_2O molecules physically adsorbed onto rice husks and C-H deformation vibrations, respectively. Siloxane bonds (Si-O-Si) bands were placed to peak at 450 cm^{-1}. Si-O network was placed to peaks between 1200 and 700 cm^{-1}. Differences between spectra of BRHA and BRH occurred at the band of 1305 and 450 cm^{-1}. This can be explained with the decrease of organic matter content and its transformation into active carbon (Turmanova et al., 2008). The bands at 1000 and 760 cm^{-1} correspond to the Si–O stretching vibration, and the bending vibration at 450 cm^{-1} appeared sharper as the organic matter was no longer present.

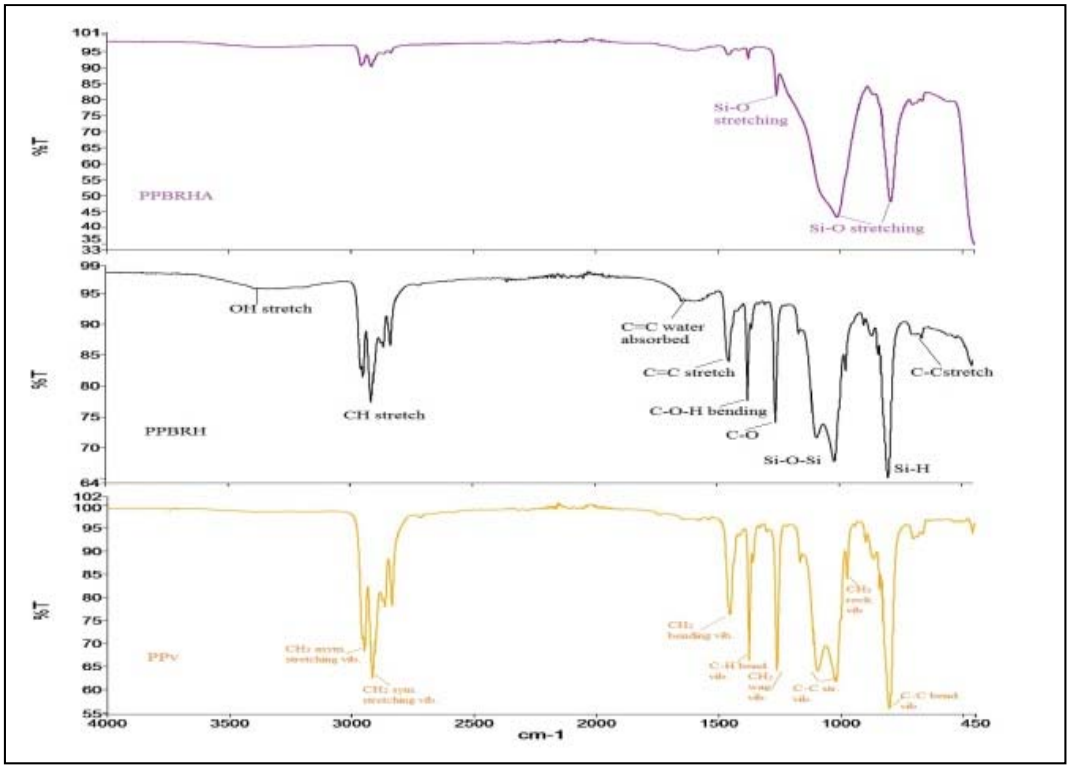

Figure 7. FTIR characterizations of composites

Morphological study of composites

Fig. 8 shows the fracture surfaces of PPGF composite after Gardner impact test. The fracture surface of matrix shows the brittle failure of PP, showing little plastic deformation resulting from fiber end (Fig. 8a). Figure 8b shows that there is a good adhesion between glass fiber and PP matrix. And also location of fibers refers a good dispersion.

Good interfacial adhesion between glass fiber and matrix enhance the stress transfer during the loading. Crack propagation is restricted by glass fiber and this cause increase of strength. Good interface between fiber and matrix also provide increase of energy absorption capacity. During impact loading, fracture propagation can be resisted by fiber-interface-matrix region (Rozman et al., 2010).

Figure 9a shows that BRHA reinforced composite have micro voids between filler and matrix. This causes poor interaction in interface. Fig. 9b reveals that presence of agglomeration on crack surface provides easy crack propagation. And also agglomeration causes lack of interfacial bonding between filler and matrix.

Figure 10a shows location of rice husk in the matrix. Figure 10b reveals that there are micro-cavities between filler and matrix due to the filler have been pulled out from polymer. These cavities result from polar-apolar incompatibility of filler-matrix. This incompatibility cause lower strength and increase of water absorption value.

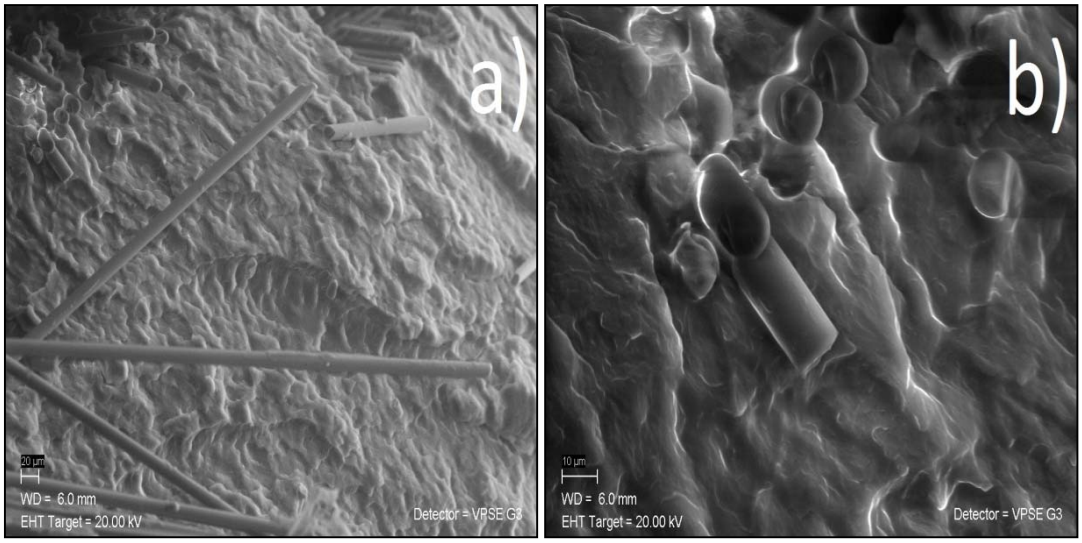

Figure 8. a) Brittle cracking of glass fiber b) Glass fiber and PP interface

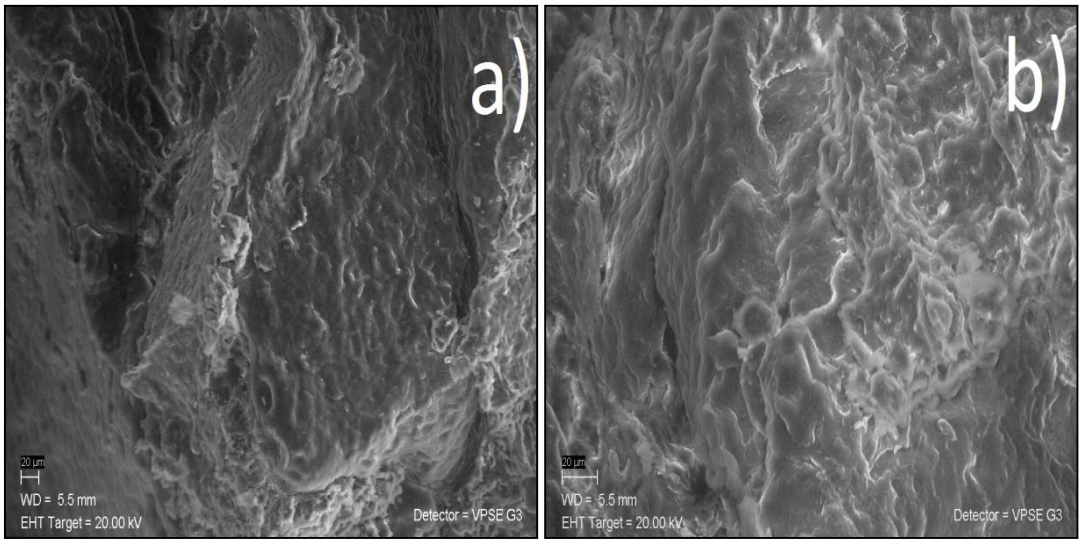

Figure 9. Failure on crack surface of composite b) BRHA agglomeration

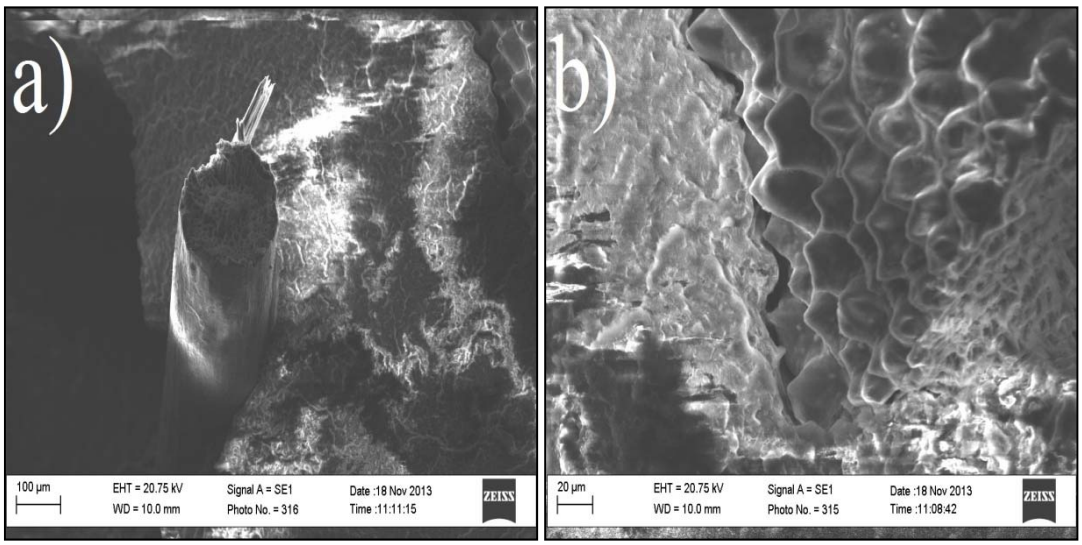

Figure 10. a) Dispersion of rice husk in the matrix b) Cavities between rice husk and matrix

Conclusion

This study reports about usage of glass fiber and rice husk/ash as reinforcement. Composite materials were prepared by incorporating of glass fiber and rice husk/ash to the PP matrix at the weight rate 10 to 30%. MAPP coupling agents have been successfully used in application as a coupling agent for various fillers. It is observed that the mechanical properties, particularly the strength of the composites are increased when MAPP is added to the system. This is because of the improved surface interaction of filler and polymer in the presence of coupling agents and the transfer of stress from one phase to the other.

The tensile and flexural strength of the glass fiber reinforced composite increased up to 30% fiber content but BRH and BRHA composite's strength decreased by filler content. The tensile and flexural modulus of composites increased with filler content. Increase rate of modulus was occurred in composite of PPGF, PPBRHA and PPBRH, respectively. BRH (10% wt) reinforced PP composite had the maximum impact energy value. Energy value decreased with filler content. The highest water absorption values were obtained in PP composites reinforced by BRH, BRHA and the lowest in glass fiber reinforced composite. Water absorption increased with the increased filler content in BRH and BRHA reinforced composites.

References

Anonymous, (2000). Approved Mthods of American Association of Cereal Chemists.10th ed. Minnesota, USA.)

Arbelaiz, A., Ferna´ndez, B., Ramos, J.A., Retegi, A., Llano-Ponte, R. & Mondragon, I. (2005). Mechanical properties of short flax fiber bundle/polypropylene composites: Influence of matrix/fibre modification, fiber content, water uptake and recycling. Composites Science and Technology, 65, 1582–1592.

Bigg, D.M. Polymer Composites, 1987, 8 -115.

Crespo, J.E., Sanchez, L., Garcıa, D. & Lopez, J. (2008). Study of the mechanical and morphological properties of plasticized pvc composites containing rice husk fillers. Journal of Reinforced Plastics And Composites. 27, 229-243.

de Carvalho, F.P., Felisberti, M.I., Oviedo, M.A.S., Vargas, M.D., Farah, M. & Ferreira, M.P.F. (2012). Rice husk/poly (propylene-co-ethylene) composites: effect of different coupling agent on mechanical, thermal and morphological properties. Journal of Applied Polymer Science, 123, 3337–3344.

Ershad-Langroudi, A., Jafarzadeh-Dogouri, F., Razavi-Nouri, M. & Oromiehie, A. (2008). Mechanical and thermal properties of polypropylene/recycled polyethylene terephthalate/chopped rice husk composites. Journal of Applied Polymer Science, 110, 1979–1985.

Franco-Herrera P.J. & Gonzalez A.V. (2005). A study of the mechanical properties of short natural fiber reinforced composites. Composites: Part B, 36, 597–608.

Fuad, M.Y.A., Ismaıl, Z., Ishak, Z.A.M. & Omar, A.K.M. (1995). Application of rice husk ash as fillers polypropylene: effect of titanate, zirconate and silane coupling agents. Eur. Polym. J. 31, 885-893.

George, J., Sreekala, M.S. & Thomas, S. (2001). A review on interface modification and characterization of natural fiber reinforced plastic composites. Polymer Engineering Science, 41, 1471–85.

Gupta, A.P. Saroop, U.K. Jha, G.S. & Verma, M. (2006). Studies on effect of coupling agent on glass fiber filled polypropylene. Polymer-Plastics Technology and Engineering, 42, 297-309.

Hummel, D.O. & Scholl, F. (1968). Atlas den Kunststoff-analyze, Band 1. Munchen: Carl Hanser Verlag, pp 131.

Jacoby, P., Sullivan, R. & Crostic, W. (2001). Wood filled high crystallinity polypropylene, The 6th International Conference on Wood-Fiber Plastic Composites, USDA Forest Service, Madison, Wisconsin.

Julson, J., L., Subbarao, G., Stokke, D.D., Gieselman, H.H. & Muthukumarappan, K. (2009). Mechanical properties of bio-renewable fiber/plastic composites, Journal Applied Polymer Science, 93, 2484.

Khalil, R. (2008). Impact of the surface chemistry of rice hull ash on the properties of its composites with polypropylene, Phd Thesis, School of Civil and Chemical Engineering Science, Engineering and Technology Portfolio, RMIT University.

Lee, N-J. & Jang, J. (1999). The effect of fiber content on the mechanical properties of glass fiber mat/polypropylene composites. Composites: Part A, 30, 815–822.

Nourbakhsh, A., Baghlani, F.F. & Ashori, A. (2011). Nano-SiO2 filled rice husk/polypropylene composites: Physico-mechanical properties. Industrial Crops and Products, 33, 183–187.

Premalal, H.G.B., Ismail, H. & Baharin, A. (2002). Comparison of the mechanical properties of rice husk powder filled polypropylene composites with talc filled polypropylene composites. Polymer Testing, 21, 833–839.

Razavi-Nouri, M., Jafarzadeh-Dogouri, F., Oromiehie, A. & Langroudi, A.E. (2006). Mechanical properties and water absorption behavior of chopped rice husk filled polypropylene composites. Iranıan polymer journal, 15, 757-766.

Rozman, H.D., Zuliahani, A. & Tay, G.S. (2010). Effects of rice husk (rh) particle size, glass fiber (gf) length, rh/gf ratio, and addition of coupling agent on the mechanical and physical properties of polypropylene-rh-gf hybrid composites. Journal of Applied Polymer Science, 115, 3456–3462.

Starks, N.M. & Rowland, R.E. (2003). Effects of wood fiber characteristics on the mechanical properties of wood/polypropylene composites. Wood and Fiber Science, 35, 167-174.

Thwe, M.M. & Liao, K. (2002). Effect of environmental aging on the mechanical properties of bamboo-glass fiber reinforced polymer matrix hybrid composites. Composites Part A:Applied Science and Manufactoring, 33, 43-52.

Turmanova, S., Dimitrova, A. & Vlaev L. (2008). Comparison of water absorption and mechanical behaviors of polypropylene composites filled with rice husk ash. Polymer-Plastics Technology and Engineering, 47, 809–818.

Turmanova, S., Genieva, S. & Vlaev, L. (2012). Obtaining Some Polymer Composites Filled with Rice Husks Ash-A Review. International Journal of Chemistry, 4, 62-89.

Yang, H-S., Wolcott, M.P., Kim, H-S., Kim, S. & Kim, H-J. (2006). Properties of lignocellulosic material filled polypropylene bio-composites made with different manufacturing processes. Polymer Testing, 25, 668–676.

DETERMINATION OF CONTROL LIMITS FOR ASH CONTENT OF CLEAN COARSE COAL PROCESSED BY HEAVY MEDIUM DRUM

Adem TAŞDEMİR

Eskişehir Osmangazi University, Department of Mining Engineering, Eskişehir-TURKEY

atasdem@ogu.edu.tr

Abstract: In this research, control limits of the ash content of clean coarse coal product (+18 mm) produced by a heavy medium drum at a coal preparation plant in Turkey was investigated. The importance of data normality and data independence to detect correct control limits of process control chart were shown for ash content of coal product. One year ash data obtained in 2010 which had non-normal distribution and autocorrelated were found to obey lognormal distribution well and ARIMA(1,0,1) model was the best model to remove autocorrelation. Assuming normal distribution and independence, the control limits of ash content were determined as UCL=16.97, CL=12.85, LCL=8.74 with original ash data. When considering only data non-normality and ignoring autocorrelation, the ash control limits were detected as UCL=17.49, CL=12.72, LCL=9.25. On the other hand, the control limits of ash content were implemented as UCL=19.56, CL=12.72, LCL=8.27 if we consider both lognormal distribution and autocorrelation by ARIMA(1,0,1) model. In addition, number of out-of-control points for ARIMA residual chart considering both data non-normality and auto-correlation were less than those obtained by control chart using original data.

Keywords: Non-normality, Autocorrelation, coal preparation, heavy medium drum, ARIMA chart

Introduction

Process control charts (SPCs) are widely used method to monitor and to control of a quality characteristic during an industrial production stage. Control charts provide to monitor the continuous variations in the process and can be applied and interpreted easily (Montgomery, 2011). Its application is based on two basic assumptions. These assumptions are that the data investigated obey normal distribution and independent, i.e not autocorrelated. However, these assumptions should be taken into account and verified prior to generate control charts. How data normality and autocorrelation affect the performance of control charts have been revealed in many scientific papers (Stoumbos and Reynolds, 2000; Castagliola, and Tsung, 2005; Alwan and Roberts, 1988; Bisgaard and Külahçı, 2005; Wheeler, 1991; Srinivasan, 2001; Vermat, 2006; Borror et. al., 1999; Montgomery, 2011; Montgomery, and Runger, 1997; Chou et. al., 1998; Reynolds and Lu, 1997; Lu and Reynolds, 1999; Zhang, 1997; Testik, 2005; Smeti, et. al., 2006, Psarakis and Papaleonida, 2007). It was reported in these works that, if the assumptions are not verified, the control limits determined would not be represent the process correctly and therefore, the resulted SPCs are interpreted wrong by the applicants and incorrect decisions are given about the process. If either of these assumptions is not confirmed, control limits estimated based on original data may not correctly capture the true unusual points. Hence, estimated control limits calculated by verifying assumptions would be incorrect and as a result control charts could be interpreted wrong in terms of their control limits and hence out of control points. To avoid these mistakes, the data should be checked for data normality and autocorrelation.

This research aimed to determine the control limits in terms of ash content for +18 mm clean coarse coal produced by heavy dense drum device. Some examples of SPC charts on different applications of coal production have been carried out by some researchers (Elevli, 2006; Elevli and Behdioğlu, 2006; Deniz and Umucu, 2013; Taşdemir, 2012, 2013 and 2016a). Some studies have also shown that both data normality and autocorrelation affect SPC results seriously in mining and mineral processing applications (Bhattacherjee and Samanta, 2002; Samanta and Bhattacherjee, 2001 and 2004; Elevli et. al., 2009; Taşdemir, 2012, 2013 and 2016a; Taşdemir and Kowalczuk, 2014).

The statistical properties of ash content data used in this research were investigated in detail by Taşdemir (2016b) and determined that the data obey to log normal distribution well instead of normal distribution and also not independent, i.e. autocorrelated. The autocorrelation between consequent ash content data was modelled best by ARIMA(1,0,1) model to achieve data independence (Taşdemir, 2016b). The control limits of SPC under data normality and independence assumptions and also under verification of these assumptions were presented and compared. As a result, correct control limits considering data normality and autocorrelation for the ash content of

+18 mm clean coal produced by heavy medium drum were determined and the correct out of control points were found by ARIMA residual chart.

Materials and Methods

To determine the control limits of ash content for +18 mm coarse clean coals data produced by heavy medium drum, daily data which were obtained in the year of 2010 were supplied by Ege Linyitleri İşletmesi (ELİ) for the Dereköy coal preparation plant in Soma, Turkey. This coal preparation plant has about 4.8 million ton/year coal production capacity. Fig. 1 shows the simplified flowheet of it from Şengül (2008) (Taşdemir, 2016b and 2016c). Rather detailed information about the production stage were given at the first part of this study (Taşdemir, 2016b) and also in (Taşdemir, 2016c). The +18 mm clean coarse coals are floated in the first compartment of the drum and it is shown with a star symbol in Fig. 1. Totally 355 ash content data obtained from the production in 2010 were used in order to determine its control limits.

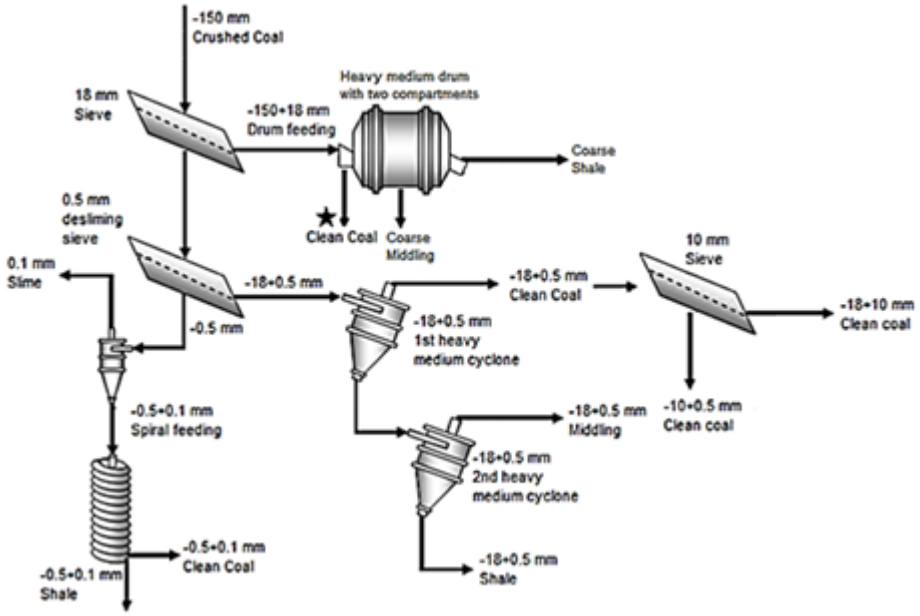

Figure 1. Modified flowsheet of Dereköy coal washing plant from Şengül (2008) and the +18 mm coarse clean coal product of heavy medium drum shown with a star symbol.

During the determination of the control limits of SPC charts, trial versions of Statgraphics XV and Minitab 16.0 softwares were used and SPC charts were generated. The data were found to obey lognormal distribution well to achieve data normality and the ARIMA(1,0,1)time series model was determined the best model based on its lowest AIC (Akaike Information Criterion) to remove autocorrelation (Taşdemir, 2016b). More detailed information for the determination of ARIMA time series models were already documented very well by Box and Jenkins (1976), Montgomery et al., (2008) and Montgomery & Runger (2011).

In this paper, the SPC charts generated under assumptions and verification conditions were presented in order to show the differences of results in terms of control limits and number of out of control points by using the data properties from Taşdemir (2016b).

Results and Discussion

Summary of statistical properties of ash content data

As stated above section, the ash content data have not obeyed normal distribution and lognormal distribution was suitable to make distribution normal (Taşdemir, 2016b). Fig. 2 compares the probability plots of normal and log transformed ash content data with resulted Anderson darling (AD) normality test statistics. The *p* value of normal distribution is very smaller than 0.05 (<0.005) indicating that the ash content data were not normally distributed. On the other hand, *p* value of log transformed ash content data distribution is 0.176 *(p>0.05)* showing that the data are represented by log normal distribution well after logarithmic transformation

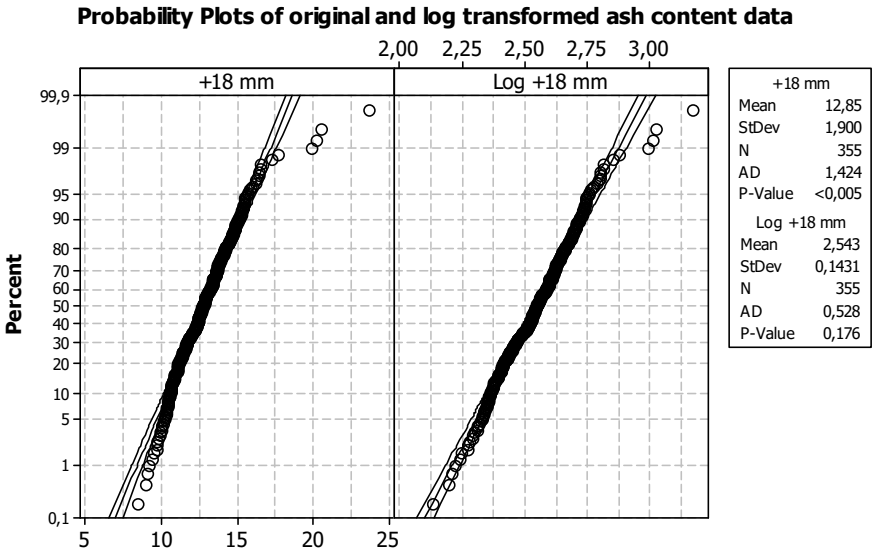

Figure 2. Probability plots of original and log transformed ash content data

Parameters of ARIMA time series model for log-transformed ash content data

After achieving data normality by log transformation, The log transformed ash content of +18 mm clean coal produced by heavy medium drum was found to be modelled by ARIMA(1,0,1) or ARMA(1,1) model well (Taşdemir, 2016b) and the details of model determination can be found there. Table 1 summarizes the ARIMA(1,0,1) model parameters.

Table 1: ARIMA(1,0,1) model summary for log-transformed ash content data (Taşdemir, 2016b)

Parameters	*Estimate*	*Stnd. Error*	*t*	*p value*
AR(1), ϕ	0.7688	0.074445	10.3271	0.000000
MA(1), θ	0.4609	0.102183	4.51042	0.000009
Mean, μ_0	2.5428	0.015762	161.324	0.000000
Constant, δ	0.5879			
WNV*, σ_a^2	0.0166	*: white noise variance		

The ARIMA (1,0,1) time series model is modelled by Eq. 1 as given the following (Castagliola and Tsung, 2005):

$$X_t = (1-\phi)\mu_0 + \phi X_{t-1} + \theta a_{t-1} + a_t \quad (1)$$

Where X_t is the observation at time t=1, 2, ,…, a_t is the random noise or white noise at time =1, 2, ,… which is assumed to have mean of zero (0) and standard deviation of σ_a, ϕ is the autoregressive parameter of the model which corresponds to p term in the model, θ is moving average parameter which corresponds to q term in the model and μ_0 is the nominal mean of the process (Castagliola and Tsung, 2005). The constant, δ, parameter in the model was calculated from $(1-\phi)\mu_0$.

By using these parameters, following ARIMA(1,0,1) time series model determined for the log transformed ash content of +18 mm clean coal produced by heavy medium drum is given in following Eq. 2 (Taşdemir, 2016b):

$$X_t = 0.5879 + 0.7688X_{t-1} + 0.4609a_{t-1} + a_t \quad (2)$$

Where, X_t is the log transformed ash content value at time, a_t is the random noise which have distribution of N(0, 0.1289).

Control limits under data assumptions

Table 2 summarizes the individual chart (I-chart) parameters obtained for the original ash content of +18 mm coarse coal under data assumptions, i.e. without data transformation and independence verification. Process sigma (σ) in Table 2 was estimated from average moving range ($\overline{MR}$) for the sample size of 2. The generated SPC and control limits under these assumptions is presented in Fig. 3. According to the Fig. 3, upper control limit (UCL) and lower control limit (LCL) were determined as 16.97 and 8.74 respectively while centre line (CL) or (CTR) was 12.85 which corresponded the mean of ash content data. Six points are out of control limits from UCL and one point is below the LCL.

If we assume that the ash content data had normal distribution and not autocorrelated, the observations of 31, 32, 53, 214, 347 and 348 were beyond the $+3\sigma$ while observation 208 was below the -3σ (Fig. 3).

Table 2: I-chart parameters of original ash content data of +18 mm clean coarse product by heavy medium drum

I-Chart Parameters	*Values*
$UCL=+3\sigma$	16.97
$CL=\bar{X}$	12.85
$LCL=-3\sigma$	8.74
$\sigma(\overline{MR}/1.128)$	1.37
$\overline{MR}$	1.55

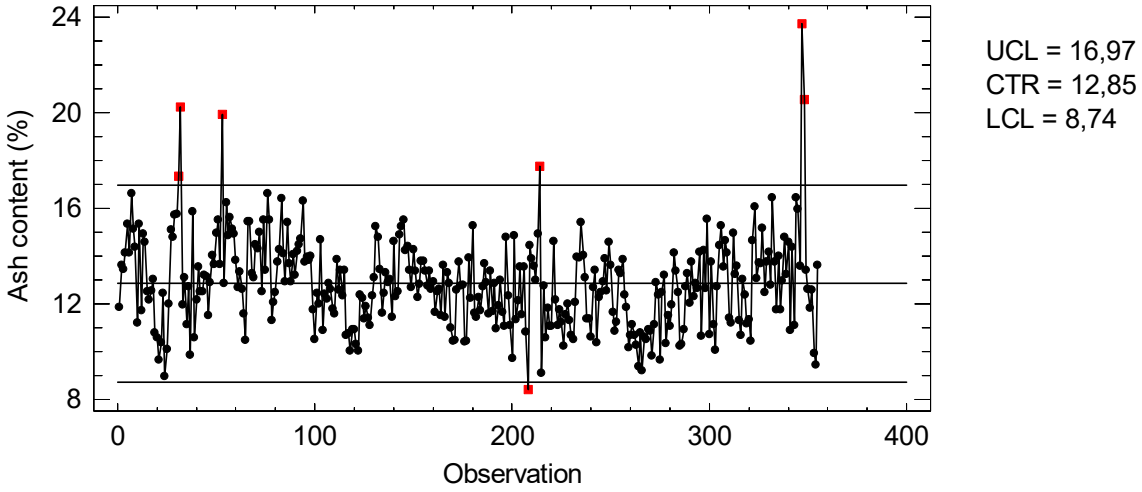

Figure 3. I-chart under normality and autocorrelation assumptions and its control limits

Control limits under verification of data normality and autocorrelation assumption

I-chart parameters after verifying the data normality by log transformation are presented in Table 2 with the corresponding original and transformed metric values. As presented in Fig. 2, the mean of log transformed ash content corresponded to 2.543 in transformed metric. Therefore, back transformed mean of ash content was equal to 12.72 in original metric.

Fig. 4 presents the control limits of ash content on SPC chart generated after data normality as in transformed metric in Fig. 4a and its back transformed metric, i.e. original unit in Fig. 4b. After log transformation, upper control limit (UCL), center line (CL) or (CTR) and lower control limit (LCL) are found as 2.86, 2.54 and 2.22 in logarithmic scale respectively. Since the log transformed values may not be meaningful or not be preferred, back transformed control limits are shown in Fig. 4b which shows the same out of control points with Fig. 4a. As seen in Fig. 4b, UCL and LCL are determined as 17.49 and 9.25 respectively. Compared to Fig. 3, the control limits are very different when the data normality is taken into account and data independence is just assumed. Larger control limits are obtained when data normality is achieved. Total number of out of control limits which beyond control limits are nine, five of them are beyond the UCL and four of them are below the LCL. These unusual points in Fig. 4a and 4b are different from the ones which are obtained in Fig. 3. The observations of 32, 53, 214, 347 and 348 are beyond $+3\sigma$ while observations of 24, 208, 215 and 266 are below -3σ.

Table 2: I-chart parameters of original ash content data of +18 mm clean coarse product by heavy medium drum

Parameters	*Transformed metric*	*Original metric*
$UCL=+3\sigma$	2.86	17.49
$CL=\ \bar{X}$	2.54	12.72
$LCL=-3\sigma$	2.22	9.25

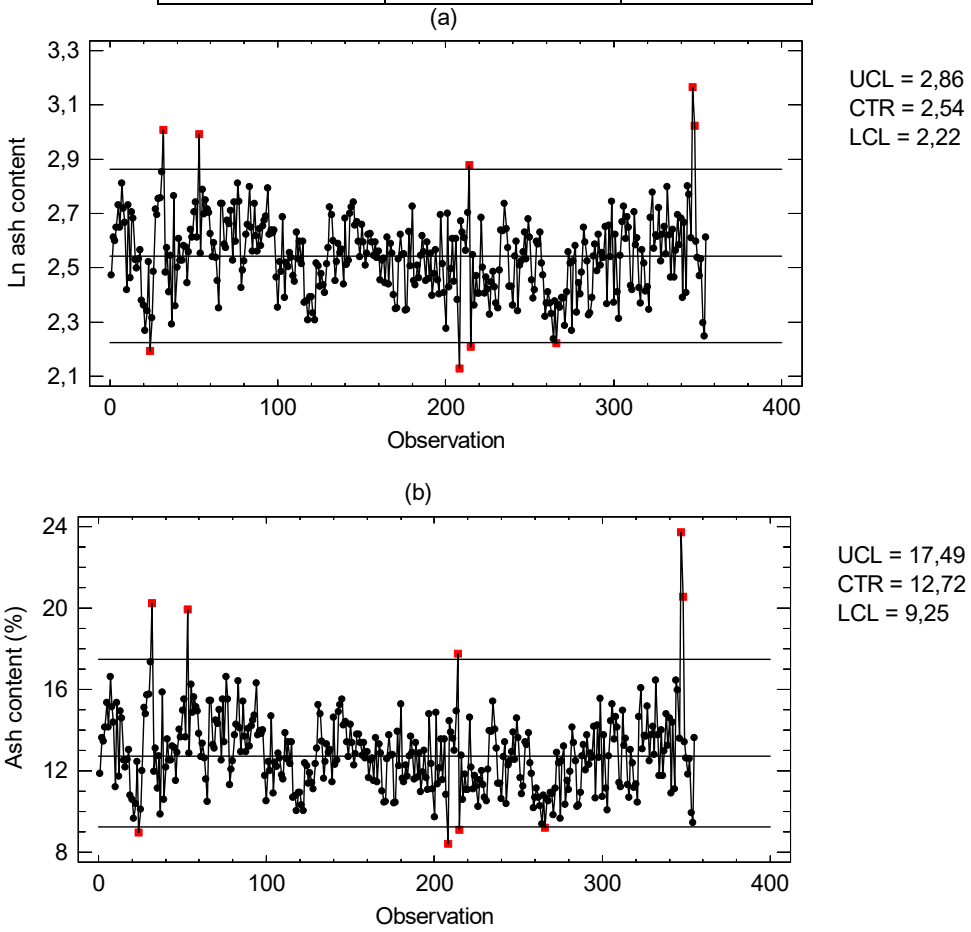

Figure 4. I-chart under normality verification and autocorrelation assumptions in transformed metric (a) and its back-transformed values of control limits in original metric (b)

Control limits under verification of both data normality and autocorrrelation

As stated above, data autocorrelation of log transformed ash content was removed successfully by ARIMA(1,0,1) time series model. While implementing control limits of SPC chart while considering autocorrelation, the process sigma, σ_x, was estimated from the both white noise or random shock and fitted ARIMA(1,0,1) model parameters (Table 1) for +18 mm clean coal product of heavy dense drum. In this chart, center line (CL) was estimated from the following formula;

$$CL = \mu_0 = \frac{\delta}{1-\phi} \quad (3)$$

The CL in Eq. 3 was determined from the parameters of ARIMA(1,0,1) model given in Table 1. Then, the control limits of data, UCL and LCL are drawn around centerline (CL) located at μ_0 by using the process sigma, σ_x;

$$\mu_0 \pm 3\sigma_x \quad (4)$$

The relation between the variance, σ_x^2, of the ARIMA(1,0,1) process, X_t, and the variation, σ_a^2, of the random noise, a_t, is calculated from the following Eq. 5 (Castagliola and Tsung, 2005):

$$\sigma_x^2 = \frac{1+\theta^2-2\phi\theta}{1-\phi^2}\sigma_a^2 \quad (5)$$

The variance of random shocks, σ_a^2, i.e. white noise variance in Eq. 5 can be estimated by both the mean squared error (*MSE*) of fitted AR(2) model and the mean range ($\overline{MR}$) of residuals (Polhemus, 2005). After solving Eq. 5, the variance of log-transformed ash content was about 1.23 times larger than the residual white noise variance ($\sigma_x^2 = 1.2318\sigma_a^2$).

The ARIMA(1,0,1) chart parameters where the random noise variance (σ_a^2) is estimated from the average moving range of ARIMA(1,0,1) residuals ($\overline{MR}$) and then process sigma (σ_x) was calculated by Eq. 5 was given in Table 3. The generated control charts are presented for log transformed metric in Fig. 5a and for back transformed metric in Fig. 5b.

Table 3: ARIMA chart parameters when the white noise variance, σ_a^2 was calculated by average moving range of ARIMA(1,0,1) residuals ($\overline{MR}$))

Parameters	*Transformed metric*	*Original metric*
UCL=$+3\sigma_x$	2.95	19.14
CL= μ_0	2.54	12.72
LCL=$-3\sigma_x$	2.14	8.45

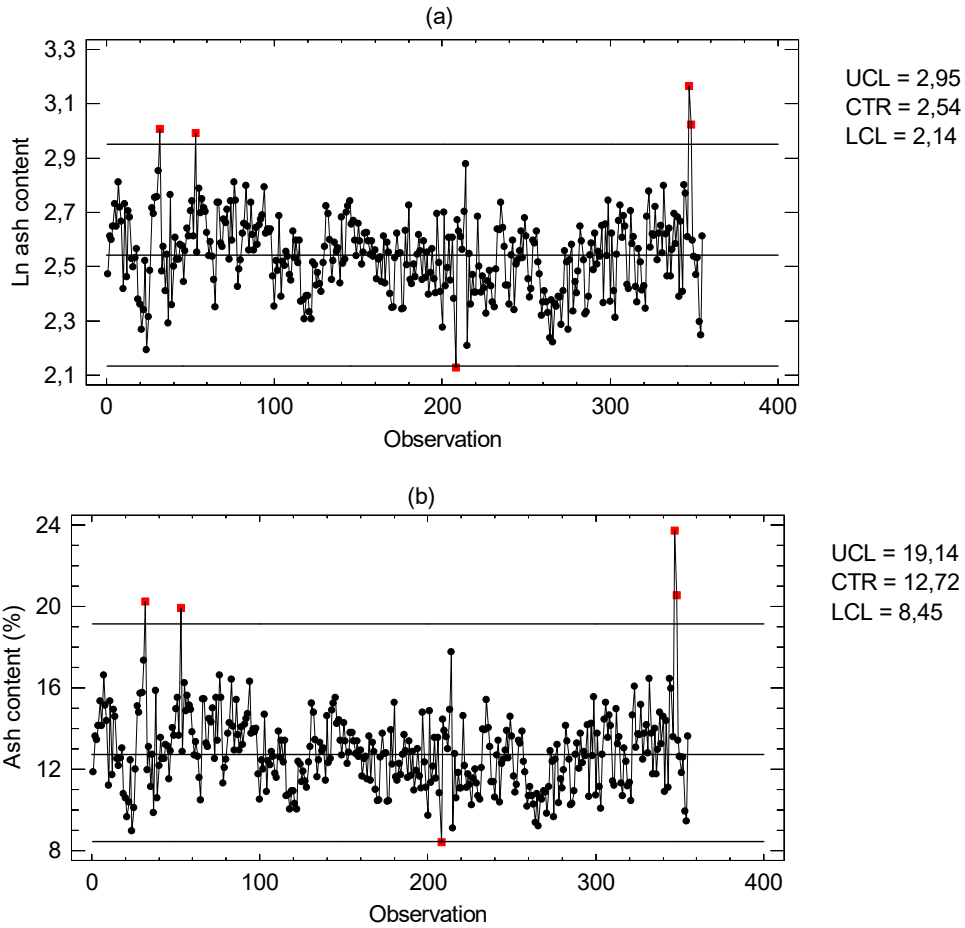

Figure 5. I-chart under normality and autocorrelation verification in transformed metric (a) and its back-transformed values of control limits in original metric (b) (white noise variance, σ_a^2 was calculated by average moving range of ARIMA(1,0,1) residuals ($\overline{MR}$))

Fig. 5a and 5b show the control limits of ash content where both normality and autocorrelation are verified. Compared to Fig 5 with Fig. 3 and Fig. 4, both control limits and out of control points are very different since the data normality and autocorrelation are taken into account when determining the control limits of ash content. The UCL and LCL were determined as 19.14 and 8.45 respectively when the data normality and autocorrelation are verified. The observations of 32, 53, 347 and 348 are beyond the $+3\sigma_x$ while the observation 208 was below the $-3\sigma_x$.

Table 4 shows the control limits of ash content determined for the ARIMA chart parameters when where white noise variance, σ_a^2 was calculated by the mean squared error, *MSE* to determine the process sigma, σ_x. The control limits of generated chart are considered as long term monitoring of the process (Polhemus, 2005). Polhemus (2005) indicates that this control limits are used to determine the process deviations from long-term mean more than expected given the dynamics of the process.

The control limits of ARIMA chart constructed in Fig. 6 shows the long term control limits for the +18 mm clean coarse coal by heavy dense drum. In this chart, process sigma, σ_x was estimated by Eq. 5 and white noise variance, σ_a^2 was calculated by *MSE* of ARIMA(1,0,1) model which was determined as σ_a = 0.1289 and given in Table 1 (Taşdemir, 2016b). As seen from the charts in Fig. 6a and 6b are considerably wider bounds than the charts in Fig. 5 and Fig. 4 since the estimated process σ_x is a function of both white noise or random shock and fitted ARIMA(1,0,1) model parameters (Table 1).

The UCL and LCL were determined as 19.56 and 8.27 for long term control limits. Total number of unusual points was four which are all beyond the UCL which corresponds to observations of 32, 53, 347 and 348.

Table 4: ARIMA chart parameters when white noise variance, σ_a^2 was calculated by *MSE* of ARIMA(1,0,1)

Parameters	*Transformed metric*	*Original metric*
$UCL=+3\sigma_x$	2.97	19.56
$CL=\ \mu_0$	2.54	12.72
$LCL=-3\sigma_x$	2.11	8.27

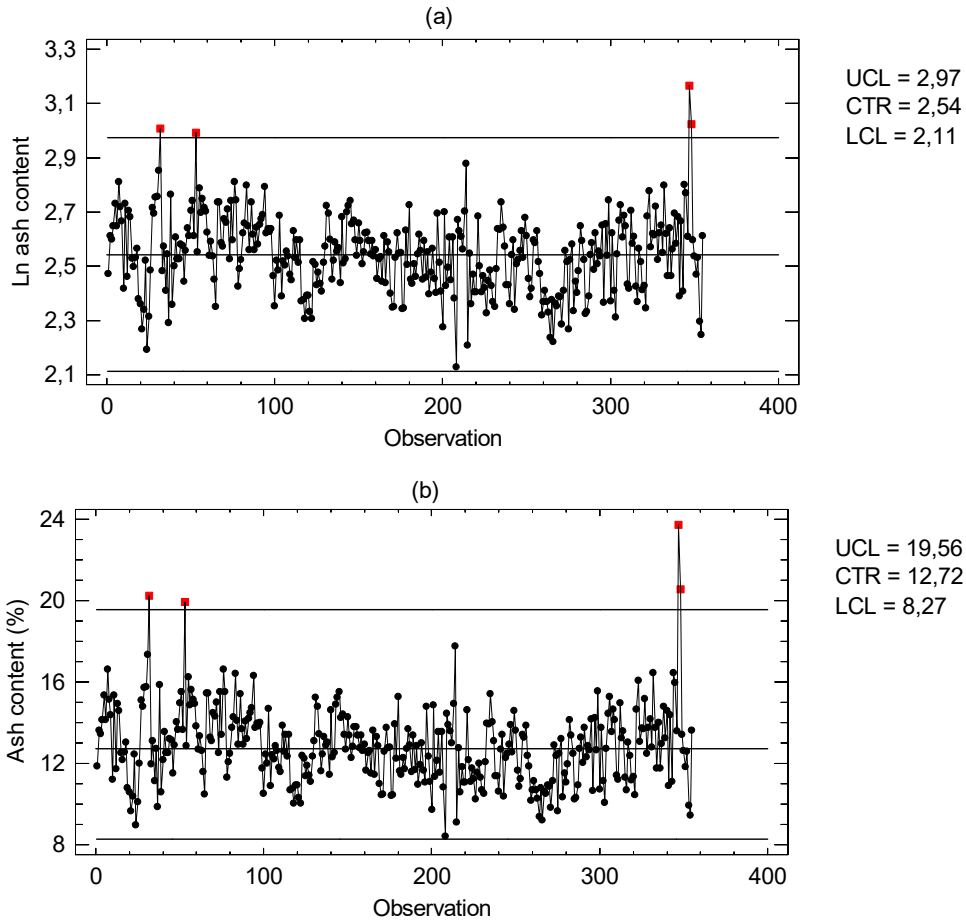

Figure 6. I-chart under normality and autocorrelation verification in transformed metric (a) and its back-transformed values of control limits in original metric (b) (white noise variance, σ_a^2 was calculated by *MSE* of ARIMA(1,0,1))

ARIMA residual chart of log-transformed ash content data

The ARIMA residuals charts were generated to detect real uncontrolled points of ash data. The ARIMA residuals were obtained from the difference between actual log transformed ash values and their forecasted values determined by ARIMA(1,0,1) model. The residuals, a_t, were calculated by rewriting the Eq. 2 as the following:

$$a_t = X_t - 0.5879 - 0.7688X_{t-1} - 0.4609a_{t-1} \quad (6)$$

Since a_t was determined to be independent and identically distributed (*i.i.d*) normal (0, σ_a), control limits of residuals, i.e., UCL and LCL which are drawn around centerline (CL) of zero (0) were calculated by the following Eq. 7 (Castagliola and Tsung, 2005):

$$CL = 0 \pm 3\sigma_a \quad (7)$$

The ARIMA residual chart, where σ_a is estimated from the residual mean of moving range ($\overline{MR}$), resulted for ash content is given in Fig. 7. From Fig. 7, number of points beyond $\pm 3\sigma_a$ limits are 3 which corresponds to observations of 53, 215 and 347. Since the aim is to reduce the ash content as soon as possible during the coal washing process, the out of point beyond LCL (observation 215) cannot be considered uncontrolled process point actually. Therefore, the process can be considered out of control for the 53rd and 347th days in terms of ash content and was in control for the rest days in 2010 based on the ARIMA residuals chart of Fig. 7.

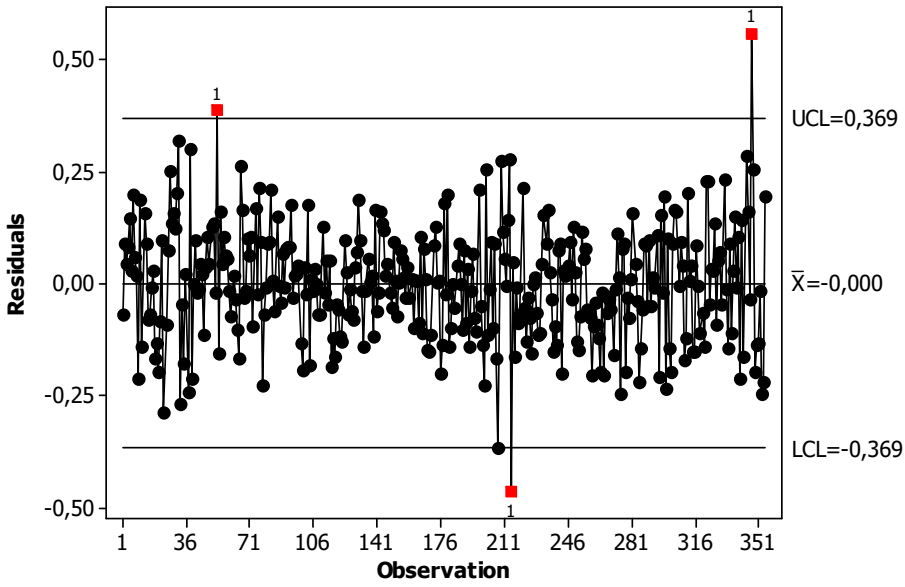

Figure 7. ARIMA residuals chart of ash content data

Conclusions

Control limits ıf ash content for the +18 mm clean coarse coal product produced by heavy medium drum was determined under data normality and data verification conditions. It was shown that the number of total out of control points were different if the assumptions were taken into account or not. In order to give right decision in monitoring and control of a process variable in terms of ash content, both data normality and autocorrelation should be verified prior to application of SPC charts. These can be done for the +18 mm clean coarse coal data by applying log transformation first to achieve data normality and then removing autocorrelation by ARIMA(1,0,1) time series model. Long term control limits were determined as 19.56 for the upper control limit and 8.27 for the lower control limit while center line was 12.72. Only two points were out of control which were determined by the ARIMA residuals chart in 2010 in terms of ash content. This result was different from the ones which were calculated by only assuming data normality and autocorrelation without verifying them.

Acknowledgement

Ege Linyitleri İşletmesi (ELİ) is gratefully acknowledged for providing the coal washing data used in this research

References

Alwan, L. C. & Roberts, H. V. (1988). Time series modeling for statistical process control, *Journal of Business and Economic Statistics,* vol. 6, pp. 86-95.

Bhattacherjee, A. & Samanta, B. (2002). Practical issues in the construction of control charts in mining applications, *The Journal of the South African Institute of Mining and Metallurgy,* pp. 173-180.

Bisgaard, S. & Külahçı, M. (2005). Quality quandaries: the effect of auto-correlation on statistical process control procedures," *Quality Engineering,* vol. 17, pp. 481-489.

Borror, C. M. Montgomery, D. C. & Runger, G. C. (1999). Robustness of EWMA control chart to non-normality, *Journal of Quality Technology*, vol. 31(3), pp. 309-316.

Box, G. E. P. & Jenkins, G. M. (1976). *Time Series Analysis Forecasting and Control*. Revised edition. Oakland, California, USA.

Castagliola, P. & Tsung, F. (2005). Autocorrelated SPC for non-normal situations, *Quality and Reliability Engineering International,* vol. 21, pp. 131-161.

Chou, Y. M. Polannsky, A. M. & Mason, R. L. (1998). Transforming nonnormal data to normality in statistical process control, *Journal of Quality Technology,* vol. 30(2), pp. 133-141.

Deniz, V. & Umucu, Y. (2013). Application of statistical process control for coal particle size, *Energy Sources, Part A: Recovery, Utilization, and Environmental Effects,* vol. 35(14), pp. 1306-1315.

Elevli, S. (2006). Coal quality control with control charts, *Coal Preparation*, vol. 26(4), pp. 181-199.

Elevli, S. & Behdioğlu, S. (2006). Determination of variation in coal quality by statistical process control techniques, *Madencilik,* vol. 45(3), pp. 19-26.

Elevli, S., Uzgören, N. & Savaş, M. (2009). Control charts for autocorrelated colemanite data, *Journal of Scientific & Industrial Research,* vol. 68, pp. 11-17.

Lu, C. W. & Reynolds, M.R. Jr., (1999). Control charts for monitoring the mean and variance of auto-correlated processes, *Journal of Quality Technology,* vol. 31, pp. 259-274.

Montgomery, D. C. (2011). *Introduction to Statistical Process Control*. 3rd edition. John Wiley & Sons, New York, NY.

Montgomery, D. C., Jennings, C. L. & Külahçı, M. (2008). *Introduction to Time Series Analysis and Forecasting*. Wiley Series in Probability and Statistics.

Montgomery, D. C., & Runger, G. C. (2011). Applied Statistics and Probability for Engineers, (p. 765), Wiley.

Polhemus, N. W. (2005). How to construct a control chart for autocorrelated data using Statgraphics Centurion, Available at http://www.statgraphics.fr/tele/Centurion/howto3.pdf.

Psarakis, S. & Papaleonida, G. E. A., (2007). SPC procedures for monitoring autocorrelated processes, *Quality Technology & Quantitative Management,* vol. 4(4), pp. 501-540.

Reynolds, M. R. Jr. & Lu, C. W. (1997). Control charts for monitoring processes with autocorrelated data, *Nonlinear Analysis, Theory, Methods & Applications,* vol. 30(7), pp. 4059-4067.

Samanta, B. & Bhattacherjee, A. (2001). An investigation of quality control charts for autocorrelated data, *Mineral Resources Engineering,* vol. 10, pp. 53-69.

Samanta, B. & Bhattacherjee, A. (2004). Problem of nonnormality in statistical process control: A case study in a surface mine, *The Journal of the South African Institute of Mining and Metallurgy,* pp, 257-264.

Smeti, E. M.,Kousouris, L. P., Tzoumerkas, P. C. & Golfinopoulos, S. K. (2006). Statistical process control techniques on auto-correlated turbidity data from finished water tank, Presented paper at *International Conference on Water Science and Technology Integrated Management on Water Resources*., Athens, Greece.

Srinivasan, A., (2001). *Application of information technology and statisitcal process control in pharmaceutical quality assurance & compliance*, Master's Thesis, Massachusettes Institute of Technology.

Stoumbos, Z. G. B. & Reynolds, Jr. M. R. (2000). Robustness to non-normality and auto-correlation of individuals control charts, *Journal of Statistical Computation and Simulation,* vol. 66(2), pp. 145-187.

Şengül, C. O. (2008). *Performance Evaluation of TKI-GLI Ömerler Coal Washing Plant*, Hacettepe University, Mining Engineering Department, Master Science Thesis, (Turkish text).

Taşdemir, A. (2012). Effect of autocorrelation on the process control charts in monitoring of a coal washing plant, *Physicochemical Problems of Mineral Processing,* vol. 48(2), pp. 495-512.

Taşdemir, A. (2013). Application of ARIMA Residuals Chart for Spiral at A Coal Preparation Plant, 23rd International Mining Congress of Turkey, Antalya, Turkey, pp. 1199-1209.

Taşdemir, A. & Kowalczuk, P. B. (2014). Application of statistical process control for proper processing of the fore-sudetic monocline copper ore, *Physicochemical Problems of Mineral Processing,* vol. 50(1), pp. 249-264.

Taşdemir, A. (2016a). Statistical Process Control of Ash Content for -10+0.5 mm Coal Product of Heavy Medium Cyclone, *3rd International Conference on Advanced Technology & Sciences (ICAT'2016),* Konya, Turkey, pp. 1418-1423.

Taşdemir, A. (2016b). Prediction of Ash Content for Coarse Clean Coal Prepared with Heavy Medium Drum by ARIMA(1,0,1) Model, *International Sciences and Technology Conference, ISTEC 2016,* Vienna, Austria, PP. 832-839.

Taşdemir, A. (2016c). Estimation of coal ash content washed in heavy medium cyclone by ARIMA time series model, 1st International Conference on Engineering Technology and Applied Sciences, Afyonkarahisar, Turkey, pp. 1399-1406.

Testik, M. C. (2005). Model inadequacy and residuals control charts for auto-correlated processes, *Quality and Reliability Engineering International,* vol. 21, pp. 115-130.

Vermat, M. B. (2006). Statistical process control in non-standard situations, Instituut Voor Bedrijfs En Industriele Statistiek.

Wheeler, D. J. (1991). *Shewhart's charts: myths, facts and competitors*, Paper presented at the 45th Annual Quality Congress Transactions ASQC.

Zhang, N. F. (1997). Detection capability of residual control chart for stationary process data, *Journal of Applied Statistics,* vol. 24(4), pp. 475-492.

FACTORS PROMOTING *STAPHYLOCOCCUS AUERUS* DISINFECTION BY TiO_2, SiO_2 AND AG NANOPARTICLES

Merve ÖZKALELİ and Ayça ERDEM*

Akdeniz University, Department of Environmental Engineering, Antalya, Turkey

ayerdem@akdeniz.edu.tr

Abstract: The use of conventional disinfection products and methods in drinking water treatment continue to fail in many undeveloped countries. Those applications need to be re-evaluated and innovative approaches to be considered to enhance the reliability and robustness of disinfection while avoiding disinfection byproducts (DBPs) formation. The rapid growth in nanotechnology has prompted significant interest in the environmental applications of nanoparticles (NPs). In order to understand the antibacterial effect of NPs, *Staphylococcus aureus* treated with TiO_2, SiO_2 and Ag NPs were studied under ambient conditions. The results indicated that the most bactericidal effect with specific die-off rates of 0,003 L/mg (TiO_2 NPs) and 0,002 L/mg (Ag NPs) were defined in the absence and the presence of photoactivation, respectively. Moreover, as ionic strength of the test media increases from 10 to 100 mM, NP-NP and NP-bacteria interactions were negatively affected.

Keywords: Disinfection, TiO_2, SiO_2, Ag, Nanoparticles, *Staphylococcus aureus*

Introduction

Among many pathogenic bacteria, Gram (+) *Staphylococcus aureus* are highly infectious and are commonly cause skin, bone and joint infections, and gastrointestinal illness in humans (Lowy 1998, Kadariya 2014). To overcome the potential serious consequences of those infectious pathogens, new technologies and materials for disinfection purposes have been proposed (Hu 2006, Parnia 2009, Oliveira 2014). The conventional disinfectants (i.e. chlorine, ozone, chlorine dioxide and chloramines) known to produce carcinogenic disinfection byproducts (DBPs) (Nieuwenhuijsen 2000, Krasner 2009). Advanced oxidation processes (AOPs) can be applied to reduce the formation of DBPs, to inactivate water pathogens and to mineralize the refractory organic compounds (Chong 2010). Among these AOPs, photocatalytic nanoparticle (TiO_2, ZnO, Fe_2O_3, etc. NPs employing systems have been highly effective on disinfecting the pathogenic bacteria. Matsunaga et al. (1985) reported for the first time that TiO_2 photocatalyst could kill bacterial cells in water by UV illumination, which could generate reactive oxygen species (ROS) in water medium. Since then, numerous photocatalytic disinfection studies under UV light (Wei 1994, Christensen 2003, Gogniat 2006, Bonetta 2013) and fewer studies under solar light (Hu 2007, Helali 2014) using TiO_2 photocatalyst studies have been reported. In addition to those studies, TiO_2 NPs (Shah 2008, Xing 2012, Barnes 2013), TiO_2 thin films (Kambala 2009), Ni doped TiO_2 NPs (Yadav 2014), Fe doped Ti-CNTs (Latif 2014), Ce_2O_3/ TiO_2 composites (Hassan 2012), Ag doped TiO_2 NPs (Kowal 2011), and Al_2O_3-TiO_2-Ag composites (Tartanson 2014) Ag-SiO_2 composite films (Lei 2014), Ag-SiO_2 particles (Sotiriou 2010), and polymer coated Ag NPs (Vukoje 2014), and nano-Ag ions (Feng 2000, Kim 2007, Jung 2008, Sotiriou 2010) were employed to inactivate *S. aureus* and other pathogenic bacteria.

The objective of this study was to evaluate the disinfection efficiency of TiO_2, SiO_2 and Ag NPs on Gram (+) *S. aureus.* Batch experiments were conducted to determine (a) the most antibacterial NP concentrations, (b) the effect of water chemistry on the antibacterial activity of NPs, and (c) the effect of both absence and presence of light on the inactivation of bacteria.

Materials and Methods

Culture of microorganisms: The Gram (+) *Staphylococcus aureus* (ATCC 43300) were cultivated in 100 mL of Luria-Bertani (LB) broth at 37°C on a rotary shaker (150 rpm) for 18 h. The cultures with an initial population of $10^6 \pm 10^2$ CFU mL^{-1} were used in the experiments.

Nanoparticles: Commercially obtained TiO_2, SiO_2 and Ag NPs were used in the experiments (Table 1). A 1000 mg/L stock suspension for each NP was prepared in 0, 10, 50 and 100 mM of deionized water using Na_2HPO_4, KH_2PO_4, NH_4Cl, and NaCl immediately before the experiments. The final concentrations of 10, 100 and 500 mg

L^{-1} NPs were prepared by serially diluting of the stock suspensions having different ionic strength. All experiments were conducted in continuously shaken aqueous slurry solutions to ensure mixing and to prevent settling of the NPs. The bacteria were added to the suspensions immediately prior to the disinfection runs.

Table 1. Nanoparticles used in the experiments.

Nanoparticle	Particle Size (nm)	Surface Area (BET, m^2g^{-1})	Physical appearance
TiO_2 (Anatase)	32	45	White powder
SiO_2	10 - 20	NA	White powder
n-Ag	20 - 40	NA	Black powder

Exposure experiments: To determine the effect of particle concentration and ionic strength of the solutions on the survival of bacteria, dose-response experiments were conducted. Forty five mLs of NP solutions and 5 mL of bacteria prepared in 0, 10, 50 and 100 mM sterile test media were added to each beaker to make initial NP concentrations of 0, 10, 100, and 500 mg L^{-1}. Four artificial light sources (color temperature of 4300 K, and total light intensity of 7000 lux), mimicking the spectrum of natural solar light, were placed 30 cm above the orbital shaker to produce light intensity of *2.1 W* cm^{-2}. The temperature inside the cabinet was maintained at 25.0 ± 1.5◦C. The shaker was set to mix at 150 rpm throughout all experiments. All antibacterial tests were triplicated in presence and absence of light lasted 1 h.

End point test: The numbers of viable cells were determined by LB agar plating. The plates were incubated at 37°C for 24 h, and then the colony counting was done using Lassany model digital colony counter. The survival fractions (N/N_0) and the specific die-off rates (k', Eq 1) (Erdem 2015) were calculated by the following equation:

$$k' \ (L \ \ mg^{-1}) = \frac{-\ln(N/N_0)}{C} \qquad \text{(Eq 1)}$$

where N_0 (CFU, colony forming unit) is the population of the control cultures, N (CFU) is the population of the NP exposed cultures after 1 h in presence and absence of light, and C (mg L^{-1}) is the NP concentration.

Results and Discussion

Nanoparticle characterization:
Particle size, surface area and zeta potential of the NPs were measured NP characterization results are shown in Table 2. Primary particle size results show the measured particle size directly sampled from the box. Nano-TiO_2 primary particle sizes measured by DLS were smaller than the measurement given by the manufacturer, whereas nano-SiO_2 primary particle sizes were bigger than that of the given size. Ag NPs showed an average size value of the primary particle size. It is clearly noted that the water chemistry of the test media affects the NP size. When 10 mM test media was used, the average particle sizes showed a 10 - 15× increase. This result is also confirmed with the SEM images of TiO_2, SiO_2 and Ag NPs that the NP aggregation in test media and NP particle sizes in µm range were observed (Figure 1). The obtained surface areas were inversely correlated to the particle sizes as expected. Zeta potential results showed that the NPs were negatively charged and were not stable in the test media.

Table 2. Characterization results of the TiO_2, SiO_2 and Ag nanoparticles used in the experiments.

	TiO_2	SiO_2	n-Ag
Primary Particle Size by DLS (nm)	26.4	27.7	30.9
Primary Surface Area (BET, m^2g^{-1})	176.34	103.72	92.16
Zeta Potential at pH 6.5 (mV)	-20.3	-17.2	-11.1
Particle Size by DLS (nm) (10 mM, pH 6.5)	287±25	421±19	342±38

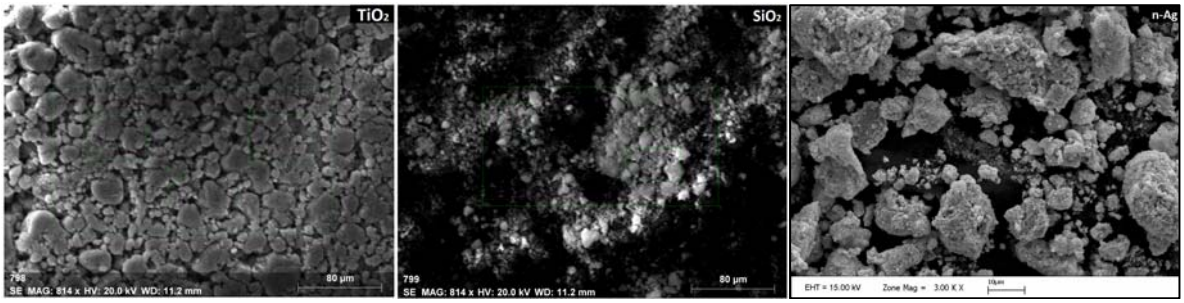

Figure 1. SEM images of TiO_2, SiO_2 and Ag nanoparticles.

Effect of nanoparticle concentration and light:

Four different TiO_2, SiO_2 and Ag NP concentrations (10, 100, 500 and 1000 mgL^{-1}), dark and light (light intensity: *2.1 W cm*$^{-2}$) conditions were used to evaluate the effect of NP concentrations and light on the survival of *S. aureus*. The results given in Table 3 show that regardless of NP type, the mortality rate of the bacteria increased when both NP concentrations increased and changing the light condition from dark to light, especially when 10 mM ionic strength of test media was used. The most effective antibacterial NP concentration in presence of light was confirmed as 1000 mg L^{-1} of TiO_2. In absence of light, when NP concentration increased, the most increase in mortality rates were observed as 57 % (500 mg L^{-1}), 47 % (500 mg L^{-1}) and 40% (1000 mg L^{-1}) in TiO_2, n-Ag and SiO_2 NP setups, respectively. The effects of SiO_2 NPs on bacterial viability were as low as 40 and 56% in absence and presence of light, respectively. TiO_2 NPs were more effective on the *S. aureus* bacteria than n-Ag and SiO_2 NPs in both absence and presence of light.

Table 3. The effect of nanoparticle concentration on the survival of *S. aureus* in absence and presence of light. (Ionic strength: 10 mM, light intensity: *2.1 W cm*$^{-2}$)

NP Concentration (mgL^{-1})	Death (%)					
	TiO_2		SiO_2		Nano-Ag	
	Dark	Light	Dark	Light	Dark	Light
10	13	75	32	33	32	41
100	45	57	27	30	34	49
500	57	76	23	52	47	75
1000	47	93	40	56	32	47

The survival ratios (N/N_0) of the *S. aureus* treated with TiO_2, SiO_2 and Ag NPs under dark (a) and light (b) conditions are depicted in Figure 2. At each concentration of NPs, k' was determined by Eq 1 for both dark/light conditions and ionic strength condition. k' values were averaged (k'_{ave}), where lower k'_{ave} value means higher antibacterial effect. In absence of light, the lowest k'_{ave} values of TiO_2, SiO_2 and n-Ag NPs were calculated as 0.003 L mg^{-1} (0 mM), 0.010 L mg^{-1} (10 mM) and 0.004 L mg^{-1} (50 mM), respectively. The lowest k'_{ave} values of 0.004 L mg^{-1} (50 mM), 0.010 L mg^{-1} (100 mM) and 0.002 L mg^{-1} (10 mM) were calculated when bacteria were exposed to TiO_2, SiO_2 and n-Ag NPs, respectively. The results in Figure 2 show that *S. aureus* was sensitive when lower ionic strength media was used in absence of light. Higher bacterial sensitivity in absence of light may be linked to the release of metal ions or NP-specific mechanisms (Cumberland 2009; Gottschalk 2011; Dobias 2013).

Figure 2. The effect of ionic strength and TiO_2, SiO_2 and Ag nanoparticle concentrations on *S. aureus* under dark (a) and light (b) conditions.

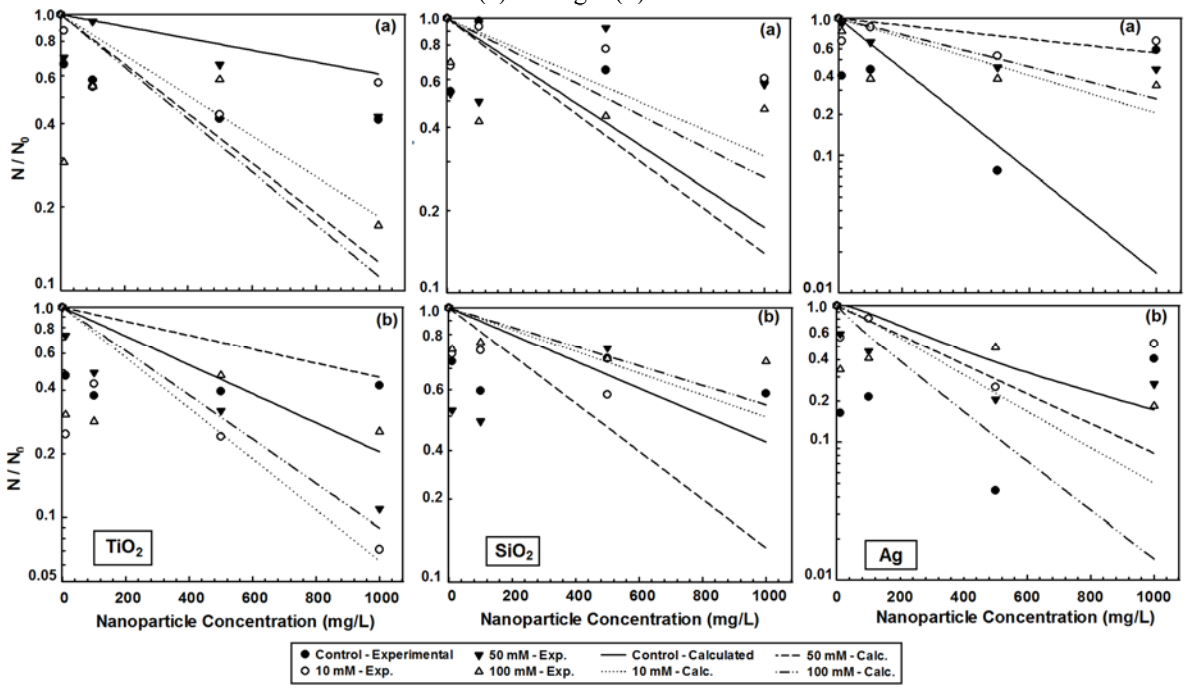

Figure 2 also shows the curve fits obtained from the calculated survival fractions. In order to implement those values, experimentally verified k'_{ave} values were used in Eq 1 and then the calculated survival fractions were estimated. R^2 values were presented in order to correspond the curve fits with experimental results. Highest correspondence ($R^2 = 0.9194$) was observed when *S. aureus* was exposed to TiO_2 NPs under dark, while lowest correspondence ($R^2 = 0.5625$) was observed when SiO_2 NPs were employed. In presence of light, lowest R^2 value of 0.4626 was calculated from bacteria- SiO_2 NPs reactions and highest R^2 value of 0.9563 was observed when *S. aureus* was exposed to nano-Ag particles.

Conclusion

In order to define the factors promoting the disinfection of the *S. aureus* specific die-off rates (k') of the NPs were calculated and were used in this study. It was clearly revealed that TiO_2, SiO_2 and Ag NPs promoted the inactivation of *S. aureus* in both absence and presence of light conditions. The bacteria showed higher sensitivity to TiO_2 and Ag NPs than SiO_2 NPs respectively. The SEM images confirmed that the aggregation/agglomeration of the NPs in test media with different ionic strengths negates the antibacterial activity of the NPs. Therefore, effect of water chemistry on dispersion and retention of NPs needed to be considered. Moreover due to the conduction of the experiments in a relatively clean laboratory conditions, the sustainability of antimicrobial activities of NPs in natural or waste water need to be clarified. Therefore, more research should be conducted to further assess the applicability and sustainability of NPs in disinfection processes.

References

Barnes, R., Molina, R, Xu, JB, Dobson, PJ, Thompson, IP (2013). "Comparison of TiO_2 and ZnO nanoparticles for photocatalytic degradation of methylene blue and the correlated inactivation of gram-positive and gram-negative bacteria." J Nanopart Res 15(2): 1432.

Bonetta, S., Bonetta, S, Motta, F, Strini, A, Carraro, E. (2013). "Photocatalytic bacterial inactivation by TiO_2-coated surfaces." AMB Express 3(59): 8 pages.

Chong, M., Jin, B, Chow, CWK, Saint, C (2010). "Recent developments in photocatalytic water treatment technology: A review." Water Res 44: 2997-3027.

Christensen, P., Curtis, TP, Egerton, TA, Kosa, SAM, Tinlin, JR (2003). "Photoelectrocatalytic and photocatalytic disinfection of *E. coli* suspensions by titanium dioxide " Appl Cat B 41: 376-386.

Feng, Q., Wu, J, Chen, G, Cui, F, Kim, T, Kim, J (2000). " A mechanistic study of the antibacterial effect of silver ions on *Escherichia coli* and *Staphylococcus aureus*." J Biomed Mater Res 52: 662-668.

Gogniat, G., Thyssen, M, Denis, M, Pulgarin, C, Dukan, S (2006). "The bactericidal effect of TiO_2 photocatalysis involves adsorption onto catalyst and the loss of membrane integrity." Fems Microbiol Let 258(1): 18-24.

Hassan, M., Amna, T, Al-Deyab, SS, Kim, HC, Oh, TH, Khil, MS (2012). "Toxicity of Ce_2O_3/TiO_2 composite nanofibers against *S. aureus* and *S. typhimurium*: A novel electrospun material for disinfection of food pathogens." Colloids and Surfaces A 415 268-273.

Helali, S., Polo-López, MI, Fernández-Ibánez, P, Ohtani, B, Amanoc, F, Malato, S, Guillard, C (2014). "Solar photocatalysis: A green technology for *E. coli* contaminated water disinfection. Effect of concentration and different types of suspended catalyst." J Photochem Photobiol A: Chem 276: 31-40.

Hu, C., Guo, J, Qu, J, Hu, X. (2007). "Photocatalytic degradation of pathogenic bacteria with AgI/TiO_2 under visible light irradiation." Langmuir 23: 4982-4987.

Hu, C., Hu, X, Guo, J, Qu, J. (2006). "Efficient destruction of pathogenic bacteria with NiO/ $SrBi_2O_4$ under visible light irradiation." Environ. Sci. Technol. 40: 5508-5513.

Jung, W., Koo, H, Kim, K, Shin, S, Kim, S, Park, Y (2008). "Antibacterial activity and mechanism of action of the silver ion in Staphylococcus aureus and *Escherichia coli*." Appl Environ Microbiol 74: 2171-2178.

Kadariya, J., Smith, TC, Thapaliya, D (2014). "*Staphylococcus aureus* and Staphylococcal Food-Borne Disease: An Ongoing Challenge in Public Health." BioMed Research International 2014(Article ID 827965): 9 pages.

Kambala, V., Naidu, R (2009). "Disinfection Studies on TiO_2 Thin Films Prepared by a Sol-Gel Method." J Biomed Nanotechnol 5(1): 121-129.

Kim, J., Kuk, E, Yu, K, Kim, J, Park, S, Lee, H, Kim, S, Park, Y, Park, Y, Hwang, C, Kim, Y, Lee, Y, Jeong, D, Cho, M (2007). "Antimicrobial effects of silver nanoparticles." Nanomed Nanotechnol 3: 95-101.

Kowal, K., Wysocka-Krol, K, Kopaczynska, M, Dworniczek, E, Franiczek, R, Wawrzynska, M, Vargova, M, Zahoran, M, Rakovsky, E, Kus, P (2011). "In situ photoexcitation of silver-doped titania nanopowders for activity against bacteria and yeasts." J Colloid Interface Sci 362 (1): 50-57.

Krasner, S. (2009). "The formation and control of emerging disinfection by-products of health concern." Phil. Trans. R. Soc. A 367: 4077-4095.

Latif, W., Qazi, IA, Hashmi, I, Arshad, M, Nasir, H, Habib, A (2014). "Novel Method for Preparation of Pure and Iron-Doped Titania Nanotube Coated Wood Surfaces to Disinfect Airborne Bacterial Species *Pseudomonas aeruginosa* and *Staphylococcus aureus*." Environ Eng Sci 31(12): 681-688.

Lei, L., Liu, X,Yin, YQ, Sun, Y, Yu, M, Shang, J (2014). "Antibacterial Ag-SiO_2 composite films synthesized by pulsed laser deposition." Materials Lett 130: 79-82.

Li, Q., Mahendra, S, Lyon, DY, Brunet, L, Liga, MV, Li, D, Alvarez, PJJ (2008). "Antimicrobial nanomaterials for water disinfection and microbial control: Potential applications and implications." Water Research 42 4591-4602.

Lowy, F. (1998). "Medical progress: Staphylococcus aureus infections." The New England Journal of Medicine 339(8): 520-532.

Matsunaga, T., Tomoda, R, Nakajima, T, Wake, H. (1985). "Photoelectrochemical sterilization of microbial cells by semiconductor powders." FEMS Microbiol. Lett. 29 211-214.

Nieuwenhuijsen, M., Toledano, MB, Eaton,NE, Fawell, J, Elliott, P. (2000). "Chlorination disinfection byproducts in water and their association with adverse reproductive outcomes: a review." Occup Environ Med 57: 73-85.

Oliveira, P., Souza, SG, Campos, GB, da Silva, DCC, Sousa, DS, Araújo, SPF, Ferreira, LP, Santos, VM, Amorim, AT, Santos, AMOG, Timenetsky, J, Cruz, MP, Yatsuda, R, Marques, LM. (2014). "Isolation, pathogenicity and disinfection of *Staphylococcus aureus* carried by insects in two public hospitals of Vitória da Conquista, Bahia, Brazil." Braz J Infect Dis 18(2): 129-136.

Parnia, F., Hafezeqoran, A, Moslehifard, E, Mahboub, F, Nahaei, M, Dibavar, MA. (2009). "Effect of Different Disinfectants on *Staphylococcus aureus* and *Candida albicans* Transferred to Alginate and Polyvinylsiloxane Impression Materials " Journal of Dental Research, Dental Clinics, Dental Prospects 3(4): 122-125.

Shah, R., Kaewgun, S, Lee, BI, Tzeng, TRJ (2008). "The Antibacterial Effects of Biphasic Brookite-Anatase Titanium Dioxide Nanoparticles on Multiple-Drug-Resistant *Staphylococcus aureus*." J Biomed Nanotechnol 4(3): 339-348.

Sotiriou, G., Pratsinis, SE (2010). "Antibacterial Activity of Nanosilver Ions and Particles." Environ Sci Technol 44(14): 5649-5654.

Tartanson, M., Soussan, L, Rivallin, M, Chis, C, Penaranda, D, Lapergue, R, Calmels, P, Faur, C (2014). "A new silver based composite material for SPA water disinfection." Water Res 63: 135-146.

Vukoje, I., Dzunuzovic, ES, Vodnik, VV, Dimitrijevic, S, Ahrenkiel, SP, Nedeljkovic, JM (2014). "Synthesis, characterization, and antimicrobial activity of poly(GMA-co-EGDMA) polymer decorated with silver nanoparticles." J Materials Sci 49(19): 6838-6844.

Wei, C., Lin, WY, Zainal, Z, Williams, NE, Zhu, K, Kruzic, AP, Smith, RL, Rajeshwar, K. (1994). "Bactericidal activity of TiO_2 photocatalyst in aqueous media: toward a solar-assisted water disinfection system." Environ. Sci. Technol. 28 934-938.

Xing, Y., Li, XH, Zhang, L, Xu, QL, Che, ZM, Li, WL, Bai, YM, Li, K (2012). "Effect of TiO_2 nanoparticles on the antibacterial and physical properties of polyethylene-based film." Prog Org Coatings 73 (2-3): 219-224.

Yadav, H., Otari, SV, Bohara, RA, Mali, SS, Pawar, SH, Delekar, SD (2014). "Synthesis and visible light photocatalytic antibacterial activity of nickel-doped TiO_2 nanoparticles against Gram-positive and Gram-negative bacteria." J Photochem Photobiol: A Chem 294 130-136.

FRICTION WELDING OF AL 7075 ALLOY AND 316 L STAINLESS STEEL

Osman TORUN

Afyon Kocatepe University, Bolvadin Vocational School, Afyonkarahisar, Turkey

otorun@aku.edu.tr

Abstract: Friction welding of Al 7075-T6 alloy and 316 L stainless steel carried out for different times under a constant friction and forging pressure, a forging time, rotational speeds. Microstructures of the welds were examined by scanning electron microscopy and optical microscopy. The results showed that all of the welded samples were free of any or crack along the weld interface. The chemical compositions of the interface of the welded joints were determined by using energy dispersive spectroscopy. The micro hardness of the welded samples was measured. The strength of the welds was determined by the shear tests. It was observed that the shear strength of the welds depended on the welding time. The maximum shear strength was 210, 7 MPa.

Keywords: Al7075, 316 L Stainless steel, Friction welding

Introduction

Cr–Ni austenitic stainless steels, especially, AISI 316 exhibit considerably better corrosion resistance than martensitic or ferritic steels and also have excellent strength and oxidation resistance at elevated temperatures (Kumar 2014, Kumar 2015, Marshal 1984, Oshima 2007). The fusion weld of these steels is usually the part of a system with reduced corrosion resistance and low-temperature toughness, and therefore in many cases it is the limiting factor for material application. The heat of fusion welding also leads to grain coarsening in the heat-affected zone and solidification cracking in the weld metal of stainless steels (ASM Handbook 1999). Aluminum is currently the most widely used metallic material besides steel. The mechanical characteristics of aluminum offer an increasing application field, especially where lightweight constructions are required (Kurt 2007, Lugscheider 1995) Al 7075-T6 alloy which is used in this study has low specific weight, high strength-to-weight ratio, as well as high electrical and thermal conductivity.

Friction welding is well known among solid-state welding methods and used for welding similar and dissimilar materials (Satyanarayana 2005, Torun 2011, Çelikyürek 201, Ates 2007). This method is very useful for the welding of dissimilar combination, and the welding process is easily automated. Also, this welding method has several advantages over fusion welding methods such as high energy efficiency, narrower heat affected zone (HAZ), and low welding cost. In particular, the friction welding is able to easily produce joints with high reliability; it is widely used in the automobile industry and applied to fabricate important parts such as drive shafts and engine valves. Moreover, this welding method can also provide the joint of dissimilar combination as well as the circular pipe. Some researchers have reported that the mechanical and metallurgical properties of the friction-welded joints of circular pipes of dissimilar combination show desirable characteristic (Wang 1975, Maalekian 2007, Kimura 2016)

Materials and Methods

Al 7075-T6 alloy and AISI 316 L stainless steel were received from a private company. The cylindrical samples 50 mm in length and 8 mm in diameter were machined from 316 L stainless steel and Al 7075-T6 alloy. The friction welding experiments were carried out by a continuous-drive friction welding machine for different times under a constant friction and forging pressure, a forging time and a rotational speed (Table 1). After welding, the welded samples were cut perpendicular to the welding interface. The surfaces of the welded samples were ground with 1200 grinding paper and polished with 1 µm diamond paste, then 316 L sides of welded samples were etched with a mixture of H2O (30 ml), HNO3 (30 ml), HCl (20 ml) and HF (20 ml) and The Al 7075-T6 sides were etched with Keller. The microstructures were observed with light microscopy and scanning electron microscopy (SEM). The chemical compositions of the weld zone and the base alloys were determined using energy dispersive spectroscopy (EDS). Microhardness values were measured to both sides from center of the

Table 1. Parameters of the friction welding.

Friction Speed, rmp	Friction Pressure, (MPa)	Forging Pressure (MPa)	Friction Time (s)	Forging Time (s)	Burn-off (mm)
1000	50	100	6	10	0,4
1000	50	100	8	10	0,9
1000	50	100	10	10	1,5
1000	50	100	12	10	2,2

welded samples by means of Vickers indenter with a load of 100 g. Shear tests were performed to determine the strength of the weld interface using an electromechanical universal test machine (Shimadzu AG-IS-250) at room temperature. A specially designed specimen holder was used to measure the shear strength. Three samples were tested for each welding condition.

Results and Discussion

Optical micrograph of the sample welded for 10 s is presented in Fig. 1. All of the welded samples were of sound quality, and they did not exhibit any pores or crack formation along the weld interface. Three main regions are observable on the Al 7075 side of the interface of all of the welded samples: a dynamically recrystallized zone with very fine grains (DRX), thermo-mechanically affected zone (TMAZ) and heat affected zone (HAZ) (Fig. 1a) (Khalid 2010). The width of the DRX for all of the welded samples was approximately 250-330µm. The micrographs demonstrated a slight variation in the width of DRX independent on the friction time. There was not any change on the 316 L stainless steel side (Fig. 1b).

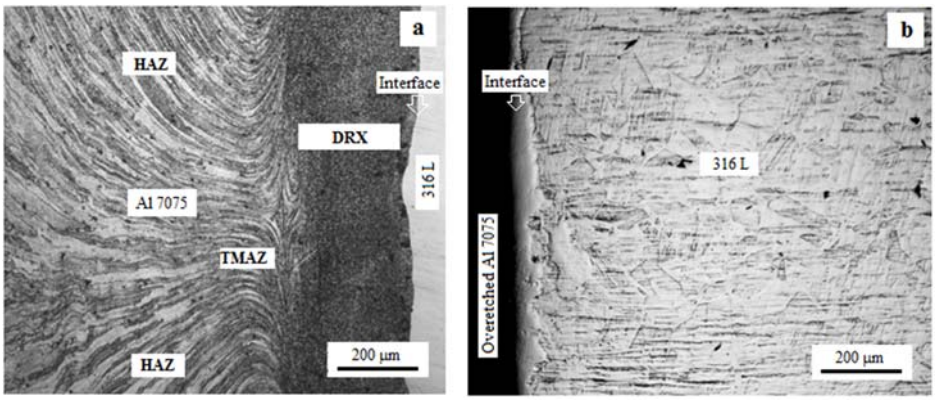

Figure 1.Optical micrograph of the sample welded for 10 s.

SEM micrograph and EDS analysis for welded samples for 10 s are shown in Fig. 2. It cannot be clearly observed that a diffusion zone at the weld interface for all of the welded samples (Fig 2a). However, EDS analysis results showed that there was a diffusion zone at the weld interface all the welded samples (Fig. 2b).

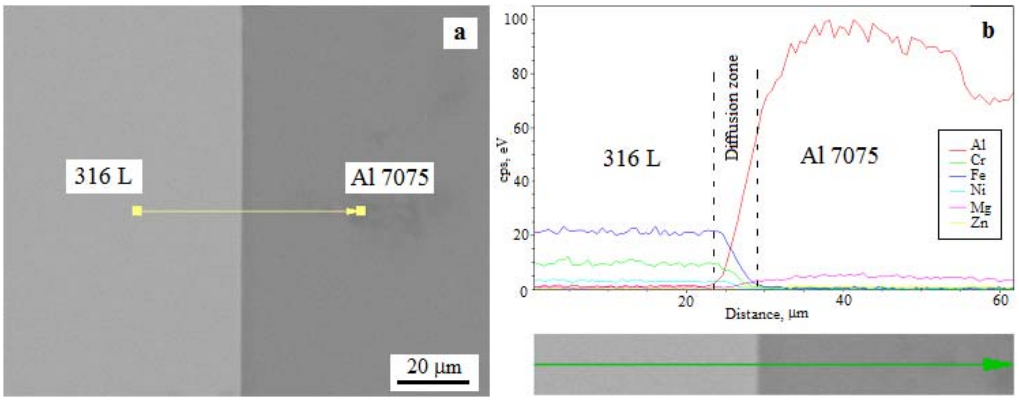

Figure 2.SEM micrograph and EDS analysis of welded samples for 10 s.

The diffusion zone present at the weld interface consists of Fe, Al, Cr, Ni, Mg atoms. The diffusion zone is rich in Fe and Al atoms and has lower amounts of Cr, Ni and Mg atoms.

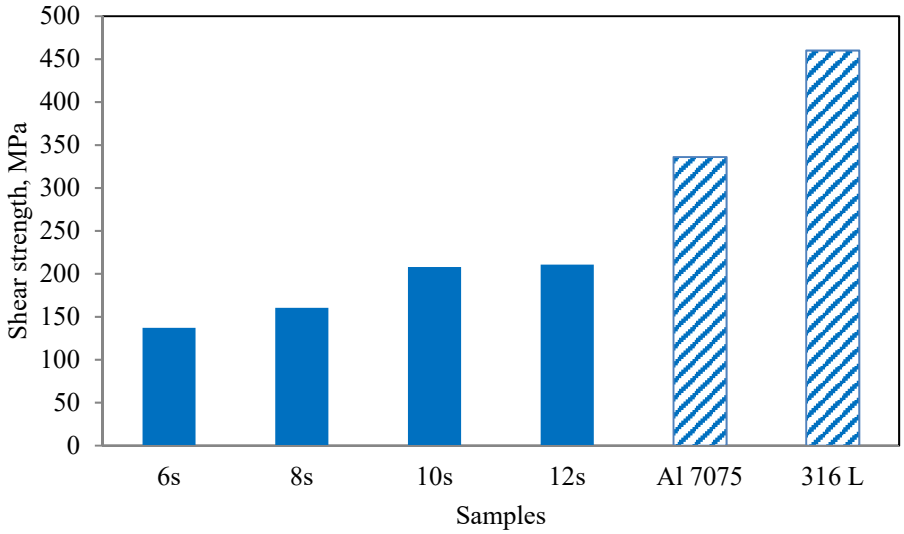

Figure 3.The shear strengths of the welds and the base alloys.

The shear strengths of the welds and the base alloys are shown in Fig. 3. The results showed that the values of the shear strength of the welded samples increase with increase in friction time. Under these experimental conditions, it can be said that the shear strength of welds was dependent on the friction time. This observation indicates that the increase in the shear strength is related to the magnitude of the accumulated heat input, which depends on the friction time. Especially, 6 s and 8 s friction times were not high enough to produce the required heat for the friction welding, compared with the 10 and 12 s treatments. Microhardness values were measured in the direction from the center of the weld to both sides of the welded samples. The micro hardness profiles for all of the friction welding times were found to be similar. Fig. 4 shows the hardness values obtained from all welded samples.

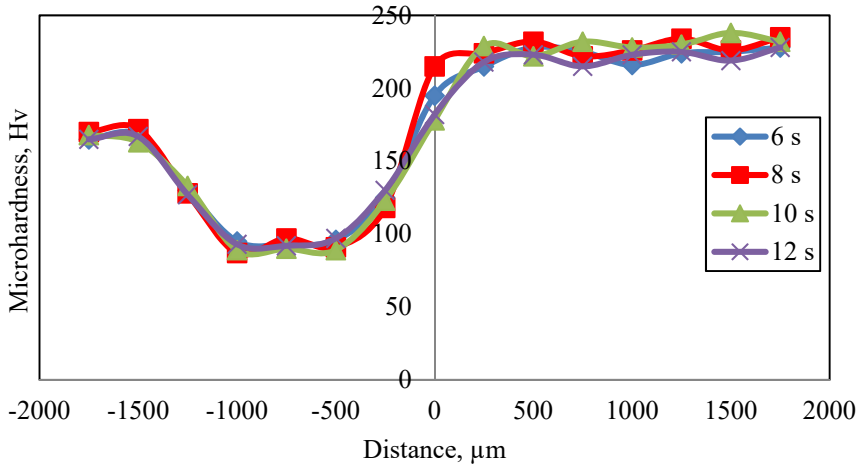

Figure 4. The hardness values obtained from all welded samples.

The hardness of the DRX, HAZ and TMAZ is lower than that of the base alloy on the Al7075-T6 side. The DRX hardness is not as low as the HAZ/TMAZ because of its extremely fine grained microstructure. The drop in HAZ and TMAZ can be explained based on strengthening precipitation. Al 7075 base metal in T6 condition contains a large number of submicroscopic Mg_2Zn and AlCuMg precipitate particles, which confer high strength and hardness to the alloy. During friction welding, The HAZ/ TMAZ experiences high enough temperatures for causing dissolution or coarsening of these strengthening precipitates. During cooling, the cooling rates are high enough to allow any reprecipitation of these strengthening phases. Therefore, the HAZ/ TMAZ hardness is lower than the base alloy harness (Khalid 2010). There was not any change on hardness of 316 L stainless steel side.

Conclusion

Al 7075-T6 alloy and 316 L stainless steel were welded by friction welding methods. All of the welded samples were of sound quality, and they did not exhibit any pores or crack formation along the weld interface. The friction time play an important role in flash formation and welds shear strength. The welds shear strength samples and burn-off increase with increase in the friction time. After welding, while three different zone observed in the Al 7075-T6 side, there was not any difference on the 316 L stainless steel side. The hardness profiles for all friction time are similar. It was observed that Al 7075-T6 side has different hardness values.

Acknowledgements

The author is grateful to Afyon Kocatepe University Scientific Research Committee since this study is supported (Project No. 16.KARİYER.67).

References

Kumar M.V., Balasubramanian V., (2014), Int J Pres Ves Pip 113 (p. 24).
Washko S. D., and Aggen G., (2005), ASM handbook vol 1: properties and selection, 3rd ed, ASM International, New York (p. 1303).
Marshal P., (1984), Microstructure and Mechanical Properties, 1st ed, Elsevier Science Publishing, New York (p. 80).
Oshima Y H T, and Kuroda K, (2007), ISIJ Int 47 (p. 359).
ASM Handbook (1999), Properties and Selection: Irons, Steels, and High Performance Alloys. Materials Park, E-Publishing Inc..
Kurt B., (2007), J. of Mater. Proc. Technol 190 (p. 138).
Lugscheider E, Krämer G, Barimani C., and Zimmermann H., (1995), Surf and Coat Techn. 74 (p. 497).
Khalid H. R., Janaki Ram G. D., Phanikumar G., Prasad R. K.. (2010), Mater. and Des., 3123 (p. 75).
Satyanarayana VV., Reddy GM., Mohandas T., (2005), J Mater Process Technol, 160 (p.128).
Torun O., Çelikyürek I., Baksan B., (2011), Intermetallics 19 (p. 1076).
Çelikyürek İ., Torun O., Baksan B., (2011), Mater Sci and Eng A528 (p. 8530).
Ates H., Turker M., Kurt A., (2007), Materials and Design, 28 (p. 948).
Wang KK., (1975), Weld Res Counc Bull 204 (p. 1).
Maalekian M., (2007), Sci Technol Weld Join 12(8) (p. 738).
Kimura M., Kusaka M., Kaizu1K., Nakata K., Nagatsuka K., (2016) Int J Adv Manuf Technol 82 (p. 489).

HIGH RISE BUILDINGS IN HISTORIC CITIES

Elif Süyük Makaklı,
Serpil Özker

Işık University, Department of Architecture, Istanbul-Turkey
Işık University, Department of Interior Architecture, Istanbul-Turkey
elif.suyuk@isikun.edu.tr
serpil.ozker@sikun.edu.tr

Abstract: High rise building was the most remarkable new building type to emerge in the late 19th century which has entirely changed the scale, appearance, concept and image of cities with its great visual impact. With advanced technologies the skylines of the cities dominated by high rise buildings all over the world in 20th century. In the 21st century it can be expected that more and more innovative high rise buildings will be built, utilizing the cutting-edge techniques also in historic cities with World Heritage Sites. High rise buildings' relationship with their context is more problematic than any other structure, the subject of what they add and what they take away to the city is quite controversial. Introducing a new building in a historic city has a dramatic impact on traditional urbanistic structure. In this study high rise buildings in historic cities with World Heritage Sites, their development, and impact on the city and the urban image are examined by selected examples from different historic cities. The current approaches for designing high rise buildings in a historical setting will be also examined.

Key words: High rise building, historic city, architecture

Introduction

High rise buildings which are an indispensable part of our cities, will continue to exist in the future due to certain reasons such as evolving and changing social needs, rapid urbanization and population growth. There are different terms that define this building type; such as tall buildings, high rise buildings, skyscrapers depending on various contexts. In this study the term high-rise building is used which is substantially taller than their neighbours and/or which significantly changes the skyline.

High rise buildings have the potential to create a powerful image in the context of urban memory, even the potential to change the climate of the region. Technically, architecturally, socially and spatially their impact on the environment is quite strong. High rise buildings' relationship with their context is more problematic than any other structure, the subject of what they add and what they take away to the city is quite controversial. The most intense debates take place in historic cities while the separation or harmony between traditional and contemporary is more sharp and decisive here. High rise building was the most remarkable new building type to emerge in the late 19th century which has entirely changed the scale, appearance, concept and image of cities with its great visual impact. A high-rise building, can be a residential block an office tower or has a mixed use function. With advanced technologies the skylines of the cities dominated by high rise buildings all over the world in 20th century. In the 21st century it can be expected that more and more innovative high rise buildings will be built, utilizing the cutting-edge techniques also in historic cities with World Heritage Sites (WHS).

The global urban population has increased from 0.7 billion in 1950 to 3.9 billion in 2014. UN forecasts another 60 percent by 2050, as 6.3 billion people are projected to live in urban settlements (UN, 2014). A majority of people will be living in urban areas and vertical development is inevitable for the urban growth in the future cities. Cities, which can only be analyzed and understood by interdisciplinary study, are growing and developing constantly day by day. Christine Boyer, the author of 'The City of Collective Memory', suggests in her book that the city consists of three major layers; the city as a work of art (one common to the traditional city), the city as panorama(one characteristic of the modern city) and the city as spectacle (one appropriate to the contemporary city) (Boyer, 1994). These different architectural layers touch each other heterogeneously and form the diversity.

Every new proposed high rise building in a historic city should have a good architectural quality and bring a sustainable approach (Abel, 2006). By the architectural quality of the building is meant; scale, form and massing proportion and silhouette, facing materials, relationship to other structures, effect on the skyline, effect on streetscape and near views (CABE 2007). These type of buildings should be more urban and as well as respectful to a historic city as its impact on public space and the skyline is distinctive due to its scale and density. In this study high rise buildings in historic cities with World Heritage Sites, their development, and impact on the city and the urban image are examined by selected examples from different historic cities. The current approaches for designing high rise buildings in a historical setting will be also examined.

Historic City – High Rise Building

Historic cities with World Heritage Sites have more exclusive place among world cities while they have common value for all humanity with Outstanding Universal Value. The urban conservation for these cities is important for the human history. Introducing a new building in a historic city has a dramatic impact on traditional urbanistic structure. High rise building and a historic city is perceived as two contrasting concepts while high rise building concept is fundamentally different from other contemporary building due to their scale and visual impact on the surrounding. Building a high rise building in a historical setting the protection of the authenticity and integrity is essential as it is an instantly recognizable addition to the city's skyline.

Historic area or city is defined in 1976 UNESCO Recommendation as: *"Historic and architectural (including vernacular) areas" shall be taken to mean any groups of buildings, structures and open spaces including archaeological and palaeontological sites, constituting human settlements in an urban or rural environment, the cohesion and value of which, from the archaeological, architectural, prehistoric, historic, aesthetic or sociocultural point of view are recognized. (URL1)*

Cities are changing and developing rapidly and uncontrolled development can deteriorate the urban heritage with its tangible and intangible values that has shaped through the history. UNESCO defines its approach for the management of historic urban landscape as holistic; the goal is to integrate the conservation and social and economic development. It is crucial[1] to manage the urban development around a World Heritage site and there are two important factors that should be considered; buffer zone regulation, maintenance. Buffer zone is intended to protect World Heritage sites from negative influences. It defines a neighboring zone that may influence a World Heritage site. Although it is not a must the majority of World Heritage sites have a buffer zone which guarantees the protection of the sites. They are not formal components but they contribute to the attributes of the Outstanding Universal Value and to the setting.

High-rise buildings in historical settings are added as new layers into the city and may become the elements which enrich the urban texture without destroying the local environment. CABE (Commission for Architecture and the Built Environment) and English Heritage published Guidance on Tall Buildings in 2007. The main principle is defined as: *to secure high quality design and ways to enhance and improve places in which people live their lives and conserve heritage assets for this and future generations*. Well-designed tall buildings in the right place can be a force for good, but that they also have the potential to cause a destruction of the historical fabric. The destruction can occur in two ways; *Visual character, Urban life quality.*

City can have various silhouettes depending on the viewing direction and the viewpoint. Silhouettes of cities possess their personal individuality, gives the first emotion, first perception for that city thus the first image is created in our minds. Key elements, historic -cultural landmarks and its historic characters of the setting can be observed by a viewer and tall buildings have the potential to determine and create a silhouette or to break the existing. Besides forming the built heritage some buildings in historic cities become the symbol of the city they characterized the urban policies, new developments or new decisions about tall buildings which will be analyzed

[1] New development which can affect the World heritage site has the risk for the site to be admitted to the list of endangered World Heritage.

in the case cities. Preserving the free sky and vistas around these specific buildings is directly related to the perception of the image of the city.

Lynch specifies three separate components of the city's image as follows: "identity, structure & meaning" and verifies that "in reality they always appear together" and determines the image. (Lynch, 2010). The Urban identity is created by urban images in long time process through the history and composed of various components. In the historical process cities have been shaped by various factors such as wars, religion and economy. Initially they were designed for defensive purposes then in medieval times religion shaped the city and religious structures became the focal point and identified the silhouette and image of the city. It is an indisputable fact that the image or identity of a city is not merely identified by the silhouette. The Urban identity of a city is determined by its own idiosyncratic features that are its geography, socio-cultural values of the community and the architectural production. In this respect the urban identity is dependent on meeting the needs of the present with the preservation of the past.

The Case of İSTANBUL

The city of İstanbul is a harmonised combination of the works of nature and man and one of the most significant centers for Civilization and Culture of the world. During Marmaray excavations it has been observed that the history of the city starts in BC 8500. The city protected its status as a capital from Constantine the Great until the 20th century. Great empires like the Eastern Roman, Byzantine and Ottoman made this city their capital for 16 centuries long (Batur, 2011). Among its history the unique geography makes the city special, which is located on three pieces of land separated by the sea. The city was founded on a peninsula and surrounded by the Golden Horn (Halic) on the north, the Bosphorus on the east and the Marmara Sea on the south. Its relationship with the sea and its topography formed the original character of the city. Throughout the history peninsula has radically changed in the context of social-culturally and spatially and also through the fire and the impact of earthquakes. The four regions of Istanbul Historic Peninsula were declared as World Heritage Site on 06.12.1985 by UNESCO.

Figure 1. The Location of Historic Peninsula in the City

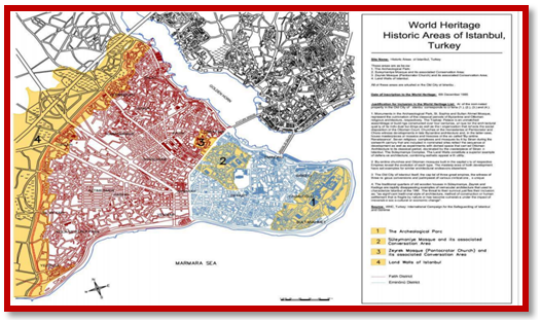

Figure 2.WHS of İstanbul

1. **Sultanahmet Archeological Park** (First Degree Archeological Site and Urban Archeological Site)

2 The Süleymaniye Mosque and Environs Protected Area

3 Zeyrek Mosque (Pantokrator Church) and Environs Protected Area

4 İstanbul Land Walls

The four sites of the property are first Degree Conservation Sites, the masterpieces are the ancient Hippodrome of Constantine, the 6th-century Hagia Sophia and the 16th-century Süleymaniye Mosque. The Historic Peninsula was surrounded by ancient walls which were built by Theodosius in the early fifth century.

Figure 3.View of Istanbul's historic peninsula, looking from Galata. Abdullah Fréres, ca. 1880-93 and a collage of WHS.

The total area is 2,110 hectares; 1,562 hectares of which is covered by the Historic Peninsula and 548 hectares by the Buffer Zone. The "Buffer Zone" is determined in the Management Plan lying parallel to the Land Walls is within the boundaries of Eyup, Bayrampasa and Zeytinburnu Districts. The skylines of the Historic Peninsula express the Outstanding Universal Value of the property. In the Prost's İstanbul Master Plan (1936-58)[2] the first principles and regulations were determined to protect the silhouette of the Historic Peninsula. He put 40 m height limit: that allows max. 3-storey buildings with heights not exceeding 9.50 meters in locations those are above sea level by 40 meters or more, with the purpose of protecting the silhouette of the Historic Peninsula. (Bilsel,C,Pinon, P.,2010)

After the proclamation of the Republic, Ankara became the capital city and contrariwise to other metropolises the population of Istanbul has reduced in 1930s. In 1950s the city started witnessing demographic expansion due to migration which still continues increasingly. High rise buildings appeared first in 1950s and until to the mid 1970s averaging 25 stories office and hotel buildings were built. 1980s were megapolization period (Akdağ, et.al 2010), after 1980s the new urban regeneration process is started (Tekeli, 2014). The remarkable high-rise buildings were built in 1990s in new commercial districts (Zincirlikuyu, Maslak and Beşiktaş) in European side. In the 20th and 21th century the number of high rise buildings is increased rapidly in the city. There are 43 high rise buildings taller than 150 m and 33 of them are completed. The tallest completed building is the Sapphire Tower (2010) with 261 m height. 56 percent of these buildings have residential functions, 21 percent have mixed-use and the rest have hotel and office function. The Cluster of tall buildings are established around Levent-Maslak district and forming a highly visible and attractive symbol of the modern metropolis which change the symbolic perception. The number of tall buildings increasing in both sides of the city and from different locations of the city various characteristics of skylines can be observed. (CTBUH)

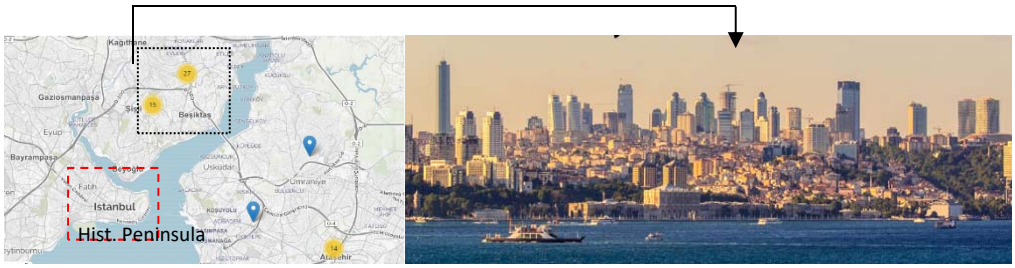

Figure 4: Cluster of tall buildings in İstanbul (CTBUH)

The startling development is occured with the construction of 16/9 residential tower complex with 3 buildings of 27, 32 and 37 storeys in the western district of Zeytinburnu which began in 2010 and damaged the silhouette of the highly valued Historic Peninsula when viewed from Bosphorus. Many objections were raised by public before and during the construction of the buildings regarding the negative impacts that they could cause, but somehow the legal procedures have been fitted or changed in order to complete the construction. Despite all these objections and the on-going court processes the buildings were completed. The 3 blocks obstructed the view and caused an

2 Prof. Henri Prost, Head City Planner of Paris Region was invited to Istanbul in 1936 to make a Master Plan for Istanbul. Although he is criticized for not having evaluated Istanbul within a general development perspective and for transforming the fabric of the city's historic core to rationalize the traffic circulation, his role was significant in the protection of the unique silhouette of the historic peninsula . He mentioned that the Marmara shore of the old city was endowed with "one of the most beautiful views of the world" (Bilsel,C,Pinon, P.,2010)

adverse impact by changing the background setting of the Blue Mosque, Topkapi Palace and Hagia Sophia. The court ruled that those buildings were illegally built as they "negatively affected the world heritage site that the Turkish government was obliged to protect" (URL 2). According to the expert report[3] these 3 buildings located in the buffer zone area and they harm the appreciation of the Outstanding Universal Value of the World heritage Site from different viewpoints. Even though Turkish top administrative court affirmed a decision which imposes the demolition of the buildings it has not been implemented yet.

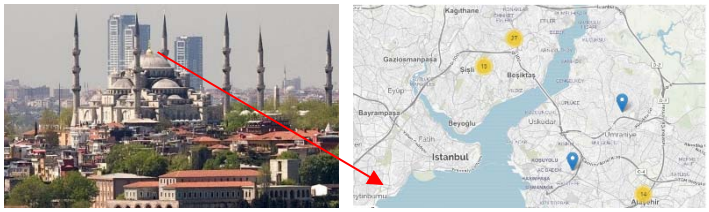

Figure 5: 16/9 Buildings and Historic Peninsula

The 1/100.000 scale Istanbul Master Plan is a reference document that shapes Istanbul's future silhouette concerning the spaces and guiding plans which emphasize a holistic silhouette main plan for the districts including the Historic Peninsula, the Golden Horn and the Bosphorus. Those districts have a direct influence on the silhouette of Istanbul and therefore it is very important to consider them while preparing a study regarding Istanbul's silhouette. Several significant viewpoints like the Bosporus Bridge, the Üsküdar coastline, Harem, Haydarpaşa, Kadıköy Center coastline, Moda, Kabataş coast, the Unkapanı Bridge, the Galata Bridge etc. were identified in order to observe the effects of high buildings on the silhouette. While doing this the natural surface differences and average eye level observation were taken into the consideration. By digital analysis the ultimate height of the buildings that would not affect the silhouette of the Historic Peninsula was defined. (İstanbul Hist.Penin. Site M.P. 2011)

The Case of LONDON

Another historic city that changed its silhouette in time due to the high rise development is London, which is one of the world cultural capital with its 2000 years history. St Paul's Cathedral (1711) has been the tallest building in London until the early twentieth century. After the construction of Faraday Building and Unilever House in the 1930s, the views of St. Paul's Cathedral from the River Thames were obstructed. Consequently 'St Paul's Heights Policy' (a local view protection policy) was implemented in 1937 to protect and enhance important local views from different directions. Until 1970 during post war reconstruction period some high rise building were built in city as the number increased in 1980s the sensitivity to conservation and heritage considerations and also view protection agenda revived.(part 2) . Through history the dynamics of building high-rise buildings in the city has been shaped by different policies and in the 2000s, a cluster of tall buildings were built in the east of the City. They are set in the background of The Tower of London4 which is a palace-fortress and the best-preserved example of a royal Norman castle. The Tower of London(3) (Insc. 1988) is one of the four (The Royal Botanic Gardens at Kew(1), The Palace of Westminster (2), Maritime Greenwich) inscribed prominent UNESCO World Heritage Sites in London. The relationship between the Tower of London and the city in the background is a very sensitive point that should not harm the appreciation of the Outstanding Universal Value of the World heritage Site. In order to conserve the cultural heritage and to protect the skyline of the four towers of the White Tower some visual separation should be obtained between the upper parts of the White Tower and the tall buildings in the background.

[3] According to the İstanbul 4th Administrative Court expert report. The impact of the skyscrapers on the silhouette of the city has been documented after it has been observed from several points such as the ferry passing the Bosphorus, Bosphorus Bridge, Salacak, Harem, Maiden's Tower, Kadıköy and Çamlıca. (URL 3)

[4] The centrepiece is the 11th century White Tower - "white" because of its massive whitewashed walls.

Figure 6:WHS in London

The free sky space around the White Tower enhances the value of its visual dominance and where this space has been compromised then the visual appearance has been depreciated. Some prominent tall buildings of the late20th and early 21st centuries and earlier periods such as spires of city churches are rising behind the tower(Konuk, G. 2008).

Figure 7. Tower of London

In 1991 to protect the strategic views the Secretary of State for the Environment determined Protected Vistas and directions with planning guidance. However, in 2007, the Government's Strategic Views protection was devolved on the Mayor of London and in this year narrow-scoped Mayor's London View Management Framework (LVMF) was published which has been revised and significantly widened in 2010. Although new regulations implemented to protect the perspectives and views of historic monuments in 2007, it failed to ease tensions between different actors (Appert 2015). The London Plan 2011 and the City of London Local Plan are the planning policies that manage the construction of high rise buildings in the city. Conservation areas and also the areas where would adversely affect the protected views are considered as inappropriate areas for the construction of high rise buildings. These determined protected views are 'protected views of St Paul's Cathedral', 'the Tower of London' and 'Views from the Monument'

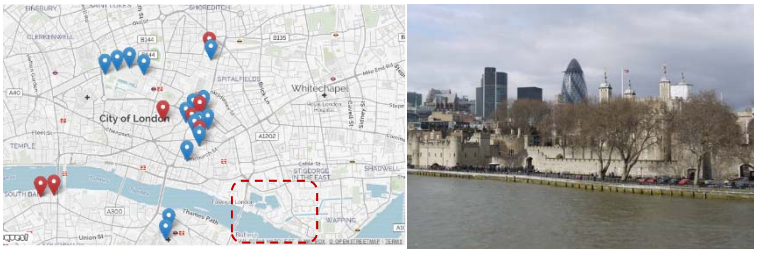

Figure 8: Buildings 100 m+ completed/under construction around Tower Of London

64 percent of tall buildings in London have office functions, 20 percent have residential and the rest have mixed-use function. There are 49 high rise buildings taller than 100 m and 16 of them are taller than 150 m. The tallest completed building in London is the Shard (2013) with 306 m height. (CTBUH)

Tall buildings are permitted to be proposed on suitable sites only if they have potential effect on (city of London):

- *the City skyline*
- *character and amenity of their surroundings including their relationship with existing tall buildings*
- *significance of heritage assets and their setting*
- *effect on historic skyline features*

Figure 9: The LVMF protected vistas map

Conclusion

Each city has its own unique dynamics of urbanization and those dynamics differ depending on the cultural, political, economical and geographical position of the country that the city belongs to. Cities, which can only be analyzed and understood by interdisciplinary study, are growing and developing constantly day by day and this is also valid for historic cities. Building a high rise building in a historical setting has a direct effect on the surrounding heritage and unfortunately there are many examples of unsightly designed, improperly settled buildings which have visually adverse impact over a wide neighborhood. High rise buildings which are an indispensable part of our cities will continue to exist in the future due to certain reasons such as evolving and changing social needs, rapid urbanization and population growth. These building types have the potential to create a powerful image in the context of urban memory, even the potential to change the climate of the region. Technically, architecturally, socially and spatially their impact on the environment is quite strong. Where should they fit in a city and their relation to existing heritage and their height should be clearly determined by needed planning guidance with the participation of different stakeholders. Every new proposed high rise building in a historic city should have a good architectural quality and bring a sustainable approach and not destruct the Visual character and Urban life quality of the city. These type of buildings should be more urban and as well as respectful to a historic city as its impact on public space and the skylines[5] is distinctive due to its scale and density. In the historical process different urban policies, political decisions, global actors and economic systems influenced decision-making mechanism. Regarding urban interventions which are produced by legal policies change the urban image and shaped the historic cities as analyzed in case cities above. The Urban identity of a city is determined by its own idiosyncratic features that are its geography, socio-cultural values of the community and the architectural production therefore each city has its own story.

Historic cities with World Heritage Sites have more exclusive place among world cities while they have common value for all humanity with Outstanding Universal Value. Any proposed building in a historic city has to consider the existing skyline and should not harm the views and the major landmarks of the city. These assessments have to be done by digital analysis methods to understand the effects of those buildings on the context and the silhouette. Not only conservation of the cultural and historical heritage of the city has to be considered but also the fulfillment of the needs of a living and dynamic city has to be taken into the consideration. A sensitive balance has to be obtained between both phenomenon as high rise buildings have the potential to create a powerful and positive image in the context of collective urban memory, and may become the elements which enrich the urban texture. Urban identity is dependent on meeting the needs of the present with the preservation of the past.

References

Abel, C., (2006), 'High Rise and Genius Loci', CTBUH Technical Paper, Building Case Study Urban Design

Appert M., Montes C., (7, 2015) 'Skyscrapers and the redrawing of the London skyline: a case of territorialisation through landscape control', Articulo, Journal of Research, Tales of the City

Akdağ, S.G., Çağdaş, G., Güney C., (2010), 'Analyzing the Changes of Bosporus Silhouette', Future Cities: ECAADE 2010

Batur, A., (2011), 'İstanbul "İstanbul Mimarlik Rehberi" Farkli Ve Yeni', İstanbul Mimarisi, İBB

5 Skylines are "the outline or silhouette of a building or number of buildings or other objects seen against the sky," (Oxford English Dictionary)

Bilsel, C., Pinon, P., 2010,'The Imperial Capital to the Republican Modern City: Henri Prost's Planning of Istanbul (1936-1951)', İstanbul Araştırmaları Enstitüsü, İstanbul, 2010

Boyer, M. C., (1994). The City of Collective Memory: Its Historical Imagery and Architectural Entertainments, MIT Press, Cambridge, Mass.

CABE (Commission for Architecture and the Built Environment) and English Heritage published Guidance on Tall Buildings in 2007

CTBUH, Skyscraper Center, www.skscrapercenter.com (Retrieved 2016-May)

Greater London Authority, 2007. London view management Framework, LVMF. London, Greater London Authority.

Greater London Authority, 2010. Revised London view management Framework, LVMF. London, Greater London Authority.

İstanbul Historic Peninsula Site Management Plan 2011

United Nations, (August 2014/3) Population Facts, Department of Economic and Social Affairs Population Division

Lynch, Kevin, 2010, Kent İmgesi, Çev. İrem Başaran, T. İş Bankası yayınları.İstanbul.

Tekeli,İ.,(2014), 'Türkiye'nin Kentleşme Deneyiminden Öğrenebileceklerimiz', TEPAV

Martin, O., Piatti, G., (2009) 'World Heritage and Buffer Zones', International Expert Meeting on World Heritage and Buffer Zones Davos, Switzerland UNESCO

'Tall Buildings in the City of London' (February 2015 Part 2) Published by the City of London Corporation, Department of the Built Environment,

Figure 1. The Location of Historic Peninsula in the City , İstanbul Historic Peninsula Site Management Plan 2011

Figure 2. WHS of İstanbul, İstanbul Historic Peninsula Site Management Plan 2011

Figure 3.View of Istanbul's historic peninsula, looking from Galata. Abdullah Fréres, ca. 1880-93, Library of Congress and a collage by the authors.

Figure 4: Cluster of tall buildings in İstanbul (CTBUH), www.skscrapercenter.com/city/istanbul

Figure 5: 16/9 Buildings and Historic Peninsula, photo source:URL 2 , map CTBUH.

Figure 6. WHS in London, whc.unesco.org

Figure 7. Tower of London, A collage by the authors, Unesco World Heritage Convention/whc.unesco.org

Figure 8: The LVMF protected vistas map, Greater London Authority, 2010. Revised London view management Framework, LVMF. London, Greater London Authority.

URL 1:http://portal.unesco.org/en/ev.php-URL_ID=48857&URL_DO=DO_TOPIC&URL_SECTION=201.html (Retrieved 2016-May)

URL 2: 'Istanbul's 'Illegal' Towers To Be Demolished After Landmark Court Ruling', https://www.theguardian.com/artanddesign/architecture-design-blog/2014/aug/21/istanbuls-illegal-towers-to-be-demolished-after-landmark-court-ruling. (Retrieved 2016-May.)

URL3: http://www.yapi.com.tr/haberler/silueti-kurtaracak-rapor_107809.html

URL4:Konuk, Güzin(2008) 'Planlamada, Yüksek Yapı Politikasını Oluştururken "Esneklik" Önemlidir', http://v3.arkitera.com/s105-planlamada-yuksek-yapi-politikasini-olustururken-esneklik-onemlidir.html

IMPLEMENTATION OF BERNSEN'S LOCALLY ADAPTIVE BINARIZATION METHOD FOR GRAY SCALE IMAGES

Can EYUPOGLU

Istanbul Commerce University, Department of Computer Engineering, Istanbul-Turkey

ceyupoglu@ticaret.edu.tr

Abstract: In digital image processing, binarization (two-level thresholding) is a commonly used technique for image segmentation. It is the process of converting a gray scale image to a binary image. Furthermore, binarization methods are divided into two groups as global binarization and locally adaptive binarization. A number of binarization techniques have been proposed over the years. Bernsen's method is one of locally adaptive binarization methods developed for image segmentation. In this study, Bernsen's locally adaptive binarization method is implemented and then tested for different gray scale images.

Keywords: Digital Image Processing, Image Segmentation, Binarization, Thresholding, Locally Adaptive Binarization, Bernsen's Method

Introduction

Binarization is a well-known method for image segmentation due to applicability to many fields in digital image processing (Sahoo et al., 1988). In order to separate objects from background, it is an effective technique. A number of binarization applications have been proposed over the years such as document image analysis for extracting printed characters, logos, graphical content or musical scores, map processing for finding place of lines, legends or characters, scene processing for detecting a target, quality inspection of materials, extraction of edge field and spatio-temporal segmentation of video images (Sezgin and Sankur, 2004).

In recent years, the field of document image analysis has received significant attention and has become one of the important parts of digital image processing. There are various researchers which are seeking to design systems for extracting information from extensive documents as maps, magazines, newspapers, engineering drawings, forms and mails. In most of these systems, binarization is applied as the first step (Trier and Taxt, 1995a). The aim of the binarization of document images is extracting text from images, removing noise and reducing image size. This process is performed with removing useless information in order to increase visibility of useful information in an image (Bataineh et al., 2011). In the work of Kefali et al. (2010), it is asserted that the purpose of binarization is to decrease the existence of undesirable data and conserve the desired data in document images. This operation is done by converting all gray levels of images into two levels as black and white.

Binarization techniques are divided into two groups. These are global binarization and locally adaptive binarization (Singh et al., 2011). Global binarization methods compute a single threshold value for the entire image. Pixels having a gray level darker than the threshold value are marked as black (foreground). In the contrary case, the other pixels are labeled as white (background) (Trier and Jain, 1995). Some of the global binarization methods existing in the literature are Abutaleb's method (Abutaleb, 1989), Kapur et al.'s method (Kapur et al., 1985), Kittler and Illingworth's method (Kittler and Illingworth, 1986) and Otsu's method (Otsu, 1979). Besides, locally adaptive binarization methods calculate a threshold value for each pixel on the basis of information contained in a neighborhood of the pixel. Some of these methods compute a threshold surface over the entire image. In the input image, if a pixel (x, y) has a higher gray level than threshold surface evaluated at (x, y), then the pixel (x, y) is marked as background, otherwise it is marked as foreground (Trier and Jain, 1995). In the literature, some of the locally adaptive binarization methods are Bernsen's method (Bernsen, 1986), Chow and Kaneko's method (Chow and Kaneko, 1972; Nakagawa and Rosenfeld, 1979), Eikvil et al.'s method (Eikvil et al., 1991), Mardia and Hainsworth's method (Mardia and Hainsworth, 1988), Niblack's method (Niblack, 1986), Taxt et al.'s method (Taxt et al., 1989), Yanowitz and Bruckstein's method (Yanowitz and Bruckstein, 1989), White and Rohrer's dynamic threshold algorithm (White and Rohrer, 1983), White and Rohrer's integrated function algorithm (White and Rohrer, 1983), Parker's method (Parker, 1991) and Trier and Taxt's method (Trier and Taxt, 1995b).

The rest of the paper is organized as follows. In materials and methods section, Bernsen's locally adaptive

binarization method is explained. In results and discussion section, the results of applying Bernsen's method on gray scale images are showed for different neighborhood values and contrast limits. Finally, conclusions being under study are summarized in conclusion section.

Materials and Methods

In this paper, Bernsen's locally adaptive binarization method is used in order to extract texts from gray scale images. Furthermore, it is implemented and tested for different neighborhood values and contrast limits. In Bernsen's method (Bernsen, 1986), the threshold value is calculated for each pixel (x, y) according to the following equation (1).

$$T(x, y) = (Z_{low} + Z_{high}) / 2 \quad (1)$$

where Z_{low} and Z_{high} are the lowest and highest gray level pixel values in a square r x r neighborhood centered at (x, y). The contrast measure is calculated for each pixel (x, y) according to the following equation (2).

$$C(x, y) = Z_{high} - Z_{low} \quad (2)$$

If the contrast measure $C(x, y) < l$, then the neighborhood consists only of one class, foreground or background. In addition, r and l values vary depending on the used images and areas. Applying Bernsen's method for gray scale images is shown in Figure 1.

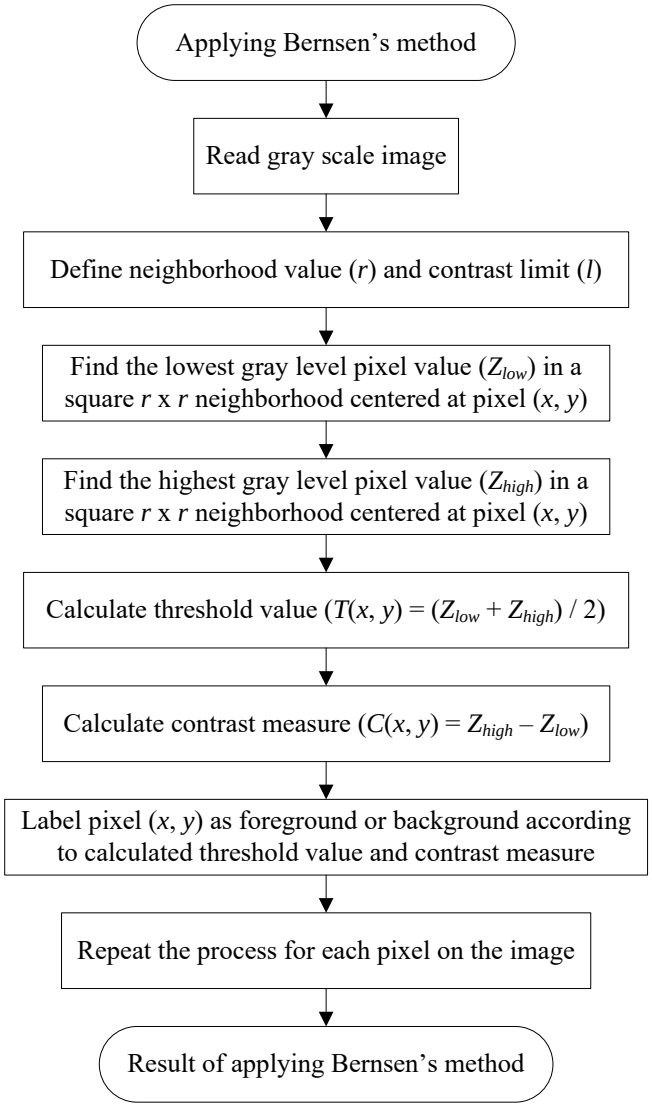

Figure 1. Flowchart of applying Bernsen's locally adaptive binarization method for gray scale images.

As seen in the flowchart, firstly, the gray scale image used for testing is read. Secondly, the neighborhood value

and contrast limit are defined. After that the lowest and highest gray level pixel values in a square r x r neighborhood centered at (x, y) are found and then the threshold value and contrast measure are computed. In the sequel, the pixel (x, y) is labeled as foreground or background according to calculated threshold value and contrast measure. Finally, this process is repeated for each pixel on the image.

Results and Discussion

In this study, in order to extract texts from gray scale images, Bernsen's locally adaptive binarization method is used. The application used for binarization is implemented using MATLAB R2014a. The application is tested for different neighborhood values and contrast limits on various gray scale images. The neighborhood values are chosen as 3, 5 and 15. Moreover, the contrast limits are selected as 15 and 50 for testing the performance of Bernsen's method. As an example, one of the original gray scale images used in this work is shown in Figure 2. The size of this gray scale image is 202 x 202 pixels.

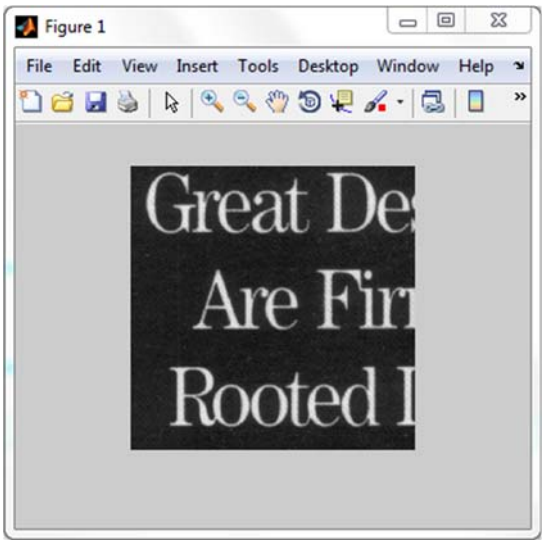

Figure 2. Orijinal gray scale image used for testing Bernsen's method.

The results of applying Bernsen's method on the original gray scale image for r=3 are shown in Figure 3.

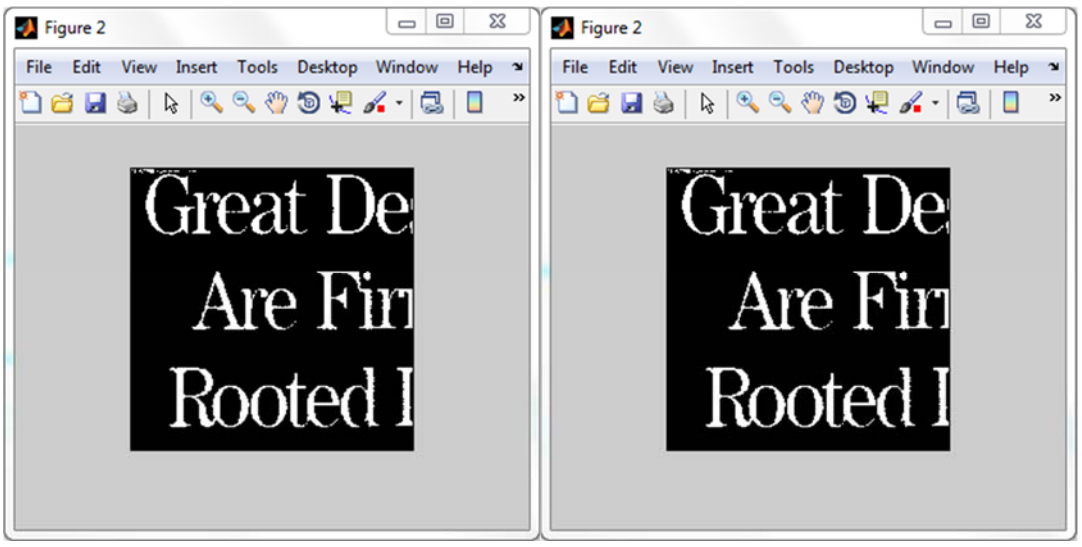

Figure 3. Applying Bernsen's method on the original image for r=3 (l=15 and l=50 respectively).

The results of applying Bernsen's method on the original gray scale image for r=5 are shown in Figure 4.

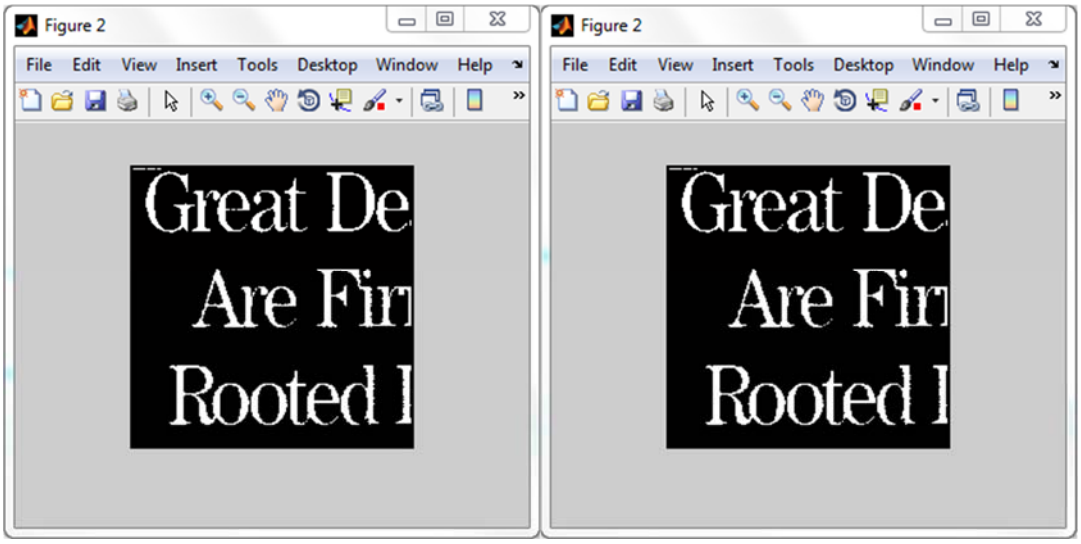

Figure 4. Applying Bernsen's method on the original image for *r*=5 (*l*=15 and *l*=50 respectively).

The results of applying Bernsen's method on the original gray scale image for *r*=15 are shown in Figure 5.

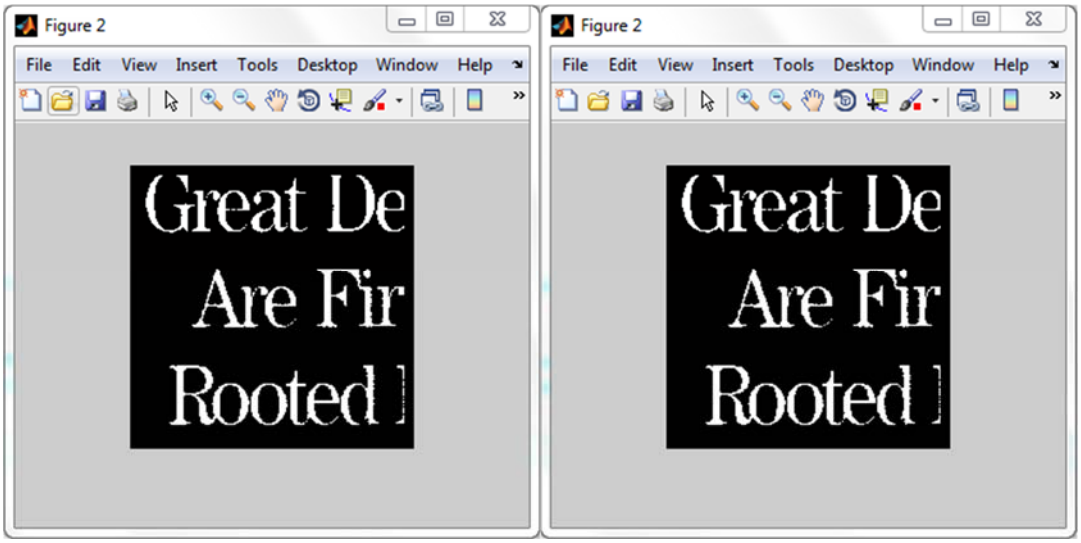

Figure 5. The results of applying Bernsen's method on the original image for *r*=15 (*l*=15 and *l*=50 respectively).

As seen in Figure 3, 4 and 5, the useless information is removed from the original gray scale image and the visibility of the useful information is increased. Consequently, the texts are successfully extracted using Bernsen's binarization method. It is observed that this method is efficient for different *r* and *l* values. However, the increase of neighborhood value and contrast limit raises the process time of the method. Besides, the process time is inversely proportional to the processing speed of Bernsen's method.

Conclusion

In recent years, document image analysis has become a significant research topic in the area of digital image processing. Binarization is applied as the first step in most of the document image analysis applications. The purpose of the binarization of document images is to remove useless information and noise in order for extracting text and useful information from images. In this paper, Bernsen's locally adaptive binarization method is implemented and then it is evaluated for different neighborhood values and contrast limits. According to the study results, it is seen that the texts are successfully extracted and Bernsen's method is effective for various neighborhood values and contrast limits. In addition, the more neighborhood value and contrast limit raise, the more the process time of the method increases.

References

Abutaleb, A.S. (1989). Automatic thresholding of gray-level pictures using two-dimensional entropy. *Computer Vision, Graphics and Image Processing, 47*, pp. 22-32.

Batainehb, B., Abdullah, S.N.H.S., & Omar, K. (2011). An adaptive local binarization method for document images based on a novel thresholding method and dynamic windows. *Pattern Recognition Letters 32*, pp. 1805-1813.

Bernsen, J. (1986). Dynamic thresholding of grey-level images. *Proc. Eighth Int'l Conj Pattern Recognition*, pp. 1,251-1,255, Paris.

Chow, C.K., & Kaneko, T. (1972). Automatic detection of the left ventricle from cineangiograms. *Computers and Biomedical Research, 5*, pp. 388-410.

Eikvil, L., Taxt, T., & Moen, K. (1991). A fast adaptive method for binarization of document images. *Proc. First Int'l Conf. Document Analysis and Recognition*, pp. 435-443, Saint-Malo, France.

Kapur, J.N., Sahoo, P.K., & Wong, A.K.C. (1985). A new method for gray-level picture thresholding using the entropy of the histogram. *Computer Vision, Graphics and Image Processing, 29*, pp. 273-285.

Kefali, A., Sari, T., & Sellami, M. (2010). Evaluation of several binarization techniques for old Arabic documents images. *The First International Symposium on Modeling and Implementing Complex Systems (MISC'2010)*, pp. 88-99, Algeria.

Kittler, J., & Illingworth, J. (1986). Minimum error thresholding. *Pattern Recognition, 19* (1), pp. 41-47.

Mardia, K.V., & Hainsworth, T.J. (1988). A spatial thresholding method for image segmentation. *IEEE Trans. Partern Analysis and Machine Intelligence, 10* (6), pp. 919-927.

Nakagawa, Y., & Rosenfeld, A. (1979). Some experiments on variable thresholding. *Pattern Recognition, 11* (3), pp. 191-204.

Niblack, W. (1986). *An Introduction to Digital Image Processing*, pp. 115-116. Englewood Cliffs, N.J.: Prentice Hall.

Otsu, N. (1979). A threshold selection method from gray-level histograms. *IEEE Trans. Systems, Man, and Cybernetics, 9* (1), pp. 62-66.

Parker, J.R. (1991). Gray level thresholding in badly illuminated images. *IEEE Trans. Pattern Analysis and Machine Intelligence, 13* (8), pp. 813-819.

Sahoo, P.K., Soltani, S., & Wong, A.K.C. (1988). A survey of thresholding techniques. *Computer Vision, Graphics, and Image Processing, 41* (2), pp. 233-260.

Sezgin, M., & Sankur, B. (2004). Survey over image thresholding techniques and quantitative performance evaluation. *Journal of Electronic Imaging, 13* (1), pp. 146-165.

Singh, T.R., Roy, S., Singh, O.I., Sinam, T., & Singh, K.M. (2011). A New Local Adaptive Thresholding Technique in Binarization. *International Journal of Computer Science Issues, 8* (6), pp. 271-277.

Taxt, T., Flynn, P.J., & Jain, A.K. (1989). Segmentation of document images. *IEEE Trans. Pattern Analysis and Machine Intelligence, 11* (12), pp. 1,322-1,329.

Trier, O.D., & Jain, A.K. (1995). Goal-Directed Evaluation of Binarization Methods. *IEEE Transaction on Pattern Analysis and Machine Intelligence, 17* (12), pp. 1191-1201.

Trier, O.D., & Taxt, T. (1995a). Evaluation of Binarization Methods for Document Images, *IEEE Transaction on Pattern Analysis and Machine Intelligence, 17* (3), pp. 312-315.

Trier, O.D., & Taxt, T. (1995b). Improvement of 'integrated function algorithm' for binarization of document images. *Pattern Recognition Letters, 16* (3), pp. 277-283.

White, J.M., & Rohrer, G.D. (1983). Image thresholding for optical character recognition and other applications requiring character image extraction. *IBM J. Research and Development, 27* (4), pp. 400-411.

Yanowitz, S.D., & Bruickstein, A.M. (1989). A new method for image segmentation. *Computer Vision, Graphics and Image Processing, 46* (1), pp. 82-95.

IMPORTANCE OF SKETCHING IN THE DESIGN PROCESS AND EDUCATION

Serpil Özker, Elif Süyük Makaklı

Işık University, Department of Interior Architecture, Istanbul-Turkey
Işık University, Department of Architecture, Istanbul-Turkey

serpil.ozker@isikun.edu.tr
elif.suyuk@isikun.edu.tr

ABSTRACT
Design education adopts different education models that changes constantly due to differences among disciplines. Education models can be varied with different training techniques. The design approaches introduced during the design process, which forms the basis of design education, gain meaning through sketching "with free-hand drawing" which is an effective communication tool for the profession. Sketching ensures fast development and introduction of opinions, serving as an active transmitter of visual expression. The computer technologies that are advancing rapidly today turns the traditional design, the "free-hand technique", into an element with a conceptual impact on the design process. The study aims to discuss the "process of sketching" behind the design factor in the architecture and interior architecture education in Turkey and to analyse the method of sketching as well as its application styles, design, presentation, education, process and results, discussing the importance of sketching process in the education. Finally, the sketching process is associated with the concept of design, emphasizing that it is essential for the architecture and interior architecture design education and it is a skill that must be enhanced through education.

Key Words: Architecture and Interior Architecture Education, Design, Sketching process.

Introduction

Design is to look at the design problem in a different way considering operational, functional, aesthetic concerns by developing new methods. Design, acting towards its personality in this process, is to tangibly provide transfer of ideas in conceptual meaning. Therefore, the effect of visual transfer on persons gains importance. The most efficient method to embody an intangible expression in the design process is to transfer the ideas on a paper fast, in a way to benefit from freehand technique which is a traditional expression method. The most used visualization techniques are freehand drawing, technical drawing and drawing digitally (Gümüş, 2007). Research, thinking, application methods and developing unique design ideas is aimed in design education. In a sense, transfer of unique design ideas tangibly stresses on the importance of sketching namely design data. Sketching is the most influential means of communication in design jobs such as architect and interior architect. Sketching helps to become skillful at fulfilling and developing the idea in design process in a short time and brings continuity with it. It can produce different processes by being supported with visual presentation. In this regard, examining sketching process which is an important element in design education is aimed in this study. Design process and consequences of design education in the Interior Architect and Architect disciplines is studied; Design, design knowledge, design education, the importance of freehand and sketching process in education is examined. In this regard, it is stressed out in this study that sketching process behind the design has a required place in design education.

Design and Design Education

Design is envisaging, shaping or an envisaged fact produced to make a plan or sketch. It is a mental project or scheme in which steps to make a consequence is set forth (Bayazıt, 1994). At present, Interior Architect and Architect are among the modern and renewed jobs with the effect of socio-cultural and economic changes. Therefore, it is inevitable that Interior Architect and Architect education to be shaped under different approaches (Özker, Makaklı, 2015). In the Interior Architect and Architect education especially project/design studio courses are steering and shaping education. According to James Reswick, design which is a creative action is a fact involves creating a new and useful thing which has not existed (Ketizmen, 2002). Design is a creative process; solving problems, sketching, thinking and producing process in a sense. On the other hand, design education is to develop individual behaviors with education and guidance. The aim of design jobs such as Architect and Interior Architect is to transfer the method and fiction of design education to the student. In this sense Interior Architecture education program is consists of design courses such as basic design, project/design studio, furniture design which are design-oriented courses out of technical courses. On the other hand, design courses such as basic design,

project/design studio which are design-oriented courses out of technical courses are in the education program of Architect. Sketching is highly important in design courses in which the student can express herself/himself or becomes skillful at that. Developing design skills, having an idea about what is design is provided with design courses.

Education quality of these jobs which are shown among the popular jobs and increased rapidly is a crucial matter to be examined. In design education especially which is gained at Design studios, questioning the relation between education and design by transferring the definition and process of design correctively is necessary. Design is a new experience for students. Design education is an education type which is continuously open to development and change. It is necessary to properly form the foundation of design education which will adapt developing and changing life conditions (Çetinkaya, 2011). Sketching and visually thinking skills should be gained to the student. So designers' visual communication means in which they express abstract and concrete concepts in way to reflect their own identities, likes and purposes is mostly possible with sketching.(İslamoğlu, 2012). Some works include superficial, fast produced, unclear creative ideas while others include detailed and clear design ideas. Both are necessary for design methods and they are elements that support each other (Silav, 2013). Therefore the purpose of Design education is to raise individuals who think individually and critically, have an aesthetic perception, can interpret its neighborhood by perceiving it, developed his/her expression power. Students, thanks to design courses in design education, learns about unclarity of sketching; that each line crossed has a potential meaning and opens to different interprets; concepts such as visualization, analyzing, determination and nourished from them (Adıgüzel and others, 2012a). Design action is an action that creativity matters. Developing, interpreting and transferring ideas in a paper improve the individual creativity in a sense. What is expected from design education is transferring design conceptualization which students will use in their educational and professional life through a variety of courses, teaching sketching language to them in order to express themselves.

Sketch in the Design Process

Sketch, is a draft data occurs through thinking, it is the first stage, it does not represent "the perfect", it is the language among individuals. As for sketch process is the process of making lots of sketches, "freehand drawing". According to İnceoğlu and others, if writing is the means of expression in literature, drawing is the means of expression in architect. In this sense, sketching in the architect, interior architect and similar design education is important as writing. This process is the preliminary draft of project; a part of design; effective element which produce the outcome. In this regard, sketch is the thinking method which gives meaning to the project in the design courses. Goldschmidt name this process as sketch dialect. Sketching provide with interprets and new deductions of this process to occur (Goldschmidt, 1991). Sketches are dynamic production which can appear in every stage of whole design process. It does not stop, develops continuously, and this dynamic act continues in every stage of whole process (Yakın, 2012a). Sketch is the best sentence describes the idea, finding the idea through sketch is the most important factor of the design process. Spontaneous drawings arise from sketch, it brings the continuity but it is not permanent, the solution shows up while the image is becoming clear (Dodsworth, 2011). The principle aim of design disciplines which look differently at various subjects and try to find a solution is to achieve the same goal. In this context, the objective of Design jobs is to create the design fast and think fast. In order to determine the problem and reach out the solution, the ability to make sketches is crucial. Making the problem and its definition properly, offering the right solutions make the sketch necessary. Even though some designers limit their design process with various criteria, design, indeed, is a process shaping unique for each designer. Sketching is an important part of the design process, it shapes with creative actions. Drawing which is a process of thinking and interpretations starts with expression of visual image with hands and it improves while disciplined eyes and mind evaluate and change the image. Drawing is accepted as whole process or rather as cycle (Hanks, Belliston, 1977). In this regard, sketching "freehand drawing" appears as the most effective means of expression, language of thinking.

Sketching has an interactive role of unifying the ideas in mind, defined functions and the meaning of drawings; finding new forms and adapting them to the design (Edwards, 1979). It is possible to divine sketching studies in two groups as "Searching" and "Interpreting". While the Searching sketches is to find solution to a problem which has not discovered yet, Interpreting sketches is to expressing an existing concrete or tangible actions as newly and uniquely by filtering it with interpreting (Yakın, 2012b). The result expected from drawing in the design process is not the product but its semantic value that is going to show up is important. Therefore, researching, interpreting, develop unique design ideas shows that sketching is important indesign process.

Importance of Sketching In the Design Process and Education

Design education express an entirety with sketching "freehand style", presentation and application methods and there is no matter for distinctive for design jobs. Design is complicated process; designer or project coordinator manages this process by using their knowledge, experience and creativity. While making analysis by examining

certain parameters such as environmental design, historical process relating to architecture and its neighborhood, user needs, functional analysis; concept developing suggestions related to design are offered (Adıgüzel and others, 2012b). In this context, analysis, synthesis along with sketch drawings contributes to design. In this regard, it is possible to examine design education and process like this:

Design Education,
Design education is type of education in which student gains lots of ideas such as thinking, researching, acquiring of knowledge, questioning, and solving problems. Design education namely project courses in disciplines of Architect and Interior Architect is a creative process for creating the new. Establishing common working areas coordinated together with student in the supervisory of a coordinator, design method and fiction are transferred to the student.

Process in Design Education,
Design education process starts with determining a project subject every midterm, the project is completed with end of term jury and in the supervision of coordinator. The student, whose project subject has been decided, researches the design he/she wants to introduce with the data she acquired in the process of acquisition information through freehand sketching methods. In the Architect and Interior Architect education, the aim of the design courses, along with their weight is different from each other, is to raise individuals who defend original ideas, able to speak up and interpret their creativities. Type of education differentiates from departments to departments such as course content, hour, theory, types of teaching lessons. For Example, while design education is performed with computer aided in one department, it can be concluded with computer or hand drawings methods aided by sketching.

Presentation in Design Education,
Design education and reflecting of designer identity to opposite party appear in presentation stage. Observer has an idea about person's creativity while looking his/her presentation. Presentation stage in design education can either be with freehand sketch drawings or it can be prepared while having been benefited from computer environment.

Another supporter of traditional design methods is today's computer technology. Computers which are becoming a must technology and need of modern age are now turning into commonly used devices at the first and last stage of design. However, design first on paper, the first stage of design education, is supported with different drafts. Draft drawings which gains clarity are concluded with computer aid in the last stage of design. Today's developments in digital technology has improved, changed and brought the production process of design focused jobs to different dimensions. Digital based solutions such as parametric modeling, computational design digital design and fabrication, and Building Information Management (BIM) relation with design creation process is being started to questioned. For example, a symposium was held at Yale School of Architecture about questioning the place of a traditional drawing titled "Is Drawing Dead" in digital age.The status of traditional drawing is examined in the digital age.) Keynote speaker Peter Cook mentioned that he is interested less polished version where building remains fictional in an honest way rather than computer renderings with perfect images(URL1).

Digital technologies have developed every day and provide designer with ease of use. In design education, it is aimed that student learns utilization of computer technology and the whole process from two dimensional drawings to rendering. Transferring the ideas mind to a paper or preparing them digitally is interpreted as a mater of choice. Whatever the type of means the aim is to provide an embodiment of an idea in the end. The first sketching design created with computer in education process is only possible after learning various programs. For the students who newly started to design education the place of freehand drawing, in this context, is inevitable for the first experiences in design process. Freehand drawing is not a drawing which only capable ones can make and perfection is pursued in the end rather an expression means in which tangible ideas embody in order to solve problems in design process, and it is a method that can be improved while sparing time on it. By which method that the designer will prepare his/her sketching can be improved accordingly his/her choice at next process. In this regard, increasing of intellectual quality; being able to make computer aided visual analysis; modeling of created or existed designs or environments with computer; being able to review design rules; improving the tendency to

gain disappeared cultural values at virtual platform, what is expected from computer aided design, are benefited by utilization of them in architect education and application (Tokman, 1998). In this sense, the student who design with freehand sketching understands that intellectual quality and design is a thinking power, it is important matter to create fast designs with sketching.

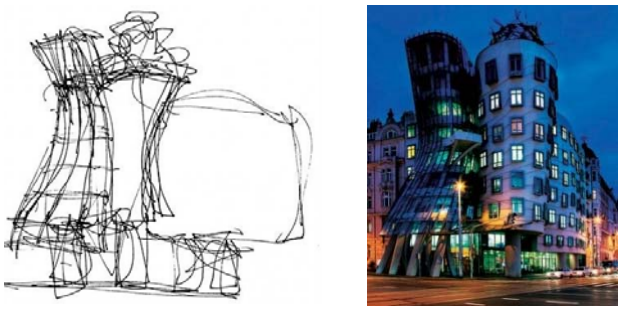

Figure 1-2. Frank O Gehry

Figure 3-4. Mario Botta

Conclusion

Design is an action that affects development of new information and production besides is a process in which design action is realized. Therefore, in design education which is a creative process, it is necessary to bring students sketching habit of which contribution to creativity can not be ignored from the beginning of design education to occupation practices. Sketching is the production first thinking, contributes significantly to making of creative designs. It should be taught that sketching is a necessity and basis of the design education especially, in project courses. In this sense, it should be shown that design education is a problem solving focused education process in which skills such as design, gaining experience, researching, analyzing, synthesizing which are being improved with different education methods and suggestions, are being gained.

In this context, suggestions of this study are ;

- Importance should be given to freehand sketch drawings in the disciplines such as Architect, and Interior Architect,
- Places that encourage creativity should be created in design process,
- Methods that can reveal student's own skill, gain him/her individual self confidence should be found out ,
- It should be transferred to the student that sketch drawing is a design thing rather than a necessity,
- It is necessary to transfer to the student with education that, for creative designs, fast thinking through freehand sketching is contributing significantly to transfer the idea to paper.

Consequently, it has been felt that freehand sketch drawing is losing its importance with today's increasing computer aided design technology environment. However, although it seems as if sketching losing its importance in Design education, freehand sketch drawing is a process attributes meaning to design. Sketch drawing which is shown as a traditional method should not lose its value, it should be aimed to gain sketch habit to the student in all of the design courses.

References

Adıgüzel D. Kutlu R. Ormancı S. Tosun V. (2012a, b), Interior Architecture Project Studio Experience in the Section of Design-Application İÇMEK / Interior Architecture Education National Congress II, İstanbul, Turkey, 20 December 2012, page 65, 131.

Bayazıt N. (1994), *Introduction to Design Methods in Industrial Designs and Architecture*, Literatür Publications.

Çetinkaya Ç. (2011), The Place of Design and Concept Relationship within the Interior Arthitecture Basic Design Education: A research on Basic Design Education through two different Universities, Hacettepe Üniversity Master Thesis, Ankara, page 1.

Dodsworth S. (2012), *Elements of Interior Design*, AVA Book Production Pte, Singapur.

Edwards B. (1979), *Drawing on the Right Side of Brain*, LA, JP Torcher.

Goldschmidt G. (1991), *Dialectics of Sketching*, Creative Research Journal, 4 (2), page 123–143.

Gümüş E. (2007), *Design Process and Computer*, Marmara University School of Fine Arts, Master Thesis, İstanbul, page 10.

Hanks K. ve Belliston L. (1977), *Draw: A Visual Approach to Thinking, Learning, and Communicating*. Los Altos, CA: William Kaufmann Inc.

İnceoğlu N. Gürer T. Çil E. (1995), *Sketches as a Means of Thinking and Expression*, Helikon Publications, İstanbul, page 7.

İslamoğlu Ö. S. (2012), Sketching in Design Process, İÇMEK/Interior Architecture Education National Congress II, İstanbul, Turkey, 20 December 2012, page 127.

Ketizmen G.Ç. (2002), Examination of Methodological and Spatial Effects in the Formation of Architectural Design Studio, Anadolu University, Institute of Science and Technology, Master Thesis, August 2002, page 3.

Özker S. Makaklı E. (2015), In the context of Interior Architecture departments in Turkey; Design studio (project) education, ERPA International Congresses on Education 2015, ERPA Congresses 2015, 4-7 June 2015.

Silav M. (2013), *Sketch in Design Education*, European Journal of Research on Education, IASSR, Art in Education, page 40.

Tokman L. (1998), The Effect of Computer Technology on Education Method, Education Policy, Working place of Design Studio in Architecture Under Graduate Program, Y.T.Ü. Education in the Faculty of Architecture, İstanbul, 1998, page 117-128.

URL1. http://archpaper.com/2012/02/is-drawing-dead-yale-searches-for-an-answer/, accessed date: 20.06.2016.

Yakın B. (2012a, b), An Analytical Approach to relationship of Visual Thinking and Visual Expression in Design Process, Hacettepe University Faculty of Fine Arts ,Master Thesis, Ankara, 2012, page 30, 59.

Figure 1, Frank O Gehry- Sketch, http://abduzeedo.com/architect-day-frank-gehry, access date: 12 Mai 2015.

Figure 2, Frank O Gehry- Figure, http://www.telegraph.co.uk/culture/film/3674871/Sketches -of-Frank-Gehry.html? image=4, access date: 12 Mai 2015.

Figure 3, Mario Botta-Sketch, http://www.arhitekton.net/crtezi-sketches-mario-botta-2/?lang=en, access date: 12 Mai 2015.

Figure 4, Mario Botta- Figure, http://www.arhitekton.net/crtezi-sketches-mario-botta-2/?lang=en, access date: 12 Mai 2015.

INVESTIGATION OF CONCRETE GRAVITY DAM BEHAVIOUR CONSIDERING DAM–FOUNDATION–RESERVOIR INTERACTION

Muhammet KARABULUT[1], Murat Emre KARTAL[2], Murat CAVUSLI[3], Seda COSKAN[4], Oguzhan DURSUN[5]

1 Bulent Ecevit University, Department of Civil Engineering, Zonguldak/TURKEY, karabulut@beun.edu.tr
2 Bulent Ecevit University, Department of Civil Engineering, Zonguldak/TURKEY kartal@beun.edu.tr
3 Bulent Ecevit University, Department of Civil Engineering, Zonguldak/TURKEY murat.cavusli@beun.edu.tr
4 Vocational School, Bulent Ecevit University, Kilimli, Zonguldak/TURKEY, sedacoskan@gmail.com
5 Bulent Ecevit University, Department of Civil Engineering, Zonguldak/TURKEY, oguzhan-dursun@hotmail.com

Abstract: Ground motion effects on a concrete gravity (CG) dam in the earthquake zone should be taken into account for design conditions. Boyabat CG dam constructed in Sinop, Turkey, is selected as an application. This study presents two-dimensional earthquake response of Boyabat CG dam including friction between dam and foundation. The two-dimensional finite element model of Boyabat CG dam is obtained using ANSYS finite element software. The unfavorable section of the dam is selected for two-dimensional numerical analyses. The contact-target element pairs are used in the dam–foundation–reservoir interaction. In this case, friction contact is considered in the numerical solutions. Empty and full reservoir cases are also considered in these solutions. The hydrodynamic pressure of the reservoir water is modeled with two dimensional fluid finite elements based on the Lagrangian approach. In the earthquake analyses, the finite element model has fixed boundary conditions. According to linear dynamic analyses, maximum horizontal displacements and maximum principle stress components are presented by dam height in the largest section. These results are evaluated considering empty and full reservoir conditions.

Keywords: Concrete gravity dam, Contact-target elements, Dam-foundation-reservoir interaction, Lagrangian approach.

Introduction

Water has been one of the most important things in human life from first era to now. People always try to live in around water resources. Because water is necessary for the continuing of life, so people had to learn how water was stored and how water usage was done. In many area, water has vital importance for instance, consumption, irrigation, climate and power.

Dam is one of the most difficult structural construction in civil engineering field because dam has huge potential risk in active seismic zones especially. A gravity dam is a massive sized dam fabricated from concrete and designed to hold back large volumes of water (Cracking Dams, 2008). By using concrete, the weight of the dam is actually able to resist the horizontal thrust of water pushing against it. This is why it is called a gravity dam. Gravity essentially holds the dam down to the ground, stopping water from toppling it over. Gravity dams are well suited for blocking rivers in wide valleys or narrow gorge ways. Since gravity dams must rely on their own weight to hold back water, it is key that they are built on a solid foundation of bedrock. The one advantage of a gravity dam is its rather simple design, with most dams being a straight vertical wall across a valley or gorge way. However, gravity dams can also be designed curved, as in the Hoover dam. Gravity dams are very durable and still highly preferred over buttress dams and arch dams (About Dams, 2008). The one drawback is that gravity dams require a large amount of material and construction to build are therefore relatively expensive (Gravity Dams, 2008). Therefore, each project should be evaluated on its own. When the conditions allow consideration of a concrete gravity dam alternative, the following points can be a plus. The method or scheme of diverting flows around or through the dam site during construction is an important consideration to the economy of the dam. A concrete gravity dam offers major advantages and potential cost savings by providing the option of diversion through alternate construction blocks, and lowers risk and delay if overtopping should occur (USACE, 1995).

This study showed that linear behavior of the concrete gravity Boyabat dam under Kocaeli earthquake. The change of maximum principal stresses and horizontal displacements by dam height were investigated. Numerical analyses were performed for empty and full reservoir cases considering fixed boundary conditions. ANSYS software was used for dam modeling and all dynamic analysis. The contact-target element pairs are used in the dam–foundation–reservoir interaction. Besides, friction is considered in the numerical solutions. It is provided by no separation

friction case.

Mathematical Model of Boyabat CG Dam

Boyabat dam, located approximately 10km south-east of Duragan county center, Sinop, was constructed in 2012 by General Directorate of State Hydraulic Works. It was established on Kızılırmak River. The reservoir is used for irrigation and energy purposes. The dam crest is 262 m in length and 8 m wide. The maximum height of the dam from base to top crest point is 195 m, respectively. The annual total power generation capacity is 1.500×10^6 kWh/year.

Figure 1. Boyabat Dam.

Boyabat concrete gravity dam was modeled in ANSYS software. Finite element model of concrete gravity dam was divided to convenient finite element sizes. Finite element mesh was carried out approximately resemble measurements for dam model. Finite element model of the dam was given in given Fig. 2.

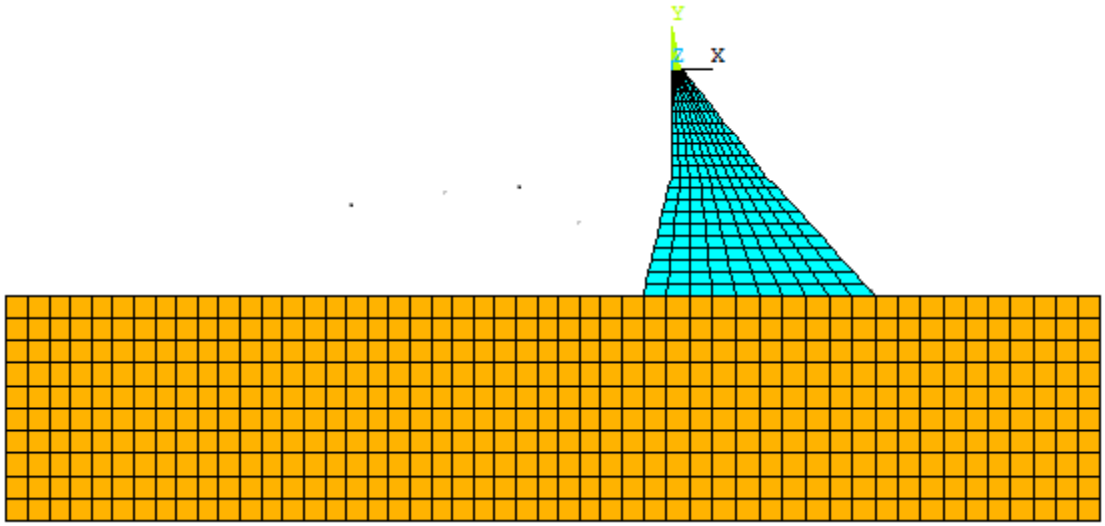

a) Empty reservoir condition

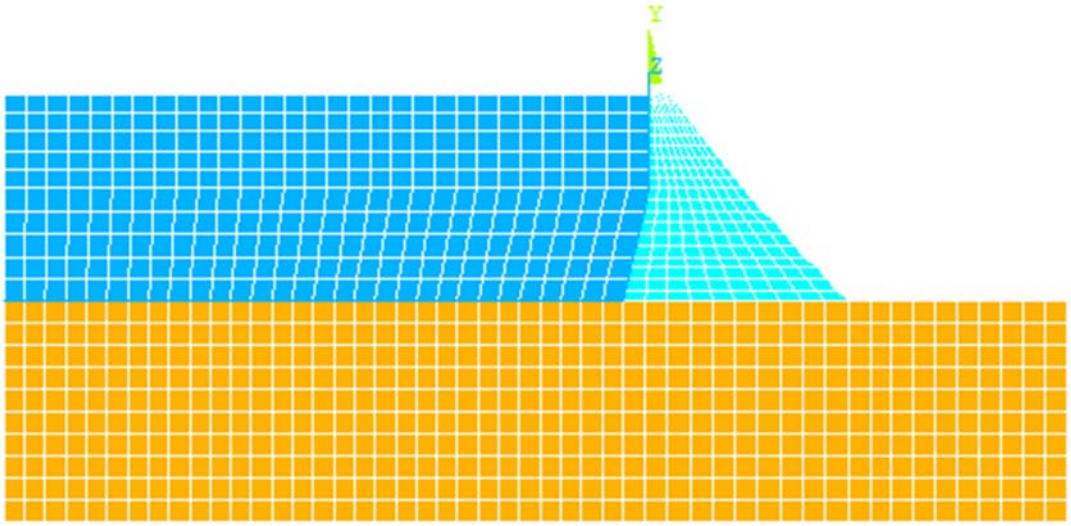

b) Full reservoir condition

Figure 2. Finite element model of Boyabat Dam

Firstly, contact-target elements were identified between dam body and foundation. Dam model includes two cases. One of these situations is empty reservoir conditions and second one is full reservoir conditions. Linear dynamic analysis was done for the both situations.

Material Properties

The material properties of dam-foundation-reservoir interaction model used in linear analyses given in Table 1.

Table 1: Material properties of Boyabat dam

	Elastic modulus (kN/m^2)	Poisson ratio (υ)	Density (γ) (kN/m^3)
concrete	2.8×10^7	0.2	2.3955
foundation	$10.5E^6$	0.17	2.73293
water	$2.07E^6$	0	0.99918

Lagrangian Approach for Dam -Reservoir -Foundation Interaction

The formulation of the fluid system based on the Lagrangian approach is presented as following (Wilson and Khalvati, 1983). In this approach, fluid is assumed to be linearly compressible, inviscid and irrotational. For a general two-dimensional fluid, pressure-volumetric strain relationships can be written in matrix form as follows,

$$\begin{Bmatrix} P \\ P_z \end{Bmatrix} = \begin{bmatrix} C_{11} & 0 \\ 0 & C_{22} \end{bmatrix} \begin{Bmatrix} \varepsilon_v \\ w_z \end{Bmatrix} \tag{1}$$

where P, C_{11}, and ε_v are the pressures which are equal to mean stresses, the bulk modulus and the volumetric strains of the fluid, respectively. Since irrotationality of the fluid is considered like penalty methods (Zienkiewicz and Taylor, 1989) rotations and constraint parameters are included in the pressure-volumetric strain equation (Eq. (1)) of the fluid. In this equation P_z, is the rotational stress; C_{22} is the constraint parameter and w_z is the rotation about the Cartesian axis y and z.

In this study, the equations of motion of the fluid system are obtained using energy principles. Using the finite element approximation, the total strain energy of the fluid system may be written as,

$$\pi_e = \frac{1}{2}\mathbf{U}_f{}^T\mathbf{K}_f\mathbf{U}_f \tag{2}$$

where U_f and K_f are the nodal displacement vector and the stiffness matrix of the fluid system, respectively. K_f is obtained by the sum of the stiffness matrices of the fluid elements as follows,

$$\mathbf{K}_f = \sum \mathbf{K}_f^e$$

$$\mathbf{K}_f^e = \int_V \mathbf{B}_f^{eT} \mathbf{C}_f \mathbf{B}_f^e dV^e \tag{3}$$

where C_f is the elasticity matrix consisting of diagonal terms in Eq. (1) is the strain-displacement matrix of the fluid element.

An important behaviour of fluid systems is the ability to displace without a change in volume. For reservoir and storage tanks, this movement is known as sloshing waves in which the displacement is in the vertical direction. The increase in the potential energy of the system because of the free surface motion can be written as,

$$\pi_s = \frac{1}{2} \mathbf{U}_{sf}^T \mathbf{S}_f \mathbf{U}_{sf} \tag{4}$$

where U_{sf} and S_f are the vertical nodal displacement vector and the stiffness matrix of the free surface of the fluid system, respectively. S_f is obtained by the sum of the stiffness matrices of the free surface fluid elements as follows,

$$\left.\begin{aligned} \mathbf{S}_f &= \sum \mathbf{S}_f^e \\ \mathbf{S}_f^e &= \rho_f g \int_A \mathbf{h}_s^T \mathbf{h}_s dA^e \end{aligned}\right\} \tag{5}$$

where h_s is the vector consisting of interpolation functions of the free surface fluid element. ρ_f and g are the mass density of the fluid and the acceleration due to gravity, respectively. Besides, kinetic energy of the system can be written as,

$$T = \frac{1}{2} \dot{\mathbf{U}}_f^T \mathbf{M}_f \dot{\mathbf{U}}_f \tag{6}$$

where $\dot{\mathbf{U}}$ and M_f are the nodal velocity vector and the mass matrix of the fluid system, respectively. M_f is also obtained by the sum of the mass matrices of the fluid elements as follows,

$$\left.\begin{aligned} \mathbf{M}_f &= \sum \mathbf{M}_f^e \\ \mathbf{M}_f^e &= \rho_f \int_V \mathbf{H}^T \mathbf{H} dV^e \end{aligned}\right\} \tag{7}$$

where H is the matrix consisting of interpolation functions of the fluid element. If (Eq. (2), (4) and (6)) are combined using the Lagrange's equation (Clough and Penzien, 1993) ; the following set of equations is obtained,

$$\mathbf{M}_f \ddot{\mathbf{U}}_f + \mathbf{K}_f^* \mathbf{U}_f = \mathbf{R}_f \tag{8}$$

where $\dot{\mathbf{U}}_f$, $\ddot{\mathbf{U}}_f$, $\mathbf{U}_f$ and $\mathbf{R}_f$ are the system stiffness matrix including the free surface stiffness, the nodal acceleration and displacement vectors and time-varying nodal force vector for the fluid system, respectively. In the formation of the fluid element matrices, reduced integration orders are used.

The equations of motion of the fluid system, (Eq. (8)), have a similar form with those of the structure system. To obtain the coupled equations of the fluid-structure system, the determination of the interface condition is required. Since the fluid is assumed to be inviscid, only the displacement in the normal direction to the interface is continuous at the interface of the system. Assuming that the structure has the positive face and the fluid has the negative face, the boundary condition at the fluid-structure interface is,

$$U_n^- = U_n^+ \tag{9}$$

where U_n is the normal component of the interface displacement. Using the interface condition, the equation of motion of the coupled system to ground motion including damping effects are given by,

$$\mathbf{M}_c\ddot{\mathbf{U}}_c + \mathbf{C}_c\dot{\mathbf{U}}_c + \mathbf{K}_c\mathbf{U}_c = \mathbf{R}_c \tag{10}$$

in which $\mathbf{M}_c$, $\mathbf{C}_c$, and $\mathbf{K}_c$ are the mass, damping and stiffness matrices for the coupled system, respectively. $\ddot{\mathbf{U}}_c$, $\dot{\mathbf{U}}_c$, $\mathbf{U}_c$ and $\mathbf{R}_c$ are the vectors of the displacements, velocities, accelerations and external loads of the coupled system, respectively (Kartal, 2012).

Kocaeli Earthquake

In this study, 1999 Kocaeli earthquake records were used in all linear dynamic analysis. The earthquake duration is 27.185 seconds. The earthquake accelerogram was given in Fig .4.

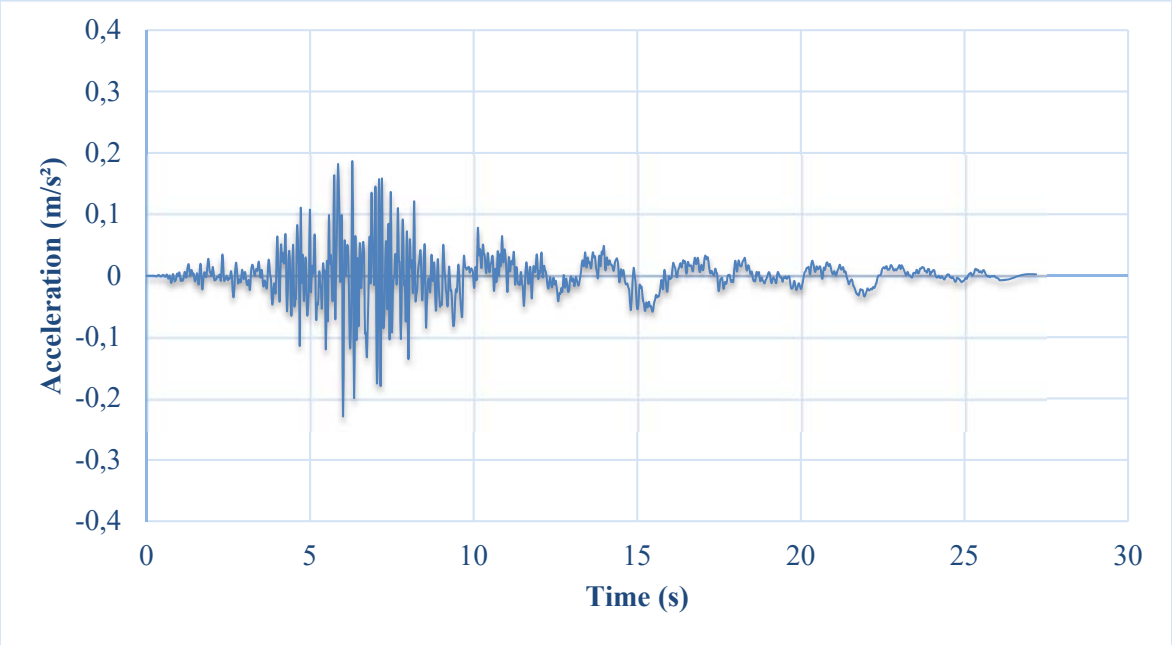

Figure 3. 1999 Kocaeli Earthquake records

Results

The displacements of upstream site of dam were calculated for empty and full reservoir cases. It is clearly seen that full reservoir case has higher displacements than empty reservoir case in linear dynamic analysis due to hydrodynamic pressure. The maximum displacement in full reservoir case is 3.2 cm and the maximum displacement in empty reservoir case is 2.7 cm for the dam. The change of displacements by dam height is given in Fig. 4 and 5.

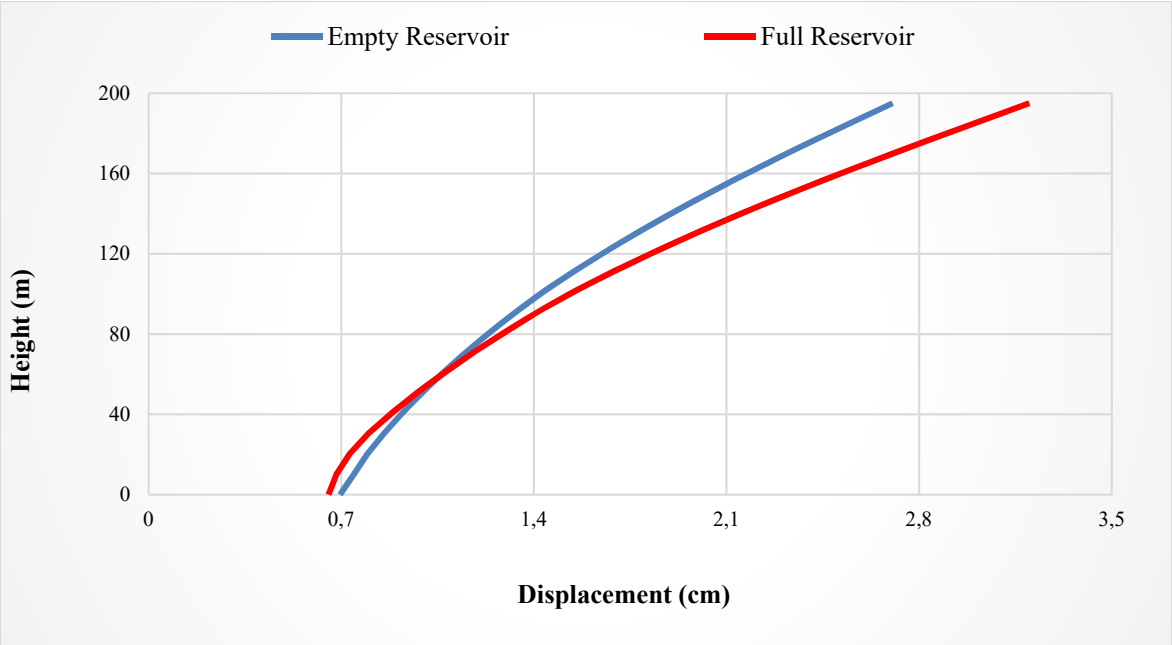

Figure 4. Maximum displacements changing

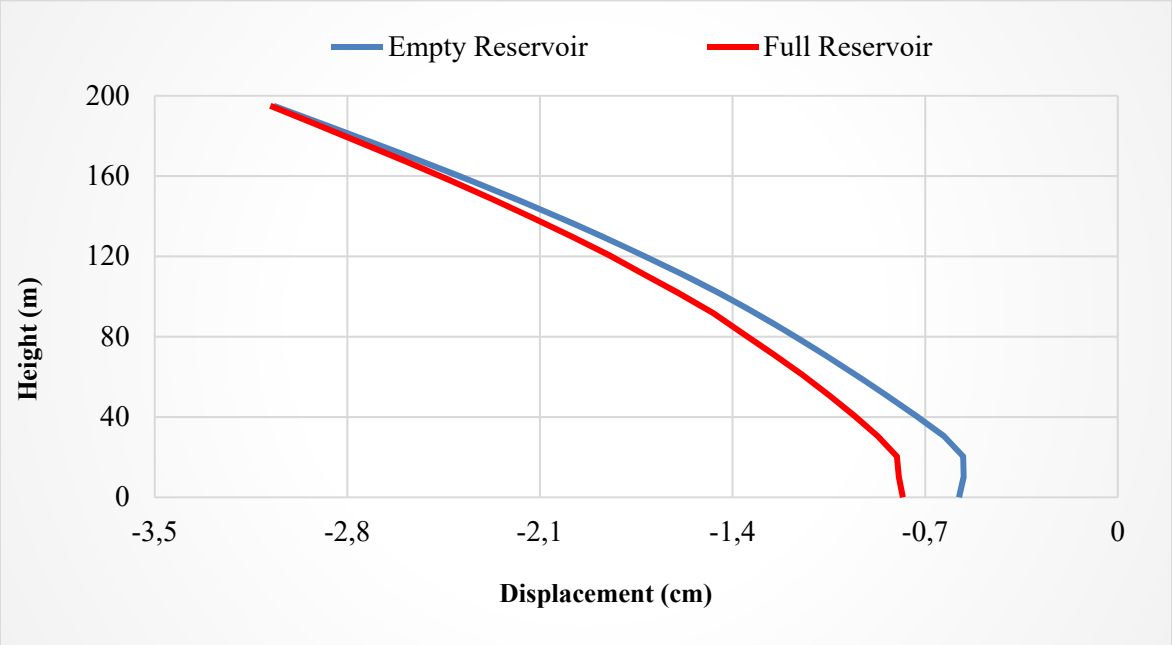

Figure 5. Minimum displacements changing

We investigated the principal stress changing by dam height under Kocaeli earthquake for linear dynamic analysis. It was expected that full reservoir case had higher principal stresses than empty reservoir case because of hydrodynamic pressure effect. According to linear dynamic analysis, it was observed that full reservoir case has higher principle stresses. The maximum principal stress is 2206.96 kN/m² in empty reservoir condition and 2904.08 kN/m² in full reservoir condition for the dam. Besides, the maximum compressive stress is 2622.44 kN/m² in empty reservoir condition and 2324.98 kN/m² in full reservoir condition for the dam. The change of maximum principal stresses and compressive stresses by dam height are given in Fig. 6 and 7.

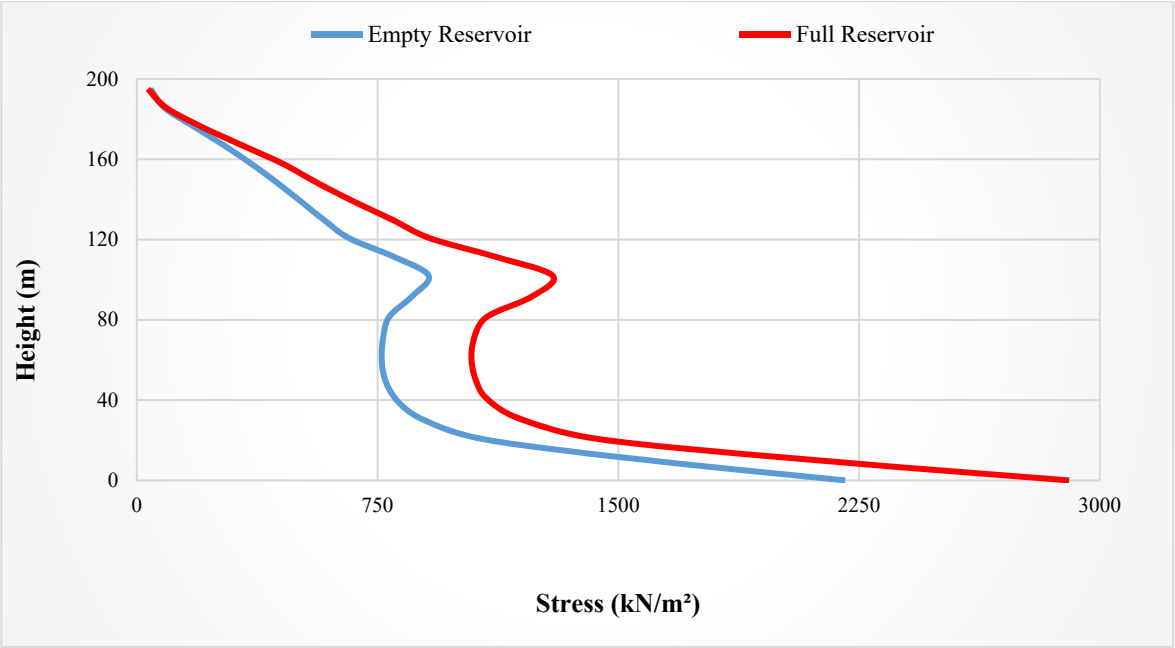

Figure 6. Maximum tensile stresses changing

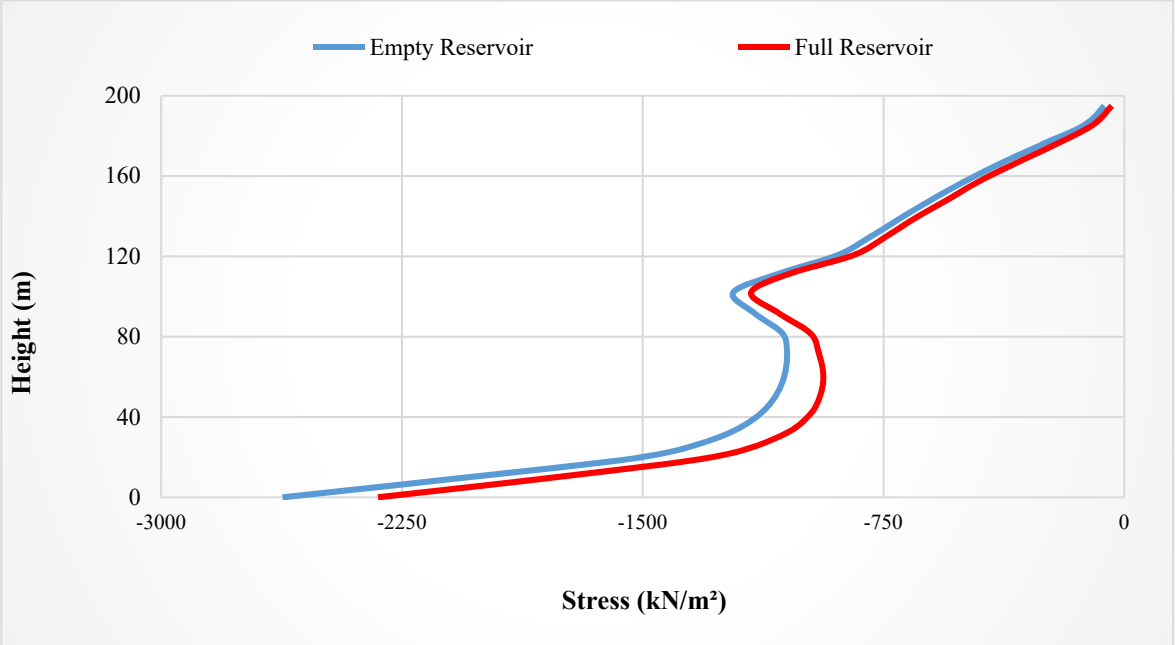

Figure 7. Maximum compressive stresses changing

Conclusion

Boyabat CG Dam geometry and the unfavorable section of the dam was examined using finite element model. Boyabat dam was modeled as two-dimensional and the material and foundation soil mechanical properties were obtained from the experimental data of the dam. After that these materials were identified to dam model by ANSYS software. Fixed boundary conditions were defined around dam and foundation. Finally, 1999 Kocaeli earthquake was selected for this application due to similar earthquake seismic zones.

In this study, we investigated the effect of strong ground motion on stresses and displacements. In addition to this, it was examined that friction, which was identified between dam body-foundation soil, effect on stress for empty and full reservoir conditions. It is clearly seen that full reservoir model has larger tensile-compressive stresses and displacements than empty reservoir model.

References

Key Developments in the History of Gravity Dams (2008). Cracking Dams, 2008-09-30
About Dams (2008) The British Dam Society, 2008-09-30.
Gravity Dams (2008) The British Dam Society, 2008-09-30.
USACE (1995). *Gravity Dam Design*. EM 1110-2-2200 (30 June 1995)
Wilson, E. L. and Khalvati, M. (1983): Finite elements for the dynamic analysis of fluid-solid systems, Int. J. Num. Meth. Eng., 19, 1657–1668. 1983.
Zienkiewicz, O. C. and Taylor R. L.(1989): The Finite Element Method, Mc Graw-Hill, 1989
Clough, R. W. and Penzien, J. (1993): Dynamics of structures, 2nd Edn., McGraw-Hill, Singapore, 1993.
Kartal, M.E. (2012) Three-dimensional earthquake analysis of roller-compacted concrete dams, Natural Hazards and Earth System Sciences, Volume 12, Issue 7, Pages 2369 - 2388, 2012. Doi:10.5194/nhess-12-2369-2012 SCIE

INVESTIGATION OF SINGLE AND MULTI-LAYER NONWOVENS THERMAL INSULATION AND AIR PERMEABILITY BEHAVIORS

Seyda EYUPOGLU*, Nigar MERDAN, Habip DAYIOGLU, Mehmet KILINC

Istanbul Commerce University, Department of Fashion and Textile Design, Istanbul-Turkey

scanbolat@ticaret.edu.tr

Abstract: Textile materials have potential importance for an alternative use on thermal insulation as their porous and fibrous structure. In this study, thermal insulation and air permeability of multi-layer nonwovens with 120, 180 and 500 g/m^2 forming single and double layer were investigated. Moreover, thermal insulation and air permeability of triple-layer and four-layer nonwovens with the weight of 180 g/m^2 were analyzed. It was found that the single layer nonwovens give better thermal insulation properties than the multi-layer nonwovens. Furthermore, the increase of weight of nonwovens causes to increase in thermal conductivity coefficients. According to the air permeability measurements, the results show that the air permeability of samples decreases with the increase of weight of samples and number of layer.

Keywords: Nonwoven, Multi-layer, Thermal Conductivity, Air Permeability.

Introduction

It is very important to have thermal insulation on daily and special habitats. The thermal insulation defined as absorbing (not reflecting) the thermal energy within the material. The textile materials being fibrous and porous have potential applications where thermal insulation is necessary.

The properties of insulation and absorption of the nonwovens differ by fiber geometry and fiber regularity within the texture. It is rather difficult to identify the microstructure of the nonwovens for their complex texture. Nonwoven structure contains not only fiber as well as air gaps. Different fiber composition within the nonwovens leads to change the total surface area (Seddeg, 2009). The sound absorption properties of the textiles having porous structure (Tascan and Vaughn, 2008; Tascan and Vaughn, 2008; Shoshani and Yakubov, 2000), different fiber blends (Nick et al. 2002; Seddeq et al., 2013), stratified composition (Lin et al., 2011; Kucuk and Korkmaz, 2015), standard and hollow polyester with different weight (Abdelfattah et al., 2011). Furthermore, the effect of the acoustic characteristic of nonwovens containing polyester, viscose, glass fiber and basalt fibers on the material thickness, weight, air permeability and porosity have been studied (Yang et al., 2001). There are also more studies on the effect acoustic properties of jute, polypropylene and polyester containing nonwovens on the bases of weight, fabric type, fiber density, number of ply, the distance between the origin of sound and material, and also fiber types (Sengupta 2010).

The energy sources are running out rapidly. This situation, leads activities on especially in developed and other countries to take control of their energy needs, and lead them to search for new energy sources. The major part of the energy saving is natural thermal energy.

Nowadays it became common to use thermal insulation materials on habitants in order to reduce the energy consumption. There are a number of researches on thermal insulation behavior of waste woven fabrics (Briga-Sa et al., 2013), waste wool and regenerated polyester fibers (Patnaik et al., 2015), nonwovens (Woo et al., 1994), stratified nonwovens (Mohammadi et al., 2003), the effect of fiber diameter and porosity dimensions (Zhu and Li, 2003), nonwovens produced by pinning methods (Saleh, 2011), glass, wool, rook wool and mineral wool (Abdou and Budaiwi, 2013).

In order to use polyester nonwovens is a various applications the behavior of air permeability behavior of the weightand pinning density of the polyester viscose blend nonwovens (Zu et al., 2015; Cincik and Koc, 2012), theoretical and experimental as well as artificial neural networks of multi-ply nonwovens (Mohammadi et al., 2002; Debnath et al., 2000), the relations, the pore size effect (Epps and Leonas, 2000), the effect of thermal insulation (Debnath and Madhusoothanan, 2010), and also the relations between air permeability and sound absorption was studied (Thilagavathi et al., 2010).

In this study, the thermal insulation and air permeability properties of nonwoven fabrics with different weight were investigated. The purpose for chosen nonwovens is for being lightweight materials, making them preferable on thermal insulation. In this context, thermal insulation and air permeability of multi-layer nonwovens with 120, 180 and 500 g/m^2 forming single and double layer were investigated. Moreover, thermal insulation and air permeability of triple-layer and four-layer nonwovens with the weight of 180 g/m^2 were analyzed. The thermal insulation and

air permeability properties of samples increase with the decrease of weight and layer numbers of samples.

Materials and Methods

Fabric

Polyester nonwovens with 45 µm fiber diameter of 120, 180 and 500 g/m^2 were used.

Preparation of Multi-Ply Nonwovens

From the polyester nonwovens having 120 and 500 g/m^2 weight of the prepared samples of single and double layer, and 180 g/m^2 polyester nonwovens single, double, triple and fourfold samples were prepared.

Measurements of the Thermal Conductivity Coefficient

Thermal conductivity coefficients of the samples were evaluated in accordance with TS 4512 Standard (TS EN ISO 10534-2) via using P.A.HILTON LTD.H940 instrument. In order to measure thermal conductivity coefficients of the samples prepared, the samples with the diameter of 25 mm was primarily experimented. The heat value (Q) in watt was determined from the digital screen of the instrument. The measurements of the thickness and area of the tested fabrics as well as heat difference between them were replaced in the following equation (Kılıc and Yigit, 2008).

$$Q = -k.A.\frac{dT}{dx}$$

In this equation, Q is the heat flow (W), A is the surface field (m^2), x is the thickness of sample (m), ΔT is the temperature difference (K) and k is thermal conductivity coefficient (W/m K). The measurements of thermal conductivity coefficient were iterated three times.

Measurements of the Air Permeability

The measurements was carried out by using 20 cm^2 circular fabric with 100 Pa pressure difference for 1 second and the results was expressed in mm/s by taken the average of five different measurement. The test was performed according to TS 391 EN ISO 923 (TS 391 EN ISO 9237) test method.

Results and Discussion

Results of Thermal Conductivity Coefficient Measurements

The thermal conductivity coefficient results of the samples with different weights and number of layers are given on Figure 1.

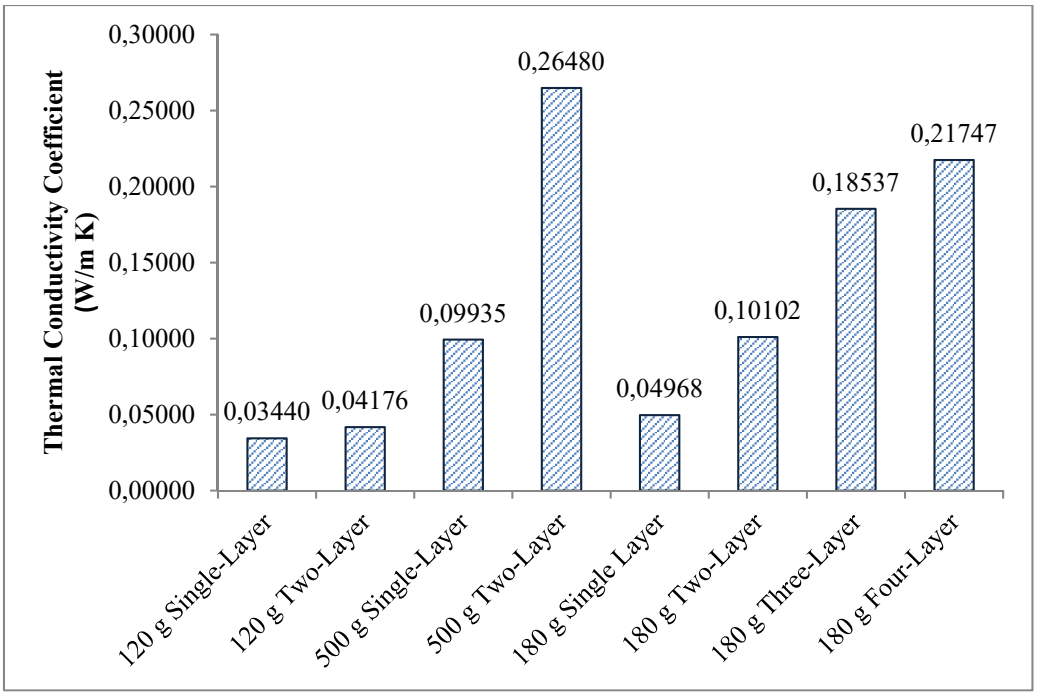

Figure 1. Thermal conductivity coefficient of samples.

Figure 1 shows that, the increased nonwoven weight increases the thermal conductivity coefficient, as a result of increased weight leads to increasing the thickness of the materials. According to the Fourier Law, the increased sample thickness and number of layers causes increasing the thermal conductivity coefficient.

The increased number of layers causes increased thickness, and as a result of this leads to increases the thermal conductivity coefficient. These results were also correlated with the air permeability of the samples decreases by increasing the number of layers and weights.

Results of Air Permeability Measurements

The air permeability results of the samples with different weights and number of layers are given on Figure 2.

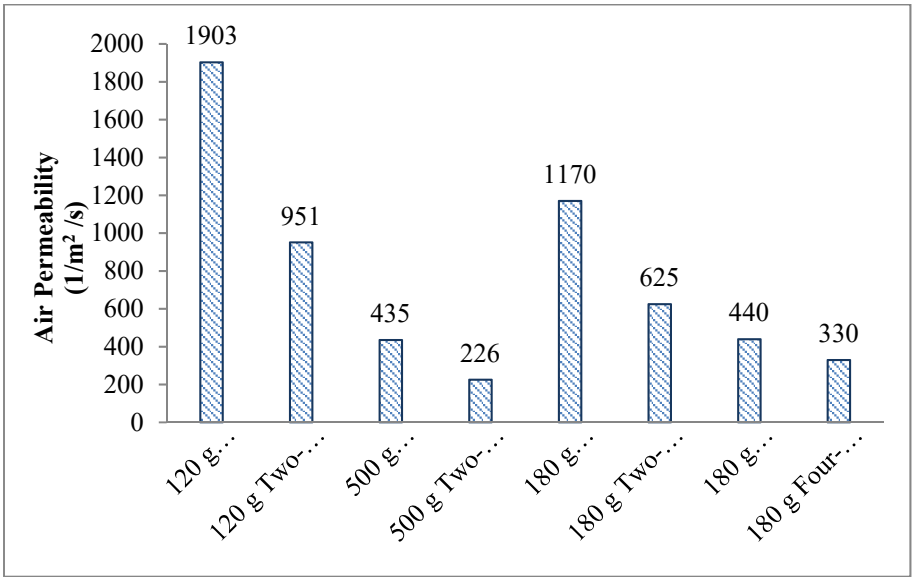

Figure 2. Air permeability measurements of samples.

The air permeability results show that, the increased sample weight decreases the air permeability. This can be explained by the weight increasing causing to density decrease. The density increase leads to decrease the air permeability. The increased number of layers of the samples causes decrease on air permeability. This can be explained by increased number of layers causing increase on the sample thickness. The increased sample thickness causes increased air flow distance during the test and this results decrease on air permeability. Besides, the increased number of layers leads density increase.

Conclusion

In this study, the thermal conductivity coefficient and air permeability of the nonwovens with different weight and number of layers was investigated. In this context, the thermal conductivity and air permeability coefficient of polyester nonwoven fabrics with 120, 180 and 500 g/m^2 weights and also their 2,3 and 4 layers samples was investigated. As a result, the increased weight and number of layers of the nonwovens leads to increase on thermal conductivity and decrease on air permeability. The prepared nonwovens found very suitable materials as having light, cheap, high air permeability and thermal insulation properties.

References

Abdelfattah, A.M., Ghalia E.I., Eman R.M. (2011). Using nonwoven hollow fibers to improve cars interior acoustic properties, Life Science Journal, 8(1), pp.344-351.

Abdou, A., Budaiwi, I.(2013). The variation of thermal conductivity of fibrous insulation materials under different levels of moisture content, Construction and Building Materials, 43, pp.533–544.

Briga-Sa, A., Nascimento, D., Teixeira, N., Pinto, J., Caldeira, F., Varum, H., Paiva, A.(2013). Textile waste as an alternative thermal insulation building material solution, Construction and Building Materials, 38, pp.155–160.

Cincik, E., Koc, E.(2012). An analysis on air permeability of polyester/viscose blended needle-punched nonwovens, Textile Research Journal, 82 (5), pp. 430-442.

Debnath, S., Madhusoothanan, M. (2010), Thermal insulation, compression and air permeability of polyester needle-punched nonwoven, IJFTR ,35 (1), pp.38-44.

Debnath, S., Madhusoothanan, M., Srinivasamoorthy, V.R.(2000). Air permeability Artificial neural network Empirical model Needle-punched nonwoven fabric, IJFTR, 25 (4), pp. 251-255.

Epps, H.H., Leonas, K.K.(2000). Pore size and air permeability of four nonwoven fabrics, International Nonwovens Journal, 9(2), pp. 1-8.

Lin, J.H., Lin, C.C., Chen, J.M., Chuang, Y.C., Hsu, Y.H., Lou, C.W.(2011). Processing technique and sound absorption property of three-dimensional recycled polypropylene nonwoven composites, Advanced Materials Research, 26 (60), pp.287-290.

Kılıc¸ M and Yigit A. Isı transferi. Bursa: Alfa Aktuel, 2008.

Kucuk, M., Korkmaz,Y.(2015). Sound absorption properties of bilayered nonwoven composites, Fibers and Polymers, 16 (4), pp. 941-948.

Mohammadi, M., Banks–Lee, P., Ghadimi, P.(2002). Air permeability of multilayer needle punched nonwoven fabrics: theoretical method, Journal of Industrial Textiles, 32 (1), pp. 45-57.

Mohammadi, M., Banks–Lee, P., Ghadimi, P.(2003). Determining effective thermal conductivity of multilayered nonwoven fabrics, Textile Research Journal, 73, pp. 802-808.

Nick, A., Becker, U., Thoma, W.(2002). Improved acoustic behavior of interior parts of renewable resources in the automotive industry, Journal of Polymers and the Environment, 7(10), pp.115-118.

Patnaik, S., Mvubu, M., Muniyasamy, S., Botha, A., Anandjiwala, R.D.(2015). Thermal and sound insulation materials from waste wool and recycled polyester fibers and their biodegradation studies, Energy and Buildings, 92, pp.161–169.

Saleh, S.S.(2011).Performance of needle-punching lining nonwoven fabrics and their thermal insulation properties, Journal of Basic and Applied Science Research, 1(12), pp.3513-3524.

Seddeq, H.S.(2009). Factors influencing acoustic performance of sound absorptive materials. Australian Journal of Basic and Applied Sciences, 3(4), pp. 4610-4617.

Seddeq, H.S., Aly, N.M., Elshakankery, M.H.(2013). Investigation on sound absorption properties for recycled fibrous materials, Journal of Industrial Textiles, 43, pp.56–73.

Sengupta,S. (2010). Sound reduction by needle-punched nonwoven fabrics. IJFTR, 35, pp. 237-242.

Shoshani, Y., Yakubov, Y.(2000). Numerical assessment of maximal absorption coefficients for nonwoven fiber webs, Applied Acoustics, 59, pp. 77–87.

Tascan, M., Vaughn, E.A.(2008). Effects of total surface area and fabric density on the acoustical behavior of needle punched nonwoven fabrics, Textile Research Journal April, 78(4), pp.289-296.

Tascan, M., Vaughn, E.A.(2008). Effects of fiber denier, fiber cross-sectional shape and fabric density on acoustical behavior of vertically lapped nonwoven fabrics, Journal of Engineered Fibers and Fabrics, 3(2), pp. 32-38.

Thilagavathi, G., Pradeep, E., Kannaian, T., Sasikala, L.(2010). Development of natural fiber nonwovens for application as car interiors, Journal of Industrial Textiles, 39, pp.267-275.

TS EN ISO 10534-2; coustics. Determination of sound absorption coefficient and impedance in impedance tubes. Transfer-function method.

TS 391 EN ISO 9237;Textiles-Determination of permeability of fabrics to air.

Woo, S.S., Shalev, I., Barker, R.L.(1994). Heat and moisture transfer through nonwoven fabrics part I: heat transfer, Textile Research Journal, 64 (3), pp. 149-162.

Yang, T.L., Chiang, D.M., Chen, R.(2001). Development of a novel porous laminated composite material for high sound absorption, Textile Research Journal, 7, pp.675-698.

Zhu, G., Kremenakova, D., Wang, Y., Militky, J.(2015). Air permeabiliıty of polyester nonwoven fabrics, AUTEX Research Journal, 15 (1), pp. 8-12.

Zhu, Q., Li, Y.(2003). Effects of pore size distribution and fiber diameter on the coupled heat and liquid moisture transfer in porous textiles, International Journal of Heat and Mass Transfer, 46, pp.5099–5111.

MINIMIZING THE ENERGY OF THE VELOCITY VECTOR FIELD OF CURVE IN R^3

Ayşe ALTIN

Hacettepe University Faculty of Science 06800 Beytepe Ankara Turkey

ayse@hacettepe.edu.tr

Abstract: The present paper considers all the unit-speed curve segments between two fixed points p and q in R^3. It obtain a condition for the critical curve of the problem of minimizing the energy of the velocity vector field among the family of all curves from p to q. It show that the condition can be expressed in terms of the curvature functions.

Keywords: Energy, Energy of a unit vector field, Sasaki metric

Introduction

The volume of unit vector fields has been studied by (Gluck and Ziller, 1986, Johnson, 1988, Higuchi, Kay and Wood, 2001) among other scientists. They define the volume of unit vector field X as the volume of the submanifold of the unit tangent bundle defined by $X(M)$. In (Wood, 1997), the energy of a unit vector field on a Riemannian manifold M is defined as the energy of the mapping $X: M \to T^1M$, where the unit tangent bundle T^1M is equipped with the restriction of the Sasaki metric on TM.

Generally, every geometric problem about curves can be solved using the curves'Frenet vectors field. Therefore, in (Altın, 2011), we focus on the curve C instead of the manifold M. For a given curve C, with a pair of parametric unit speeds (I, α) in a space R^n, on which we take a fixed point $a \in I$, we denote Frenet frames at the points $\alpha(a)$ and $\alpha(s)$ by $\{V_1(\alpha(a)), \dots, V_r(\alpha(a))\}$ and $\{V_1(\alpha(s)), \dots, V_r(\alpha(s))\}$ respectively. We calculate the energy of the Frenet vectors fields as well as the angle between the vectors $V_i(\alpha(a))$ and $V_i(\alpha(s))$, where $1 \leq i \leq r$. We observed that both energy and angle depend on the curvature functions of the curve C.

In this paper, we choose two points p and q in R^3. We obtain a condition for the critical curve of the problem of minimizing the energy of the velocity vector field among the family of all curves from p to q. We also prove that this condition can be expressed in terms of the curvature functions. For example the condition is realized for curves whose curvature functions is constant. An example is also provided to show that the curvature of the curve is linear.

Definition 1.1 A curve segment is the portion of a curve defined in a closed interval, (O'Neill 1966).

Theorem 1.1.(Frenet formulas) If $\alpha: I \to R^3$ is a unit speed curve with curvature $\kappa > 0$ and torsion τ, then

$$T' = \kappa N,$$
$$N' = -\kappa T + \tau B,$$
$$B' = -\tau N$$

Where $\{T, N, B\}$ is the Frenet frame on α (O'Neill 1966).

Proposition 1.1 The connection map $K: T(T^1M) \to T^1M$ verifies the following conditions.
1) $\pi \circ K = \pi \circ d\pi$ and $\pi \circ K = \pi \circ \tilde{\pi}$, where $\tilde{\pi}: T(T^1M) \to T^1M$ is the tangent bundle projection and $\pi: T^1M \to M$ is the bundle projection.

2) For $\omega \in T_xM$ and a section $\xi: M \to T^1M$, we have

$$K(d\xi(\omega)) = \nabla_\omega \xi.$$

Where ∇ is the Levi-Civita covariant derivative (Chacón , Naveira and Weston,2001).

Definition 1.2. For $\eta_1, \ \eta_1 \in T_\xi(T^1M)$ define

$$g_s(\eta_1, \ \eta_1) = < d\pi(\eta_1), d\pi(\eta_2) > + < K(\eta_1), K(\eta_2) >. \qquad (1)$$

This gives a Riemannian metric on TM. Recall that g_s is called the Sasaki metric. The metric g_s makes the projection $\pi: T^1M \to M$ a Riemannian submersion (Chacón , Naveira and Weston,2001).

Definition 1.3. The energy of a differentiable map $f: (M, <,>) \to (N, h)$ between Riemannian manifolds is given by

$$\varepsilon(f) = \frac{1}{2}\int_M (\sum_{a=1}^{n} h(df(e_a), df(e_a))\, \nu \qquad (2)$$

where ν is the canonical volume form in M and $\{e_a\}$ is a local basis of the tangent space (Chacón , Naveira and Weston,2001 and Wood, 1997).

A Condition on Minimizing Energy of the Velocity Vector Field of a Curve in R^3

The following theorem characterizes a critical point of the energy of the velocity vector field of a curve in R^3

Theorem 2.1. Let α be unit speed curve in R^3 and α(a) = p, α(b) = q. Let us consider the collection of all curves segments from p to q in R^3 . If the energy of the velocity vector of α along one segment is less than that along any other segment, then the following equation is valid

$$\int_a^b \lambda(s)\kappa(s)\kappa'(s)ds = 0 \qquad (3)$$

where κ is the curvature function and λ is the real-valued function n [a, b].

Proof. Let $\alpha: I \to R^3$ be a unit speed curve in R^3 and [a, b]⊂ I, α(a)= p, α(b) = q. There exists a real-valued function λ on [a, b], λ(s)=(s-a)(b-s), λ(a)=λ(b)=0 and $\lambda(s) \neq 0$ for all s∈(a, b). Let {T, N, B} be the Frenet frame field on α and

$$\lambda(s)T(s) = \big(v_1(s),\ v_2(s),\ \ v_3(s)\big), \qquad v_i: [a.b] \to R. \qquad (4)$$

Let the collection of curves be

$$\alpha^k(s) = \big(\alpha_1(s)+k\ \ v_1(s),\ \alpha_2(s)+k\ \ v_2(s),\ \ \alpha_3(s)+k\ \ v_3(s)\big) \text{ for sufficiently small } k. \qquad (5)$$

For k=0, α^0(s)=α(s) and λ(a)=λ(b)=0, we have v_i(a)= v_i(b)=0 . $1 \le i \le 3$ and $\alpha^k(a) = p,\ \alpha^k(b) = q.$ These results show that α^k is the curve segment from p to q.

Assume this collection $\alpha^k(s)$ =α(s, k) for all curves. The expression for the energy of the vector field T_k of α^k from p to q becomes $\mathcal{E}(T_k)$.

Now, let TC_k be the tangent bundle. So we have $T_k: C_k \to TC_k$, where $TC_k = \cup_{t\in I} T_{\alpha^k(t)}C_k$, $C_k = \alpha^k(I)$ and $T_{\alpha^k(t)}C_k$ denotes generated by T_k. Let $\pi: TC_k \to C_k$ be the bundle projection. By using equation (2) we calculate the energy of T_k as

$$\mathcal{E}(T_k) = \frac{1}{2}\int_a^b g_S(d\,T_k(T_k(\alpha(s,k)), dT_k(T_k\big(\alpha(s,k)\big))ds \qquad (6)$$

where ds is the differential arc length. From (1) we have

$$g_S(dT_k(T_k),\ dT_k(T_k)) = <d\pi(\ dT_k(T_k)),\ d\pi(\ dT_k(T_k))> + <K(dT_k(T_k)),\ K(dT_k(T_k)>.$$

Since T_k is a section, we have $d(\pi)\circ d(T_k) = d(\pi \circ T_k) = d\big(id_{C_k}\big) = id_{TC_k}$. By Proposition 1.1, we also have that

$$K\big(dT_k(T_k)\big) = \nabla_{T_k}T_k = T_k' = \frac{\partial T_k}{\partial s},$$

giving

$$g_S(dT_k(T_k),\ dT_k(T_k)) = <T_k,\ T_k> + <T'_k,\ T'_k>.$$

Using these results in (6) we get

$$\mathcal{E}(T_k) = \frac{1}{2} \int_a^b (< T_k, T_k > + < T'_k, T'_k >) ds \qquad (7)$$

Where $T_k = \frac{1}{w(s,k)} \frac{d\alpha}{\partial s}(s, k)$; $w(s,k) = \sqrt{< \frac{d\alpha}{\partial s}(s,k), \frac{d\alpha}{\partial s}(s,k) >}$, Suppose that $\mathcal{E}(T_k)$ is such a minimized energy for any "k" $\alpha(s, k)$ with $\alpha(s,0)=\alpha(s)$. We calculate $\frac{\partial \mathcal{E}(T_k)}{\partial k}$ and evaluate at k=0. If $\mathcal{E}(T_k)$ is a minimizing energy, then k=0 should be a critical point of $\mathcal{E}(T_k)$. Supposing that $\frac{\partial \mathcal{E}(T_k)}{\partial k}|_{k=0} = \frac{\partial \mathcal{E}(T_0)}{\partial k} = 0$, from (7) we obtain:

$$\frac{\partial \mathcal{E}(T_k)}{\partial k} = \frac{\partial}{\partial k} \left[\frac{1}{2} \int_a^b (< T_k, T_k > + < T'_k, T'_k >) ds \right] = \frac{1}{2} \int_a^b \frac{\partial}{\partial k} \left[< T_k, T_k > + < \frac{\partial T_k}{\partial s}, \frac{\partial T_k}{\partial s} > \right] ds.$$

Since $< T_k, T_k > = 1$ we have $\frac{\partial}{\partial k} < T_k, T_k >= 0$ and we get

$$\frac{\partial \mathcal{E}(T_k)}{\partial k} = \frac{1}{2} \int_a^b \frac{\partial}{\partial k} < \frac{\partial T_k}{\partial s}, \frac{\partial T_k}{\partial s} > ds = \int_a^b (< \frac{\partial^2 T_k}{\partial s \partial k}, \frac{\partial T_k}{\partial s} > ds. \qquad (8)$$

We can write

$$\frac{\partial}{\partial s} < \frac{\partial T_k}{\partial k}, \frac{\partial T_k}{\partial s} > = < \frac{\partial^2 T_k}{\partial s \partial k}, \frac{\partial T_k}{\partial s} > + < \frac{\partial T_k}{\partial k}, \frac{\partial^2 T_k}{\partial s^2} >.$$

Thus, we can deduce,

$$< \frac{\partial^2 T_k}{\partial s \partial k}, \frac{\partial T_k}{\partial s} > = \frac{\partial}{\partial s} < \frac{\partial T_k}{\partial k}, \frac{\partial T_k}{\partial s} > - < \frac{\partial T_k}{\partial k}, \frac{\partial^2 T_k}{\partial s^2} >. \qquad (9)$$

Substituting (9) in (8), for, k=0,

$$\frac{\partial \mathcal{E}(T_0)}{\partial k} = \int_a^b [\frac{\partial}{\partial s} < \frac{\partial T_k}{\partial k}(s,0), \frac{\partial T_k}{\partial s}(s,0) > - < \frac{\partial T_k}{\partial k}(s,0), \frac{\partial^2 T_k}{\partial s^2}(s,0) >] ds$$

and

$$\frac{\partial \mathcal{E}(T_0)}{\partial k} = < \frac{\partial T_k}{\partial k}(s,0), \frac{\partial T_k}{\partial s}(s,0) > |_a^b - \int_a^b < \frac{\partial T_k}{\partial k}(s,0), \frac{\partial^2 T_k}{\partial s^2}(s,0) > ds \qquad (10)$$

From (4) and (5), we obtain,

$$\frac{\partial \alpha}{\partial k}(s, k) = \lambda(s) \; T_k(s) \qquad (11)$$

and

$$\frac{\partial \alpha}{\partial k}(s, 0) = \alpha'(s) = T_k(s, 0) \qquad (12)$$

Now we calculate the partial derivatives of (12) with respect to s and k; using Frenet formulas, we get

$$\frac{\partial T_k}{\partial s}(s,0) = \frac{\partial^2 \alpha}{\partial s^2}(s,0) = \alpha''(s) = T'(s) = \kappa(s) N(s) \qquad (13)$$

and

$$\frac{\partial T_k}{\partial k}(s,k) = \frac{\partial^2 \alpha}{\partial s \partial k}(s, k) = \frac{\partial^2 \alpha}{\partial k \partial s}(s, k).$$

From (11), we have

$$\frac{\partial T_k}{\partial k}(s,k)|_{k=0} = \frac{\partial T}{\partial k}(s,0) = \lambda'(s) T(s) + \lambda(s) \kappa(s) N(s). \qquad (14)$$

It follows from (13) and (14) that

$$< \frac{\partial T_k}{\partial k}(s,0), \frac{\partial T_k}{\partial s}(s,0) > = \lambda(s) \kappa^2(s).$$

Considering the candidate function $\lambda(a) = \lambda(b) = 0$, we get:

$$< \frac{\partial T_k}{\partial k}(s,0), \quad \frac{\partial T_k}{\partial s}(s,0) > |_a^b = \lambda(b)\kappa^2(b) - \lambda(a)\kappa^2(a)=0 \qquad (15)$$

From (13), we get

$$\frac{\partial^2 T_k}{\partial s^2}(s,0) = -\kappa^2(s)T(s) + \kappa'(s)N(s) + \kappa(s)\tau(s)B(s) \qquad (16)$$

Therefore, (14) and (16) gives

$$< \frac{\partial T_k}{\partial k}(s,0), \frac{\partial^2 T_k}{\partial s^2}(s,0) > = -\lambda'(s)\kappa^2(s) + \lambda(s)\kappa(s)\kappa'(s) = [-\lambda(s)\kappa^2(s)]' + 3\lambda(s)\kappa(s)\kappa'(s). \qquad (17)$$

Substituting (15) and (17) in (10), yields

$$\frac{\partial \mathcal{E}(T_k)}{\partial k}|_{k=0} = \frac{\partial \mathcal{E}(T_0)}{\partial k} = -\int_a^b ([-\lambda(s)\kappa^2(s)]' + 3\lambda(s)\kappa(s)\kappa'(s))ds=0$$

and

$$\frac{\partial \mathcal{E}(T_0)}{\partial k} = [-\lambda(s)\kappa^2(s)]|_a^b - 3\int_a^b \lambda(s)\kappa(s)\kappa'(s)ds=0$$

We are looking the candidate function $\lambda(a) = \lambda(b) = 0$, which given $[-\lambda(s)\kappa^2(s)]|_a^b = 0$ and

$$\frac{\partial \mathcal{E}(T_0)}{\partial k} = -3\int_a^b \lambda(s)\kappa(s)\kappa'(s)ds=0.$$

This completes the proof of the theorem. Any path that minimizes the energy function $\mathcal{E}(T_k)$ must satisfy equation (3). Note that the condition is necessary, but not sufficient; not every function that satisfies (3) will produce minimal energy. If α is geodesic then it will satisfy equation (3). The following is provided as an example. This
example will also demonstrate that the curvature of the curve is linear, given the aforementioned conditions.

Example. Let $\alpha: I \to R^3$, [0,1]⊂ I, α(0)= p, α(1) = q. If we can choose $\lambda: [0,1] \to R$, λ(s)=s(1-s), λ(0)=0, λ(1)=0 and λ(s)≠ 0 for all s∈(0, 1). Let the curvature function of α be $\kappa(s) = cs + d$ where c and d are real numbers. Using equation (3), we have

$$\frac{\partial \mathcal{E}(T_0)}{\partial k} = \int_0^1 \lambda(s)\kappa(s)\kappa'(s)ds = c(c + 2d) = 0.$$

If c=0 then κ constant, or c=-2d.

References

Altın, A. (2011),. On the Energy and the Pseudo Angle of a Frenet Vectors Fields in R_v^n. *Ukrainian Mathematical journal*, Vol. 63, No 6, (pp.833-839).

Chacón, P.M. and Naveira, A.M. (2004), Corrected Energy of Distributions on Riemannian Manifold. *Osaka Journal Mathematics*,Vol 41 (pp. 97-105).

Chacón, P.M. and Naveira, A.M. and Weston , J.M. (2001), *On the Energy of Distributions, with Application to the Quarternionic Hopf Fibration*.. Monatshefte fûr Mathematik, Vol.133,(pp. 281-294).

Gluck. H. and Ziller, W. (1986), On the volume of the unit vector fields on the three sphere. *Comment Math. Helv*. Vol 61, (pp.177-192).

Higuchi, A., Kay, B. S. and Wood, C. M. (2001), The energy of unit vector fields on the 3-sphere *Journal of Geometry and Physics*. Vol 37, (pp. 137-155).

Johnson, D.L. (1988), Volume of flows, Proc. *Amer. Math. Soc*.Vol.104, (pp. 923-932).

O'Neill, B. (1966). Elementary Diffrential Geometry. *Academic Press Inc.*

Wood, C. M. (1997), On the Energy of a Unit Vector Field. *Geometrae Dedicata*. Vol.64, (pp.319-330).

MODELLING APPROACHES OF PERFORMANCE EVALUATION OF HIGH QoS OF KERBEROS SERVER WITH DYNAMICALLY RENEWING KEYS UNDER PSEUDO CONDITIONS

Yoney K. EVER [1] Eser GEMIKONAKLI[2] Kamil DIMILILER [3]
[1] Software Engineering Department, Near East University, Nicosia,
North Cyprus, Mersin 10 Turkey
Email: yoneykirsal.ever@neu.edu.tr

[2] Graduate School of Applied Sciences, University of Kyrenia, Girne, Mersin 10 Turkey
E-mail: eser.gemikonakli@kyrenia.edu.tr

[3] Electrical & Electronic Engineering Department, Near East University, Nicosia,
North Cyprus, Mersin 10 Turkey
Email: kamil.dimililer@neu.edu.tr

Abstract: In literature, some existing studies suggested different proposed approaches that interrupt temporary link/server access. Also, in order to find implications in terms of performance degradation, analytical models are used, as well as failures of the servers. Unlike previous studies, the failures of the servers are considered together with link/server interruptions for renewals. In this study, the authors mainly focused to develop a new framework for the existing authentication protocols by considering them in an unusual fashion. The performance degradations that may be caused by service interruptions are discussed with a new framework to model the interactions between the network and the authentication servers.

Keywords: Kerberos variance, Quality of Service, Performability modelling, Queueing analysis

Introduction

Last three decades use of networked computer system has been increased and become popular. Communication and distribution of large, confidential and classified information are also available electronically, which requires challenge to protect system, data as well as resources. The configuration of the system plays an important role in privacy and data integrity that affects the performance of the underlying networks. The system considered should have the ability to perform sufficient and legitimate access to resources, while considering the applied security resources.

Network authentication is one of the vital methods for network and information security communications. Kerberos which is based on Needham-Schroder Authentication Protocol (Needham1978) commonly used for this purpose. As stated in literature, Kerberos architecture is divided into two core elements Key Distribution Centre (KDC) and Ticket Granting Service (TGS) (Brennen2004). The KDC stores authentication information and uses it to securely authenticate users and services while TGS holds digital tickets to identify the network clients and servers. If an attacker can gain administrative access to the KDC, he would have access to the complete resources of the Kerberos realm. A masquerading TGS (any client) can impersonate the TGS of the network (Kirsal2007b). In addition, Kerberos exhibits some other vulnerabilities widely reported in the literature (Brennen2004).

The design of the proposed protocol, combines the properties of Kerberos and Key-Exchange protocols together, which was considered in developing a specific authentication protocol as part of a previously proposed framework (Kirsal2007a). This combined approach had been proposed to shut down external access to an enterprise network for a period of time to enable the distribution of randomly generated keys (Kirsal2007b), (Schneider1998). In research (Kirsal2007b), while authentication protocol was designed, intruder is modelled as well. While the protocol was modelled, renewing keys at various intervals was considered, in order to block potential intruders. Although the intruder had been given the power to attack, the protocol was successful in preventing replay attacks (Kirsal2007b), (Kirsal2008). Security protocols in distributed systems are time-sensitive. That is to say if time of decrypting messages are increased, intruders could be blocked and prevented. In (Kirsal2008), a new protocol is proposed based on the use of timestamps to delay decryption by potential intruders. Considering the key distribution, external network access is restricted for short time intervals (Kirsal2007b), and (Kirsal2008). This affects the performance of the network. For this purpose, an analytical model has been developed to evaluate the

performability of the proposed approach (Kirsal2007b). While key distribution times depend on network characteristics such as size, and speed, the intervals between key renewals can be determined by the mean values of decryption times.

Related Works

In this section, frequent key renewal protocol, challenges of quality of service, and performability modelling for security protocols will be explain in detail.

Frequent Key Renewal Protocol

As stated in (Kirsal-Ever2013) the proposed protocol is based on frequent key renewal under pseudo conditions. the proposed approach was shutting-down external access to an enterprise network for a period of 140 seconds, to enable the distribution of randomly generated keys to users in a relatively secure way. Details are given in (Kirsal-Ever2013).

Quality of Service Challenges

Quality of Service (QoS) refers to the ability of a network to provide better, more predictable service. It is referred as selected network traffic over various underlying technologies, specifically wireless and mobile networks (Lowe1996), (Saravanan2006), (Song2005). Last two decades wireless and mobile networks have gained widespread popularity mainly because of their low cost and relatively high data rates. In this circumstances, issues with QoS becomes extremely important. In recent years, within the use of a wireless communication system, seamless time sensitive movement of audio and video are demanded by enterprises and users. However, interruptions may be caused because of implemented security mechanisms, which can cause degradation of performance for the traffic.

In addition, as stated in (Hua2004), interruptions in wireless and mobile systems cause the packet loss, latency, congestion and jitter, which are important QoS challenges. Latency is the time delay occurred in speech by the end-to-end user communication system. The lower the latency, the better the QoS (Balsamo2003), (Baghaei2004). In order to increase QoS in terms of packet losses, less interruptions, dedicated bandwidth and controlled jitter should be improved. Researches on good QoS showed that greater levels of interruption introduce more delay and require lower network latency (Lowe1996), (Hua2004).

The major constraint is end-to-end interruption. It requires the delay to be reduced through a packet network. To support traffic reliably and enhance the QoS in WLAN, a network must therefore be able to provide packet forwarding latency, jitter, guaranteed network bandwidth and capacity for communication during periods of network congestion (Kirsal-Ever2013).

Necessity of Modelling Security Protocols for Performability Modelling

Implemented security mechanisms in wireless communication systems are one of the main reason of service interruptions (Ever2009). The wireless variants of existing protocols may prefer to shut the communication while the critical key exchange processes are taking place. That would introduce significant delays, and increased number of request awaiting for authentication.

System or server interruptions depend on the system's nature and can have different impacts on the system performance. The system may not support the ongoing process or the packet efficiently due to the interruptions hence performance may degrade. In order to overcome this problem, availability and performance of the system should be considered together (Jiang2005). In (Trivedi1994) a unified performability and reliability analysis by using Markov Reward model (MRM) is presented. In (Kirsal-Ever2013) existing performability evaluation methods are considered for evaluation of security mechanisms from a performance point of view. A new framework has also been discussed for modelling the interactions between the network and the authentication servers.

Framework

The arrivals of jobs are assumed to be independent and follow Poisson distribution with rate λ. The service times of jobs are distributed exponentially with mean $1/\mu$. The Kerberos server considered can serve jobs only during its operative periods, which means that the key distribution is being taken place (the system is not shut) and the server

is active during this process. The Kerberos server may suffer from failures and inter failure times are distributed exponentially with mean 1/ξ. At the end of this period, the server breaks down and requires an exponentially distributed repair time with mean 1/η. The distribution of time intervals between shutdowns are assumed to be exponentially distributed with given mean value 1/δ. When the system is shut, the server does not provide service to incoming request for an exponentially key distribution time which is given by 1/φ. This system can be modelled as follows:

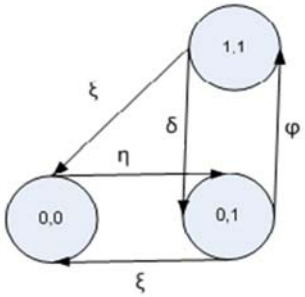

Figure 1. State diagram for availability of standalone Kerberos authentication server

The state (0, 0) denotes the event that the system is shut and the server is broken. In the state (0, 1) the server is not broken and the system is shut. Finally, the state (1, 1) represents the state where the server becomes operative since the system is not shut and the server is active. In case the server is broken in this stage, there is a direct transition from state (1, 1) to the state (0, 0). Therefore, it is assumed that the system is shut and key distribution does not take place while the server is nonfunctional.

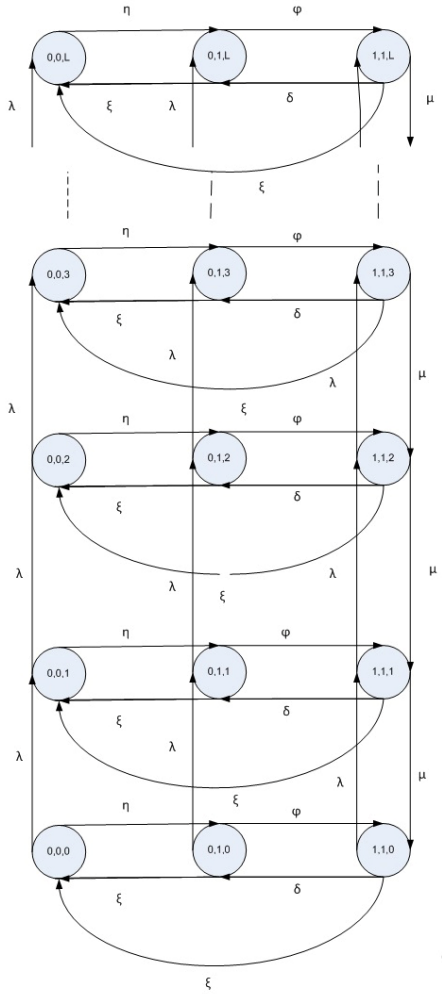

Figure 2. The state transition diagram for the performance and availability model of the system

The system state can be represented by (i, j, k) where i is the system status, j is the number of active server and k

is the number of jobs in the system. Please note that i and j can be maximum 1 since there is only one server considered for the proposed model. Therefore, in Figure 2, as long as jobs keep on arriving to the system, the system state changes one state upward until it reaches maximum number of jobs (L) in the system. The upward transition further than the state (i, j, k) is not possible since the jobs are blocked because of the limitation of L, where $k \leq L$. There is forward lateral transition from state (i, j, k) to the state (i, j+1, k) when the server is repaired. Once the system generates key, there is also forward transition from the state (i, j, k) to the state (i+1, j, k). There are two possible backward lateral transition from the state (i+1, j+1, k) to the state (i+1,j,k) and (i, j, k), when the system is shut and the server is broken respectively. Another backward lateral transition can be possible from the sate (i, j+1, k) to the state (i, j, k) in case the server is broken. Finally, when the server is operative, one job is served with a downward transition from the state (i+1, j+1, k+1) to (i+1, j+1, k).

The two dimensional process considered in (Kirsal-Ever2013) can be used for the Spectral Expansion solution method with the matrices A, B and also C as given below. Please note that the matrix A represents the lateral, the matrix B upward and also the matrix C downward transitions.

$$A = A_j = \begin{bmatrix} 0 & \eta & 0 \\ \xi & 0 & \varphi \\ \xi & \delta & 0 \end{bmatrix} \qquad B = B_j = \begin{bmatrix} \lambda & 0 & 0 \\ 0 & \lambda & 0 \\ 0 & 0 & \lambda \end{bmatrix} \qquad C_0 = (0),\ C = C_j = \begin{bmatrix} 0 & 0 & 0 \\ 0 & 0 & 0 \\ 0 & 0 & \mu \end{bmatrix}$$

Conclusions and Future Work

This paper is concerned with a modelling approach for performability evaluation of Kerberos servers which dynamically renew keys under pseudo-secure conditions as well as security variants over Kerberos authentication protocol as an example to service interruptions in wireless communication systems. As stated earlier, during key distribution, external access to the network is not allowed. The access restrictions happen for short intervals (Kirsal2007), (Kirsal2008). However, any link shut-down costs the network in terms of performance degradation. Therefore, it is essential to evaluate the impact of the proposed approach on system performance. The proposed approach in (Ever2009) also involves temporary interruption to link/server access where it has implications in terms of QoS degradation. Discussions on performance and availability evaluation of some security measures are provided.

Hence in order to enhanced QoS, the existing performance and availability modelling techniques used in the literature can be adapted to modelling of various security protocols considering the server behaviour as well as the characteristics of the networks. In order to evaluate the cost in terms of the degradation of system performance, an analytical method is used. Unlike the previous studies, the server failures are considered as well. Therefore, the approach presented in this study provides more realistic performability measures.

The model developed is highly flexible and it can be used for systems with various failure, repair, and renewal times and times between interruptions. The method can be extended for multiple Kerberos servers and for systems with backup servers especially for the KDC.

References

[1] Balsamo, S., Persone, V. D. N., & Inverardi, P. (2003). *A Review on Queueing Network Models with Finite Capacity Queues for Software Architectures Performance Prediction*. Performance Evaluation. 51(4), pp. 269-288.

[2] Chakka, R. (1998). *Spectral Expansion Solution for Some Finite Capacity Queues*, Annals of Operations Research. 79, pp. 27-44.

[3] Ever, E., Kirsal, Y. & Gemikonakli, O. (2009). *Performability Modelling of a Kerberos Server with Frequent Key Renewal under Pseudo-Secure Conditions for Increased Security*. IEEE International Conference on the Current Trends in Information Technology (CTIT). Dubai Women College, pp. 91 96.

[4] Baghaei, N. & Hunt, R. (2004). *Security Performance of Loaded IEEE 802.11b Wireless Networks*. Computer Communications, Elsevier, UK. 27(17), pp. 1746-1756.

[5] Brennen, V. A. (2004). "Kerberos Infrastructure HOW TO", CryptNET, Guerrilla Technoogy Development.

[6] Chakka, R. & Mitrani, I. (1994). *Heterogeneous Multiprocessor Systems with Breakdowns: Performance and Optimal Repair Strategies*. Theoretical Computer Science. l25, pp. 91-109.

[7] Ever, E., Kirsal, Y. & Gemikonakli, O. (2009), *Performability Modelling of Handoff in Wireless Cellular Networks and the Exact Solution of System Models with Service Rates Dependent on Numbers of Originating and Handoff Calls*. IEEE Proceedings of International Conference on Computational Intelligence, Modelling and Simulation (CSSim 2009), pp. 282-287.

[8] Ever, E., Gemikonakli, O., Kocyigit, A. & Gemikonakli, E. (2013). *A Hybrid Approach to Minimize State*

Space Explosion Problem for the Solution of Two Stage Tandem Queues. Journal of Network and Computer Applications. 36, pp.908-926.

[9] Jiang, Y., Lin, C., Shen, X., & Shi, M. (2005). *Mutual Authentication and Key Exchange Protocols with Anonymity Property for Roaming Services.* NETWORKING, pp. 114-125.

[10] Kirsal, Y. & Gemikonakli, O. (2007). *An Authentication Protocol to Address the Problem of the Trusted 3rd Party Authentication Protocols*. Novel Algorithms and Techniques in Telecommunications, Automation and Industrial Electronics, (CISSE 2006), pp. 523-526.

[11] Kirsal, Y. & Gemikonakli, O. (2007). *Frequent Key Renewal Under Pseudo- Secure Conditions for Increased Security in Kerberos Authentication and its Impact on System Performability*. Proceedings of the 3rd International Conference on Global E-Security, University of East London (UeL), 2007.

[12] Kirsal,Y. & Gemikonakli, O. (2008). *Improving Kerberos Security through the Combined Use of the Timed Authentication Protocol and Frequent Key Renewal,* 7th IEEE International Conference on Cybernetic Intelligent Systems (CIS2008), IEEE Press, pp. 153-158.

[13] Lowe, G. (1996). *Some New Attacks upon Security Protocols*. 9th IEEE Computer Security Workshops, Society Press, pp. 162-169.

[14] Mitrani, I. (2005). *Approximate Solutions for Heavily Loaded Markov- Modulated Queues*. Performance Evaluation, vol.62 (1-4), pp. 117-131.

[15] Needham, R. M. & Schroeder, M. D. (1978). *Using Encryption for Authentication in Large Networks of Computer*. Commun. ACM, ACM Press, vol. 21, pp. 993-999.

[16] Schneider, S. (1998). *Verifying Authentication Protocols in CSP*. IEEE Trans. Sofw. Eng., IEEE Press, vol. 24, pp. 741-758.

[17] Trivedi, K. S., Malhotra, M. & Fricks, R. M. (1994). *Markov reward approach to performability and reliability analysis*, pages 7-11.

[18] Mitrani, I. (2001). *Queues with Breakdowns, Performability Modelling: Techniques and Tools*, Wiley, Chichester.

[19] Trivedi, K. S., Dharmaraja, S. & Ma, X. (2003). *Performability modelling of wireless communication systems*. International Journal of Communication Systems, vol 16, pp. 561-577.

[20] Gemikonakli, O., Mapp, G., Thakker, D., & Ever, E. (2006). *Modelling and performability analysis of network memory servers*, Annual Simulation Symposium, pp.127-134.

[21] Gemikonakli, O., Mapp, G., Ever, E., & Thakker, D. (2007). *Modelling network memory servers with parallel processors, break-downs and repairs*, Annual Simulation Symposium, pp. 11-20.

[22] Kirsal, Y., & Gemikonakli, O. (2009). *Performability Modelling of Handoff in Wireless Cellular Networks with Channel Failures and Recovery*, In IEEE Proceedings of 11th International Conference on Computer Modelling and Simulation (UKSim 2009), pp. 544-547.

[23] Kirsal, Y., Ever, E., Gemikonakli O. & Mapp G. (2011). *Critical Review of Analytical Modelling Approaches for Performability Evaluation of the Handover Phenomena in Mobile Communication Systems.,* The Proceeding of IEEE 11th International Conference on Computer and Information Technology, 2th International Workshop on Dependable Service-Oriented and Cloud computing (DSOC 2011), pp. 132-137.

[24] Kirsal, Y., Gemikonakli, O., Ever, E. & Mapp, G. (2012). *Performance Analysis of Handovers to Provide a Framework for Vertical Handover Policy Management in Heterogeneous Environments*, In 45th Annual Simulation Symposium, (ANSS'12), Orlando, FL, USA, pp. 1-8.

[25] Gowrishankar, S. G.N., & Satyanarayana P.S. (2009). *Analytic Performability Model of Vertical Handoff in Wireless Networks,* Journal of Computer Science, 5(6), pp. 445-450.

[26] Trivedi, K.S. & Ma X. (2002). *Performability Analysis of Wireless Cellular Networks,* Symposium on Performance Evaluation of Computer and Telecommunication Systems (SPECTS 2002).

[27] Shensheng, T. & Wei, L. (2005). *Performance Analysis of the 3G Network with Complementary WLAN*, Global Telecommunications Conference GLOBECOM '05, vol. 5, pp. 2636-2641.

[28] W. Xia, and, L. Shen (2007). *Modeling and Analysis of Handoffs in Cellular and WLAN Integration*. IEEE International Conference on Communications, ICC '07I, pp. 385-391.

[29] Saravanan, I., Sivaradje, G. & Dananjayan, P. (2006). *QoS provisioning for cellular/WLAN interworking, Wireless and Optical Communications Networks*, 2006 IFIP International Conference, pp. 50-55.

[30] Song, W., Jiang, H., Zhuang, W. & Shen, X. (2005). *Resource Management for QoS Support in Cellular/WLAN Interworking*, IEEE Network, 19(5), pp.12-18.

[31] Hua, Z., Li, M., Chlamtac, I., & Prabhakaran, B. (2004). *A Survey of Quality of Service In IEEE 802.11 Networks*, In IEEE Wireless Communications Journals, 11(4), pp. 6-14.

[32] Kirsal-Ever, Y., Yonal Kirsal, Alberto Polzonetti, Leonardo Mostarda, Clifford Sule, Purav Shah, Enver Ever (2013), "Challenges of Kerberos Variance with High QoS Expectations", *International Conference on Security and Management (SAM), World Congress in Computer Science, Computer Engineering, and Applied Computing (WORLDCOMP)*, Las Vegas, USA.

STRATEGIC DECISION SUPPORT SYSTEM BASED HYBRID MODELS FOR COLLEGES ENROLLMENT CAPACITY PLANNING: DESIGN & IMPLEMENTATION

Said Ali El-Quliti[1], Abdul Hamid Mohamed Ragab[2], Reda Abdelaal[1], Ali Wagdy Mohamed[3], Abdulfattah Suliman Mashat[4], Amin Yousef Noaman[5], and Abdulrahman Helal Altalhi[4]

[1]Faculty of Engineering, Dept. of IE, KAU, SA
[2]Faculty of Computing and Information Technology, Dept. of IS, KAU, SA
[3]Statistics Department, Faculty of Sciences, Dept. of Statistics, UJ, SA
[4]Faculty of Computing and Information Technology, Dept. of IT, KAU, SA
[5]Faculty of Computing and Information Technology, Dept. of CS, KAU, SA

[2]aragab@kau.edu.sa (correspondence Author)

Abstract: This paper proposes a Hybrid Strategic Decision Support System (H-SDSS) for colleges' enrollment capacity planning. Three hybrid subsystems are combined for executing the task of decision making processes. The system includes students' track specified model, colleges' enrollment model and students' capacity forecast model. Data mining knowledge based rules and goal programming based methods are used for building the system. This H-SDSS is expected to help university decision makers for solving problems related to strategic decisions for enhancing university students' admission and enrollment capacity planning to satisfy future of higher educational demands as well as labor market needs.

Keywords: Strategic Decision, DSS, Goal programming, knowledge base rule, Data mining.

Introduction

DSS is an interactive computer-based system intended to help decision makers use communications technologies, data and documents, knowledge and models to identify and solve problems, to complete decision process tasks, and to make decisions. DSS enhances a person and group's ability to make decisions. DSS can be differentiated by the level of decision (Gutierrez, 2008): Strategic where the decision can be taken for two to five years, Tactical; where a decision can be taken within a few months up to two years, Operational; where a decision can be dealt within a few days or a few months, and Dispatching; where a decision can be taken just for some hours.

Standalone DSSs are limited performance and lacks efficiency specially with the fast growing in developed technology. The Hybrid DSS can solve these problems and improve the overall system performance. Hybrid DSS has been used in many specific areas and application such as medical care (Berner, 2009), finance (Kotsiantis, 2006), and architecture (Simmons, 2008). However, the literature did not cover well the HDSS in the area of Higher Education Management. The work proposed in this paper suggested a novel design and implementation for a hybrid strategies DSS. The architecture combines data mining approaches (Han & Kamber, 2006) as well as goal programming (Orumie & Ebong, 2014). This is expected to satisfy Higher Education institutions' decision makers for solving problems related to students' college admission and enrollment effectively and improving universities of achieving their goals for getting optimal capacity that satisfying their future needs.

Most of previous work are based on using single model DSS, and this lacks flexibility, adaptability, and capability. This paper introduces a novel H-SDSS based hybrid subsystem and integrated models for design and implementation for Colleges Enrollment Capacity Planning. The rest of the paper explains the following sections: literature survey, the architecture of the proposed H-SDSS system, the applied case study data resources and system implementation, the H-SDSS system results, and the conclusions, respectively.

Literature Survey

DSSs vary greatly in application and complexity, but they all share specific features. A typical DSS has four components (Power, 2008): data management, model management, knowledge management and user interface management. Decision making in a complex, dynamically changing environment is a difficult task that requires new techniques of computational intelligence for building adaptive, hybrid intelligent decision support systems (HIDSS). These hybrid systems combine several of Knowledge-Based Systems into one system (Kendal & Creen,

2007). They achieve this combination either in a loose coupling, e.g. different modules in the same system use different methods, or in a tight coupling - methods are mixed at a low level, e.g. fuzzy neural networks or fully integrated systems. These are the most promising among standalone DSS. Since, they integrate the advantages of all the methods combined, e.g. dealing with both data and expert rules, using both statistical formulas and heuristics or hints.

Authors (Fong & etal, 2009) proposed a hybrid model of neural network and decision tree classifier that predicts the likelihood of which university a student may enter, by analyzing his academic merits, background and the university admission criteria from that of historical records. Authors (Kasabov & etal, 2016) proposed hybrid intelligent decision support systems and applications for risk analysis and discovery of evolving economic clusters in Europe. Authors (Chen & etal, 2012) proposed a hybrid DSS combining several data mining techniques using an improved weighted majority voting scheme (iWMV). Authors (Mansoul & etal, 2013) proposed a hybrid DSS for application on Healthcare. They used an approach based on using a multi-criteria decision guided by a case-based reasoning (CBR) approach. Authors (Balakrishnan & etal, 2013) developed A hybrid predictive system for retinopathy. They used data mining and case based reasoning (CBR). C5.0 was used to produce the decision tree whereas k-nearest neighbor and Hamming distance algorithms were used to select the three most similar cases for every new case entered into the system.

In this paper, it is proposed to use goal programming method for managing the integrated models subsystem, and using data mining knowledge based for managing the data driven subsystem. Goal programming (GP) is a branch of multi-objective optimization, which in turn is a branch of multi-criteria decision analysis (MCDA). GP is used to perform three types of analysis (Inflibnet , 2016): (1) Determine the required resources to achieve a desired set of objectives, (2) Determine the degree of attainment of the goals with the available resources, (3) Providing the best satisfying solution under a varying amount of resources and priorities of the goals. Data Mining (DM) is the process of collecting, searching through, and analyzing a large amount of data in a database, as to discover patterns or relationships (Han & Kamber, 2006). The most commonly DM methods used in this paper including: student's classification, clustering based on association discovery rules.

Materials and Methods

Figure 1 shows the components of the hybrid SDSS system proposed. The *model management subsystem* works as model driven based DSS, and it includes three integrated models: (1) Tracks Specified model (TSM), (2) Colleges Enrollment Model (CEM) and (3) Capacity Forecast Model (CFM) as explained in details in next sections. The *Data Management subsystem* works as data driven based DSS. The *Knowledge-Base Management Subsystem* can support any of these subsystems. It provides intelligence to augment the decision maker's own. It can be interconnected with the organization's knowledge repository Organizational Knowledge Base. Knowledge can be provided via web servers. Many artificial intelligence methods have been implemented in web development systems which are easy to integrate into the other DSS components as explained in next sections.

User Interface

The *User Interface Subsystem* allows the interaction between the computer and the decision maker. It is used by the user; is part of system; to communicate with and commands the DSS. The web browser provides a familiar and consistent Graphical User Interface (GUI) structure for most DSS. The decision maker; user or manager; can be an individual or a group, depending on who is responsible for the decision, and provides the human intellect. An intermediary allows a manager to benefit form a DSS. For example: University staff assistants have specialized knowledge about management problems and some experience with decision support technology. Expert tool users perform tasks that the problem solver does not have the skill or training to perform. University business analysts have a knowledge of the application area, a formal business administration education and considerable skill in using DSS construction tools. Facilitators control and coordinate the use of software to support the work of people working in groups, and are also responsible for the conduct of workgroups sessions.

The Data Management Subsystem (DMS)

It is connected to several internal and external databases for retrieving the necessarily data required. Five databases are dealt with as shown in Figure 1. (1) Web portal university database is used for retrieving students admitted data such as age, ID, nationality and GPA. (2) The university DB it is used for retrieving the preparatory rules, as explained in (Ragab & etal, 2014). (3) The graduated history DB which help for forecasting, as explained next. (4) The colleges DB used for retrieving enrollment criteria rules explained in (Ragab & etal, 2014). (5) Ministry of higher education DB is used for retrieving the key performance indicators (KPIs) according to future suggested plans that have to be satisfied.

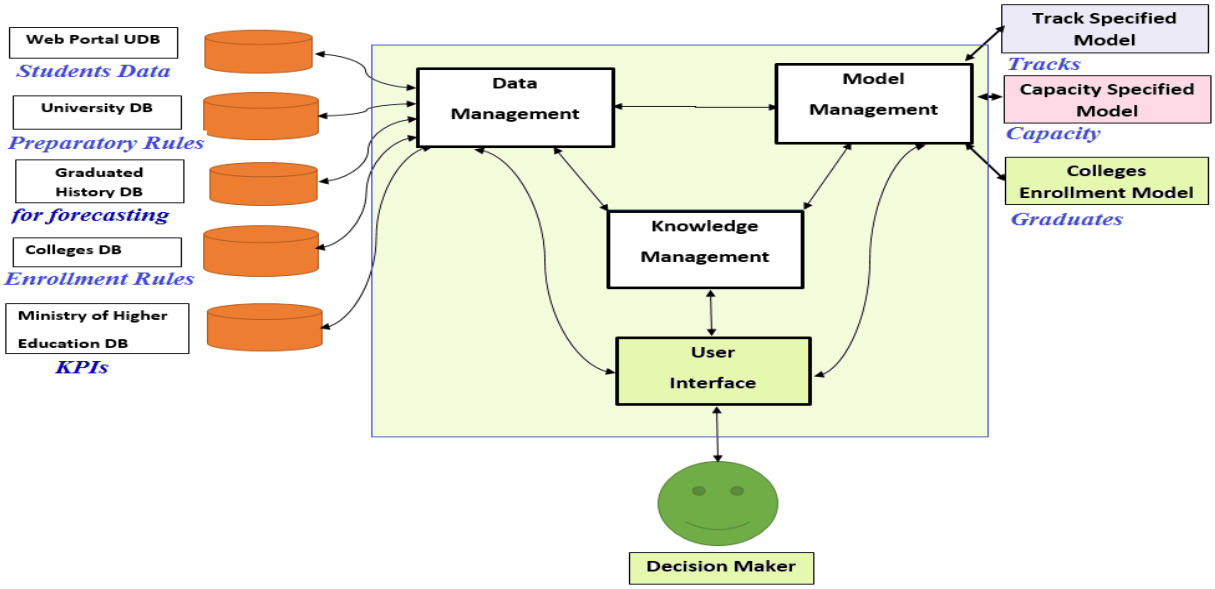

Figure 1. The architecture of the proposed SDSS.

The data Management Subsystem is implemented using data mining (DM) knowledge base rules as explained in (Ragab & etal, 2014). Where, C4.5, PART and Random Forest algorithms gave the highest performance and accuracy with lowest errors. Based on these results, the C4.5 algorithm is used in the implementation. Figure-2 shows a simplified diagram followed for implementing C4.5. A significant cleaning and transformation phase needs to take place so as to prepare the information for DM algorithm. The data we use to construct our DMS subsystem is based on Knowledge Discovery Association Rules. Web usage mining performs mining on student's web data, particularly data stored in logs managed by the web servers. The web log provides a raw trace of the students' navigation and activities on the site. In order to process these log entries and extract valuable patterns that could be used to enhance DMS subsystem and help in system evaluation.

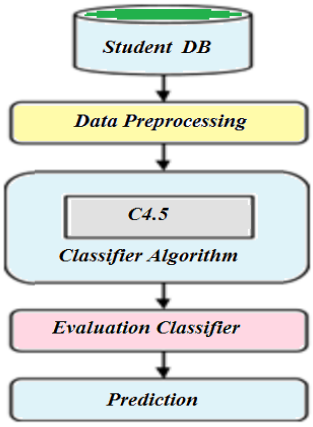

Figure 2. The C4.5 DM algorithm processing steps for implementing DMS.

The Model Management Subsystem (MMS)

It is implemented based on goal programming mathematical model explained in (El-Quliti & etal, 2016). The MMS is consists of three integrated models as follows:

(A) Tracks Specified Model (TSM)

The TSM is used for sorting the preparatory year tracks recommended for fresh students. It contains a sorter and a filter. The sorter used to sort students to several university study tracks available with 60% for Science tracks and 40% for Art tracks. The filter is used to re-arrange students onto two categories. Students who passed all courses successfully will go to college model to be enrolled to suitable colleges. Students who failed in any course are rejected and postponed for services when they are succeeded. The track model executes its' tasks based on the goal programming constrains shown in Table (1) and in the mathematical formulas shown in Appendix-Part (ii).

(B) Colleges Enrollment Model (CEM)

The standard criteria that govern college allocation are based on fulfilling the following four criteria: (1) Success of all preparatory year courses. (2) Minimum score of college prerequisite courses must be satisfied. (3) Weighted Relative Rate must be satisfied. And (4) College capacity must be valid. The CEM contains two internal components; a Classifier and Allocator, respectively. The classifier categorizes students according to their gender and their qualifications. The allocator services students who succeeded in all preparatory year courses and enrolls students into colleges fairly according to the GPA and prerequisite qualified courses stated by specialized colleges. The CEM carries out these tasks based on the goal programming constrains shown in Table (2) and in the Appendix-Part (iii).

(C) Capacity Forecast Model (CFM)

The CFM uses goal programming formulas shown in the appendix to predict the future capacity expected for next upcoming years. For the proposed SDSS forecast purposes, the following goal attributes has been taken into consideration.

1. Annual growth rate for enrolled students.
2. Percentage of the total number of students enrolled in science and engineering programs.
3. Percentage of total enrollment in higher education regardless of age, to the total population in the age group of 18-23 years.
4. Accepted percentage in higher education from high school graduates.
5. Percentage of the total number of students in each discipline of education to the total faculty members.
6. Percentage of the total number of girls to the total number of boys in higher education.
7. Not violating the available resources.
8. Annual growth rate for graduated students.
9. Ratio of graduated students to those enrolled 5 years ago.

Relevant parameters and data for the model related to the applied case study explained in next section.

H-SDSS Case Study Data Specifications

Trusted sources of our applied case study input data included the following: (1) the Kingdom of Saudi Arabia (KSA) Ministry of Education Ninth Development Plan (2010-2014) that adopts the drive towards a knowledge based economy through focusing on human development and education (MHE, 2009, 2016). The main challenges of education are improving enrolment rates, reducing dropout rates at all levels of education, and enabling education to meet the demand of labor market. (2) The twenty-five-year plan (AAFAQ) for KSA Higher Education Development (MHE, 2016). (3) The statistical KSA universities data from the web during years 2004-2015 (ISD, 2014 & CDIS, 2016). Applying these data into the proposed system implemented, the results are obtained as explained next section. The mathematical model will cover the main objectives stated in the KSA Plan and that stated in KSA Strategic Plan (AAFAQ). It will be restricted to a-3 year planning horizon as an example for application, but it can be extended to longer time span with little modifications. To design the decision variables for the case study applied, it is necessary to represent all different problem attributes as defined in Table 1.

Table1: Problem attributes and their values.

Attributes	Values
y = Year of the plan	y = 1 for the first year of the next plan 2016, 2 for the second and 3 for the last year, y = 0 for the last year in the previous plan (current year, 2015), y= -1 for year 2014 and so on.
u = University	u = a university, $u \in$ U, the set of all universities in the country.
i = Status	E for Enrolled and G for Graduated
j = Gender	b for boys section and g for girls section
k = Education Program	m = a college in the medicine specialty, m $\in$ M, the set of all colleges in the Medicine specialty, s = a college in the Science & Engineering specialty, s $\in$ S, the set of all colleges in the Science and Engineering specialty, a = a college in the arts specialty, $a \in$ A the set of all colleges in the Arts specialty and T for the total number in all specialties M, S and A in all universities U.

Table 2: The KPIs input parameters related to the applied case study.

Symbol	Meaning	Value
p_r^y	Annual growth rate for enrolled students in year y of the planned horizon.	4.5%
p_s^y	Percentage of the total number of students enrolled in science & engineering and medical programs to the total number of students enrolled in higher education in year y of the planned horizon.	60%
p_m^y	Percentage of the total number of students enrolled in medical programs to the total number of students enrolled in science & engineering and in year y of the planned horizon.	16.5%
p_p^y	Percentage of total enrollment in higher education regardless of age, to the total population in the age group of 18-23years in the same year y of the planned horizon.	50%
p_h^y	Accepted percentage in higher education from high school graduates in year y of the planned horizon.	55%
p_g^y	Percentage of the total number of enrolled girls to the total number of boys enrolled in year y of the planned horizon.	90%
Percentage of the total number of students in each discipline of university education to the total faculty (*F*) in that specialty in year y of the planned horizon is:		
β_M^y	Medicine	10 :1
β_S^y	Science & Engineering	17: 1
β_A^y	Arts	22:1
β_U^y	Total University	20: 1
q_r^y	Annual growth rate of the number of graduates for year y of the planning horizon.	7.2%.
q_d^y	The planned percentage of students who will complete their studies in year y of the planned horizon to the total number of students enrolled five years ago.	85%

Table 3: The input data in the year 2015, used as current year in the mode.

Symbol	Meaning	Value
$x_{E,b,T}^{y-1,U}$	Total number of boys enrolled in Saudi Arabia in all universities in year y-1 (2015 = last year of the previous National plan).	214,603
$x_{E,g,T}^{y-1,U}$	Total number of girls enrolled in Saudi Arabia in all universities in year y-1 (2015 =last year of the previous National plan)	199,185
$x_{G,b,M}^{y-1,U}$	Number of graduated boys in the Kingdom in year 2015 (medicine)	3,191
$x_{G,b,S}^{y-1,U}$	Number of graduated boys in the Kingdom in year 2015 (science & engineering specialty)	18,103
$x_{G,b,A}^{y-1,U}$	Number of graduated boys in the Kingdom in year 2015 (arts specialty)	13,851
$x_{G,g,M}^{y-1,U}$	Number of graduated girls in the Kingdom in year 2015 (medicine)	3,456
$x_{G,g,S}^{y-1,U}$	Number of graduated girls in the Kingdom in year 2015 (science & engineering specialty)	22,871
$x_{G,g,A}^{y-1,U}$	Number of graduated girls in the Kingdom in year 2015 (arts)	34,797

Table 4: Input data related to the Kingdom of Saudi Arabia for different years.

Symbol	Meaning	Value in Year y		
		2015	**2016**	**2017**
N_C^y	Population of Saudi Arabia in the age of 18-23 years.	1,297,000	1,335,910	1,375,987
N_H^y	Total number of High school graduates.	404,742	422955	441988
N_b^y	Number of boys for bachelor Scholarships abroad.	22,644	24,908	27,399
N_g^y	Number of girls for bachelor Scholarships abroad.	8,477	9,325	10,257
B_u^y	Total Budget for a university u in a year y (in million SAR).	32,500	35,750	39,325
c_u^y	Average cost of one student in a university u in a year y (in SAR).	56,250	61,875	68,063
$F_{bM}^{y,U}$	Number of faculty in all universities (boys section, medical specialty)	7,425	8,168	8,984
$F_{g,M}^{y,U}$	Number of faculty in all universities (girls section, medical specialty)	4,433	4,876	5,364
$F_{b,S}^{y,U}$	Number of faculty in all universities (boys section, science and engineering)	19,346	21,281	23,409
$F_{g,S}^{y,U}$	Number of faculty in all universities (girls section, science and engineering)	8,658	9,524	10,476
$F_{b,A}^{y,U}$	Number of faculty in all universities (boys section, arts specialty)	9,431	10,374	11,412
$F_{g,A}^{1,U}$	Current number of faculty in all universities (girls section, arts specialty)	9,776	10754	11829
$F_{b,T}^{y,U}$	Number of faculty in all universities (boys section, all specialties)	37,245	40,970	45,066
$F_{g,T}^{y,U}$	Number of faculty in all universities (girls section, all specialties)	23,405	25,746	28,320
		Value in Year y		
		2011	**2012**	**2013**
$x_{E,b,M}^{y-5,U}$	Number of enrolled boys (medicine).	8,518	9,370	10,307
$x_{E,b,S}^{y-5,U}$	Number of enrolled boys in year y-5, y-4 and y-3. (science & engineering specialty)	93,807	103,188	113,506
$x_{E,b,A}^{y-5,U}$	Number of enrolled boys (arts specialty)	34,301	37,731	41,504
$x_{E,g,M}^{y-5,U}$	Number of enrolled girls (medicine)	7,114	7,825	8,608
$x_{E,g,S}^{y-5,U}$	Number of enrolled girls (science & engineering)	92,867	102,154	112,369
$x_{E,g,A}^{y-5,U}$	Number of enrolled girls (arts)	38,993	42,892	47,182

Relevant parameters and data for the applied case study are collected and presented in Table 2, (MHE, 2016). Table 3 represents the input data in the year 2015; which considered as current year y in the goal programming model. Table 4 represents the input data for different years needed in the mathematical model. Based on these defined attributes and equations, the results obtained are explained in section 6.

H-SDSS System Implementation

The hybrid integrated models subsystem is implemented based on goal programming method (El-Quliti, 2016). The enrollment part is presented in equations (1-57) shown in the Appendix. The graduation part are solved directly using the inequality relations (58-69). Relevant model parameters and data for the applied case study are represented in the Tables (1-4) in the previous sections. Figure 3 shows a simplified flowchart for the algorithm implemented. Details computations are explained in next sections.

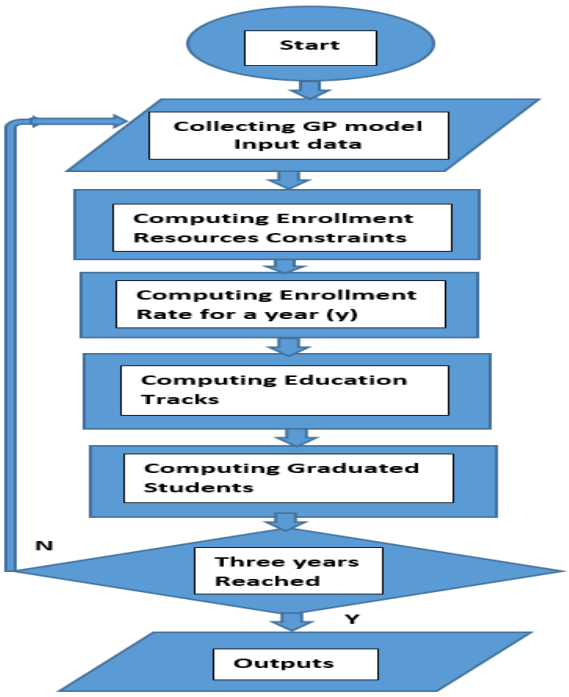

Figure 3. Simplified goal programming followed steps for the H-SDSS algorithm implemented.

Control the Education Tracks

The percentage of the total number of students enrolled in science and engineering and medical programs to the total number of students enrolled in higher education is more than or equal p_s^y and computed as shown in Appendix-part (ii-A). The percentage of the total number of students enrolled in medical programs to the total number of students enrolled in science and engineering is more than or equal p_m^y and computed as shown in Appendix part (ii-B). The Tracks Specified Model (TSM) executes these functions.

Control Students Enrollments and Graduation Rate

All the resources of the teaching process are collected in the total budget required for a University u that should not exceed a certain total limit of B_u^y at any year y of the planning horizon.

c_u^y = cost per student in a University u in a year y, and

B_u^y = Maximum budget for a university u in a year y,

The percentage of total enrollment in higher education regardless of age, to the total population in the age group of 18-23 years $\geq p_p^y$, and the accepted percentage in higher education from high school graduates in the same year $\geq p_h^y$. It is required to increase the enrollment of students in higher education with an average annual growth rate of p_r^y. The percentage of the total number of enrolled girls to the total number of enrolled boys in higher education $\geq p_g^y$. These values are computed as shown in Appendix part (iv). The number of graduates that will be increase with an average annual rate = q_r^y. Percentage of students who have completed their studies in a given year to the total number of students enrolled in universities five years before that year=q_d^y . These values are computed as shown in Appendix part (v). The Colleges Enrollment Model (CEM) and the Capacity Forecast Model (CFM) process these tasks.

Results and Discussion

Table 5 and Figure 4 show the predicted number of students enrolled and graduated in the years 2016, 2017 and 2018. Results show that the number of enrollment students increase regularly every year. So that decision makers has to take necessarily steps towards supplying required resources to cover this increase. The number of graduated students also increases regularly every year. This increased value has to be taken into consideration by labor market for offering qualified jobs suitable for the graduates excess. It is also noted that the average number of drop out students (E-G) is increases. This value is high and it should be taken care of by university decision makers to be reduced. And Higher Education Ministry plan recommended dropout rate should be within the limit of 1%.

Table 5: Optimal solution for planning per year (*y*).

#	Meaning	Decision Variable	Year (*y*)		
			2016	**2017**	**2018**
1	Enrolled boys in medical	*EBM*	12,250	13,451	13,907
2	Graduated boys in Medical	*GBM*	7,240	7,965	8,467
3	Enrolled boys in science	*EBS*	54,856	56,612	69,936
4	Graduated boys in science	*GBS*	47,736	49,710	51,639
5	Enrolled girls in medical	*EGM*	9,325	10,244	11,465
6	Graduated girls in medical	*GGM*	6,047	6,651	6,954
7	Enrolled girls in science	*EGS*	46,729	52,044	53,003
8	Graduated girls in science	*GGS*	36,937	38,831	40,638
9	Enrolled boys in arts	*EBA*	34,907	41,629	43,566
10	Graduated boys in arts	*GBA*	29,156	32,071	34,328
11	Enrolled girls in arts	*EGA*	39,666	40,901	43,632
12	Graduated girls in arts	*GGA*	33,144	36,458	39,843

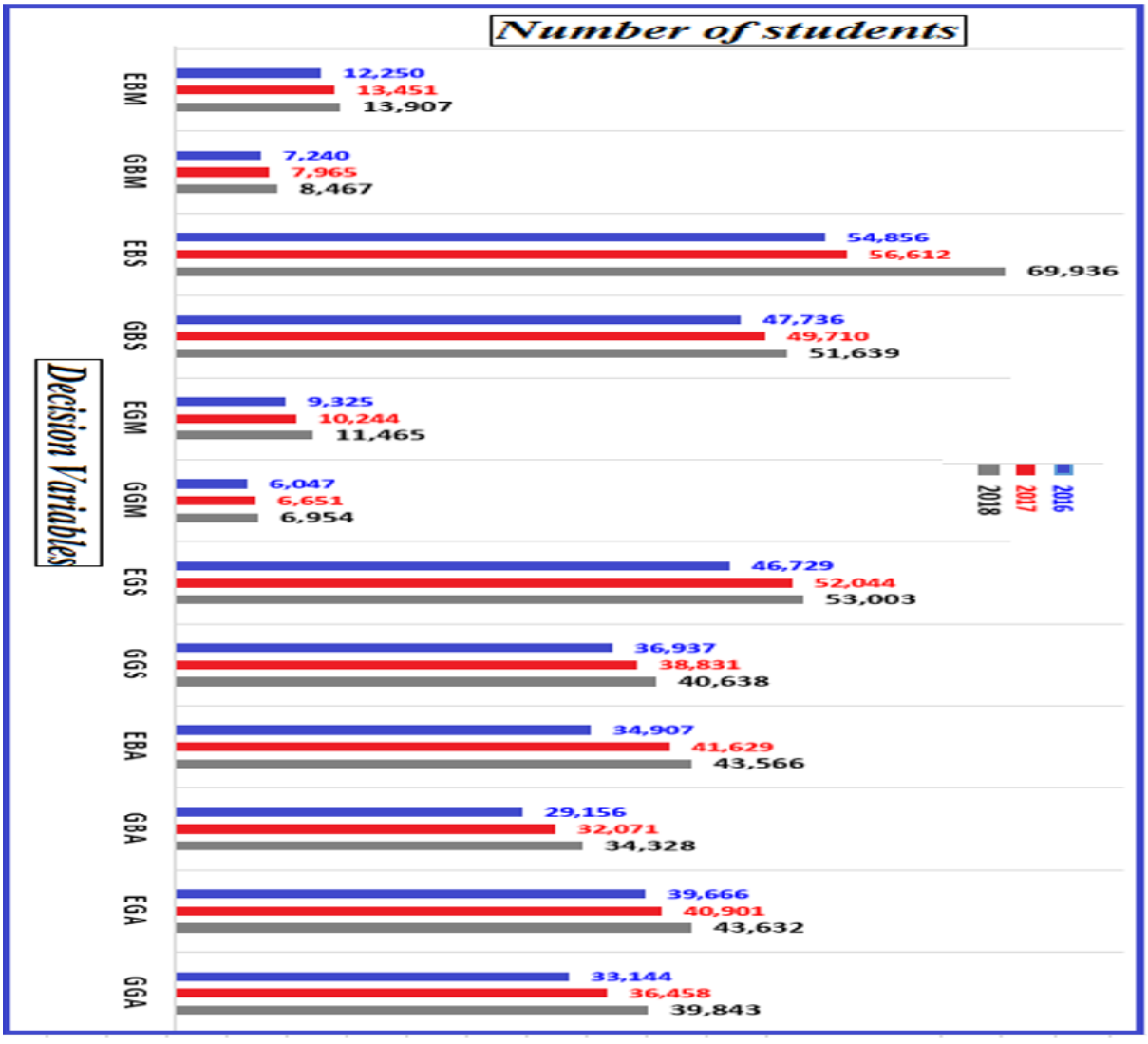

Figure 4. Enrollment and Graduated students predicted w.r.t years 2016-2018.

Conclusion

This paper introduced a new architecture of hybrid strategic decision support system (HSDSS) that can be used efficiently for colleges' enrollment capacity planning. This can help university decision makers for tackling problems related to students' college enrollments as well as to suggest required facilities that are helpful to accommodate increasing future demands and needs. The HSDSS uses goal programming methods for predicting future capacity, as well as data mining knowledge base algorithms for determine students' suitable tracks and college enrollment that satisfying students' desires and university criteria. Results; of the applied case study; show that the number of graduated students increases annually. This can be reflected on labor market needs for offering *Science* related jobs with 60% and *Art* specialist related jobs with 40%, as Ministry of Higher Education in KSA plan recommended. In addition, results show that students' dropout also increases functional to the enrollments and this cause a problem. Hence, university decision makers have to take necessarily solutions to limit this increase, the recommended value hoped to be achieved is 1%.

Acknowledgement

This work is a part of the project award number (12-INF2234-03) funded by the National Plan for Science, Technology and Innovation (MAARIFAH) – King Abdulaziz City for Science and Technology - the Kingdom of Saudi Arabia. The authors also, acknowledge with thanks Science and Technology Unit, King Abdulaziz University for technical support.

References

Gutierrez, A. & Serrano, A. (2008) .Assessing strategic, tactical and operational alignment factors for SMEs: alignment across the organization's value chain. International Journal of Value Chain Management, Vol.2 Iss.1

Berner, E. (2009). Clinical Decision Support Systems: State of the Art. AHRQ Publication No. 09-0069-EF.

Kotsiantis, S. & et.al. (2006). On Implementing a Financial Decision Support System. IJCSNS International Journal of Computer Science and Network Security, VOL.6 No.1A, (pp 103-112).

Simmons, W. (2008) .A framework for decision support in systems architecting, dspace.mit.edu, Ph. D. Thesis.

Han, J. & Kamber, M. (2006). Data Mining: Concepts and Techniques, The Morgan Kaufmann Series in Data Management Systems Series Editor: Jim Gray, Microsoft Research by Elsevier Int.

Orumie, U. & Ebong, D. (2014). A Glorious Literature on Linear Goal Programming Algorithms. American Journal of Operations Research, 4, (pp 59-71).

Power, D. (2008) .Decision Support Systems Concept. Encyclopedia of Decision Making and Decision Support Technologies, IGI.

Kendal, S. & Creen, M. (2007) .Hybrid Knowledge-Based Systems. An Introduction to Knowledge Engineering, Springer.

Fong, S. & etal, (2009). Applying a Hybrid Model of Neural Network and Decision Tree Classifier for Predicting University Admission, Information, Communications and Signal Processing, ICICS 2009, 7th International Conference.

Kasabov, N. & etal (2016).Hybrid Intelligent Decision Support Systems and Applications for Risk Analysis and Discovery of Evolving Economic Clusters in Europe., retrieved from http://www.aut.ac.nz/__data/assets/ pdf_file /0016/ 10591/hidds_final.pdf.

Chen, L. & etal, (2012). Hybrid decision making in the monitoring of hypertensive patients, e-Health Networking, Applications and Services (Healthcom), IEEE 14th International Conference, (pp32 – 37).

Mansoul, A. & etal. (2013).A Hybrid Decision Support System: Application on Healthcare. Cornell University, Computer Science, Artificial Intelligence, (PP.10-13).

Balakrishnan, Shakouri,V. & Hoodeh, M.(2013). Developing a hybrid predictive system for retinopathy. Journal of Intelligent & Fuzzy Systems, vol. 25, no. 1, (pp. 191-199).

Inflibnet (2016). An Introduction to Goal Programming, retrieved from http://shodhganga. Inflibnet.ac. in / bitstream/10603/46789/5/05_chapter%201.pdf.

Ragab, A., Mashat,A. & Khedra, A. (2014). Design and implementation of a hybrid recommender system for predicting college admission, International Journal of Computer Information Systems and Industrial Management Applications, vol. 6, (pp. 35–44).

Ragab, A. & etal, (2014) .A comparative analysis of classification algorithms for students college enrollment approval using data mining, Proceedings of the Workshop on Interaction Design in Educational Environments (IDEE '14), Albacete, Spain, (pp. 106–113).

El-Quliti, S. & etal. (2016). Higher Education Admission Capacity Planning Using a Linearized Integer Goal Programming Model., SOCIOINT 2016 ii, 3rd International Conference on education, Social Sciences and humanities , Istanbul, Turkey.

Ministry of Higher Education (MHE). (2009). *Higher Education Report.* Retrieved from www.mohe.gov.sa/en/...Educational.../Higher-Ed-Report-June-09-en.pdf.
Ministry of Higher Education (MHE). 2014. *Future Plan for Higher Education in Saudi Arabia (AAFAQ).* Retrieved from http://aafaq.mohe.gov.sa/default.aspx.
Ministry of Higher Education (MHE). (2016). Kingdom of Saudi Arabia, Website: Retrieved from http://www.mohe.gov.sa,
Information and Statistics Department (ISD). Statistical Report, Deanship of Information Technology, King Abdulaziz University.
Ministry of Economy and Planning (MEP). (2014). Ninth National Development Plan, Kingdom of Saudi Arabia. Retrieved from http://www.saudi.gov.sa.
Central Department of Statistics and Information (CDSI). (2016). Statistical Year Book, Forty Ninth Issue.

Appendix: Goal Programming Model Computing Equations.

i. Steps for computing Enrollment Rate (p_r^y)

(1) $\frac{\sum_{u\in U}\sum_{k\in K} x_{E,b,k}^{y,u} - \sum_{u\in U}\sum_{k\in K} x_{E,b,k}^{y-1,u}}{\sum_{u\in U}\sum_{k\in K} x_{E,b,k}^{y-1,u}} + d_y^- \geq \boldsymbol{p_r^y}$, y = 1, 2, 3.

(2) $\sum_{u\in U}\sum_{k\in K} x_{E,b,k}^{y,u} - \sum_{u\in U}\sum_{k\in K} x_{E,b,k}^{y-1,u} + d_y^- \geq p_r^y.(\sum_{u\in U}\sum_{k\in K} x_{E,b,k}^{y-1,u})$ y = 1, 2, 3. (1-3)

The **nonlinear** constraints is **linearized** by multiplying both sides with the denominator", then the right hand side will represent the number of students.

(3) $\frac{\sum_{u\in U}\sum_{k\in K} x_{E,g,k}^{y,u} - \sum_{u\in U}\sum_{k\in K} x_{E,g,k}^{y-1,u}}{\sum_{u\in U}\sum_{k\in K} x_{E,g,k}^{y-1,u}} + d_{y+3}^- \geq \boldsymbol{p_r^y}$, y = 1, 2, 3.

(4) $\sum_{u\in U}\sum_{k\in K} x_{E,g,k}^{y,u} - \sum_{u\in U}\sum_{k\in K} x_{E,g,k}^{y-1,u} + d_{y+3}^- \geq \boldsymbol{p_r^y}.\sum_{u\in U}\sum_{k\in K} x_{E,g,k}^{y-1,u}$, y = 1, 2, 3. (4-6)

ii. Computing Education Tracks

(A) Steps for Computing p_s^y:

(1) $\frac{\sum_{u\in U}\sum_{k=m,s} x_{E,b,k}^{y,u}}{\sum_{u\in U}\sum_{j\in J} x_{E,b,j}^{y-1,u}} + d_{y+6}^- \geq p_s^y, y = 1, 2, 3.$

(2) $\sum_{u\in U}\sum_{k=m,s} x_{E,b,k}^{y,u} + d_{y+6}^- \geq p_s^y.\sum_{u\in U}\sum_{j\in J} x_{E,b,j}^{y-1,u}, y = 1, 2, 3.$ (7-9)

(3) $\frac{\sum_{u\in U}\sum_{k=m,s} x_{E,g,k}^{y,u}}{\sum_{u\in U}\sum_{k\in K} x_{E,g,k}^{y-1,u}} + d_{y+9}^- \geq p_s^y, y = 1, 2, 3.$

(4) $\sum_{u\in U}\sum_{k=m,s} x_{E,g,k}^{y,u} + d_{y+9}^- \geq p_s^y.\sum_{u\in U}\sum_{k\in K} x_{E,g,k}^{y-1,u}, y = 1, 2, 3.$ (10-12)

(B) Steps for Computing p_m^y:

(1) $\frac{\sum_{u\in U}\sum_{k=m\in M} x_{E,b,k}^{y,u}}{\sum_{u\in U}\sum_{k=s\in S} x_{E,b,j}^{y-1,u}} + d_{y+12}^- \geq p_m^y, y = 1, 2, 3.$

(2) $\sum_{u\in U}\sum_{k=m\in M} x_{E,b,k}^{y,u} + d_{y+12}^- \geq p_m^y.\sum_{u\in U}\sum_{k=s\in S} x_{E,b,j}^{y-1,u}, y = 1, 2, 3.$ (13-15)

(3) $\frac{\sum_{u\in U}\sum_{k=m\in M} x_{E,g,k}^{y,u}}{\sum_{u\in U}\sum_{k=s\in S} x_{E,g,k}^{y-1,u}} + d_{y+15}^- \geq p_m^y, y = 1, 2, 3.$

(4) $\sum_{u\in U}\sum_{k=m\in M} x_{E,g,k}^{y,u} + d_{y+15}^- \geq p_m^y.\sum_{u\in U}\sum_{k=s\in S} x_{E,g,k}^{y-1,u}, y = 1, 2, 3.$ (16-18)

(C) Steps for Computing p_h^y.

$\sum_{u\in U}\sum_{j\in J}\sum_{k\in K} x_{E,j,k}^{y,u} + d_{y+18}^- \geq \max[(\frac{1}{5}.p_p^y.N_C^{y-1}), (p_h^y.N_H^{y-1})]$, y = 1, 2, 3 (19-21)

iii. Steps for computing Student-to-Faculty Ratio

(1) $\sum_{u\in U}\sum_{m\in M} x_{E,b,m}^{y,u} - d_{y+21}^+ \leq \frac{1}{t_M}.\beta_M^y.\boldsymbol{F_{b,M}^{y,U}}, y = 1, 2, 3.$ (22-24)

(2) $\sum_{u\in U}\sum_{m\in M} x_{E,g,m}^{y,u} - d_{y+24}^+ \leq \frac{1}{t_M}.\beta_M^y.\boldsymbol{F_{g,M}^{y,U}}, y = 1, 2, 3.$ (25-27)

Continue Appendix

$$(3)\ \sum_{u\in U}\sum_{s\in S} x_{E,b,s}^{y,u} - d_{y+27}^{+} \le \frac{1}{t_S}.\beta_S^y\ .\boldsymbol{F_{b,S}^{y,U}}, y = 1, 2, 3. \quad (28\text{-}30)$$

$$(4)\ \sum_{u\in U}\sum_{s\in S} x_{E,g,s}^{y,u} - d_{y+30}^{+} \le \frac{1}{t_S}.\beta_S^y\ .\boldsymbol{F_{g,M}^{y,U}}, y = 1, 2, 3. \quad (31\text{-}33)$$

$$(5)\ \sum_{u\in U}\sum_{a\in A} x_{E,b,a}^{y,u} - d_{y+33}^{+} \le \frac{1}{t_A}.\beta_A^y\ .\boldsymbol{F_{b,A}^{y,U}}, y = 1, 2, 3. \quad (34\text{-}36)$$

$$(6)\ \sum_{u\in U}\sum_{a\in A} x_{E,g,a}^{y,u} - d_{36}^{+} \le \frac{1}{t_A}.\beta_A^y\ .\boldsymbol{F_{g,A}^{y,U}}, y = 1, 2, 3. \quad (37\text{-}39)$$

$$(7)\ \sum_{u\in U}\sum_{k\in K} x_{E,b,k}^{y,u} - d_{y+39}^{+} \le \frac{1}{t_M}.\beta_U^y\ .\boldsymbol{F_{b,T}^{y,U}}, y = 1, 2, 3. \quad (40\text{-}42)$$

$$(8)\ \sum_{u\in U}\sum_{k\in K} x_{E,g,k}^{y,u} - d_{y+42}^{+} \le \frac{1}{t_M}.\beta_U^y\ .\boldsymbol{F_{g,T}^{y,U}}, y = 1, 2, 3. \quad (43\text{-}45)$$

iv. Steps for computing Enrolled Girls-to-Boys Ratio ($\boldsymbol{p_g^y}$)

$$(1)\ \frac{\sum_{u\in U}\sum_{k\in K} x_{E,g,k}^{y,u}}{\sum_{u\in U}\sum_{k\in K} x_{E,b,k}^{y,u}} + d_{y+45}^{-} \ge \boldsymbol{p_g^y}, \text{y} = 1, 2, 3.$$

$$(2)\ \sum_{u\in U}\sum_{k\in K} x_{E,g,k}^{y,u} + d_{y+45}^{-} \ge \boldsymbol{p_g^y}.\sum_{u\in U}\sum_{k\in K} x_{E,b,k}^{y,u}, \text{y} = 1, 2, 3. \quad (46\text{-}48)$$

vi. Enrollment Resources Constraints

for c_u^y = cost per student in a University u in a year y, and

B_u^y = Maximum budget for a university u in a year y,

Then: $\sum_{u\in U}\sum_{j\in J}\sum_{k\in K} x_{E,j,k}^{y,u} - d_{y+48}^{+} \le \sum_{u\in U} B_u^y / c_u^y$, y = 1, 2, 3. (49-51)

v. Steps for computing number of Graduated Students

$$(1)\ \sum_{u\in U}\sum_{m\in M} x_{G,b,m}^{y,u} \ge \max\left[(1+q_r^y).\sum_{u\in U}\sum_{m\in M} x_{G,b,m}^{y-1,u}, \boldsymbol{q_d^y}.\sum_{u\in U}\sum_{m\in M} x_{E,b,m}^{y-5,u}\right], \text{y} = 1, 2, 3. \quad (52\text{-}54)$$

$$(2)\ \sum_{u\in U}\sum_{s\in S} x_{G,b,s}^{y,u} \ge \max\left[(1+q_r^y).\sum_{u\in U}\sum_{s\in S} x_{G,b,s}^{y-1,u}, \boldsymbol{q_d^y}.\sum_{u\in U}\sum_{s\in S} x_{E,b,s}^{y-5,u}\right], \text{y} = 1, 2, 3. \quad (55\text{-}57)$$

$$(3)\ \sum_{u\in U}\sum_{a\in A} x_{G,b,a}^{y,u} \ge \max\left[(1+q_r^y).\sum_{u\in U}\sum_{a\in A} x_{G,b,a}^{y-1,u}, q_d^y.\sum_{u\in U}\sum_{a\in A} x_{E,b,a}^{y-5,u}\right], \text{y} = 1, 2, 3. \quad (58\text{-}60)$$

$$(4)\ \sum_{u\in U}\sum_{m\in M} x_{G,g,m}^{y,u} \ge \max\left[(1+q_r^y).\sum_{u\in U}\sum_{m\in M} x_{G,g,m}^{y-1,u}, q_d^y.\sum_{u\in U}\sum_{m\in M} x_{E,g,m}^{y-5,u}\right], \text{y} = 1, 2, 3. \quad (61\text{-}63)$$

$$(5)\ \sum_{u\in U}\sum_{s\in S} x_{G,g,s}^{y,u} \ge \max\left[(1+q_r^y).\sum_{u\in U}\sum_{s\in S} x_{G,g,s}^{y-1,u}, q_d^y.\sum_{u\in U}\sum_{s\in S} x_{E,g,s}^{y-5,u}\right], \text{y} = 1, 2, 3. \quad (64\text{-}66)$$

$$(6)\ \sum_{u\in U}\sum_{a\in A} x_{G,g,a}^{y,u} \ge \max\left[(1+q_r^y).\sum_{u\in U}\sum_{a\in A} x_{G,g,a}^{y-1,u}, q_d^y.\sum_{u\in U}\sum_{a\in A} x_{E,g,a}^{y-5,u}\right], \text{y} = 1, 2, 3. \quad (67\text{-}69)$$

WEAR PERFORMANCE OF HDPE/ ZnO – SiO_2 - $CaCO_3$ – $Mg(OH)_2$ NANO-FILLER POLYMER COMPOSITES

Sezgin Ersoy[1] and Münir Taşdemir[2]
[1] Marmara University Tech. Edu. Faculty, Dep. of Mechatronic Istanbul 34722, Turkey
sersoy@marmara.edu.tr
[2] Marmara University Technology Faculty, Dep. of Met. and Materials Eng., Istanbul 34722, Turkey
munir@marmara.edu.tr

Abstract: Polymer technology is developing products for diverse needs. However, the expected properties of materials are rapidly increasing. Many new products have been developed using nanotechnology in the development of polymer production. These products can be illustrating change properties as physical, structural, morphological, electrical and mechanical properties when compared to the microstructure. Detection of these changes can be determined by an examination of these materials. In this study, the investigation of the effect of high-intensity polyethylene is filled by zinc oxide, magnesium hydroxide, calcium carbonate and silicon dioxide. The experiments show that It varies according to the tribological properties of nano contribution rates. High density polyethylene with zinc oxide, magnesium hydroxide, calcium carbonate and silicon dioxide have been mixed at % 5, %10, %15 and % 20 proportion. After the mixing activity the dehydrated materials have been changed into granule.
Key Words: Wear Performance, Nano powder, HDPE

INTRODUCTION

In recent years micro-and nano-fillers have attracted great interest, both in industry and in academia, because they often exhibit remarkable improvement in materials properties when compared to conventional composites made by using macro-fillers. These micro-/nano-composites can be made with very low loading of micro-/nano-fillers as compared with macro particle sized fillers (Ray, 2003). High density polyethylene (HDPE) is widely used as a commodity polymer with high-tonnage production due to its distinctive mechanical and physical properties. Because of its low toughness, weather resistance, and environmental stress cracking resistance as compared to engineering polymers, its application in many areas has been limited. To improve these disadvantages, HDPE has been reinforced with fillers [Wang, 2009; Rothon, 1995-1999; Ersoy, 2012). Wear is defined as the loss of materials at the rubbing surfaces. Wear rate on the type of material, to the shape of the rubbing surfaces of the friction conditions and depends on the chemical effects of the environment. Maintained a certain period of effect of a given force to the test parts for wear reduction in the amount or size reduction by weight or volume are measured (Ersoy, 2015).

Determined by the literature and the results of similar studies have been examined. Dhoka et have examined the effect of the addition of nano ZnO on silicone modified alkyd- based coatings with water based on the mechanical and heat resistance. In this study, nano- ZnO was added in different proportions. Contribute to the increase of the rate of increase has caused the wear rate (Shailesh, 2009).

In a study conducted; PP - $Mg(OH)_2$ which size is 50 nm were mixed. Mixing ratios caused the reduction of wear. The change in the wear rate of the material has been found to be associated on hardness value. (Saçaklı, 2012).

In another study performed on mechanical and wear behavior of vinyl ester resins investigated the effect of nano silica filler. In this study, vinyl ester resin was mixed SiO_2. This abrasion test was applied to the obtained material. Results of an increase in contribution rates indicate that the wear rate increases. Another study on the ZnO nano-composites and aluminum were also examined and compared with SiO_2 and their wear rate comparison with other samples and their result values were found to be better than other nano-materials filler composites (Elansezhian, 2011).

Experimental Details

High-density polyethylene (HDPE) Was supplied by Petkim (Izmir-Turkey). Specific gravity is 0,970 g/cm^3. Melt flow rate is 5.2 g/10 min (190^o C–2.16 Kg). Yield strength is 28,0 MPa and notched Izod impact (23^o C) is 12 kJ/m^2. Zinc oxide nano powder was supplied by MK nano. Particle size is ≤50 nm and white powder. Its purity is 99.9 %. Magnesium hydroxide nano powder was supplied by MKnano. Its purity is 99 %. Particle

size is 50 nm. Calcium carbonate (calcite- CaCO3) Nano powder was supplied by Cales de Llierca. Its purity is 98 %. Particle diameter is 50 nm (Ersoy, 2012)

SiO_2, ZnO and $Mg(OH)_2$ were dried in a Vacucell VD 55 vacuum oven at 105ºC for 24 hours before being blended with HDPE. Mechanical premixing of solid compositions was done using a blender for 15 min. Samples with various proportions of HDPE/SiO_2, HDPE/ZnO and HDPE/$Mg(OH)^2$ polymer composites were produced between 180-220 oC at 20-30 bar pressure, and a rotation rate of 30 rpm, with a co-rotating twin-screw extruder. L/D ratio is 30, Ø: 25 mm. To prepare the samples for thermal and mechanical tests, the following injection conditions were used: Injection temperature was 180-220 ºC, injection pressure was 110-130 bar, dwelling time in mold was 10 s, and screw rotation was 25 rpm, Polymer composites were also dried in vacuum oven at 105 ºC for 4 hours after extrusion (Saçaklı, 2012).

METHODS

Wear rate that the fragment of material is determined by counting the amount by mechanical rubbing, scraping and erosion. The cylinder is wearing to polymer without overheating wherein the force applied is 10N. Test, according to the type of the sample, 10, 20 and 40 are made according to one of meters. The result of this operation indicates deliver the ratio of the wear resistance. This value is expressed as volume loss or abrasion (ASTM D638). Figure I. shows operating principle of the abrasion tester. The device has TS EN 12770 as a reference number which is containing the abrasion test method that used in the standard [6]. The device used in the assay is Devotrans brand. This device is located at Marmara University Faculty of Technology and Metallurgy Laboratory. Test samples have 4 mm thick and 16 mm diameter. The weight of the test sample is determined. Samples should be in full contact with the abrasive system as TS EN 12770 and TS 11007.

Figure 1. The abrasion test device

The device reaches 40 meters by 84 cycles. Thereafter the test stops and the part is ejected. And then the weight of the sample is determined. This process is repeated for 5 samples which is TS 1731. The wear tests were done according to the DIN 53 516 method with Devotrans DA5 (Devotrans, Istanbul-Turkey) abrasion test equipment. The friction coefficients and wear rates reported in the present study were the averages of three measurements. The thickness of the test specimens was 7.0 mm and diameter was 15.5 mm. The mass loss of the specimen was measured after the wear test, in order to calculate the specific wear rate by the equation:

$$Ws = \frac{\Delta m}{\rho \,.Fn.L} \text{ (mm}^3\text{/Nm)} \qquad (1)$$

where Δm: mass loss,
ρ: density (0.958),
FN: normal load,
L: sliding distance

RESULTS

The abrasion test result values are presented in this section. The results indicate that wear rate value of pure HDPE was identified as 0.000172 cm^3/Nm as reference value. All these measurements compose on this reference. Material increase in the contribution rate caused by corrosion of the values were determined.

HDPE - ZnO nano-composite examination of the wear rate values which is 5% ZnO reinforced materials

was 0.00018 cm^3 / Nm. This corrosion rate is seen that an increase in value arrive 4.6%. ZnO wear rate 10% contribution values has led to an increase of 16.3% (0.00020 cm^3 / Nm). 15% ZnO contributing which is metal-based materials was studied and the wear rate determined 0.00021 cm^3/Nm, it increase 22.1% on wear rate ratio. Contribution of 20% ZnO grew by 27.9% in value of the wear rate 0.00022 cm^3 / Nm is. It was observed that the wear rate increases. Contribution of 20% ZnO grew by 27.9% on value of the wear rate (0.00022 cm^3/ Nm)

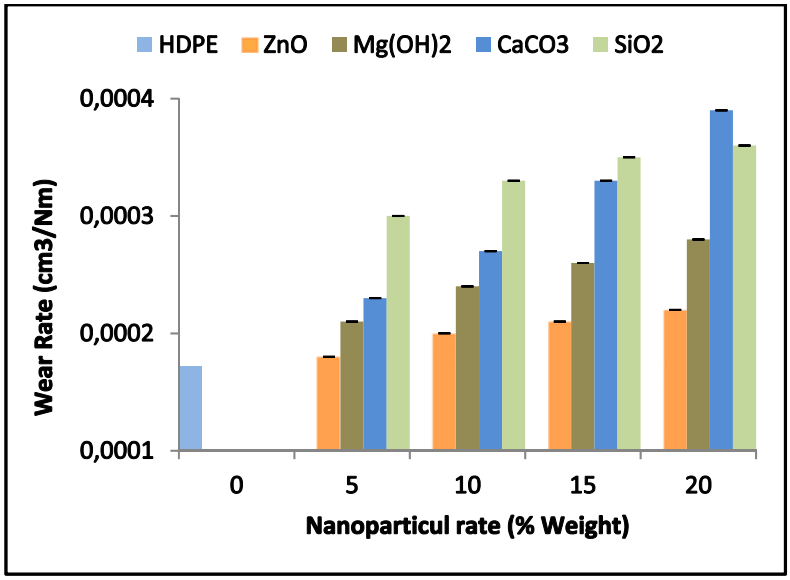

Figure 2. The wear rate as a result of abrasion test values (cm^3/Nm)

Metal materials such as ZnO, which class of Mg $(OH)_2$ addition of HDPE nano-composite wear rate values are examined, depending on the surface roughness increased wear rate. Examined the contribution of 5% of this value, the wear rate of 22,1% was observed with the increase in 0.00021 cm^3/Nm. Additives 10% ZnO, the increase in wear rate is 39.5%. The wear rate of 15% ZnO increased 0.00026 cm3/nm value (51.2%). In 20% of the additive reaches 0.00028 cm^3/ Nm seen.

Organic materials such as $CaCO_3$ and SiO_2 were found to contain high increase in the wear rate. HDPE - $CaCO_3$ contributing 5% of nanocomposite was determined as 0.00023 cm^3/ Nm, where in wear rate increased 33.7% by reference values of HDPE. Wear value with 10% fill rate increased by 57% and reached 0.00027 cm^3/ Nm. Contribution rate of 15% $CaCO_3$ on the wear rate is 0.00033 cm^3/ Nm (91.9% increase). 20% $CaCO_3$ additive caused an increase in the rate of 127%. Here the value of wear rate cm^3 / Nm 0.00039. HDPE - SiO_2 by mixing additives with the HDPE increases were observed very high in wear ratio. 5% SiO_2 added increased wear rate value 74.5% (0,00030 cm^3/Nm). Wear value contribution of 10% SiO_2 was determined to be 0.00033 cm^3/nm. Here increase in wear values as 91.8%. Attrition values of 15% of additives identified as 0.00035 cm^3/nm. This indicates an increase in the rate of 103.5%. Contribution rate of 20% indicate that increase wear value as 109.3% (0.00036 cm3/nm).

Additives used in the study of the ZnO and Mg $(OH)_2$ depending on the contribution rates of nano-powders of the wear rate is understood that a linear increase. $CaCO_3$ and SiO_2 nano powder additives for wear rate was determined at the highest level in test groups.

SEM - EDAX

Nano- powder were conducted in order to determine the content by EDAX analysis. The data obtained are presented in Figures.

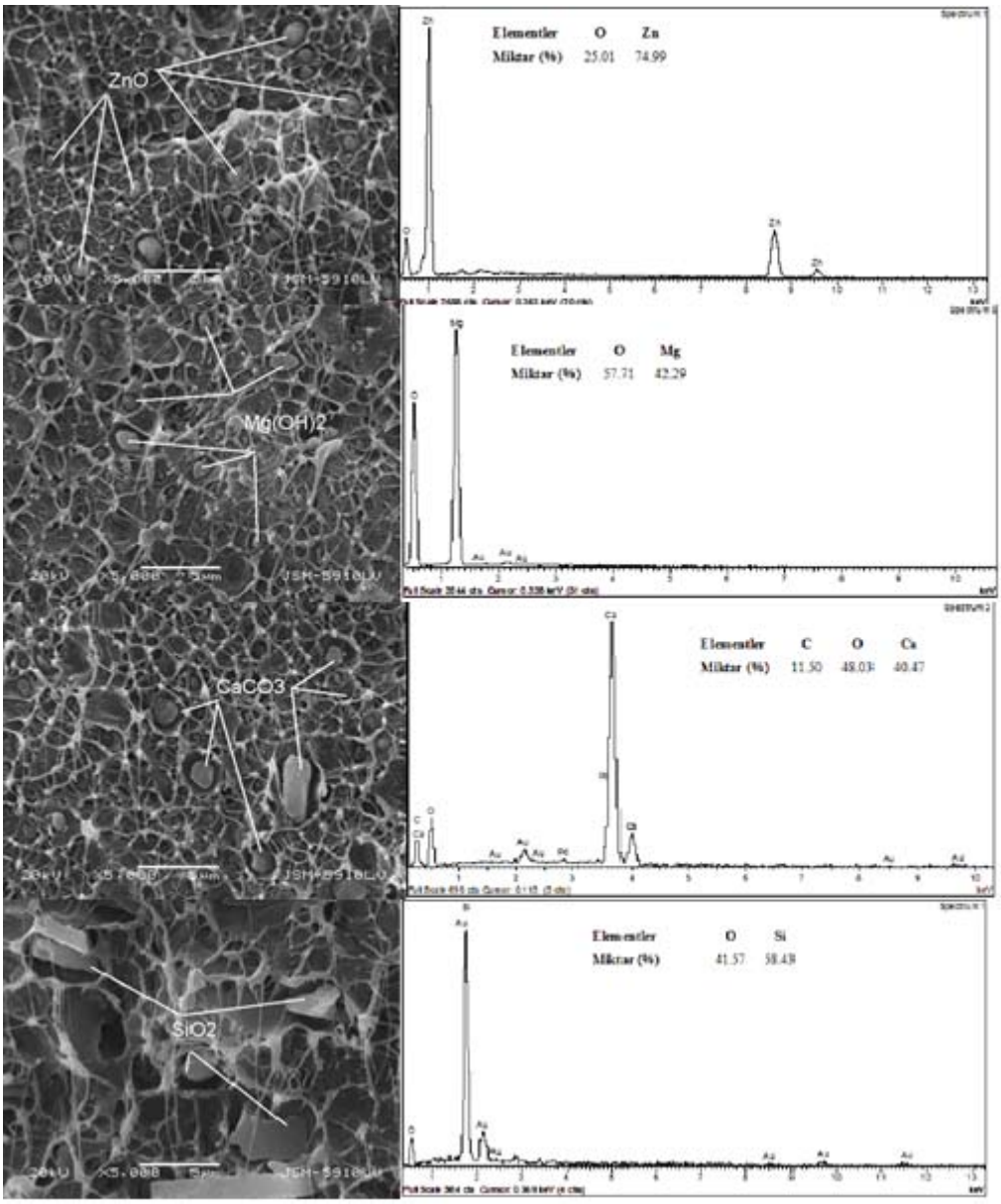

Figure 3. EDAX analysis results for ZnO, $Mg(OH)_2$, $CaCO_3$and SiO_2

CONCLUSION

Wear is the loss of material from the rubbing surfaces and its calculate quantity, by weight or volume or size reduction. Wear is the loss of material from the rubbing surfaces and it can be calculated quantity, weight and volume or size reduction. In this study; high density polyethylene incorporated nano powders were found to improve wear rate. Contribution rates have increased abrasion values. All material contribution rate, the highest values were observed in the highest wear. ZnO - HDPE composite materials for wear values increased about 20%. This increase was determined at Mg $(OH)_2$ at 27%, 109% in the addition of SiO_2, 126% of $CaCO_3$ filler respectively. Finally, it seen that wear rate of SiO_2 did not change at %20. It is understood that the SiO_2 nano-fill is not effective after this at 15%. After this work, researcher can work on filled new rate and their statistical analyses.

REFERENCE

Ray SS, Okamoto M. (2003). Polymer/layered silicate nanocomposites: a review from preparation to processing, *Prog Polym Sci* , (pp. 1539-1641)

Wang, Y., Shi, J., Han L., Xiang F. (2009). Crystallization and mechanical properties of T-ZnOw/HDPE composites, *Mater Sci Eng A* , (pp. 220-228).

Rothon, R. N. (1995). Particulate-Filled Polymer Composites; *Longman Scientific and Technical*: Harlow.

Rothon, R. N. (1999). Mineral fillers in thermoplastics: filler manufacture and characterization, *Adv Polym Sci,* (pp. 67-107).

Ersoy S., Taşdemir, M. (2012). Properties of polymer composites filled with SiO_2, ZnO and $Mg(OH)_2$ nano powder, *15th International Conference on Experimental Mechanics,* Rio de Janeiro, Brezil

Ersoy, S. (2015). Friction And Wear Performance Of High Density Polyethylene / Styrene - Butadiene Rubber Polymer Blends, *Revista Romana de Materiale* (pp. 267-271).

Shailesh K. Dhoke, S.K.; Bhandari, R.; Khanna, A.S. (2009). Effect of Nano – ZnO Addition on The Silicone-Modified Alkyd-Based Waterborne Coatings on Its Mechanical and Heat-Resistance Properties. *Progress in Organic Coatings* (pp. 39-46).

Saçakli, Y., Taşdemir, M. (2012) The Properties of Polymer Composites filled with $Mg(OH)_2$ Powder. *Journal of Polymer Materials*, (pp. 9-20).

Elansezhian, R.; Saravanan, L. (2011). Effect of Nano Silica Fillers on Mechanical and Abrasive Wear Behaviour of Vinyl Ester Resin. *International Journal of Applied Research in Mechanical Engineering*. (pp. 105-108).

Ersoy, S., Taşdemir, M. (2012). Zinc oxide (ZnO), magnesium hydroxide [Mg(OH)2] and calcium carbonate (CaCO3) filled HDPE polymer composites. Journal of of Pure and Applied Sciences. (pp 4,8).

ASTM D638. (2010). Standard Test Method for Tensile Properties of Plastics, *American National Standards Institute,* Washington, ABD.

TS EN 12770. (2004) Abrasion Resistance, *Turkish Standards Institution*, Ankara, Turkey.

TS 11007. (1993). By a rotating cylinder Tambor Determination of Abrasion Resistance. Turkish Standards Institution, Ankara, Turkey.

TS 10731. (1993). Determination of Abrasion Resistance. Turkish Standards Institution, Ankara, Turkey

